NOVEL CONDUCTING POLYMER CONTAINING COMPOSITE COATINGS FOR THE CORROSION PROTECTION OF METAL ALLOYS

A Dissertation
Submitted to the Graduate Faculty
of the
North Dakota State University
of Agriculture and Applied Science

By

Niteen Gangaram Jadhav

In Partial Fulfillment
for the Degree of
DOCTOR OF PHILOSOPHY

Major Department:
Coatings and Polymeric Materials

April 2013

Fargo, North Dakota

North Dakota State University
Graduate School

Title

Novel conducting polymer containing composite coatings for the corrosion protection of metal alloys

By

Niteen Jadhav

The Supervisory Committee certifies that this ***disquisition*** complies with North Dakota State University's regulations and meets the accepted standards for the degree of

DOCTOR OF PHILOSOPHY

SUPERVISORY COMMITTEE:

Dr. Victoria Johnston Gelling
Chair

Dr. Stuart Croll

Dr. Andriy Voronov

Dr. Sanku Mallik

Approved:

1st July 2013
Date

Dr. Dean Webster
Department Chair

ABSTRACT

Corrosion is persistent problem faced by manmade structures made up of metal alloys. Aluminum 2024-T3 is high strength, light weight alloy used in aerospace applications. It suffers from the problem of corrosion due to its composition. Cold rolled steel is employed in structural applications but undergoes severe corrosion when exposed to corrosive conditions. Coatings are one of the best avenues to protect metal alloys from the corrosion. Traditional coating systems such as barrier type coatings, metal rich coatings, and inhibitor containing coatings have their own drawbacks. Conducting polymers (CPs), such as polypyrrole (PPy) can be used for the corrosion protection of the metals. Redox activity in conjunction with corrosion inhibiting ion release ability make CPs as a promising candidate for the replacement for hexavalent chromates. However CPs porous nature, inherent insolubility, stiff chains, and poor mechanical properties pose significant hindrance towards their implementation in coatings. In order to overcome the problems associated with the CPs and to extract maximum functionality out of them, conducting polymer containing composites (CPCC) were developed. CPCC combines CPs with inorganic pigments in unique ways and pave for excellent properties.

In this work, series of composites of PPy/Inorganic pigments (aluminum flakes, iron oxide, micaceous iron oxide, and titanium dioxide) were synthesized by ecofriendly, facile chemical oxidative polymerization. Core and shell morphologies of PPy with titanium dioxide and iron oxide were synthesized and employed for the corrosion protection of cold rolled steel substrate. Various dopants such as phosphate, nitrate, molybdate, vanadate, and tungstate were incorporated in the backbone of PPy. These composites were characterized for morphology, elemental composition, and conductivity by various techniques. Furthermore coatings based on these composite pigments were formulated on Aluminum 2024-T3 and cold rolled steel substrates. These coatings were exposed to salt spray and prohesion test conditions and

electrochemically evaluated against corrosion by Electrochemical Impedance Spectroscopy (EIS), DC Polarization, galvanic coupling and Scanning Vibrating Electrode Technique (SVET). Effect of solvent in the composite synthesis and PPy morphology in the final composite on the protective properties of coating was investigated. Effect of corrosion inhibiting anions on the final performance properties was also evaluated.

ACKNOWLEDGEMENTS

I would like to take this opportunity to express my deep gratitude to Dr. Victoria Johnston Gelling, my dissertation committee chair for all her help and guidance through my study, research and dissertation.

I am grateful to my other dissertation committee members, Dr. Stuart Croll, Dr. Andriy Voronov, and Dr. Sanku Mallik, who spent their time generously and conveyed their knowledge unreservedly to improve my research work.

I would like to acknowledge the support of this research by US Army Research Laboratory under grant no. W911NF-09-2-0014, W911NF-10-2-0082, and W911NF-11-2-0027. Many thanks to Scott Pyane and Jayma Moore of electron microcopy center for their help with SEM and TEM characterizations. I am also grateful to the students, staff, and faculty of Department of Coatings and Polymeric Materials at North Dakota State University for providing me wonderful ambiance to work.

TABLE OF CONTENTS

LIST OF TABLES

LIST OF FIGURES

LIST OF SCHEMES

Scheme Page

CHAPTER 1. INTRODUCTION

1.1. Introduction

Corrosion is an electrochemical phenomenon in which metal transforms to its original oxide form. It is also described as extractive metallurgy in reverse (Figure 1.1). The metal oxide obtained from ore is subjected to tremendous energy in order to obtain its metal form. So there is thermodynamically favorable tendency of metals to regress to lower energy form (metal oxide) in contact with conducive environmental conditions. We live in the civilization which is heavily dependent on the metals and their alloys. Corrosion of metals and their alloys impacts several aspects of human life including utilities, manufacturing, transportation, infrastructure and several more. Corrosion leads to a compromise with health and safety. The useful system life is also lost requiring for expensive maintenance and repair. Corrosion also affects cosmetic appearance of the object. The worldwide annual coast of corrosion is at 2.2 trillion U.S dollars which is approximately equivalent to over 3% of worlds total GDP [1].

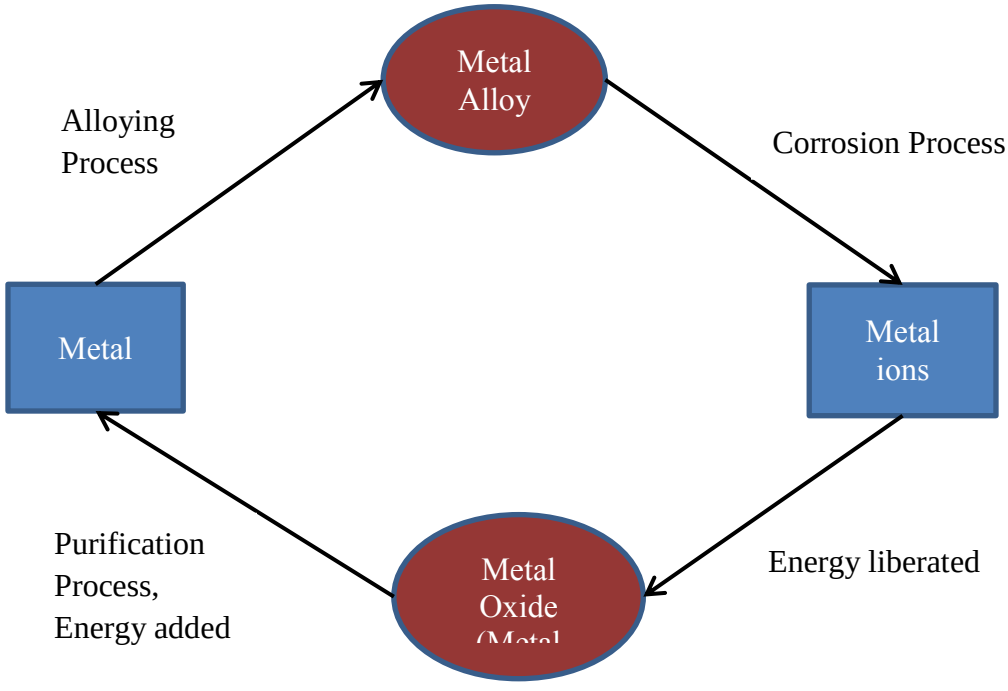

Figure 1.1: Process of corrosion, an extractive metallurgy in reverse.

Corrosion can not be completely stopped, but it can be mitigated. Several strategies have been employed for the protection of metals and their alloys from corrosion. These include proper material selection and design, cathodic protection, inhibitors, and coatings. Coatings are the most widely used techniques for the prevention of the corrosion. For the protection and the decoration of metal structures one-third of the total paint produced is utilized [2]. Traditional paint systems such as barrier type coatings fail once a defect is made on the coating. Well know corrosion inhibitors hexavalent chromates, are carcinogenic and toxic in nature. Metal rich primers need very high pigment volume concentration (PVC) for the metal to metal contact. Again these metals (zinc or magnesium) have environmental impacts. In the changing environment of the 21st century with increasing pollutants in the ecosystem and taking into consideration the drawbacks of existing coating systems, there is a need to discover possible ecofriendly alternatives to the exiting coating systems for the corrosion protection of the metals and metal alloys. New coating systems should exhibit not only corrosion inhibiting properties for prolonged durations in severe environments but also should provide extra functionality such as self-healing and smart protection.

1.2. Conducting polymers for corrosion protection

Conducting polymers (CPs) are new class of materials which have shown promise over the last three decades for the corrosion protection of metals and metal alloys [3-7]. Polyaniline (PAni), Polypyrrole (PPy), and Polythiophene (PTh) are the representative CPs studied for corrosion protection [8-10]. CPs exhibit desirable properties such as good electrical conductivity, ease of synthesis by chemical and electrochemical polymerization methods, good thermal stability, and environmental friendly nature [11-12]. However there are several disadvantages as per as application in coatings is concerned. CPs are insoluble in commonly used solvents in

coatings. They exhibit porosity and poor to moderate adhesion to the substrate [13]. There is a possibility of irreversible charge consumption which is stored in the CPs due to the redox reactions, in presence of small corrosive anions which might result in catastrophic corrosion failures [12].

In order to overcome problems associated with CPs several avenues have been explored by researchers. These include chemical modification of CP monomers in order to render them solubility. Dopant ion solutions as well as use of composites of CPs, nanocomposites of CPs, bilayer's and multilayer's of CPs, copolymers of CPs are some of the possible ways attempted by researchers in recent past. The subject of the current research is synthesis and characterization of conducting polymer containing composite (CPCC) with varying morphologies and various corrosion inhibiting dopants for corrosion protection of metal alloys. The synthesis method employed is facile, room temperature chemical oxidation polymerization of monomers of CP. It is possible to synthesize CPCC on larger scale by employing a chemical oxidation polymerization method. Corrosion inhibiting anions can be easily incorporated on to the backbone of CPs by this method, and their quantities can be easily monitored. Resultant pigment composite can be handled industrially and easily incorporated into coating systems. However, the protection offered by the CPs strongly depends on the type of substrate, substrate preparation, CPs synthesis and application process, and the type of dopant and electrolyte used in CP synthesis [14].

Several mechanisms have been proposed for the corrosion protection of metal alloys by CPs [9-10]. However, ambiguity persists in literature about the generally accepted corrosion protection mechanism by CPs [15]. Suggested mechanisms for the corrosion protection in the case of PAni are barrier effects, as corrosion inhibitors, anodic protection, corrosion inhibiting

dopant release, shift in corrosion potential, inhibition of the diffusion rates, and healing in pinholes. Suggested mechanisms for the corrosion protection in the case of PPy are anodic protection, ennobling, passivation, and corrosion inhibiting dopant release [10].

1.2.1. Polypyrrole for corrosion protection

PPy is one of the most important members of the family of CPs. PPy exhibits interesting properties such as environmental stability, good conductivity, excellent thermal stability and eco-friendly nature [16-17]. Conjugated π-system and doping due to chemical and electrochemical methods is responsible for the conductivity exhibited by PPy. Doping and de-doping results in oxidized form of PPy (Figure 1.2) and in neutral form (Figure 1.3) respectively. Positive charge is balanced with counter anion to maintain charge neutrality. Doping results from the anion of oxidant or electrolyte used in reaction [18].

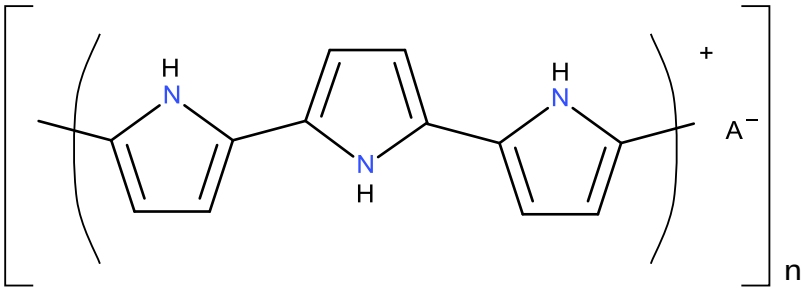

Figure 1.2: Oxidized form of PPy (A^- is anion).

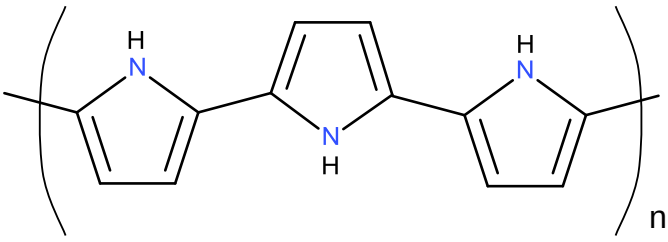

Figure 1.3: Neutral form of PPy.

PPy finds applications in sensors [19] biosensors [20], actuators [21], rechargeable batteries [22], capacitors [23], tissue engineering [24], optoelectronic devices [18], electromagnetic interference (EMI) shielding [25], fuel cells [26], drug delivery [27], and anti corrosion coatings [28]. Taking into consideration earlier mentioned drawbacks of CPs, PPy has been modified for various applications. Composites and nanocomposites of PPy are finding applications in the corrosion protection of metal and their alloys. Doped PPy is also used as a additive pigment in small proportion in the coatings or as a primer alone with or without topcoat, or as a blend with conventional coating binders [29].

1.2.1.1. Composites and nanocomposites of PPy for corrosion protection

Composites bring together diverse properties of different materials for the enhancement in property and performance. Nanocomposites exert added advantage of increased surface area resulting in the manipulation of the final properties for intended applications.

A composite of PPy with TiO_2 was synthesized by anodic co-deposition on the surface of AISI 1010 steel substrate. Higher anodic corrosion potential in case of PPy/TiO_2 films than just PPy and steel suggested improvement in corrosion resistance properties [30]. This composite PPy/TiO_2 might serve as a possible replacement material for phosphatized layers on mild steel [31]. Again for replacing phosphatized layers on mild steel, PPy/zinc phosphate composite coatings were formed on mild steel surfaces with sodium salicylate as a medium by electrochemical polymerization. Protective ability of PPy/zinc phosphate composite coatings was demonstrated in salt spray and weight loss experiments [32]. PPy/carboximethylcellulose (CMC) was synthesized on the surface of steel by electrodeposition process. Positive shift in corrosion potential and reduction in oxidation current was observed suggesting uniform and protective films of PPy/CMC [33].

Soluble PPy in m-cresol was added to methyl methacrylate (MMA) and Azobisisobutyronitrile (AIBN) initiator and was applied on iron substrate by spin coating which was furthermore polymerized at 80°C in vacuum. This resulted in the formation of PMMA/PPy composite on iron substrate. A positive shift in potential by 200 mV and two orders of magnitude decrease in anodic current than bare steel was observed for PMMA/PPy composite in Tafel curves suggesting better corrosion protection offer by composite material to the iron substrate [34]. In another study, diglycidylether of bisphenol A (DGEBA)/PPy composite material based coatings were applied on mild steel substrate. It was claimed that the stable passive film was formed on the surface of mild steel due to presence of PPy resulting in the shift in open circuit potential (OCP) values in positive direction [35]. Composite of PPy, carbon black with epoxy resin was applied on steel substrate. PPy with 1% concentration in this composite showed corrosion performance in 480 hours of exposure in saline solution [36]. In another study, in presence of dihydroxybenzene, pyrrole monomer was polymerized on alumina surface to form nanocomposite particles of PPy and alumina. These particles were employed as filler in coating for the corrosion protecting of AA-2024-T3. Impedance measurements exhibited better corrosion protection offered by nanocomposite particles [37]. Other researchers studied PPy deposited alumina particles incorporation in zinc rich primers. Increase in the corrosion protection ability of zinc rich primers was observed at lower concentrations of PPy deposited alumina particles in the coating [38].

Epoxy coating (E), Epoxy-montmorillonite (MMT) coating (EM), Epoxy-PPy coating (EP), and Epoxy-PPy-MMT coatings (EPM) were applied on Al 5000 substrate [39]. At 10 wt% concentration of MMT, PPy or PPy/MMT corrosion studies were performed by employing electrochemical impedance spectroscopy (EIS). It was observed that, superior coating resistance

(Rcoat) values were obtained for Epoxy-PPy-MMT coating ever after 100 days of immersion in 3.5% NaCl solution (Figure 1.4) suggesting better corrosion protection than E, EM, and EP coatings. This improvement was attributed to the denser and compact films of EPM. Increased hydrophobicity and adhesion of EPM coatings with combination with PPy electrochemical activity resulted in better corrosion resistance.

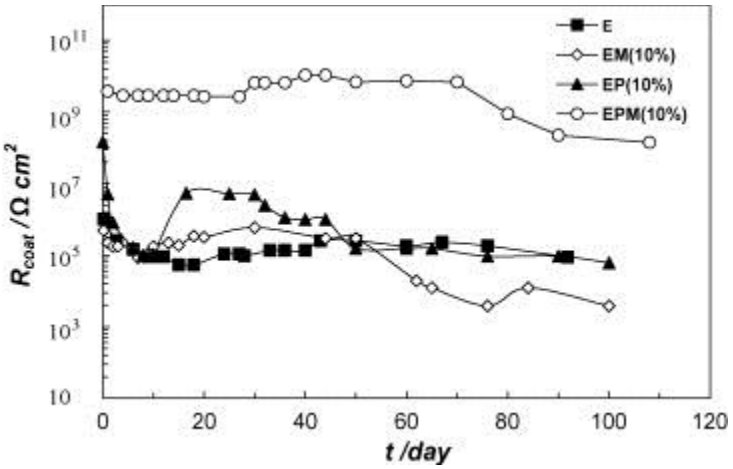

Figure 1.4: Time dependence of coating resistance of E, EP, EM and EPM coatings in 3.5% NaCl solution, "Reprinted from ref. [39] (Progress in Organic Coatings, 66(3), M.G. Hosseini, M. Raghibi-Boroujeni, I. Ahadzadeh, R. Najjar, M.S. Seyed Dorraji, Effect of polypyrrole–montmorillonite nanocomposites powder addition on corrosion performance of epoxy coatings on Al 5000, 321-327, 2009), with permission from Elsevier.

PPy-epoxy polyamide composite coatings were studied for the corrosion protection of steel. In this study, potassium permanganate and potassium persulfate were used as oxidants for synthesis of PPy. Higher impedance values were observed for PPy-epoxy polyamide composite coatings after 30 days of immersion in 3% NaCl solution. Passive layer formation due to the release of dopant ions was indicated for improved corrosion protection [40]. In another study, by electrodeposition, PPy and PPy-ZnO nanocomposites were synthesized on the mild steel substrate. The EIS and Tafel test results indicated that PPy-ZnO nanocomposite coatings exhibited better corrosion protection due to the nanozised dimensions and compactness of the

coating leading to the increase in the charge transfer resistance thereby reducing corrosion rate. Positive shift in the OCP value was observed for PPy-ZnO nanocomposite coatings [41].

PPy/polyaminobenzene sulfonic acid-functionalized single-walled carbon nanotubes (CNT-PABS) and PPy/carboxylic acid-functionalized single-walled carbon nanotubes (CNT-CA) composite coatings were synthesized by galvanostatic method on carbon steel substrate. In presence of PPy positive shift in potential and reduced current was observed indicating better corrosion protection. The protection provided by PPy/CNT-PABS and PPy/CNT-CA was attributed to increased conductivity of the composite coating [42].

PPy/Sn-doped TiO_2 nanocomposites were synthesized and were employed as pigments at 1 wt% and were added to epoxy-polyamide coating which was applied to steel substrate. Increase in anticorrosion performance was attributed to the increased surface area of PPy which could lead to greater interaction with substrate and resistance to hole transport in the p-n type semiconductor formed due to p-type PPy and n-type TiO_2 [43]. PPy/Ni-doped TiO_2 nanocomposites were synthesized and employed at 1 wt% in the coating. The nanocomposites exhibited improved corrosion performance owing to same reasons mentioned earlier [44].

Poly (N-methylpyrrole) (PMPy) was electrodeposited in presence and absence of TiO_2 nanoparticles using dodecyl benzene sulfonic acid and oxalic acid as the electrolytes. Presence of TiO_2 nanoparticles resulted in the increase in surface area for PMPy leading to increased ability of PMPy/ TiO_2 nanocomposite coating to interact with ions in the corrosion reaction. Coating capacitance (C_c) and pore resistance (R_{po}) values confirmed lesser water uptake and increased corrosion protection offered by PMPy/ TiO_2 nanocomposite coating as shown in Figure 1.5.[45].

Lamellar shape materials can lengthen the path of corrosive species thereby delaying the onset of corrosion. It has been found that; inorganic flake can reduce the electrolyte

permeability by the factor of 10 in the polymeric coating [46]. Inorganic flakes such as aluminum and mica can be combined with CPs and composite can be formed. This composite can exert the properties of both, inorganic pigment and CPs. Inorganic flake will provide barrier protection and CP will provide protection by its redox mechanism involving anodic protection, ennobling, passivation or inhibition [47]. CPCP are the novel materials in which CPs are in-situ synthesized on the surface of inorganic flakes. PPy/Aluminum flake pigments were incorporated in epoxy primer and applied on aluminum 2024-T3 substrate [48]. In galvanic contact with aluminum flake and underlying aluminum substrate, PPy tended to be reduced and activated aluminum flakes towards the sacrificial protection of the substrate aluminum 2024-T3. Reduced PPy also reoxidized by oxygen and decreased corrosion rate.

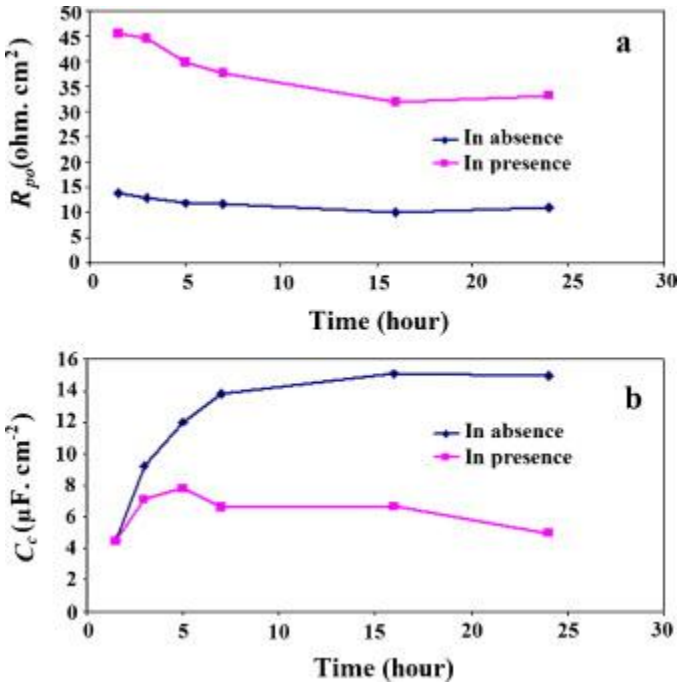

Figure 1.5: The comparison of (a) the pore resistance, R_{po} (b) the polymer coating capacitance, C_c, coated steel with synthesized PMPy in the presence and the absence of TiO_2 NPs, as a function of immersion time, "Reprinted from ref. [45] (Applied Surface Science, 257, M.R. Mahmoudian, W.J. Basirun, Y. Alias, Synthesis and characterization of poly(N-methylpyrrole)/TiO_2 composites on steel, 3702-3708, 2011), with permission from Elsevier.

1.2.1.2. Doped PPy for corrosion protection

PPy can be doped with corrosion inhibiting anions, serving as reservoir of the anions which can be released when PPy changes its redox state. The released corrosion inhibiting anions can combine with metal cations of the substrate and form a passivating layer in scratch resulting in smart corrosion protection mechanism [49-50]. The depleted charge of the PPy can again be replenished by the oxygen doping. However the protection proved by doped PPy depends upon the size of dopant, level of doping, method of synthesis, type of substrate, and nature of dopant (organic or inorganic).

It has been found that, large size dopants provide better corrosion protection than the small size dopants [51]. PPy doped with polystyrenesulfonate (PSS) dopant anion has shown better corrosion protection than, oxalate or tosylate doped PPy films electropolymerized iron substrate. Large size anion, PSS gets trapped in polymer matrix resulting in decreased mobility which furthermore reduces the ingress of corrosive chloride ions resulting in decreased corrosion rate [51]. Larger anion also provides steric effect and prevents OH- ion exchange, thereby reducing corrosion rate [52]. Dodecylsulfate doped PPy was electropolymerized on the surface of 1Cr18Ni9Ti stainless steel substrate. Positive shift in corrosion potential was observed (600 mV vs SCE) in the acidic electrolyte [53]. Sulfonated PPy was electropolymerized on stainless steel surface [54]. Anodic dissolution of stainless steel was inhibited by sulfonated PPy as well as pitting corrosion was reduced. Sulfonated PPy catalyzed the stainless steel surface to form protective ferric oxides.

Dodecylsulphate and bis(2-ethylhexyl) sulfosuccinate doped PPy were electrodeposited on pure aluminum substrate [55]. A drastic increase in corrosion potential and decrease in corrosion rate was observed improving corrosion protection for the pure aluminum substrate

[56]. Sodium dodecylbenzene sulfonate doped PPy was electropolymerized on aluminum alloy 1100 surface. An increase in impedance, corrosion potential and decrease in corrosion current density was observed for sodium dodecylbenzene sulfonate doped PPy coated on aluminum alloy 1100 surface. Various doping agents such as para-toluene sulfonic acid, camphor sulfonic acid, oxalic acid, phenylphosphonic acid, and cerium nitrate salt were employed in PPy electrosynthesis on the surface of aluminum alloy 2024-T2 [57]. Improved corrosion resistance performance was observed for cerium nitrate doped and camphor sulfonic acid doped PPy. Salicylate doped PPy was electrochemically synthesized on the copper substrate. A positive shift in potential was observed for salicylate doped PPy coated copper substrate [58]. Better corrosion protection performance was attributed to the redox reaction between salicylate doped PPy and the copper substrate.

Mobility of the corrosion inhibiting anions is very helpful for the corrosion protection in the cases where the anion release finally is responsible for the passivation. Molybdate doped PPy was electrochemically synthesized on the surface of mild steel. Dopant anion molybdenum was released when PPy was coupled with mild steel and corrosion was started in the defect. Sufficient mobility of molybdenum anion migration through PPy film lead to the formation of the passive layer in the defect [59]. In the same study, hexafluorophosphate doped PPy was compared with molybdate doped PPy for the corrosion protection of mild steel by potentiodynamic experiment. Hexafluorophosphate doped PPy was not able to passivate the mild steel as hexafluorophosphate anion is not corrosion inhibiting in nature whereas in case of molybdate doped PPy about 0.4V (vs SCE) shift in positive direction was observed indication passivation and corrosion protection (as shown in Figure 1.6).

In another study molybdate and phosphomolybdate anion doped PPy were employed for the corrosion protection of iron substrate. It was found that the release of phosphomolybdate anion is electrochemical process and not affected by the high pH at the metal/polymer interface [60]. The same observation was not evident in case of molybdate anion even though partial passivation was possible. It was also observed that in some cases care should be taken where small cation incorporation in high pH conditions is possible. Phosphotungstate doped PPy was electrosynthesized on carbon steel substrate [61]. Two fold increase in charge transfer resistance was observed for coating in comparison with bare steel indicated better corrosion protection. Phosphate and tungstate doped PPy films were electrochemically prepared on mild steel substrate [62]. Formation of primary passive layer was responsible for the improvement in corrosion resistance properties.

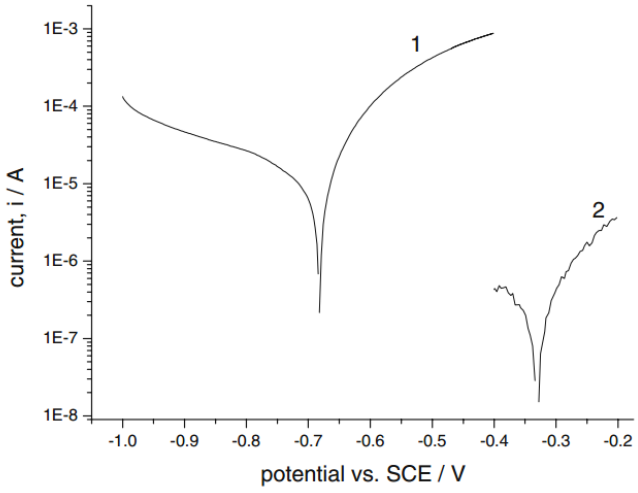

Figure 1.6: Potentiodynamic curves of PPy films with defect in 0.1 M NaCl 1: mild steel/PPy(PF6), Icorr=8x10^{-4} A 2: mild steel/PPy(-MoO_4), icorr=8x10^{-6} A, "Reprinted from ref. [59] (Journal of Applied Electrochemistry, 35(12), U. Rammelt, L. Duc, W. Plieth, Improvement of protection performance of polypyrrole by dopant anions, 1225-1230, 2005), with permission from Springer.

In another study, tungstate doped PPy was electropolymerized on carbon steel substrate. It was found that the tungstate increased stored charge of PPy coating and improved

corrosion resistance. A primary protective passive layer was observed which was responsible for the corrosion protection [12]. A similar increase in storage charge of PPy doped with phosphate anion was observed with increased corrosion protection as result of passivation on carbon steel substrate [63]. Polyphosphate doped PPy was electrodeposited on the surface of steel [64]. Bulky polyphosphate posses possibility to remain in PPy matrix and exhibiting hindrance to chloride ion ingress and can also give rise to passivation improving the corrosion protection properties of doped PPy. Phosphate doped PPy was electropolymerized on mild steel substrate [65]. Improvement in corrosion performance on mild steel was attributed to the formation of phosphate layer on mild steel surface which restricted the anodic dissolution of the metal substrate. In another study phosphate doped PPy was electrodeposited on the mild steel substrate [66]. Phosphate doped PPy increases potential and decreases corrosion current and rate (Figure 1.7). Electrochemical impedance spectroscopy (EIS), showed increase in charge transfer resistance indicating decreased corrosion rate.

Bi-layers of doped PPy were employed for the corrosion protection of steel. An inner layer of PPy was doped with molybdophosphate and phosphate anion where as outer layer was of PPy doped with various organic dopants such as dihydroxynaphthalenedisulfonate, dodecylsulfate, naphthalenedisulfonate, and anthraquinonedisulfonate anions. An outer layer helps for extended corrosion protection. Better corrosion performance was obtained for PPy doped with dodecylsulfate anion. In 3.5% NaCl solution coating maintained its passive domain for 7 days which was the result of highly oxidized state of PPy and dense nature of PPy doped with dodecylsulfate anion [67]. In another study single layer of oxalate doped PPy and dual layer of oxalate doped PPy and poly(styrene sulfonate) doped PPy was electrochemically synthesized on steel substrate [68]. The dual layer showed six fold more time to failure in 0.1M

NaCl solution than single layer. The large size of poly(styrene sulfonate) was responsible for preventing ingress of chloride ions thereby improving the corrosion protection provided by the dual layer for the steel substrate

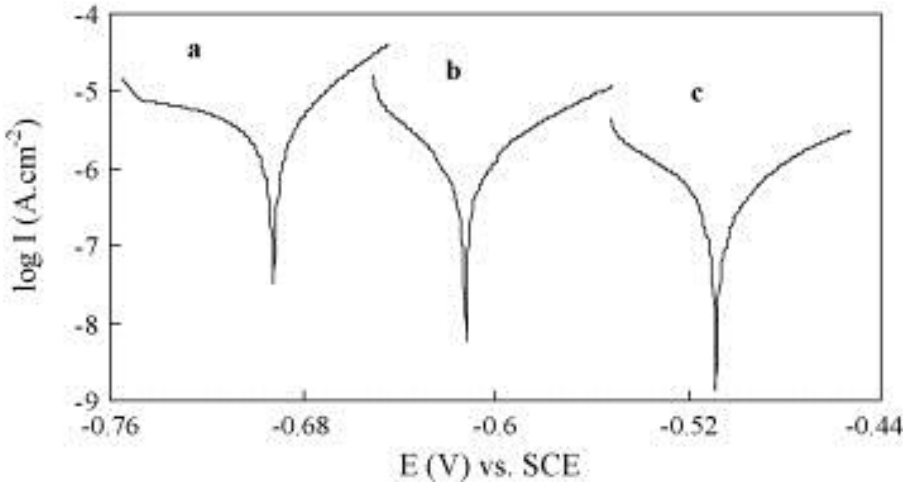

Figure 1.7: Tafel plots of (a) bare mild steel, (b) mild steel/Ppy and (c) mild steel/Ppy–phosphate electrodes in 3.5% NaCl solution after 1 h immersion; scan rate: 0.166 mV s−1, "Reprinted from ref. [66] (Progress in Organic Coatings, 60(3), M.G. Hosseini,M. Sabouri,T. Shahrabi, Corrosion protection of mild steel by polypyrrole phosphate composite coating, 178-185, 2007), with permission from Elsevier.

Co-doping with oxalate and dodecyl benzenesulfonate was performed for PPy electrodeposited on stainless steel substrate [69]. Smooth and adherent films with increased doping level were responsible for the corrosion protection offered by co-doped PPy. Nitrate and molybdate co-doped PPy was electropolymerized on pure aluminum substrate [70]. Increased pitting potential in neutral chloride media was observed which was attributed to the inhibiting action provided by dopant anions.

Co-doped PPy as well as doped PPy have shown improved corrosion protection ability as compared with just doped with single dopant or with single layer of PPy. However co-doping can also be dependent on the chemical nature of the different dopants employed in the synthesis

and in case of multilayer formation care should be taken for the adhesion and interactions between different layers.

1.3. Conclusions

A combination of CPCC and dopant ion incorporation in the backbone of the CP can pave for the unique properties for the corrosion protection. The galvanic protection offered by aluminum flakes can be combined with the dopant release which will further lead to the passivation and improved corrosion protection. In this dissertation, various CPCCs were synthesized based on inorganic pigments such as aluminum flakes, iron oxide, micaceous iron oxide, and titanium dioxide in combination with PPy and PAni. Different dopants were incorporated on the backbone of the CPs in CPCC. Composites were characterized by SEM, TEM, EDS, XPS, C-AFM, four point probe conductivity, and density tests. The resultant composites were employed in the coatings on aluminum and steel alloys. The corrosion protection ability of coatings exposed to accelerated corrosion tests was monitored by EIS, anodic polarization, SVET, and galvanic coupling experiments.

In chapter 2 of the dissertation, which is being accepted for publication in Electrochimica Acta, different morphologies of PPy were synthesized on the surface of aluminum flakes and their effect on the final corrosion performance on the aluminum 2024-T3 substrate was studied. Wire morphology of PPy was found to be offering better corrosion protection for aluminum 2024-T3 substrate for 120 days of Salt spray exposure. This PPy/Al flake pigment also provided sacrificial protection in the lager defects.

In chapter 3, which was published in ECS Transactions, phosphate and nitrate doped PPy/Al flake pigments were synthesized by chemical oxidative polymerization method. Dopants, phosphate and nitrate provided passivation in the defect areas as observed in anodic polarization

experiments and no corrosion activity was detected on the defect areas as evidenced in SVET experiments.

In chapter 4, which was published in Proceedings of CoatingsTech Conference, American Coatings Association, Rosemont, Illinois, March 11-13, 2013, tungstate and vanadate doped PPy/Al flake composite pigments were synthesized and electrochemically characterized for the corrosion protection of aluminum 2024-T3. Cathodic protection was provided by the tungstate and vanadate PPy/Al flake composite to the aluminum 2024-T3. However protection provided by the composite pigments was dependent on the type and amount of dopant as well as the conductivity of the composite pigment.

In chapter 5, which was published in Proceedings of CoatingsTech Conference, American Coatings Association, Rosemont, Illinois, March 11-13, 2013, core and shell TiO_2/PPy composite, TiO_2/PPy (Tungstate doped) composite, and TiO_2/PAni composite were synthesized and employed in coating for the corrosion protection of cold rolled steel substrate. Incorporation of CP to form composite with TiO_2 improved corrosion protection due to CPs redox ability.

In chapter 6, which was published in Polymeric Materials: Science & Engineering (PMSE) Preprints, core and shell morphology of iron oxide/PPy was synthesized by chemical oxidative polymerization. The synthesized core and shell composite was incorporated in the coatings for the corrosion protection of mils steel. For 40 days of Salt spray exposure, coating containing core and shell iron oxide/PPy composite pigments showed improved corrosion performance owing to the ability of PPy to act an oxidizer to form dense protective layer.

In chapter 7, which will be communicated to the corrosion journal, micaceous iron oxide (MIOX)/PPy composites were synthesized and characterized for corrosion protection of cold rolled steel. Smaller drop in impedance was observed for MIOX/PPy composite pigment based

coating at 100 days of Salt spray exposure than MIOX30 pigment coatings for the same duration of exposure. Lamellar nature of MIOX provided increased barrier protection and PPy added extra functionality due to its redox nature resulting in better corrosion protection than only MIOX containing coatings.

1.4. References

[1] G.F. Hays, Corrodia (2010) 1-2.

[2] Z. Ahmad, Principles of Corrosion Engineering and Corrosion Control, Elsevier Science, 2006.

[3] Y. Wei, J. Wang, X. Jia, J.-M. Yeh, P. Spellane, Polymer, 36 (1995) 4535-4537.

[4] W.-K. Lu, R.L. Elsenbaumer, B. Wessling, Synthetic Metals, 71 (1995) 2163-2166.

[5] J.-M. Yeh, S.-J. Liou, C.-Y. Lai, P.-C. Wu, T.-Y. Tsai, Chemistry of Materials, 13 (2001) 1131-1136.

[6] M. Fahlman, S. Jasty, A.J. Epstein, Synthetic Metals, 85 (1997) 1323-1326.

[7] A.J. Epstein, J.A.O. Smallfield, H. Guan, M. Fahlman, Synthetic Metals, 102 (1999) 1374-1376.

[8] S. Sitaram, J. Stoffer, T. O'Keefe, Journal of Coatings Technology, 69 (1997) 65-69.

[9] D. Tallman, G. Spinks, A. Dominis, G. Wallace, Journal of Solid State Electrochemistry, 6 (2002) 73-84.

[10] G. Spinks, A. Dominis, G. Wallace, D. Tallman, Journal of Solid State Electrochemistry, 6 (2002) 85-100.

[11] K. Castagno, D. Azambuja, V. Dalmoro, Journal of Applied Electrochemistry, 39 (2009) 93-100.

[12] M. Sabouri, T. Shahrabi, H.R. Faridi, M.G. Hosseini, Progress in Organic Coatings, 64 (2009) 429-434.

[13] M. Trueba, S. Trasatti, Journal of Applied Electrochemistry, 39 (2009) 2061-2072.

[14] E. Armelin, R. Oliver, F. Liesa, J.I. Iribarren, F. Estrany, C. Alemán, Progress in Organic Coatings, 59 (2007) 46-52.

[15] M. Rohwerder, A. Michalik, Electrochimica Acta, 53 (2007) 1300-1313.

[16] L.-X. Wang, X.-G. Li, Y.-L. Yang, Reactive and Functional Polymers, 47 (2001) 125-139.

[17] P.-G. Su, Y.-P. Chang, Sensors and Actuators B: Chemical, 129 (2008) 915-920.

[18] N.P. Gaponik, D.V. Talapin, A.L. Rogach, A. Eychmuller, Journal of Materials Chemistry, 10 (2000) 2163-2166.

[19] W.-D. Lin, H.-M. Chang, R.-J. Wu, Sensors and Actuators B: Chemical, 181 (2013) 326-331.

[20] M. Ates, Materials Science and Engineering: C, 33 (2013) 1853-1859.

[21] Y. Wu, G. Alici, G.M. Spinks, G.G. Wallace, Synthetic Metals, 156 (2006) 1017-1022.

[22] D. Kundu, F. Krumeich, R. Nesper, Journal of Power Sources, 236 (2013) 112-117.

[23] J.-H. Kim, Y.-S. Lee, A.K. Sharma, C.G. Liu, Electrochimica Acta, 52 (2006) 1727-1732.

[24] J.H. Collier, J.P. Camp, T.W. Hudson, C.E. Schmidt, Journal of Biomedical Materials Research, 50 (2000) 574-584.

[25] J.A. Pomposo, J. Rodríguez, H. Grande, Synthetic Metals, 104 (1999) 107-111.

[26] H. Zhao, L. Li, J. Yang, Y. Zhang, Journal of Power Sources, 184 (2008) 375-380.

[27] S. Geetha, C.R.K. Rao, M. Vijayan, D.C. Trivedi, Analytica Chimica Acta, 568 (2006) 119-125.

[28] J.I. Martins, T.C. Reis, M. Bazzaoui, E.A. Bazzaoui, L. Martins, Corrosion Science, 46 (2004) 2361-2381.

[29] E. Armelin, Á. Meneguzzi, C.A. Ferreira, C. Alemán, Surface and Coatings Technology, 203 (2009) 3763-3769.

[30] C.A. Ferreira, S.C. Domenech, P.C. Lacaze, Journal of Applied Electrochemistry, 31 (2001) 49-56.

[31] D.M. Lenz, M. Delamar, C.A. Ferreira, Journal of Electroanalytical Chemistry, 540 (2003) 35-44.

[32] D.M. Lenz, M. Delamar, C.A. Ferreira, Progress in Organic Coatings, 58 (2007) 64-69.

[33] P. Herrasti, P. Ocón, Applied Surface Science, 172 (2001) 276-284.

[34] Y.-T. Kim, W.-S. Kim, H.-W. Rhee, M.-K. Song, Molecular Crystals and Liquid Crystals, 445 (2006) 193/[483]-200/[490].

[35] U. Riaz, S.M. Ashraf, S. Ahmad, Progress in Organic Coatings, 59 (2007) 138-145.

[36] E. Armelin, R. Pla, F. Liesa, X. Ramis, J.I. Iribarren, C. Alemán, Corrosion Science, 50 (2008) 721-728.

[37] D.E. Tallman, K.L. Levine, C. Siripirom, V.G. Gelling, G.P. Bierwagen, S.G. Croll, Applied Surface Science, 254 (2008) 5452-5459.

[38] A. Gergely, É. Pfeifer, I. Bertóti, T. Török, E. Kálmán, Corrosion Science, 53 (2011) 3486-3499.

[39] M.G. Hosseini, M. Raghibi-Boroujeni, I. Ahadzadeh, R. Najjar, M.S. Seyed Dorraji, Progress in Organic Coatings, 66 (2009) 321-327.

[40] M. Selvaraj, S. Palraj, K. Maruthan, G. Rajagopal, G. Venkatachari, Journal of Applied Polymer Science, 116 (2010) 1524-1537.

[41] M.G. Hosseini, R. Bagheri, R. Najjar, Journal of Applied Polymer Science, 121 (2011) 3159-3166.

[42] M. Ioniţă, A. Prună, Progress in Organic Coatings, 72 (2011) 647-652.

[43] M.R. Mahmoudian, W.J. Basirun, Y. Alias, M. Ebadi, Applied Surface Science, 257 (2011) 8317-8325.

[44] M.R. Mahmoudian, W.J. Basirun, Y. Alias, Progress in Organic Coatings, 71 (2011) 56-64.

[45] M.R. Mahmoudian, W.J. Basirun, Y. Alias, Applied Surface Science, 257 (2011) 3702-3708.

[46] C. Yang, W.H. Smyrl, E.L. Cussler, Journal of Membrane Science, 231 (2004) 1-12.

[47] M. Rizzi, M. Trueba, S.P. Trasatti, Synthetic Metals, 161 (2011) 23-31.

[48] M. Yan, C.A. Vetter, V.J. Gelling, Electrochimica Acta, 55 (2010) 5576-5583.

[49] H. Nguyen Thi Le, B. Garcia, C. Deslouis, Q. Le Xuan, Electrochimica Acta, 46 (2001) 4259-4272.

[50] M. Kendig, M. Hon, L. Warren, Progress in Organic Coatings, 47 (2003) 183-189.

[51] H. Nguyen Thi Le, B. Garcia, C. Deslouis, Q. Le Xuan, Journal of Applied Electrochemistry, 32 (2002) 105-110.

[52] K. Qi, Y. Qiu, Z. Chen, X. Guo, Corrosion Science, 60 (2012) 50-58.

[53] T. Zhang, C.L. Zeng, Electrochimica Acta, 50 (2005) 4721-4727.

[54] E. Hür, G. Bereket, Y. Şahin, Materials Chemistry and Physics, 100 (2006) 19-25.

[55] V. Brânzoi, L. Pilan, F. Golgovici, F. Brânzoi, Molecular Crystals and Liquid Crystals, 446 (2006) 305-318.

[56] K.R.L. Castagno, V. Dalmoro, D.S. Azambuja, Materials Chemistry and Physics, 130 (2011) 721-726.

[57] A.C. Balaskas, I.A. Kartsonakis, G. Kordas, A.M. Cabral, P.J. Morais, Progress in Organic Coatings, 71 (2011) 181-187.

[58] V. Annibaldi, A.D. Rooney, C.B. Breslin, Corrosion Science, 59 (2012) 179-185.

[59] U. Rammelt, L. Duc, W. Plieth, Journal of Applied Electrochemistry, 35 (2005) 1225-1230.

[60] G. Paliwoda-Porebska, M. Stratmann, M. Rohwerder, K. Potje-Kamloth, Y. Lu, A.Z. Pich, H.J. Adler, Corrosion Science, 47 (2005) 3216-3233.

[61] J. Bonastre, P. Garcés, J.C. Galván, F. Cases, Progress in Organic Coatings, 66 (2009) 235-241.

[62] M.G. Hosseini, M. Sabouri, T. Shahrabi, Journal of Applied Polymer Science, 110 (2008) 2733-2741.

[63] M. Sabouri, T. Shahrabi, H.R. Faridi, M. Salasi, Corrosion Engineering, Science and Technology, 44 (2009) 51-56.

[64] A. Mollahosseini, E. Noroozian, Synthetic Metals, 159 (2009) 1247-1254.

[65] M.G. Hosseini, M. Sabouri, T. Shahrabi, Materials and Corrosion, 57 (2006) 407-410.

[66] M.G. Hosseini, M. Sabouri, T. Shahrabi, Progress in Organic Coatings, 60 (2007) 178-185.

[67] D. Kowalski, M. Ueda, T. Ohtsuka, Corrosion Science, 49 (2007) 3442-3452.

[68] L. Koene, W.J. Hamer, J.H.W. de Wit, Journal of Applied Electrochemistry, 36 (2006) 545-556.

[69] W. Prissanaroon, N. Brack, P.J. Pigram, J. Liesegang, Surface Review and Letters, 13 (2006) 319-327.

[70] I.L. Lehr, S.B. Saidman, Electrochimica Acta, 51 (2006) 3249-3255.

CHAPTER 2. THE EFFECT OF POLYMER MORPHOLOGY ON THE PERFORMANCE OF A CORROSION INHIBITING POLYPYRROLE/ALUMINUM FLAKE COMPOSITE PIGMENT

(Accepted for publication in Electrochimica Acta

http://dx.doi.org/10.1016/j.electacta.2013.03.128)

2.1. Abstract

Two different morphologies of polypyrrole (PPy) aluminum flake composites, namely spherical PPy/Al flake composites and wire PPy/Al flake composites, were synthesized by chemical oxidative polymerization. These composites were characterized by Fourier transform infrared spectroscopy (FT-IR), four point probe conductivity, conductive atomic force microscopy (C-AFM), scanning electron microscopy (SEM), and X-ray photoelectron spectroscopy (XPS). These composites were incorporated into an epoxy primer and coatings were applied on an aluminum alloy (AA 2024-T3) substrate. The coatings were exposed to salt spray according to ASTM B117 and prohesion conditions according to ASTM G85-A5. The corrosion resistance properties were monitored via electrochemical impedance spectroscopy (EIS). The current produced by corrosion reactions on the surface of the substrate was mapped using the scanning vibrating electrode technique (SVET). Galvanic coupling experiments were performed for measurement of galvanic current and mixed potential in controlled environment. It was observed that the morphology of PPy on the surface of aluminum flake has an effect on the conductivity and anticorrosion performance of the pigment. The wire PPy/Al flake composite coatings exhibited better anticorrosion performance than the spherical PPy/Al flake composite coatings and as received aluminum flake coatings. The enhancement in anticorrosion performance was attributed to the unique morphology and electrochemical activity of the PPy on

the surface of aluminum flakes. It was also revealed that the wire PPy/Al flake composite coating was sacrificially protecting the AA 2024-T3 substrate in larger defects.

2.2. Introduction

The protection of assets from corrosion remains as challenging as ever before. Metals and their alloys are the backbone of human civilizations and their protection from corrosion remains an area of high interest to materials scientists. Due to changes in environmental conditions in the 21st century, the commonly used methods for protection are not always sufficient for multipurpose protection. Organic coatings are the most widely used method of corrosion mitigation. Coatings typically protect either by barrier, sacrificial or by inhibitor release mechanisms [1]. Barrier protection by coatings is only effective as long as the coating remains intact and defect free. Once a defect has been introduced into a barrier coating, due to exposure to corrosive conditions, it leads to diffusion of corrosive ions through the coating. At this point, delamination at the metal/coating interface occurs and a barrier coating ceases to perform its protective function [2]. Sacrificial protection in the case of zinc rich primers requires a high pigment volume concentration (PVC) of zinc for the coating to offer protection to the substrate. Such high PVCs often decrease the flexibility of the primer which limits its application to substrates that do not undergo large strains [3]. Many of the corrosion inhibitors released by coatings are toxic in nature. For example, one of the most effective corrosion inhibitors, hexavalent chromate, is carcinogenic and mutagenic in parts per million concentrations [4]. One solution to the some of the problems associated with traditional corrosion prevention strategies may be conducting polymers (CPs) such as polypyrrole. Due to their redox activity, CPs are able to actively inhibit corrosion once barrier protection has been compromised. Additionally, CPs do not possess the toxicity of other corrosion inhibitors such as hexavalent chromates.

CPs are used in various applications including batteries [5], sensors [6], electromagnetic interference shielding [7], drug delivery [8], corrosion inhibition [9], actuators [10], solar cells [11], light emitting diodes [12], and printing electronic circuits [13]. CPs possess properties such as electrical conductivity, low toxicity, simplistic synthesis procedure, ease of doping by both chemical and electrochemical polymerization, good environmental stability, eco-friendly nature, and excellent thermal stability [14-16]. Polyaniline, polypyrrole (PPy), and polythiophene are the most commonly used CPs for corrosion inhibition [17-25]. Amongst these, PPy seems to be promising due to its facile synthesis, good environmental stability, and high conductivity [26].

Several mechanisms have been proposed to account for the corrosion inhibition by CPs on active metal substrates [27]. One proposed mechanism involves the formation of a passive layer. Most commonly, CPs must be oxidized in order to be conductive, and this is the form in which they are often applied to metal substrates. When in an oxidized state, the electroactive nature of CPs allows them to be fairly strong oxidizing agents which can oxidize the underlying substrate, thereby forming and maintaining a passive oxide layer at the interface between the CP and metal substrate [28]. CPs have also been shown to protect ferrous substrates via anodic protection. Due to their positive open circuit potentials and electroactive nature, CPs are able to form an electrochemical couple with the underlying metal substrate. A mixed potential then establishes between the CP coating and the metal substrate that maintains the potential of the metal substrate at a more positive potential in the passive region of the metal, leading to reduced corrosion rates [29]. CPs can also serve as a store house for corrosion inhibiting anions that can be released on demand to inhibit corrosion. This mechanism is proposed for CPs that are in an oxidized state which have a positive charge associated with them. Counter anions are then incorporated onto the polymer backbone to achieve charge neutrality. The electrons produced by

a corroding substrate will then reduce the CPs to a neutral state. The negatively charged counter ions (corrosion inhibiting anions) are then expelled from the CP, thereby protecting the metal from corrosion. Proper conditions are needed for these mechanisms to realize their effects [30]. If the proper conditions are not present, CPs can, in some circumstances, actually accelerate corrosion. One example of this would be that CPs can act as an electrochemical mediator between the metal and O_2 resulting in severe, accelerated corrosion. This happens when passivation is not maintained in some conditions such as in the presence of large defects.

There are some disadvantages associated with the application of CPs. In the case of PPy, a lack of solubility in common solvents makes the processing and application of PPy difficult. Its porous nature and moderate to poor adhesion also pose problems towards its application as a coating. The possibility of the consumption of stored charges due to redox reactions inherent in PPy and its ion exchange properties can also cause a loss of its anticorrosion function [31, 32]. In order to overcome these disadvantages, several approaches have been tried including copolymers of CPs, derivatives of CPs, and various multilayers of CPs. Another approach is to use a CP primer with a conventional topcoat [34, 35]. The technique of adding small amounts of CPs as anticorrosive additives is also used [36-38]. CPs blended with conventional polymer coating is another avenue for their use [39].

CPs can be used as primers alone by electrochemical deposition on to a metal substrate. In electrochemical polymerization of CPs, dissolution of the working electrode due to anodic polarization must be controlled by using proper electrochemical deposition conditions [33]. The electrochemical polymerization method has limitations in terms of the bulk synthesis of CPs. Chemical oxidation methods can be more easily used for the large scale synthesis of CPs.

Conducting polymer containing composite (CPCC) coating is another method to alleviate the problems associated with the successful application of CPs in coatings for corrosion protection. A polyaniline-TiO_2 composite was studied on steel for its ability to protect against corrosion [40, 41]. In this case, the passivation of steel by polyaniline resulted in improved anticorrosion performance. Several studies have been performed to synthesize and evaluate CPCCs for the corrosion protection of metals and their alloys [42, 43].

The deposition of CPs onto inorganic flakes serves several purposes. The flakes can impart some barrier protection to the substrate which compensates for the porous nature of the conducting polymer. In our group, we have deposited PPy on the surface of aluminum flakes via chemical oxidation of pyrrole to form a PPy/Al flake composite pigment [30, 44]. By controlling synthesis parameters, different morphologies can be obtained on the surface of aluminum flakes.

In the present work, two different morphologies of PPy (spherical and wire) were obtained on the surface of aluminum flakes. Resultant composites were characterized for their morphology, chemical and elemental composition, and conductivity. Using these composites and as received aluminum flakes, coatings were prepared with an epoxy binder and applied on AA 2024-T3 substrate. The anticorrosive properties of the composite coatings were evaluated by electrochemical methods (EIS, galvanic coupling, and SVET) and salt spray, prohesion exposure via ASTM methods B117 and G85-A5.

2.3. Experimental work

2.3.1. Materials

Aluminum flakes (Stapa® Aloxal® PM 2010) were provided by Eckart America. The chemical composition of as received aluminum flakes was 39% aluminum, 26% aluminum oxide, and 35% 1-methoxy-2-propanol. For the synthesis, pyrrole monomer and 1-methoxy-2-

propanol were procured from Alfa Aesar Co. Ammonium Persulfate (APS) was purchased from BDH. Aluminum alloy AA 2024-T3 panels (dimensions-0.063”x6”x3”) were obtained from Q-Panel Lab Products. EPON 830 and Epikure 3015 were supplied by Momentive Specialty Chemicals Inc. Methyl isobutyl ketone (MIBK) was purchased from Aqua solutions. Pyrrole monomer was distilled prior to its use in the synthesis. All other chemicals were used as received without further purification. In this synthesis, 18.2 MΩ Millipore® water was used.

2.3.2. Synthesis procedure of the wire PPy/Al flake composite and the spherical PPy/Al flake composite

To synthesize the wire PPy/Al flake composite, 1000 ml of Millipore® water was added into an Erlenmeyer flask. This was followed by the addition of 30 grams of as received aluminum flake. After complete dispersion of the flakes, 22.8 grams of APS was added. After the APS was completely dissolved, 13.9 ml of pyrrole was added. The reaction was performed at ambient temperature and was continued for 24 hours. After 24 hours, the coated flakes were separated from the reaction mixture via vacuum filtration and were washed with Millipore® water until the filtrate was colorless.

This product was maintained overnight in an oven at 60°C for drying. After drying, it was ground using a mortar and pestle to obtain a fine pigment powder. Finally, the resultant material was sieved through a sieve with a 106 µm opening diameter to obtain a fine powder. For the synthesis of the spherical PPy/Al flake composite, 500 ml of Millipore® water and 500 ml of 1-methoxy-2-propanol were initially added to an Erlenmeyer flask. The other materials and procedures were the same as mentioned for the synthesis of the wire PPy/Al flake composite.

2.3.3. Coatings preparation

Prior to use, AA 2024-T3 panels were sandblasted with 100 µm alumina grit and then degreased thoroughly with hexanes. The composite pigment was added in the required quantity to the EPON 830 and then the cross linker (Epikure 3015) was added in a stoichiometric ratio of 1:1. The coatings were prepared at 20% PVC for the wire PPy/Al flake composite, spherical PPy/Al flake composite, and as received aluminum flakes. These are bi-component coatings with epoxy resin, hardener, and pigment without any additives. The coatings were allowed to cure at room temperature for a week in order to have full development of the mechanical and barrier properties of the coating.

2.3.4. Instrumentation

To investigate the morphology of the samples, A JEOL JSM-6490LV scanning electron microscope (SEM) was used. The sample preparation was performed by sprinkling ground powder onto carbon tape attached to aluminum mounts. To determine the elemental composition of the samples, X-ray photoelectron spectroscopy (XPS) measurements were performed on an SSX-100 system (Surface Science Instruments) equipped with a monochromatic Al K_α X-ray source, a hemispherical sector analyzer (HSA), and a resistive anode detector. The base pressure of the XPS system was 1.0×10^{-9} Torr. During the data collection, the pressure applied was *ca.* 1×10^{-8} Torr. The size of the X-ray spot was 1x1 mm^2, which correlated to an X-ray power of 200 W. Each survey spectrum was collected with 16 scans at 150 eV pass energy and 1 eV/step. The atomic percentages were calculated using the ESCA 2005 software provided with the XPS system. Fourier transform infrared spectroscopy (FT-IR) measurements were performed on a NICOLET 8700 spectrophotometer from Thermo Scientific. The data of FT-IT was collected in transmittance mode.

Conductive Atomic Force Microscopy **(**C-AFM) studies were performed using a Veeco Dimension 3100 atomic force microscope in contact mode and a current sensing probe to obtain the surface morphology and surface current density. A four-point probe instrument consisting of a Keithley®2000 multimeter, a Keithley® 220 programmable current source, and Signatone® probes was employed to measure conductivity.

Electrochemical Impedance spectroscopy (EIS) studies were performed using Gamry Reference 600 Potentiostats with Gamry Framework Version 5.58/EIS 300 software. Dilute Harrison's solution (DHS, 0.35% ammonium sulfate and 0.05% sodium chloride) was used as an electrolyte and the measurements were carried in triplicates. A three electrode assembly was used with a saturated calomel reference electrode, platinum mesh counter electrode, and coated substrate as a working electrode. The frequency range for the measurements was 100,000-0.01Hz, collecting 10 points/decade using 10 mV RMS of AC perturbation potential.

Scanning vibrating electrode technique (SVET) measurements were performed using instruments from Applicable Electronics, Inc. Microprobe, Inc. supplied vibrating probes which were Pt-Ir microelectrodes with platinum black deposited on their tips. The Quasi-reference electrode was a platinum wire coated with platinum black. SVET measurements were carried out in DHS solution in duplicate and representative samples are demonstrated here. An artificial defect was made through the coatings with a razor blade and the measurement area was masked off with tape. This scribed sample was immersed in DHS in a petri dish and the vibrating probe was brought as close as 100 μm to the surface. This distance was measured using the optic system on the SVET instrument. The SVET results were graphed in Origin software as current density maps where cathodic and anodic activity over the scanned area was displayed as a function of position in the X and Y directions in the space.

Galvanic coupling experiments were performed by employing the experimental setup described elsewhere [30]. It is two compartment enclosed cell with one compartment of bare aluminum 2024-T3 as a working electrode and second compartment with coated metal as another working electrode. The compartment with bare aluminum 2024-T3 was bubbled with air while compartment with coated metal was bubbled with nitrogen. For both the compartments, working areas were 1 cm^2 each, yielding area ratio of 1. Gamry Reference 600 Potentiostats were employed for the measurement of coupling current and mixed potential between coated metal and bare aluminum 2024-T3. A galvanic corrosion technique was employed using potentiostat in zero resistance ammeter (ZRA) mode with DHS as an electrolyte in both the compartments.

2.3.5. Accelerated corrosion tests

Coatings were exposed to salt spray test (ASTM B117) and to the prohesion test (ASTM G85-A5) for 120 days. In ASTM B117, 5% sodium chloride solution is continuously sprayed over coatings at 35°C at 100% relative humidity. In ASTM G85-A5, DHS mist is sprayed for an hour at 25˚C followed by an hour of a dry stage at 35°C.

2.3.6. Pull-off adhesion test

Pull-off adhesion tests were performed on coated samples of as received Al flake coating, wire PPy/Al flake composite coatings, and spherical PPy/Al flake composite coatings. Minimum of six measurements were performed by employing PosiTest® Pull-Off Adhesion Tester with dolly size 14 mm glued to substrate with Hysol® epoxy two-component adhesive. Pull-off adhesion tests were performed according to ASTM 4541.

2.4. Results and discussions

2.4.1. Scanning electron microscopy (SEM)

Microscopic morphology investigations of the prepared composites were performed using SEM. The morphology of the as received aluminum flakes, as shown in Figure 1.1, appeared fairly smooth. In the preparation of CPs, synthesis parameters such as the dopant anion, pH of the solution, temperature of reaction, method of synthesis, and nature of solvent can affect the final morphology of CPs [45-50]. The surface morphology of CPs plays an important role in their electrochemical responses and doping-undoping behavior [51]. By modifying the synthesis parameters, unusual microstructures of PPy were obtained on the surface of the AA 2024-T3 [52].

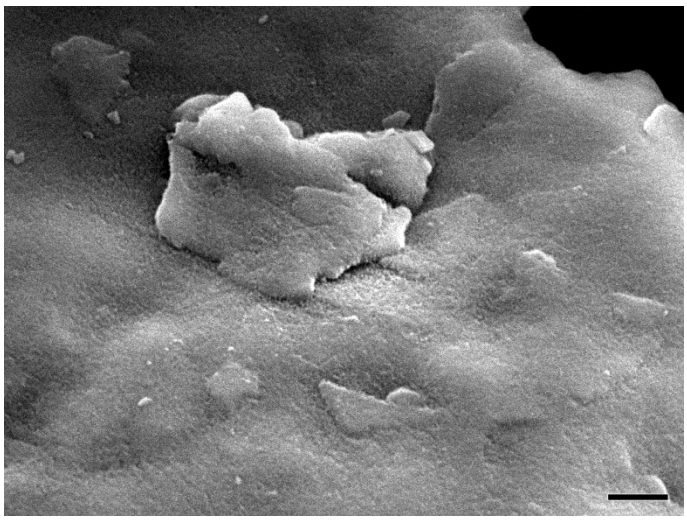

Figure 2.1: SEM micrographs of as received Al flake (scale bar =1µm).

In current study, a partial amount of the reaction solvent (50% water) was replaced with another solvent (50% 1-methoxy-2-propanol). With 100% water in the synthesis, wires like structures of PPy along with spherical PPy particles were observed on the surface of the aluminum flakes as shown in Figure 2.2(A and C). This structure will be treated as the wire PPy/Al flake composite throughout this paper. With 50% 1-methoxy-2-propanol and 50 % water

in the synthesis, regular and spherical structures of PPy were formed on the surface of the aluminum flake which covers the entire flake surface as shown in Figure 2.2(B and D). As observed in the higher magnification micrograph of wire PPy/Al flake composite and of spherical PPy/Al flake composite, the PPy wire diameter observed through SEM was *ca.* 200-300 nm (Figure 2.3(A)) and the diameter of PPy spheres was *ca*. 100-200 nm (Figure 2.3(B)).

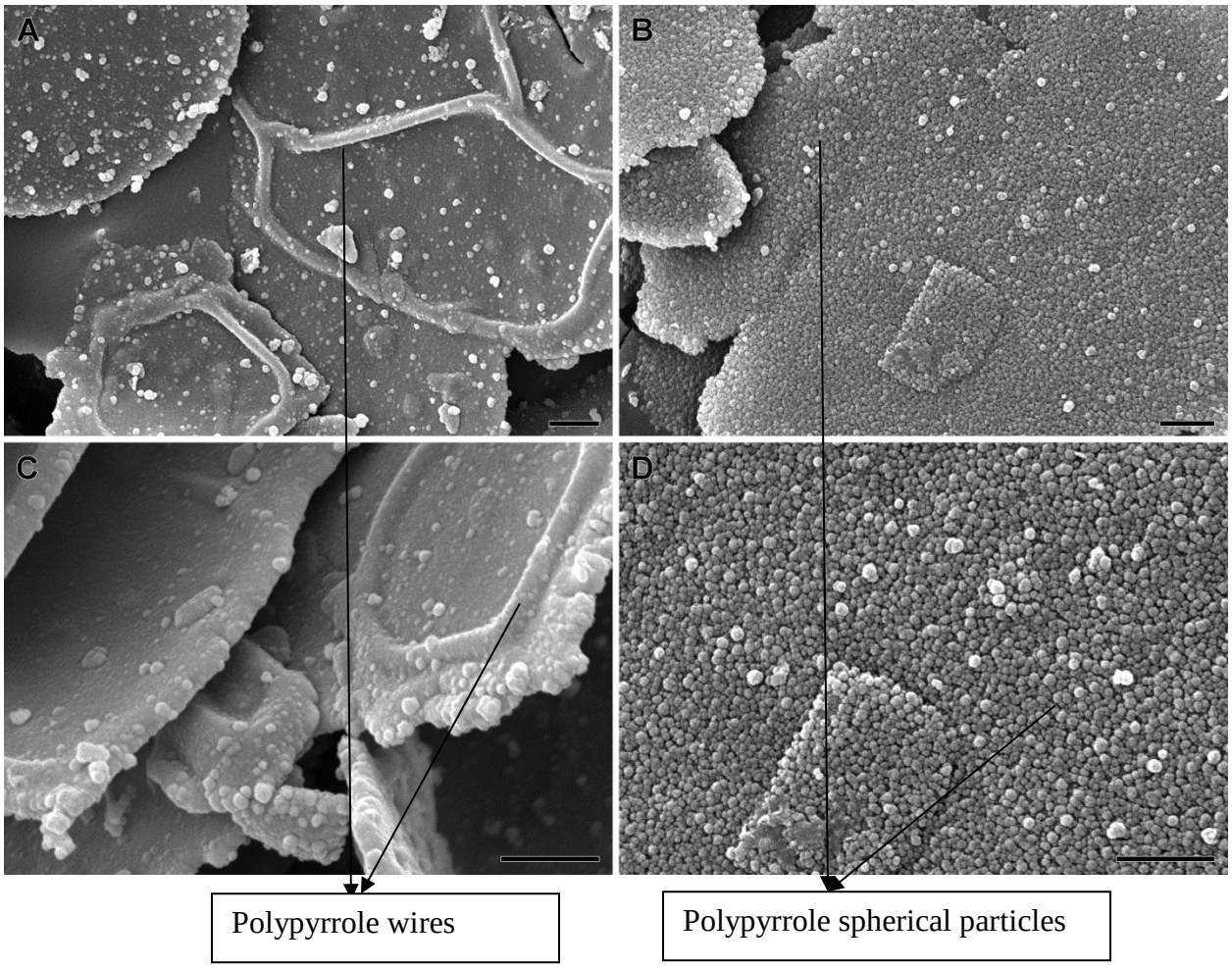

Figure 2.2: SEM micrographs of wire PPy/Al flake (images A and C), and spherical PPy/Al flake (images B and D) (scale bar =2µm).

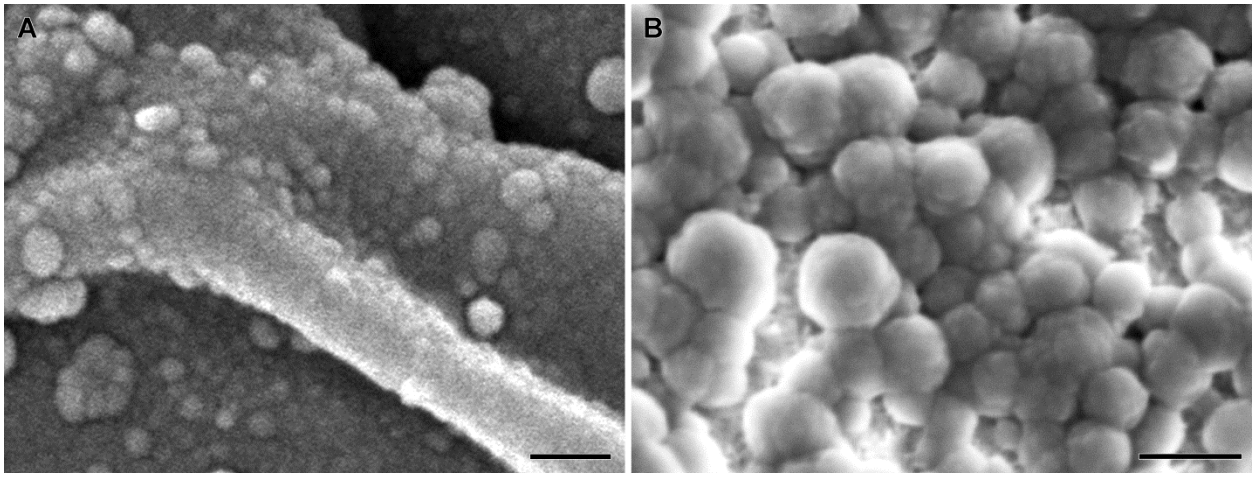

Figure 2.3: SEM micrographs for wire PPy/Al flake (image A) and spherical PPy/Al flake (image B) (scale bar =200 nm).

The structures of PPy are characteristic of the solvent used in the synthesis [48]. By changing the synthesis parameters and procedure, it is possible to prepare nanometer sized PPy [56]. The PPy was likely able to maintain its structure after solvent washing and grinding in a mortar and pestle due to its stiff, inflexible chains and insoluble nature in commonly used solvents [53]. Changes in the surface morphology due to different solvents can be influenced by the concentration and type of solvent present in the reaction mixture [46, 47]. The combination of organic solvents and water has been shown to lead to thicker and denser films of CPs [54]. The polarity and the hydrophilicity of the reaction media influence the rate of polymerization and the size of polymer particles formed. The water and 1-methoxy-2-propanol mixture is less polar and more hydrophobic than pure water, resulting in a decreased rate of polymerization and increased particle size [55]. A decrease in the rate of polymerization allows enough time for the nucleation and growth of PPy particles. This may be the factor responsible for the spherical and dense morphology of PPy on the surface of the aluminum flakes.

2.4.2. Fourier transform infrared spectroscopy (FT-IR)

Figure 2.4 represents the FT-IR spectra of pure PPy, as received aluminum flakes, the wire PPy/Al flake composite, and the spherical PPy/Al flake composite. As received flakes were composed of aluminum, aluminum oxide, and 1-methoxy-2-propanol. In the as received aluminum flake spectra, a Al-O stretching vibration was observed at 750-490 cm^{-1}[57]. Weak, variable, symmetric C-O-C stretching was observed at 1040-820 cm^{-1} and very strong asymmetric C-O-C stretching was observed at 1150-1060 cm^{-1} due to the presence of 1-methoxy-2-propanol [57]. Variable OH stretching was seen at 3428 cm^{-1}, which signified the hydroxyl groups on the aluminum flake surface due to 1-methoxy-2-propanol [58]. The strong OH band was also evident at 1400 cm^{-1}, which was attributed to aluminum oxide [59].

In the case of pure PPy, the peak at 1558 cm^{-1} represented ring stretching vibrations of C-C and C=C bonds, whereas the band at 1476 cm^{-1} signified a combination of C-N and C=C stretching modes [60]. At 1292 cm^{-1}, C-H and C-N in plane deformations were identified [60]. In pure PPy, the 1046 cm^{-1} band showed C-H deformation. The characteristic bands of PPy were observed at 917 cm^{-1} due to ring breathing and at 789 cm^{-1} due to C–H ring out-of-plane bending mode [61, 62]. Stretching vibrations of 3446-3340 cm^{-1} were absent in pure PPy which was consistent with work performed by other researchers [60, 63]. N-H out of plane vibration at 616 cm^{-1} overlapped with that of the sulfate anion [63].

In the cases of both the wire structures and the spherical structures of PPy on the aluminum flake surface, combinations of bands due to PPy and as received aluminum flakes were observed. The FT-IR spectra of the wire PPy/Al flake composite and spherical PPy/Al flake composite did not show significant differences. Ring stretching vibrations of C-C and C=C bands were observed at 1566 cm^{-1} in the wire PPy/Al flake composite and at 1573 cm^{-1} in the

spherical PPy/Al flake composite. C-N and C=C stretching modes were observed at 1465 cm^{-1} in the wire PPy/Al flake composite whereas it was seen at 1447 cm^{-1} in the spherical structured PPy on aluminum flakes. OH stretching at 3431 cm^{-1} in the wire structured PPy and at 3425 cm^{-1} in the spherical PPy/Al flake composite was observed. This signified aluminum oxide was present with aluminum flakes on its surface. It can be concluded from the FT-IR results that the PPy was deposited on the surface of aluminum flakes.

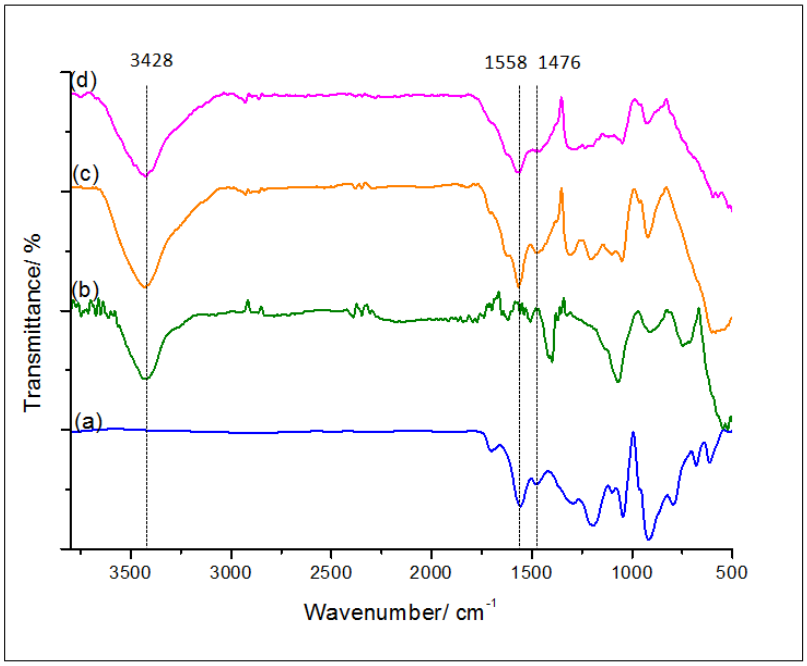

Figure 2.4: FTIR spectrum of (a) PPy, (b) as received Al flakes, (c) wire PPy/Al flake composite, and (d) spherical PPy/Al flake composite.

2.4.3. X-ray photoelectron spectroscopy (XPS)

The elemental compositions of the as received Al flake, the wire PPy/Al flake composite, and the spherical PPy/Al flake composite were obtained by XPS and are shown in Figure 2.5. As received Al flake contained 39% aluminum, 26% aluminum oxide, and 35% 1-methoxy-2-propanol. This accounted for the presence of large quantities of aluminum on surfaces along with organic matter contributed from 1-methoxy-2-propanol. Phosphorous and little amount of

nitrogen was also observed due to the presence of trace quantities of proprietary phosphonic acid and undisclosed additive on the as received aluminum flakes. In the case of the wire PPy/Al flake composite and spherical PPy/Al flake composite, higher nitrogen concentrations were observed on their surfaces. This was due to the formation of PPy on the surface of aluminum flakes. The presence of sulfate ions in the wire PPy/Al flake composite and spherical PPy/Al flake composite indicated sulfate anion incorporation in the PPy chains as dopant counter ions. The ratio of S/N in the case of the wire structured PPy was 0.1 and in the case of the spherical PPy was 0.132 which indicated a low level of doping of sulphate anions [64]. The presence of very low concentrations of aluminum on the wire PPy/Al flake composite and spherical PPy/Al flake composite indicated extensive coverage of the aluminum flakes by PPy.

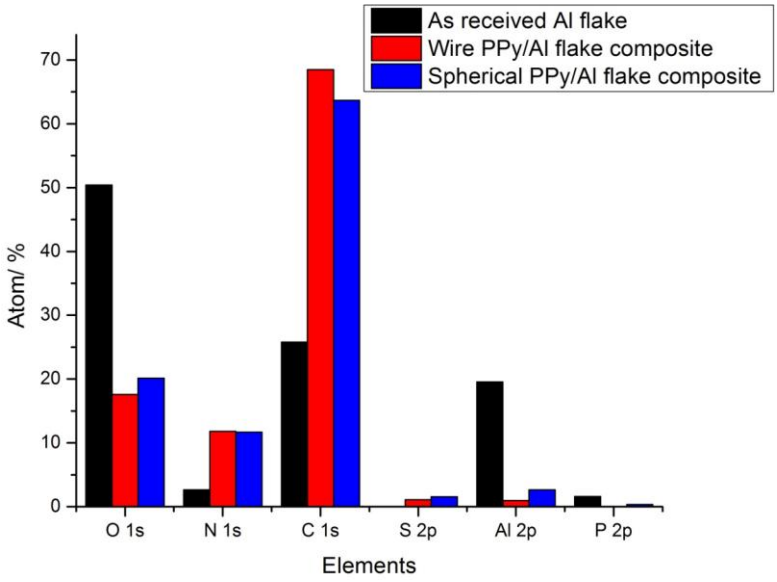

Figure 2.5: Elemental composition results obtained by XPS.

For the composite pigments consisting of PPy and aluminum flakes, high resolution spectra of the N 1s was obtained for the wire PPy/Al flake composite as shown in Figure 6(a). The peak for the N 1s at 400 eV was split into two distinct high intensity peaks at 400 eV and 401 eV. One small intensity peak was also observed at 402.6 eV. The peak at 400 eV was due to

the presence of neutral amine nitrogens (-NH-). The peaks at 401 and 402.6 eV were due to the presence of positively charged amine species of N^{+} and N^{2+} respectively [65-69]. The very small peak around 398 eV is suggestive of an imine (-N-R).

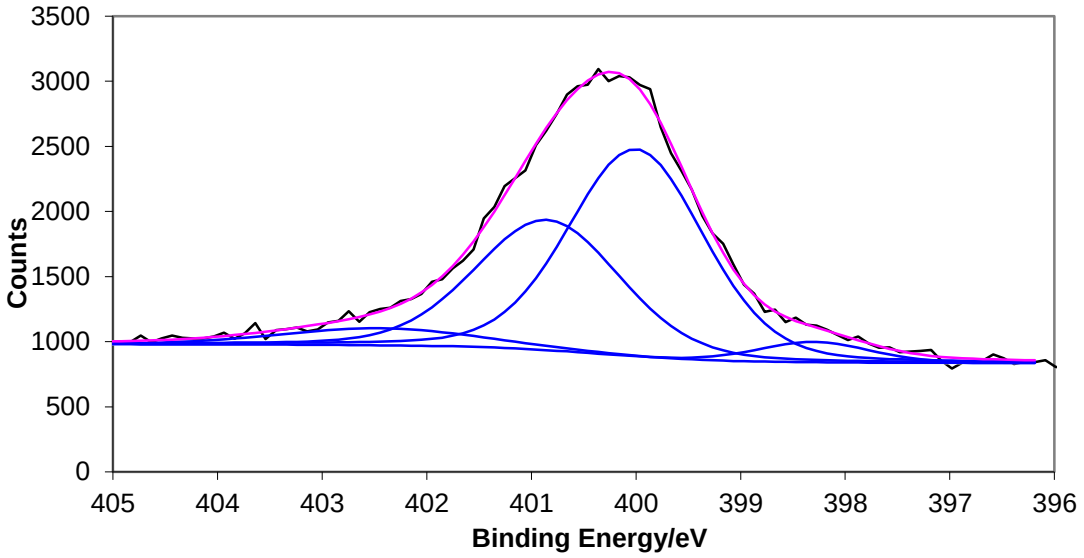

Figure 2.6 (a): High resolution spectra for N 1s obtained by XPS for wire PPy/Al flake composite.

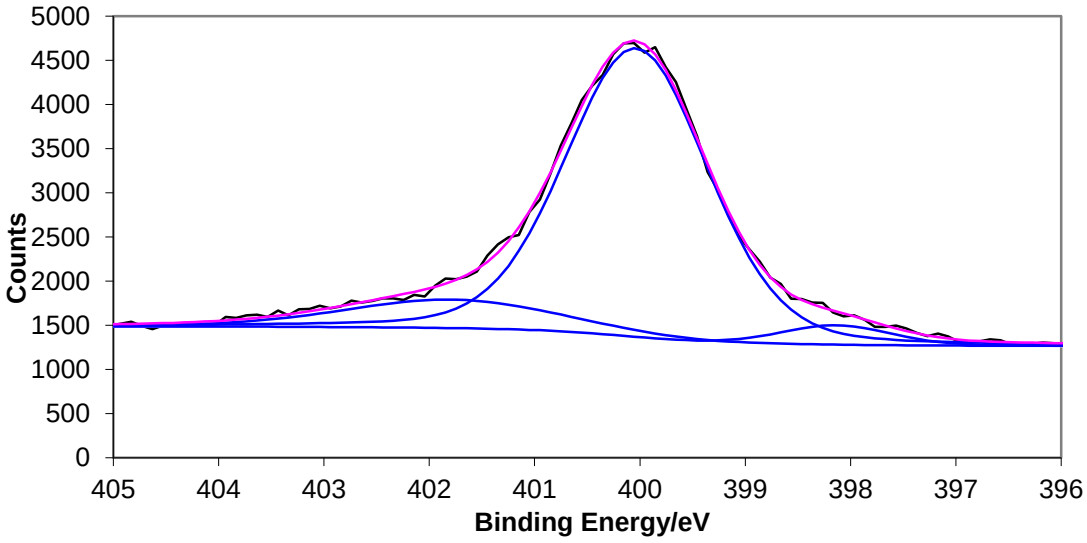

Figure 2.6 (b): High resolution spectra for N 1s obtained by XPS for spherical PPy/Al flake composite.

The high resolution spectrum of the N 1s for the spherical PPy/Al flake composite is shown in Figure 2.6(b). The major difference between the high resolution spectra for the N 1s orbital of the wire PPy/Al flake composite and the spherical PPy/Al flake composite is the absence of 401 eV peak due to positively charged amine N^+ in the spherical PPy/Al flake composite. This signified less conductivity in case of the spherical PPy/Al flake composite. The intensity of the N^+ peak is a good indicator of the conductivity of PPy which is dependent upon bipolaron formation during PPy synthesis. From the high resolution spectra obtained through XPS, it was evident that the PPy/Al flake composites obtained were conductive in nature.

2.4.4. Conductivity

The morphology and current flow through the composites were studied via C-AFM. The as received aluminum flakes exhibited no measurable current signals on a current density image (as shown in Figure 2.7(a)). In contrast, both the wire PPy/Al flake composite, and the spherical PPy/Al flake composite exhibited current on a current density image as shown in Figure 2.7(b) and Figure 2.7(c) respectively.

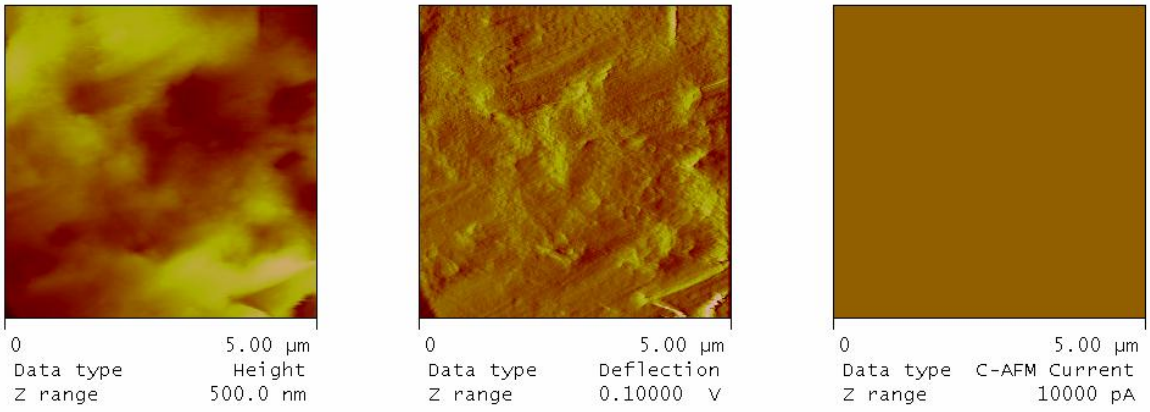

Figure 2.7 (a): Height, deflection and current image of as received aluminum flakes.

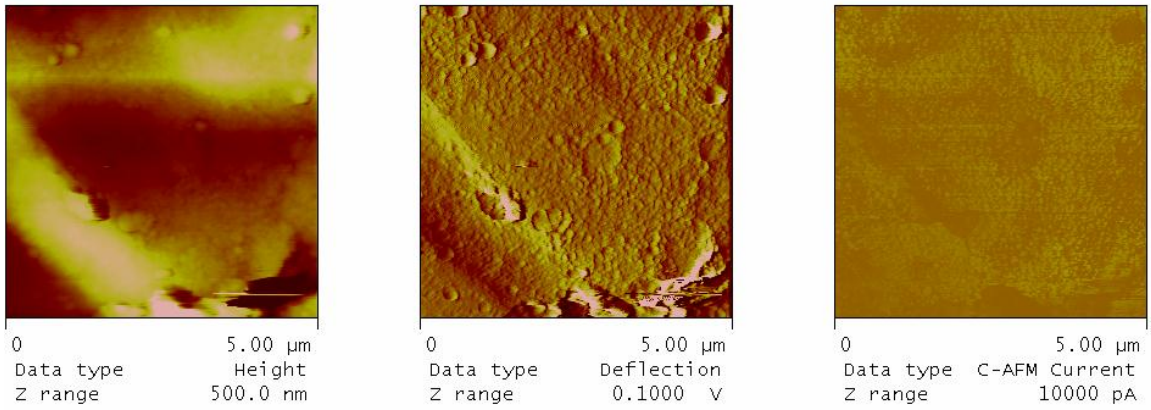

Figure 2.7 (b): Height, deflection and current image of wire structure of PPy on aluminum flakes.

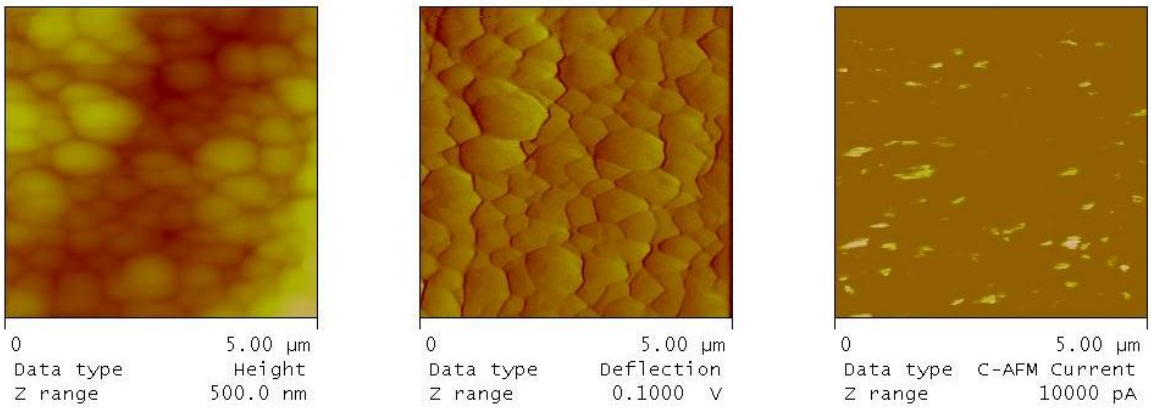

Figure 2.7 (c): Height, deflection and current image of spherical structure of PPy on aluminum flakes.

When conductivity was measured by the four point probe method, it was observed that the wire structured PPy on the aluminum flakes exhibited a conductivity value of 1.05 S/cm and the spherically structured PPy on the aluminum flake displayed a conductivity value of 0.1S/cm. This data is shown in Table 2.1.

Table 2.1
Conductivity measurements obtained using the four point probe technique

	Average conductivity (S/cm)	Standard Deviation
Wire PPy/Al flake composite	1.05	0.07
Spherical PPy/Al flake composite	0.1	0.01

This difference in conductivity was attributed to factors as described in the following discussion. The stacking of monomer units between polypyrrole chains determines the charge transfer properties between polypyrrole chains. This is dictated by the microscopic morphology which is responsible for the conducting properties of CPs [70]. A more ordered structure causes greater interaction between chains and therefore increases the macroscopic conductivity of the polymer. This morphology is dependent on the synthesis parameters including the solvents used in the synthesis [71].

The relationship between morphology, conductivity, and reaction conditions can be found by equation 2.1:

$$\sigma = ne\mu \tag{2.1}$$

Here, "n" is the density of charge carriers, "e" is electron charge, "σ" is conductivity, and "μ" is the mobility of charge carriers. As the conductivity value observed in the wire PPy was greater than that of the spherical PPy in the four point probe and the density of charge carriers was less (in XPS, S/N in the case of the wire structured PPy was 0.1 and in the case of the spherical PPy was 0.132), it can be concluded that the mobility of the charge carrier was greater in the case of the wire like structures due to their greater interconnectivity and interaction between polymer chains as observed in SEM and C-AFM [72, 73]. These results elucidate interdependence between morphology, conductivity, and reaction conditions. All other reaction conditions were constant in both synthesis of wire PPy and spherical PPy on aluminum surface except the variation in the solvent. This variation resulted in a change in morphology and conductivity.

2.4.5. Electrochemical impedance spectroscopy (EIS) and equivalent circuit modeling

AA 2024-T3 panels coated with an epoxy primer containing as received aluminum flakes, the wire PPy/Al flake composite, and the spherical PPy/Al flake composite at 20% PVC

were exposed to prohesion test conditions according to ASTM G 85-A5. EIS measurements were conducted initially and then on the exposed panels at 14 days, 28 days, 56 days, and 120 days using DHS as an electrolyte. Bode plots for the as received Al flake coating, the wire PPy/Al flake composite, and the spherical PPy/Al flake composite are represented in Figure 2.8(a), (b), and (c) respectively. Bode plots are the representation of impedance and phase angle with respect to the varied frequency. As observed in Figure 2.8(a), the low frequency (0.01Hz) impedance of the as received Al flake coating was initially between 10^5 and 10^6 ohms. As the duration of exposure increased, the low frequency impedance of the as received Al flake coating was observed to be decreasing to a value less than 10^5 ohms as seen in Figure 2.8(a). In the case of the wire PPy/Al flake coating and spherical PPy/Al flake coating, the initial low frequency impedance was approximately 10^5 ohms as shown in Figure 2.8(b) and Figure 2.8(c) respectively. As the duration of exposure to prohesion test conditions was increased, the coatings exhibited decrease in the low frequency impedance to approximately 10^4 ohms which is an order of magnitude less than the as received flake coatings.

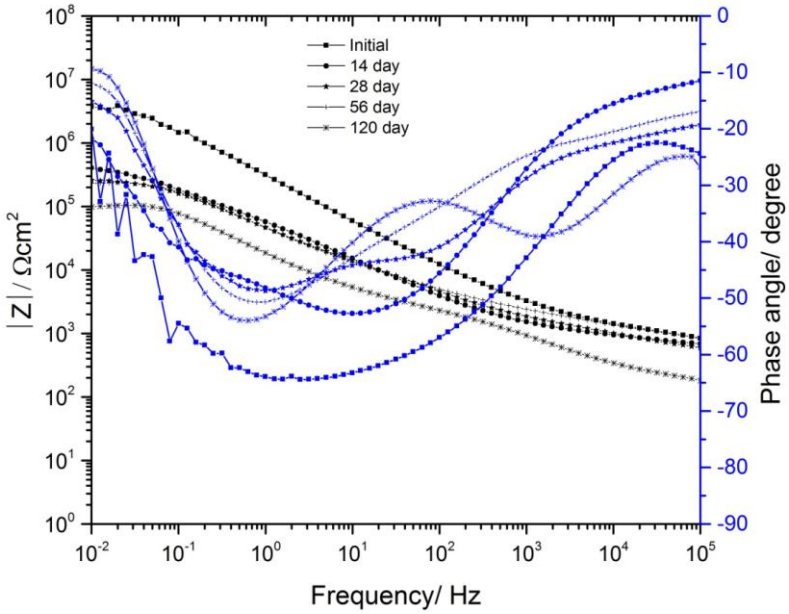

Figure 2.8 (a): Bode plot of as received Al flake coating.

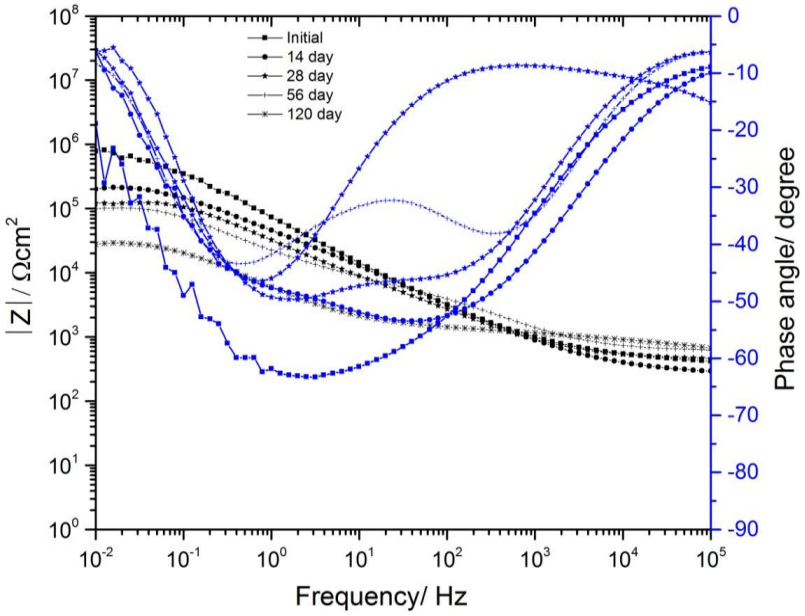

Figure 2.8 (b): Bode plot of wire PPy/Al flake composite coating.

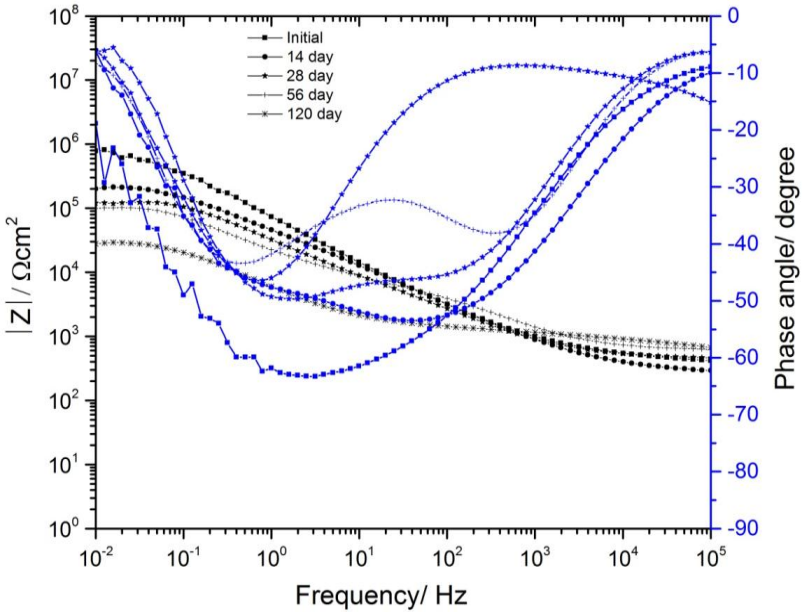

Figure 2.8 (c): Bode plot of spherical PPy/Al flake composite coating.

The decrease in the low frequency impedance can be attributed to the ingress of corrosive ions, resulting in the progressive loss of protective properties of the coating due to exposure to corrosion environment of prohesion test. This was true in case of as received Al flake coating. The impedance of both the wire PPy/Al flake coating and the spherical PPy/Al flake coating was

lower than that of as received Al flake coating owing to the conductive nature of PPy. The conducting ability of PPy forces AC current (as in EIS experiment) to take conducting pathways of PPy, thereby resulting in the decrease of impedance. This has been confirmed by earlier results [30]. A lower impedance value of coatings containing PPy does not imply that those are not protective in nature. Salt spray and prohesion exposure observations explained in later in this paper reaffirm this statement. As demonstrated by EIS results, the wire PPy/Al flake coating and the spherical PPy/Al flake coating appear not to act by barrier protection mechanism. Their redox active, conductive nature has caused another mechanism of protection to occur as evidenced by SVET and galvanic coupling measurements in following sections.

The EIS data was fitted to model circuits by using ZView 2 software (Scribner Associates Inc.). The equivalent circuit (Randles circuit model) provided in Figure 2.9(a) was used to model all the coatings except 120 hours exposure coatings of as received Al flake composite and spherical PPy/Al flake composite. In circuit modeling, R1 is the uncompensated solution resistance, R2 is the coating resistance, in this case it is pore resistance, and CPE is the constant phase element which represents pseudo capacitance and is presented by equation 2.2:

$$Z_{(CPE)} = 1/[(T)(j\omega)^{P}] \quad (2.2)$$

where, T is capacitance, j is an imaginary component, , ω is the angular frequency ($\omega = 2\pi f$, f is the frequency), P is the power ($0 \leq n \leq 1$), and $Z_{(CPE)}$ is the impedance of CPE.

Figure 2.9(b), represented the circuit modeling for 120 hours exposure coatings of as received Al flake composite and spherical PPy/Al flake composite. In this case R3 was polarization resistance and Cdl was the double layer capacitance. This is due to the appreance of second time constant. Circuit modeling results are shown in Table 2.2. It was observed that the actual data obtained from EIS experiments closely matches with that of results obtained from

equivalent circuit modeling. At 120 days of exposure, the as received Al flake coatings and the spherical PPy/Al flake coatings exhibited an order of lower magnitude of pore resistance than that of wire PPy/Al flake composites as observed in Table 2.2. Figure 2.9(c) represents an example of the fit for 120 days exposure coatings of as received Al flake composite.

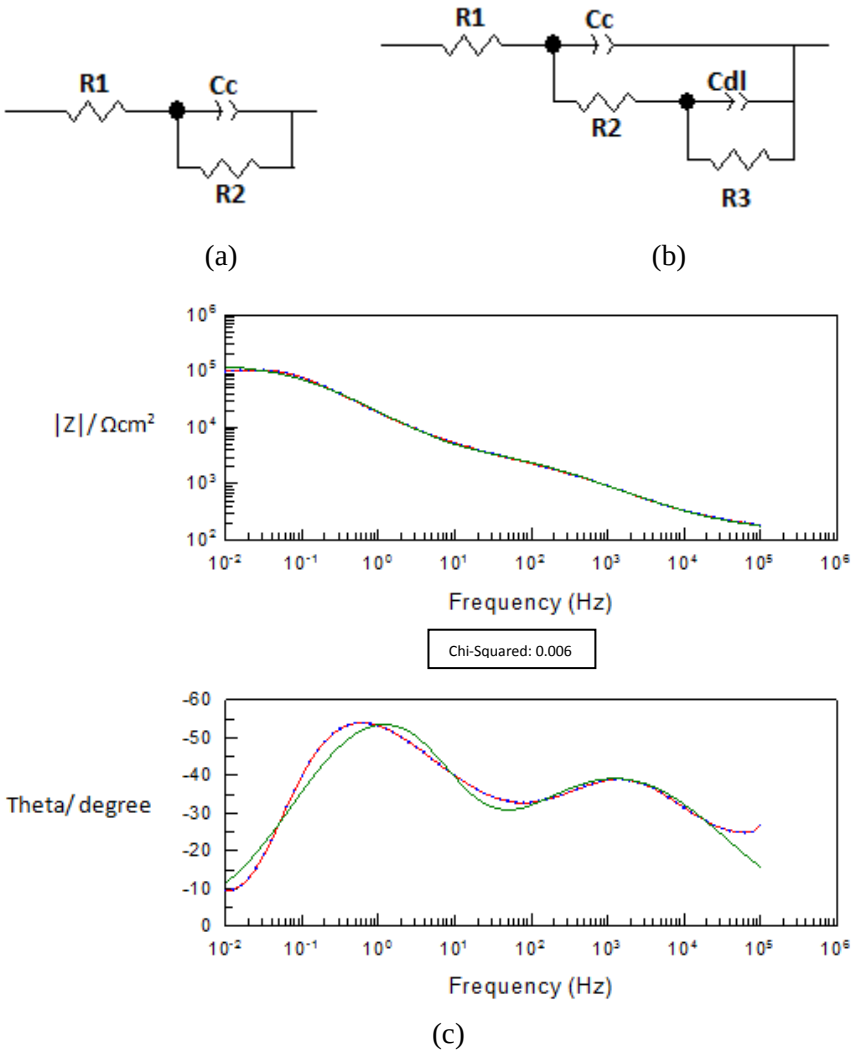

Figure 2.9: Equivalent Circuits Models (a) Randles cell, (b) Model for 120 days exposure coatings of as received Al flake composite and spherical PPy/Al flake composite, (c) Example of the fit for 120 days exposure coatings of as received Al flake composite (green curve is fit result and red curve is actual EIS data).

Table 2.2
Results of equivalent circuit modeling obtained from EIS data

Exposure duration/Days	R2/ Ωcm^2	CPE1		R3/ Ωcm^2	CPE2	
		Coating Capacitance/ Fcm^{-2}	P1		Double Layer Capacitance/ Fcm^{-2}	P2
	As received Al flake coating					
0	6.8 x 10^6	8.7 x 10^-7	0.70			
14	6.3 x 10^5	5.7 x 10^-6	0.60			
28	5.1 x 10^5	7.3 x 10^-6	0.54			
56	4.9 x 10^5	7.3 x 10^-6	0.53			
120	4.8 x 10^3	6.2 x 10^-6	0.59	1.3 x 10^5	7.5 x 10^-6	0.82
	Wire PPy/Al flake composite coating					
0	1.1 x 10^6	3.6 x 10^-6	0.70			
14	2.8 x 10^5	6.1 x 10^-6	0.62			
28	1.7 x 10^5	8.3 x 10^-6	0.61			
56	1.9 x 10^5	1.5 x 10^-5	0.48			
120	3.8 x 10^4	5.1 x 10^-5	0.62			
	Spherical PPy/Al flake composite coating					
0	4.8 x 10^5	2.3 x 10^-6	0.68			
14	3.6 x 10^5	5.9 x 10^-6	0.58			
28	2.9 x 10^5	5.9 x 10^-6	0.60			
56	3.2 x 10^5	8.5 x 10^-6	0.48			
120	5.2 x 10^3	2.9 x 10^-6	0.52	7.1 x 10^4	1.6 x 10^-5	0.72

2.4.6. Pull-off adhesion test

Force of 305 psi with standard deviation of 60 psi was observed for the cohesive failure of the coating in case of as received Al flakes. In case of spherical PPy/Al flake composite coatings it was 335 psi with standard deviation of 33 psi and in case of wire PPy/Al flake composite coatings it was observed to be 336 psi with standard deviation of 26 psi for the cohesive failure of the coating. In all three cases no adhesive failure between coating and substrate was observed. Results suggest that wire PPy/Al flake composite coatings has better adhesion as compared to the as received Al flake coating and spherical PPy/Al flake composite coatings.

2.4.7. Accelerated salt spray and prohesion tests

The x-shaped scribed panels exposed to prohesion test conditions for 120 days were examined. The optical images of the exposed panels are shown in Figure 2.10. The corrosion performance was monitored by visual inspection of blistering and delamination along the scribe. All coatings did not exhibit blistering on the coating or around the scribe whereas delamination was evident along the scribe in the prohesion chamber after 120 days (Figure 2.10).

Another set of x-shaped coated panels were exposed to ASTM B117 salt spray for 120 days. The results are shown in Figure 2.10. It was observed that the best corrosion protection was observed for the wire PPy/Al flake composite coated panels as compared to spherical PPy/Al flake composite coated panels and as received Al flake coated panels. The largest amount of blistering was observed on the as received Al flake coated panels. The formation of large blisters along the scribe on the as received aluminum flake coating signified delamination along the scribe as well. Small blisters were apparent on the spherical PPy/Al flake coating.

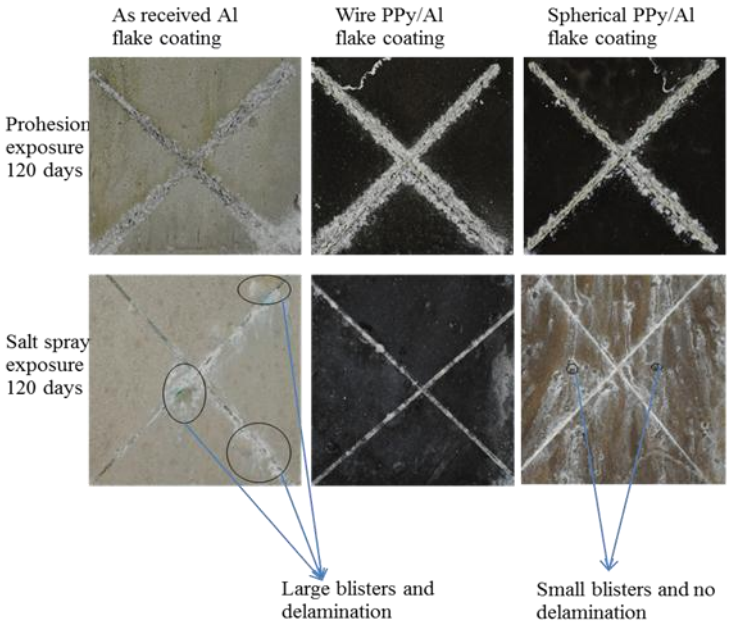

Figure 2.10: Prohesion and salt spray exposure results.

2.4.8. Scanning vibrating electrode technique (SVET)

Current density maps obtained from SVET measurements for the as received Al flake coatings, spherical PPy/Al flake coatings, and wire PPy/Al flake coatings are represented in Figure 2.11, 2.12, and 2.13 respectively. All SVET measurements were performed with scribes of approximately the same size. The SVET measurements were carried out on 20 % PVC coatings in order to have insights into the electrochemical reactions happening above the substrate. For the as received Al flake based coating, an anodic peak was observed due to the anodic metal dissolution just after 5 minutes of the immersion in DHS (Figure 2.11(a)). This behavior did not last for longer times. After 48 hours of immersion in DHS, anodic and cathodic currents were observed in the scribe as is shown in Figure 2.11(b). The cathodic current at this point was likely to be associated with the reduction of oxygen in the scribe. This suggested the establishment of a complete corrosion cell within the scribe [74]. The magnitudes of the currents observed in this case were not large which is likely due to the formation of corrosion products in the scribe.

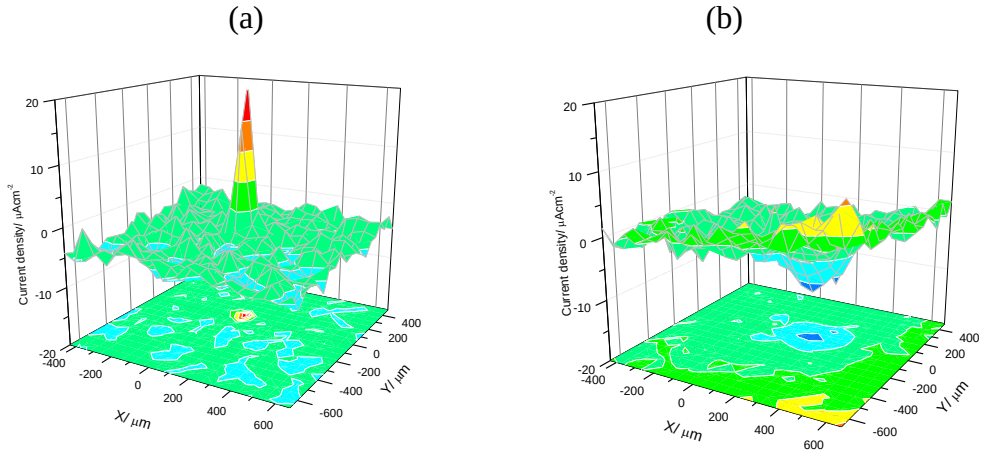

Figure 2.11: SVET current density maps on as received Al flake coatings, (a) Initial, and (b) 48 hours.

In the case of the spherical PPy/Al flake composite, an initial well defined peak of anodic activity was observed (as shown in Figure 2.12(a)) in the defect and the cathodic activity was distributed on the coating surface. The current density associated with this anodic area was ~ 40 $\mu A/cm^2$. This behavior continued after 48 hours of immersion in DHS solution (as shown in Figure 2.12(b)).

For the wire PPy/Al flake composite coatings, a cathodic peak was observed in the scribe after 5 minutes of immersion in DHS solution (as shown in Figure 2.13(a)). This behavior continued after 48 hours of immersion in DHS solution (as shown in Figure 2.13(b)). In this case, anodic current was distributed on the coating surface. The presence of cathodic activity in the defect implied a sacrificial protection mechanism by the wire PPy/Al flake composite pigmented coating. This sacrificial behavior continued beyond 385 hours of immersion in DHS solution.

However, the magnitude of cathodic current density (~25$\mu A/cm^2$) associated with the scan decreased at 385 Hours (as shown in Figure 2.14(a)). The optical image superimposed with current density vectors for the wire PPy/Al flake composite coating is shown in Figure 2.14(b). As shown in Figure 2.14(b), the defect was still shiny without any sign of visual corrosion after 385 hours of immersion in DHS solution; the blue color vector on the defect signifies cathodic activity whereas a red vector signifies anodic activity.

This situation was inverted and the area in the scribe switched to anodic behavior after 407 hours of immersion in DHS solution (as shown in Figure 2.15(a) and 2.15(b)). The magnitude of the anodic current density in the defect was ~ 12 $\mu A/cm^2$.

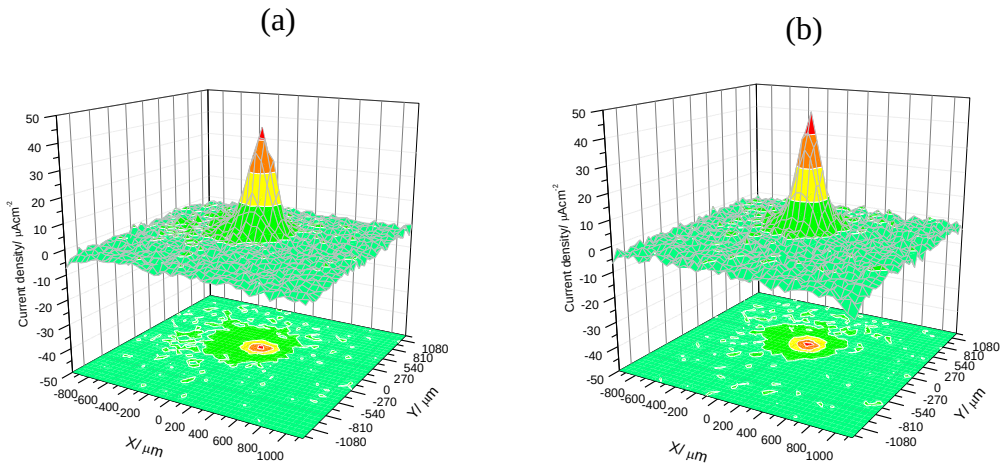

Figure 2.12: SVET current density maps on spherical PPy/Al flake coatings, (a) Initial, and (b) 48 hours.

The initial cathodic current density observed in the case of the wire PPy/Al flake composite coatings had very high magnitudes (~ 300 μA/cm^2) in comparison with the anodic current density of spherical PPy/Al flake composite coatings (~ 40 μA/cm^2). In both of these cases the defect was still shiny after 48 hours of immersion in DHS with no visible signs of corrosion product.

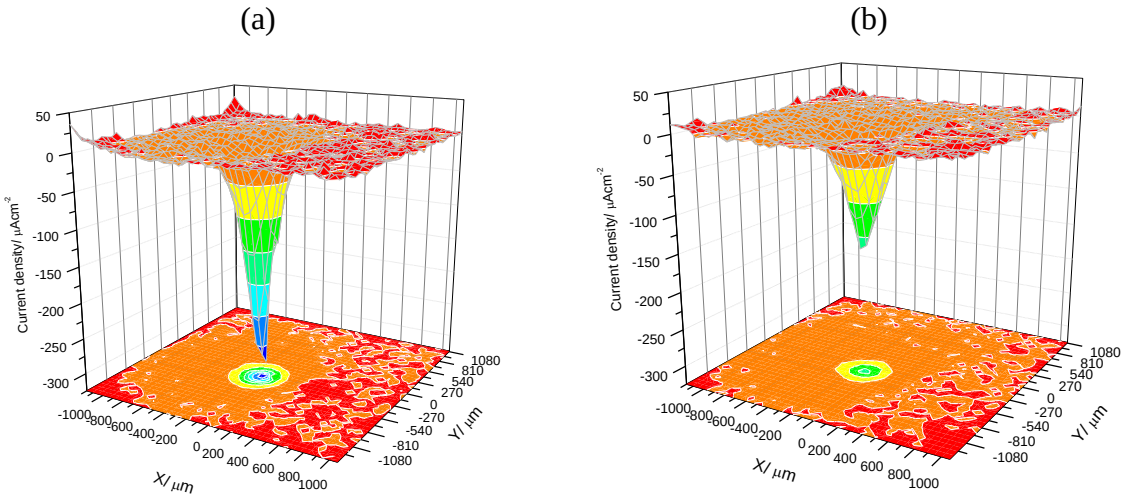

Figure 2.13: SVET current density maps on wire PPy/Al flake coatings, (a) Initial, and (b) 48 hours.

(a) (b)

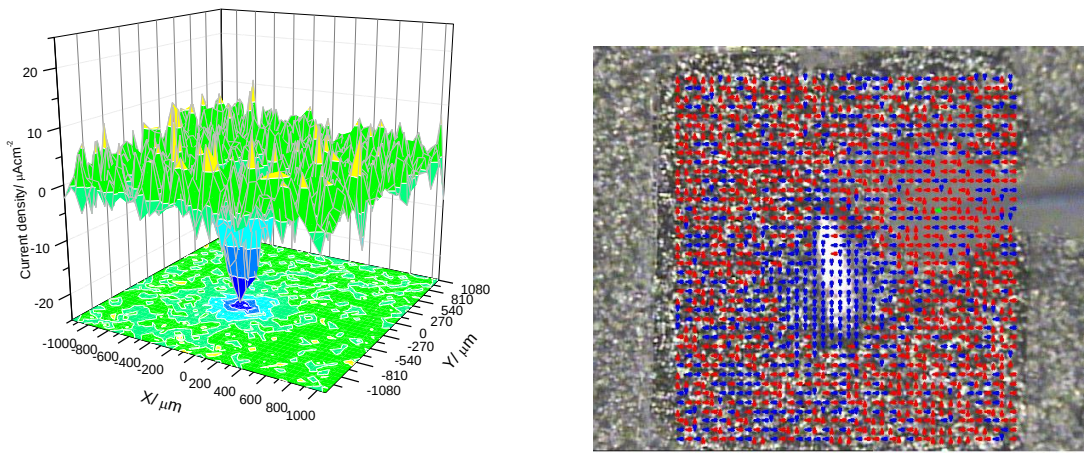

Figure 2.14: (a) SVET current density map and (b) Optical micrograph superimposed by current density vectors for wire PPy/Al flake coatings on AA 2024-T3 after 385 hours of immersion in DHS solution.

Several interactions are possible in these PPy/Al flake composite with the exposure to the accelerated corrosion conditions. When CPs are in contact with active metals the corrosion performance is mostly governed by redox, nonredox, and chemical interactions. These interactions are dependent on the conductivity and connectivity CPs in contact with active metals [75].

The anodic current in the SVET experiments is due to the anodic dissolution of aluminum, re-oxidation of PPy and cathodic current was associated with reduction of PPy or oxygen. The SVET experiments were open to air and it was difficult to control the environment with existing SVET setup. So it was not clear about the origin of the cathodic and anodic areas arising on the defect and coating for different morphologies (wire and spherical) of the PPy/Al flake composite pigment coating. In order to simulate oxygen free situation, and for highlighting more on galvanic interactions between PPy, aluminum flakes, and underlying aluminum substrate, galvanic coupling experiments were performed in controlled environment.

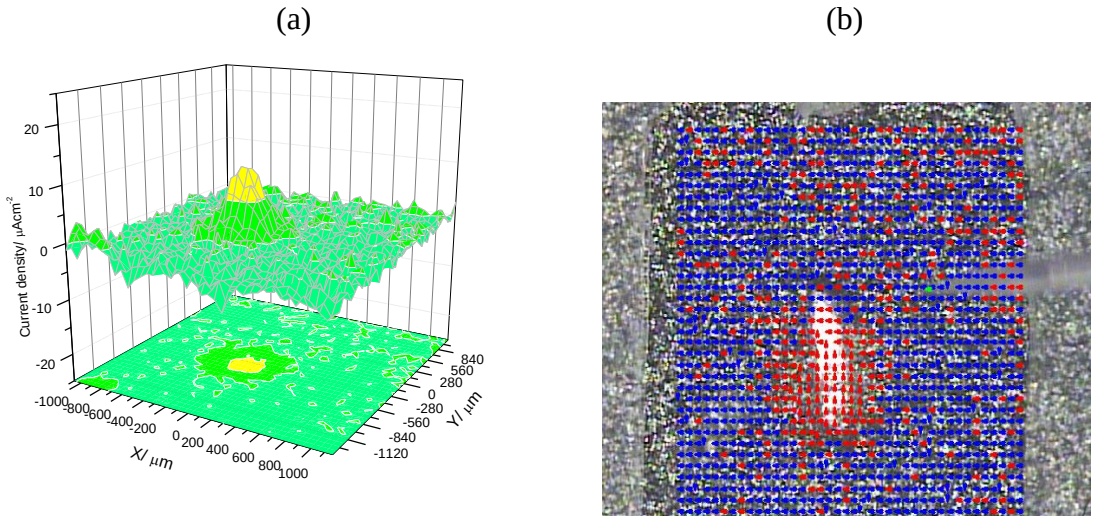

Figure 2.15: (a) SVET current density map and (b) Optical micrograph superimposed by current density vectors for wire PPy/Al flake coatings on AA 2024-T3 after 407 hours of immersion in DHS solution.

2.4.9. Galvanic coupling measurements

In galvanic coupling experiments, DHS in bare aluminum compartment was purged with air to simulate presence of oxygen whereas the coated metal compartment was purged with nitrogen to simulate de-aerated conditions. This also indicated that coated metal is behaving as it is under topcoat. In this setup, positive current signified cathode for bare aluminum 2024-T3 in substrate compartment. As shown in Figure 2.16, both wire PPy/Al flake coating and spherical wire PPy/Al flake coating displayed negative coupling current for initial period of time. This was due to the PPy which is originally in the oxidized form due to its p-doped nature. In de-aerated conditions this PPy in contact with aluminum tends to be reduced [76]. This reduction of PPy results into the oxidation of aluminum flakes which is in its contact. Thus aluminum flakes are activated. Activated aluminum flakes have found to sacrificially protect underlying aluminum 2024-T3 substrate [30]. Therefore the combination of PPy and aluminum flakes has resulted in the increased galvanic coupling current when they are coupled, thereby protecting the underlying aluminum 2024-T3 substrate. After first few hours of the experiment, the coupling current in

case of the wire PPy/Al flake coating increased rapidly and continued to increase for the duration of the experiment. The initial delay in the increase could be attributed to the possibility of presence of native aluminum oxide layer on the surface of aluminum flakes which then dissolved by the action of electrolyte and then electrical contact between PPy and aluminum flakes became possible. Whereas in case of the spherical PPy/Al flake coating, coupling current stayed low for almost first 36 hours. Eventhogh in this case also there was presence of aluminum oxide layer on the surface of aluminum flakes, it would take same amount of time for the dissolution as in case of the wire PPy/Al flake coating. In case of the spherical PPy/Al flake coating where along with long induction time (36 hours), increase in the galvanic coupling current was very low as compared to wire PPy/Al flake coating for the complete duration of the experiment as shown in Figure 2.16.

High galvanic coupling current in case of the wire PPy/Al flake coating indicates that it was providing strong cathodic protection the aluminum 2024-T3. As PPy and Al flakes are in contact with each other, the galvanic interactions between them (as PPy is conductive and in oxidized form) will reduce PPy which will then serve as an oxygen scavenger by redox reaction. This will inherently decrease the corrosion rate as the oxygen is consumed by PPy [30]. Along with this, in the atmospheric conditions where there is presence of oxygen, an oxygen doping mechanism might be occurring due to the presence of the neutral form of PPy along with its oxidized form as was shown in the XPS (results as displayed in as Figure 2.6) [76]. Neutral and reduced form of PPy has found to providing cathodic protection to the underlying aluminum 2024-T3 substrate [22]. Oxygen doping mechanism in this case involves the re-oxidation of the reduced PPy due to oxygen. Re-oxidized PPy again ensured continuous oxidation of aluminum

flakes till the point they completed transformed to aluminum oxide. This can be observed in salt spray and prohesion results after 120 days of exposure as shown in Figure 2.10.

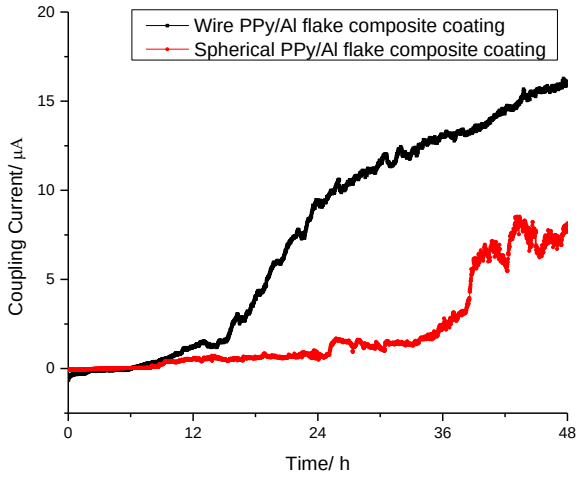

Figure 2.16: Galvanic current plot for bare aluminum 2024-T3 and PPy/Al flake coatings.

The mixed potential values observed for the wire PPy/Al flake coating was more negative than the spherical PPy/Al flake coating as shown in Figure 2.17. For the wire PPy/Al flake coating, mixed potential was -100mV more negative which signified more cathodic polarization and higher level of coupling current.

There is still question of how the wire PPy/Al flake coating and the spherical PPy/Al flake coating showing different behaviors. SVET experiments were performed in open to air conditions whereas galvanic coupling experiments were performed in controlled environment. In the previous results it was concluded that in open to air SVET conditions it is difficult to observe the electrochemical interactions between PPy and aluminum flakes [30]. Similar behaviors for as received aluminum flake coating, PPy coating and PPy/Al flake coating was observed in SVET experiment without any distinctions [30]. In the current research also it is difficult to conclusively comment on the SVET results. For more convincing results, galvanic coupling experiments in controlled environment were helpful. For the wire PPy/Al flake coating strong

positive coupling current was observed in comparison to the spherical PPy/Al flake coating where little positive coupling current was observed. Also in case of the wire PPy/Al flake coating, fast reduction of PPy was observed as compared to slow reduction of PPy in case of the spherical PPy/Al flake coating. Again there was less induction period for the wire PPy/Al flake coating as compared to the spherical PPy/Al flake coating. It is possible to attribute this to the conductivity and the connectivity of the PPy chains in case of the wire PPy/Al flake coating. In another research it was observed that high conductivity of CP results in the easy reduction of PPy [75]. In case of the wire PPy/Al flake coating, it was an order of magnitude more conductive than the spherical PPy/Al flake coating along with wire morphology of the PPy provided easy and faster mobility for electrochemical reactions including reduction of PPy as observed in galvanic coupling experiments. Again reduced PPy was found to be providing the cathodic protection to the aluminum 2024-T3 [22]. Therefore the combination of the conductivity and the connectivity in case of wire PPy/Al flake coating might be responsible for the behavior shown by it in galvanic coupling experiments.

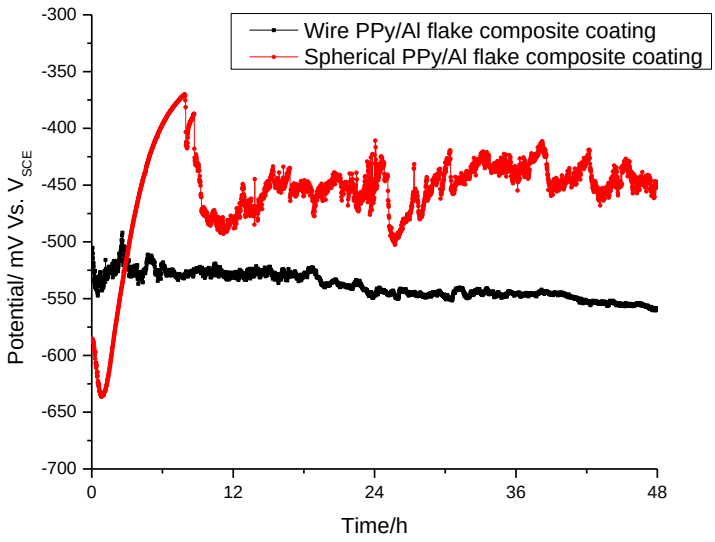

Figure 2.17: Mixed potential plot for bare aluminum 2024-T3 and PPy/Al flake coatings.

2.4.10. Defect size study by SVET

The SVET and galvanic coupling results indicated that the wire structured PPy/Al flake composite coating may be sacrificially protecting the substrate in the smaller defects. It has been found in other studies that coatings based on pure CPs are often unable to protect a substrate in the presence of large defects [77].

It has been suggested that the inherent problems with pure PPy coatings can be overcome using conducting polymer containing composite coatings [78]. To investigate the effect of a large defect on the performance of the wire PPy/Al flake composite coating, a circular defect of 3.6 mm in diameter was made on the surface of the wire PPy/Al flake composite coating using a milling bit.

As is shown in Figure 2.18 and 2.19, initially, the coating showed very little cathodic activity in the defect. As the exposure duration to the DHS was increased, cathodic activity was increased in the defect area and the coating around the defect exhibited anodic activity.

These SVET results indicate that even with a fairly large defect, the coating was providing sacrificial protection to the substrate. However, due to the increased defect area, the intensity of the cathodic current density was not as high as observed in presence of small defects. This sacrificial protection provided by the coating eventually will be lost as the oxide layer over aluminum flakes becomes thick enough or the aluminum flake in the coating is consumed, not allowing any galvanic contact between the PPy and the flakes. Therefore the wire structured PPy/Al flake composite coating was able to protect substrate even in larger defects.

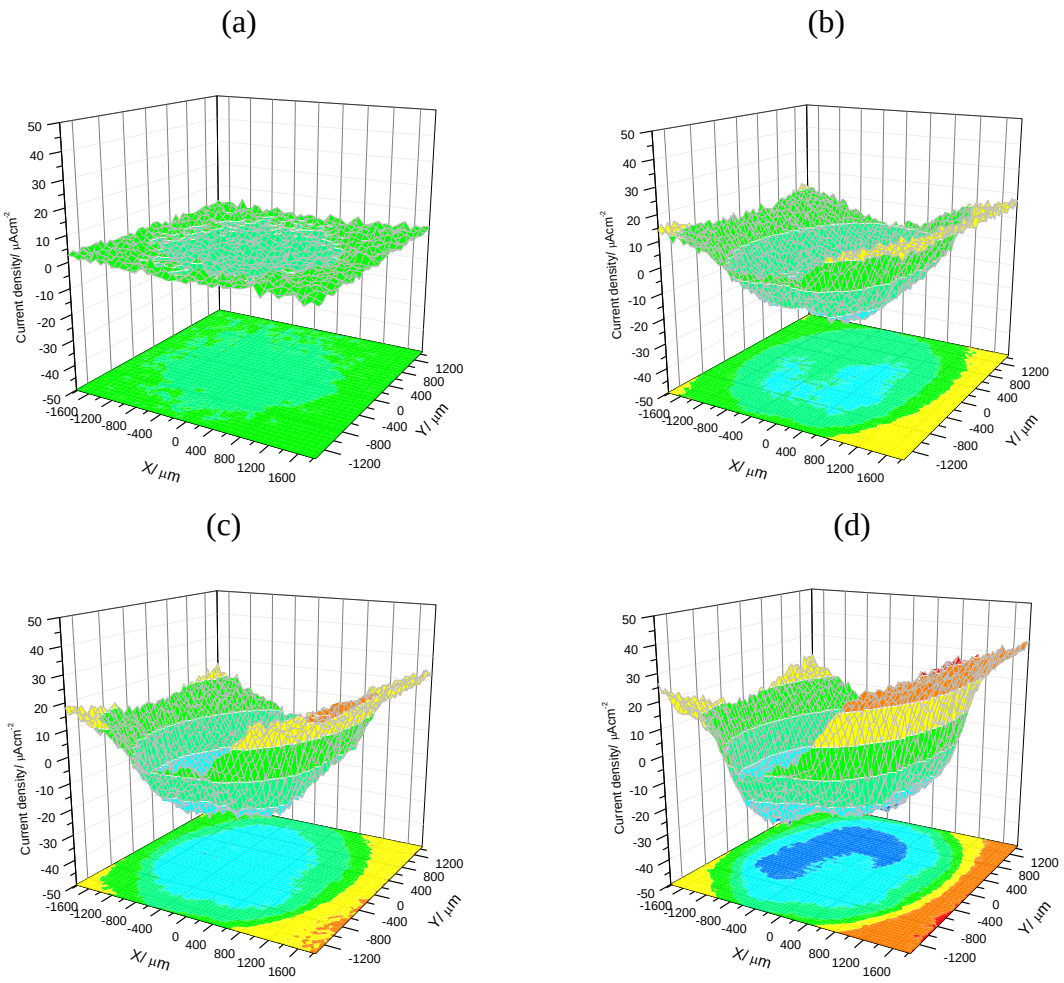

Figure 2.18: SVET current density maps on wire PPy/Al flake coatings, (a) Initial, (b) 24 hours, (c) 48 hours, and (d) 84 hours.

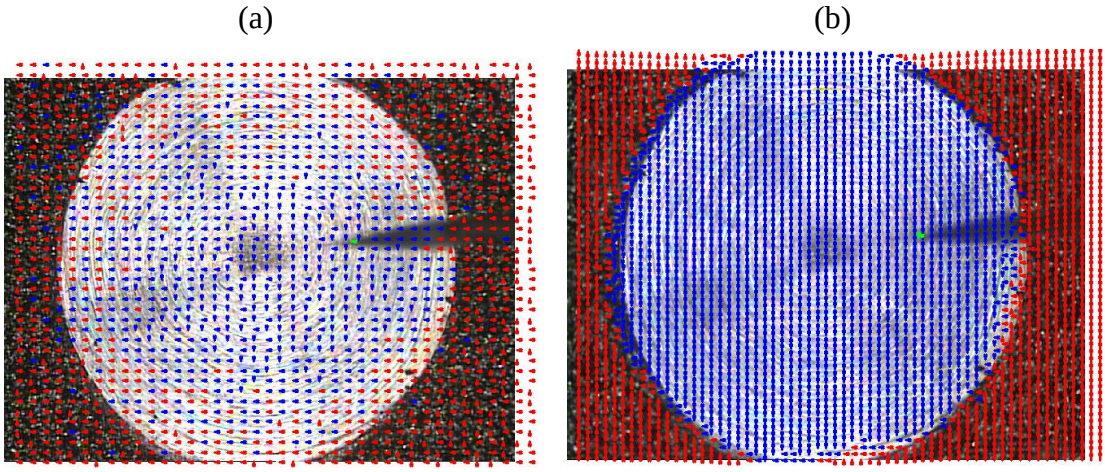

Figure 2.19: Optical micrograph superimposed by current density vectors for wire PPy/Al flake coatings on AA 2024-T3, (a) Initial, (b) after 84 hours.

2.5. Conclusions

In this study, aluminum flakes were combined with PPy in unique way by forming the composite and the incorporation of this pigment into an epoxy primer on AA 2024-T3 substrate was performed. These coatings were studied for their anticorrosive properties. The wire PPy/Al flake and the spherical PPy/Al flake composites were successfully prepared via facile chemical oxidative polymerization by varying the type and amount of solvent in the synthesis. The wire PPy/Al flake composite was found to be more conductive than the spherical PPy/Al flake composite. This was the result of wire morphology of the deposited PPy which enhanced the connectivity of the PPy deposited onto the aluminum flake surface. During 120 days of salt spray exposure, the wire PPy/Al flake composite coatings showed the best performance. It was determined that the wire PPy/Al flake composite coating provided sacrificial protection to the AA 2024-T3 substrate possibly by activating the aluminum flakes. This was reconfirmed with galvanic coupling experiments which showed increasing coupling current (sacrificial protection) and more negative mixed potential (cathodic polarization) for wire PPy/Al flake composite coating in controlled environment. It was also determined that the wire PPy/Al flake composite was able to sacrificially protect the substrate even in a much larger defect as evidenced by SVET results.

2.6. Acknowledgements

Authors gratefully acknowledge the support of this research by US Army Research Laboratory under grant no. W911NF-09-2-0014, W911NF-10-2-0082, and W911NF-11-2-0027.

2.7. References

[1] N.S. Sangaj, V.C. Malshe, Prog. Org. Coat. 50 (2004) 28.

[2] H. Leidheiser, Ind. Eng. Chem. Prod. Res. Dev. 20 (1981) 547.

[3] E. Armelin, R. Pla, F. Liesa, X. Ramis, J.I. Iribarren, C. Alemán, Corros. Sci. 50 (2008) 721.

[4] M.D. Cohen, B. Kargacin, C.B. Klein, M. Costa, Crit. Rev. Toxicol.23 (1993) 255.

[5] B.L. He, B. Dong, W. Wang, H.L. Li, Mater. Chem. Phys. 114 (2009) 371.

[6] D. Nicolas-Debarnot, F. Poncin-Epaillard, Anal. Chim. Acta. 475 (2003) 1.

[7] S. Geetha, K.K.S. Kumar, C.R.K. Rao, M. Vijayan, D.C. Trivedi, J. Appl. Polym. Sci. 112 (2009) 2073.

[8] S. Geetha, C.R.K. Rao, M. Vijayan, D.C. Trivedi, Anal. Chim. Acta. 568 (2006) 119.

[9] X.H. Wang, J. Li, J.Y. Zhang, Z.C. Sun, L. Yu, X.B. Jing, F.S. Wang, Z.X. Sun, Z.J. Ye, Synth. Met. 102 (1999) 1377.

[10] E. Smela, Mater. Res. Bull. 33 (2008) 197.

[11] D. Gendron, M. Leclerc, Energy Environ. Sci. 4 (2011) 1225.

[12] W.J. Bae, C. Scilla, V.V. Duzhko, W.H. Jo, E.B. Coughlin, J. Polym. Sci., Part A: Polym. Chem. 49 (2011) 3260.

[13] Y.S. Hwang, Y. Son, Y. Lee, Mol. Cryst. Liq. Cryst. 472 (2007) 503.

[14] A. Tsirimpis, I. Kartsonakis, I. Danilidis, P. Liatsi, G. Kordas, Prog. Org. Coat. 67 (2010) 389.

[15] S. Zor, F. Kandemirli, E. Yakar, T. Arslan, Prot. Met. Phys. Chem. Surf. 46 (2010) 110.

[16] J.O. Iroh, C. Williams, Synth. Met. 99 (1999) 1.

[17] R. Akid, M. Gobara, H. Wang, Electrochim. Acta 56 (2011) 2483.

[18] F.H. Shi, X.T. Wang, J.Q. Yu, B.R. Hou, Anti-Corros. Method M. 58 (2011) 111.

[19] H. Bhandari, R. Srivastav, V. Choudhary, S.K. Dhawan, Thin Solid Films 519 (2010) 1031.

[20] S.U. Rahman, Surf. Coat. Technol. 205 (2011) 3035.

[21] G. Bereket, E. Hur, Prog. Org. Coat. 65 (2009) 116.

[22] M.C. Yan, D.E. Tallman, S.C. Rasmussen, G.P. Bierwagen, J. Electrochem. Soc. 156 (2009) C360.

[23] C. Ocampo, E. Armelin, F. Liesa, C. Aleman, X. Ramis, J.I. Iribarren, Prog. Org. Coat. 53 (2005) 217.

[24] U. Rammelt, P.T. Nguyen, W. Plieth, Electrochim. Acta 46 (2001) 4251.

[25] T. Tuken, B. Yazici, M. Erbil, Prog. Org. Coat. 51 (2004) 205.

[26] M. Sharifirad, A. Omrani, A.A. Rostami, M. Khoshroo, J. Electroanal. Chem. 645 (2010) 149.

[27] M. Rohwerder, Int. J. Mater. Res. 100 (2009) 1331.

[28] B. Wessling, Adv. Mater. 6 (1994) 226.

[29] J. Reut, A. Öpik, K. Idla, Synth. Met. 102 (1999) 1392.

[30] M. Yan, C.A. Vetter, V.J. Gelling, Electrochim. Acta 55 (2010) 5576.

[31] M. Sabouri, T. Shahrabi, H.R. Farid, M.G. Hosseini, Prog. Org. Coat. 64 (2009) 429.

[32] M. Trueba, S.P. Trasatti, J. Appl. Electrochem. 39 (2009) 2061.

[33] A. Mollahosseini, E. Noroozian, Synth. Met. 159 (2009) 1247.

[34] V.J. Gelling, M.M. Wiest, D.E. Tallman, G.P. Bierwagen, G.G. Wallace, Prog. Org. Coat. 43 (2001) 149.

[35] D.E. Tallman, Y. Pae, G.P. Bierwagen, Corrosion 56 (2000) 401.

[36] J. Iribarren, C. Ocampo, E. Armelin, F. Liesa, C. Aleman, J. Appl. Polym. Sci. 108 (2008) 3291.

[37] F. Liesa, C. Ocampo, C. Aleman, E. Armelin, R. Oliver, F. Estrany, J. Appl. Polym. Sci. 102 (2006) 1592.

[38] E. Armelin, Á. Meneguzzi, C.A. Ferreira, C. Alemán, Surf. Coat. Technol. 203 (2009) 3763.

[39] J.H. Huh, E.J. Oh, J.H. Cho, Synth. Met. 137 (2003) 965.

[40] S. Sathiyanarayanan, S.S. Azim, G. Venkatachari, Electrochim. Acta 52 (2007) 2068.

[41] S. Sathiyanarayanan, S. Syed Azim, G. Venkatachari, Synth. Met. 157 (2007) 205.

[42] A. Kalendová, I. Sapurina, J. Stejskal, D. Veselý, Corros. Sci. 50 (2008) 3549.

[43] S. Sathiyanarayanan, S. Syed Azim, G. Venkatachari, Electrochim. Acta 53 (2008) 2087.

[44] X. Qi, C. Vetter, A.C. Harper, V.J. Gelling, Prog. Org. Coat. 63 (2008) 345.

[45] J. Unsworth, P.C. Innis, B.A. Lunn, Z. Jin, G.P. Norton, Synth. Met. 53 (1992) 59.

[46] S.J. Sutton, A.S. Vaughan, Synth. Met. 58 (1993) 391.

[47] G.A. Wood, J.O. Iroh, Polym. Eng. Sci. 36 (1996) 2389.

[48] J. Ouyang, Y. Li, Polymer 38 (1997) 1971.

[49] D.S. Maddison, J. Unsworth, Synth. Met. 30 (1989) 47.

[50] O.A. Semenikhin, L. Jiang, T. Iyoda, K. Hashimoto, A. Fujishima, Electrochim. Acta 42 (1997) 3321.

[51] T. Silk, Q. Hong, J. Tamm, R.G. Compton, Synth. Met. 93 (1998) 59.

[52] G.L. Chen, D.E. Tallman, G.P. Bierwagen, J. Solid State Electrochem. 8 (2004) 505.

[53] M.-L. Abel, J.-L. Camalet, M.M. Chehimi, J.F. Watts, P.A. Zhdan, Synth. Met. 81 (1996) 23.

[54] S. Carquigny, O. Segut, B. Lakard, F. Lallemand, P. Fievet, Synth. Met. 158 (2008) 453.

[55] D. Horák, B. Rittich, A. Španová, Effect of reaction parameters on properties of dispersion-polymerized hydrophilic microspheres as supports for immobilization of proteins Aqueous Polymer Dispersions, K. Tauer (Ed.), vol. 124, Springer Berlin / Heidelberg, 2004.

[56] Y.-Z. Long, M.-M. Li, C. Gu, M. Wan, J.-L. Duvail, Z. Liu, Z. Fan, Prog. Polym. Sci. 36 (2011) 1415.

[57] G. Socrates, Infrared and Raman Characteristic Group Frequencies, Tables and Charts 3rd ed. John Wiley and Sons, Ltd., Chichester, UK, 2001.

[58] Spectral database of organic compounds, http://riodb01.ibase.aist.go.jp/sdbs/cgi bin/cre_index.cgi?lang=eng (last accessed 30th October 2011).

[59] H.A. Al-Abadleh, V.H. Grassian, Langmuir 19 (2003) 341.

[60] S.V. Kasisomayajula, X.N. Qi, C. Vetter, K. Croes, D. Pavlacky, V.J. Gelling, J. Coat. Technol. Res. 7 (2010) 145.

[61] B. Tian, G. Zerbi, J. Chem. Phys.92 (1990) 3886.

[62] B. Tian, G. Zerbi, J. Chem. Phys.92 (1990) 3892.

[63] M. Omastová, M. Trchová, J. Kovářová, J. Stejskal, Synth. Met. 138 (2003) 447.

[64] W. Prissanaroon, N. Brack, P.J. Pigram, J. Liesegang, T.J. Cardwell, Surf. Interface Anal. 33 (2002) 653.

[65] K. Idla, A. Talo, H.E.M. Niemi, O. Forsén, S. Yläsaari, Surf. Interface Anal. 25 (1997) 837.

[66] P. Pfluger, J. Chem. Phys. 80 (1984) 544.

[67] P. Bätz, D. Schmeisser, W. Göpel, Phys. Rev. B: Condens. Matter Mater. Phys. B 43 (1991) 9178.

[68] C. Malitesta, I. Losito, L. Sabbatini, P.G. Zambonin, J. Electron Spectrosc. Relat. Phenom. 76 (1995) 629.

[69] H. Ge, G. Qi, E.-T. Kang, K.G. Neoh, Polymer 35 (1994) 504.

[70] H.C.F. Martens, H.B. Brom, J.A. Reedijk, D.M. de Leeuw, Synth. Met. 101 (1999) 821.

[71] Y. Cao, J. Qiu, P. Smith, Synth. Met. 69 (1995) 187.

[72] C. He, C. Yang, Y. Li, Synth. Met. 139 (2003) 539.

[73] K.W. Oh, H.J. Park, S.H. Kim, J. Appl. Polym. Sci. 91 (2004) 3659.

[74] J. He, V.J. Gelling, D.E. Tallman, G.P. Bierwagen, J. Electrochem. Soc. 147 (2000) 3661.

[75] J. He, D.E. Tallman, G.P. Bierwagen, J. Electrochem. Soc. 151 (2004) B644.

[76] M. Yan, D.E. Tallman, G.P. Bierwagen, Electrochim. Acta 54 (2008) 220.

[77] M. Rohwerder, A. Michalik, Electrochim. Acta 53 (2007) 1300.

[78] M. Rohwerder, S. Isik-Uppenkamp, C.A. Amarnath, Electrochim. Acta 56 (2011) 1889.

CHAPTER 3. CHARACTERIZATION AND ELECTROCHEMICAL INVESTIGATIONS OF POLYPYRROLE/ALUMINUM FLAKE COMPOSITE PIGMENTS ON AA 2024-T3 SUBSTRATE

(Published as "Characterization and Electrochemical Investigations of Polypyrrole/Aluminum Flake Composite Pigments on AA 2024-T3 Substrate" ECS Transactions 2012, 41 (15), 75-89)

3.1. Abstract

Phosphate and nitrate doped Polypyrrole (PPy)/Aluminum (Al) flake pigments were synthesized by chemical oxidative polymerization method. Coatings were formulated from the phosphate doped PPy/Al flake pigment, nitrate doped PPy/Al flake, and as received Al flakes at 20% pigment volume concentration (PVC). The anticorrosion properties of coatings on aluminum alloy (AA 2024-T3) were monitored by exposure with accelerated salt spray (ASTM B 117), electrochemical impedance spectroscopy (EIS), scanning vibrating electrode technique (SVET), and anodic polarization experiments. Phosphate and nitrate doped PPy/Al flake coatings showed enhanced anticorrosion ability in comparison with as received Al flake coating as observed in accelerated salt spray test. In the anodic polarization experiments, phosphate and nitrate doped PPy/Al flake coatings exhibited a positive shift in the potential suggesting the passivation of the substrate. Additionally, SVET experiments did not detect appreciable corrosion activity for the samples demonstrating better corrosion protection ability of phosphate and nitrate doped PPy/Al flake coatings.

3.2. Introduction

Conducting polymers (CPs) are an important class of materials with distinguishable properties and a wide range of applications [1, 2]. Extended conjugated backbone separates CPs

from insulating polymers and results in interesting redox properties imparting conductivities to CPs in the semiconducting to conducing ranges [3]. CPs are environmentally stable, non-toxic, and relatively easily synthesized [4]. Correspondingly, CPs have numerous applications such as sensors [5-8], batteries [9, 10], solar cells [11, 12], light emitting diodes [13, 14], and coatings for corrosion protection (15-23). Polyaniline (PAni), polythiophene, and polypyrrole (PPy) are often studied CPs and have been employed for the corrosion protection of metals and their alloys [24-30].

PPy is amongst one of the most studied CPs for corrosion protection. This is attributed to its good environmental stability, conductivity and facile synthesis [31]. PPy is non-toxic, environment friendly, and can be prepared by both chemical and electrochemical means [32]. PPy has been studied as a replacement for hexavalent chromate which is used in coatings for corrosion inhibition; however, due to toxicity the use of hexavalent chromate will be limited in the future [33]. Even though there is controversy over the protection mechanism provided by CPs, the overall general mechanism has been surface ennobling and anodic passivation [34]. Also, CPs can be doped with corrosion inhibiting anions and when reduced can release these anions resulting in passivation the substrate [35]. It is important to note that it has been observed that if passivation is not achieved an enhancement in the rate of corrosion can occur [36, 37]. PPy possesses disadvantages such as poor mechanical properties, lack of sufficient adhesion, porosity, and insolubility in the solvents used in the coatings [34, 38, 39]. This results in problems with its application to coatings. Conducting polymer containing composites (CPCC) are one of the possible avenues to overcome the problems associated with use of CPs [39]. For example, PAni-TiO_2 composites were synthesized by in-situ chemical oxidative polymerization of aniline [40]. This composite improved corrosion resistance of acrylic resin based primer on

steel substrate. A similar performance improvement was observed on several other composites containing PAni [41, 42]. PPy containing composites were synthesized in the past [34, 39]. In another example, PPy was synthesized on the surface of aluminum flakes by in-situ chemical oxidative polymerization. Aluminum flakes lengthened the path of corrosive ions reaching the coatings and PPy electrical contact with aluminum flake provided corrosion protection by electrochemical activity.

Often the incorporation of corrosive inhibiting dopants in backbone of CPs improves corrosion resistance ability [43]. For example, vinyl coatings with sulphonate doped PAni protected steel in neutral and acidic media [44]. PPy films formed on bare aluminum substrate in presence of molybdate and nitrate dopants displayed greater resistance to corrosive chloride ions [45]. PPy-phosphate composite coatings have also been studied and were found to exhibit enhanced corrosion protection on the mild steel substrate. This study also demonstrated that dopant ion can influence the morphology of resultant conducting composite [46]. It has been suggested that the active release of dopants is dependent on specific conditions occurring with the release rate of anions dependant on the defect environment.

In the reported work, PPy containing phosphate and nitrate as dopants were synthesized on the surface of aluminum flakes. This pigment combined the barrier protection provided by aluminum flakes and the active release of corrosive inhibiting anions from PPy. The corrosion inhibiting pigment was formed via chemical oxidative polymerization enabling the synthesis of composite pigment on a large scale. Additionally, the synthesis procedure provided an easy method for the incorporation of PPy in a coating matrix with the optimum amount of dopant with respect to PPy. It is proposed that the PPy inhibitor will function as a reservoir of phosphate or nitrate which will allow for the passivation of the substrate.

3.3. Experimental

3.3.1. Preparation of PPy/Al flake composite coating (doped with phosphate or nitrate) and as received Al flake coating

In order to synthesize PPy/Al flake pigment, 500 ml of Millipore® water and 500 ml of 1-methoxy-2-propanol (Alfa Aesar Co.) were added to an Erlenmeyer flask. This was followed by addition of the required quantity of the dopant (sodium phosphate monohydrate (BDH) or sodium nitrate (Mallinckrodt Chemical, Inc.). After addition of dopant and its complete dissolution, 30 grams of aluminum flakes (Stapa Aloxal PM 2010 from Eckart America) were added. The aluminum flakes had composition of 39% aluminum, 26% aluminum oxide, and 35% 1-methoxy-2-propanol. After the dispersion of aluminum flakes, 22.8 grams of ammonium persulfate (BDH) was added. The final step of the synthesis was the addition of 13.9 ml of pyrrole (Alfa Aesar Co) to the reaction mixture. For this synthesis, the pyrrole monomer was vacuum distilled prior to use. The reaction was continued at ambient temperature for 24 hours. The reaction mixture was then filtered and washed with water. The product was placed in an oven for drying at 60°C. It was ground in mortar and pestle and the product was collected after sieving it through # 140 sieve (with 106 μm opening diameter).

3.3.2. Scanning electron microscopy (SEM)

A JEOL JSM-6300 scanning electron microscope (SEM) was employed for the morphology investigations of as received Al flakes, phosphate doped PPy/Al flake composite, and nitrate doped PPy/Al flake composite. The sample for SEM was prepared by sprinkling ground powder onto carbon tape which was attached to the aluminum mounts followed by sputter coating with gold using a Balzers SCD 030 sputter coater. The magnification, accelerating voltage used, and scale bars are listed on each SEM micrograph.

3.3.3. Coatings preparation

Coatings were prepared on AA 2024-T3 substrate (Q-panel, dimensions-6”x3”). Prior to the coating application, the substrate was sandblasted with 100 µm alumina grit and degreased with hexane. As received Al flake, PPy-Al flake composite, either phosphate or nitrate doped, was mixed with EPON 830 (Momentive Specialty Chemicals Inc.) followed by addition of the hardener, Epicure 3015 (Momentive Specialty Chemicals Inc.) in stoichiometric ratio (1:1). The pigment volume concentration (PVC) of the prepared coating was 20%. The application viscosity was adjusted with solvent methyl isobutyl ketone (MIBK from Aqua solutions). The coating application was performed via a drawdown bar. The dry film thickness (DFT) of the coatings was approximately 80-90 µm.

3.3.4. Accelerated salt spray exposure test

The scribes of ca. 1mm width were made on fully cured panels. The “x” scribes were made with Gravograph IM4 engraving system (Gravograph, USA) assisted with Gravostyle Quick software. After scribing, the samples were exposed to accelerated environment according to ASTM B 117 (5% NaCl solution at 35°C). The corrosion resistance performance was then monitored by visual inspection of blistering and delamination along the scribe.

3.3.5. Electrochemical impedance spectroscopy (EIS)

A Gamry Instruments R600 Potentiostat/Galvanostat/ZRA with Gamry Framework Version 5.58/EIS 300 software was employed for the EIS measurements. The measurements were performed in a three electrode cell with a saturated calomel reference electrode, platinum mesh counter electrode; coated substrate as a working electrode, and 5% NaCl was used as an electrolyte so that the coating was exposed to the same electrolyte as was used in the exposure cabinet. The frequency range was from 100,000 to 0.01Hz with 10 points/decade using 10 mV

RMS of AC signal amplitude. The area of the working electrode exposed to electrolyte was 7 cm^2. Three replicates of each coating were examined.

3.3.6. Scanning vibrating electrode technique (SVET) measurements

Current distributions due to corrosion reactions occurring in a damaged sample were monitored by SVET measurements. A SVET system from Applicable electronics was employed in this study. A Pt-Ir microelectrode (Microprobe, Inc.) was deposited with a Pt black of sphere with ca. 20 µm in diameter. The vibration amplitude of microelectrode was 20 µm in X and Y direction. The scan was performed over the coating with artificial defect at the center with the microprobe approximately 200 µm above the sample. The coating on aluminum panel was taped with polyester tape to expose an area of approximately 2mm x 2mm. The defect was approximately .3mm in width and 1mm in length. This electrochemical cell was filled with dilute Harrison solution (DHS, 0.35% ammonium sulfate and 0.05% sodium chloride). Scans were started within 5 minutes of immersion in DHS solution. The noise of the instrument is estimated to be ±2 $\mu A/cm^2$. The scans were obtained in a 20x20. Data obtained from the SVET measurement is often presented in two ways. In the first representation, the vertical component of current density is graphed in a 3D surface graph. The positive current density signifies anodic current and negative current density signifies cathodic current. The second representation of the data is with vectors representing current densities superimposed on optical image of the sample. Two replicates of each coating were examined.

3.3.7. Anodic polarization

Anodic polarization scans were obtained using a similar procedure as with the EIS experiments. However, in this experiment the panels were scribed for a defect of 1.5 cm in length and 1 mm in width. Measurements were performed in a linear sweep from -0.1V to 2V

vs. open circuit potential with scan rate of 5 mV/s. DHS was used as electrolyte and the electrolyte was purged with nitrogen for 30 minutes prior to the experiment. Two replicates of each coating were examined.

3.4. Results and discussions

3.4.1. Scanning electron microscopy (SEM)

Synthesis conditions as well as parameters including reaction temperature, pH of the reaction, method of synthesis, the type of dopant, and nature of solvent can influence the resulting morphology of CPs [47-52]. In this synthesis equal amounts of water and 1-methoxy-2-propanol were used along with the dopants (sodium phosphate monohydrate and sodium nitrate respectively). As observed from SEM micrographs in Figure 3.1, the spherical and uniform morphology of PPy was obtained on the surface of aluminum flakes in both synthesis procedures, phosphate doped PPy/Al flake composite, and nitrate doped PPy/Al flake composite. Formation of PPy was more prominent in case of nitrate doped composite than phosphate doped composite.

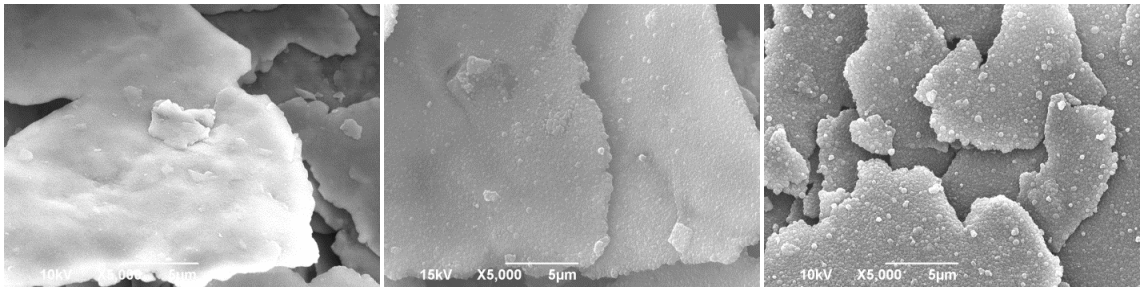

Figure 3.1: SEM micrographs of as received Al flakes (left image), phosphate doped PPy/Al flake (middle image), and nitrate doped PPy/Al flake (right image).

In the preparation procedure, phosphate doped PPy/Al flakes, and nitrate doped PPy/Al flakes were ground in a mortar and pestle. The resulting composite maintained the structure of PPy formed on aluminum flakes during the synthesis. This robustness of the composites can be

attributed to the stiff and inflexible chains of PPy along with its insoluble nature in commonly used solvents [53].

3.4.2. Electrochemical impedance spectroscopy (EIS)

EIS is used for quantitative monitoring of corrosion processes occurring at the surface of corroding metal or underneath the coating on metal surface [54-57]. Based on equivalent circuit elements and physical processes occurring in the coating and estimation of the degradation resulting from electrochemical reactions due to corrosion can be predicted [54].

The Bode and Nyquist plots for as received Al flake coating, phosphate doped PPy/Al flake composite coating, and nitrate doped PPy/Al flake composite coating are shown in Figure 3.2, 3.3, and 3.4, respectively. Bode plot represents the modulus of impedance verses frequency whereas Nyquist plot represents real and imaginary components of impedance. Phase angles for varying applied frequencies are also provided in the Bode graph.

As shown in the Bode plot of as received Al flake coating (Figure 3.2), the initial impedance was very high, indicating a sufficiently high barrier property. This high impedance was maintained for initial 350 hours. This behavior was attributed to the high aspect ratio of as received Al flakes as well as to the pigment volume concentration (PVC) of the coating which was below the critical pigment volume concentration (CPVC). This resulted in a barrier to corrosive ions diffusion as any aggressive species would proceed via tortuous paths to reach to the substrate [59]. Only one time constant was observed in as received Al flake coatings after 350 hours of exposure to salt spray conditions. After 750 hours of exposure, the resistance provided by coating was breached resulting in decrease in impedance. In the Nyquist plot of as received Al flake coating (Figure 3.2) after 750 hours of exposure, one complete conductive loop along with start of second semicircle with diffusion controlled portion was evident The diffusion

controlled portion was modeled with Warburg impedance, equation 3.1, according to Fick's second law partial differential equation (58).

$$Z_w = 1/\sigma(i\omega)^{(-1/2)} \quad (3.1)$$

Where, Z_w is Warburg impedance, i is imaginary component, σ is Warburg capacitance, and ω is the angular frequency. Warburg impedance implied development of pathways through the coating due to prolonged exposure to corrosive environment. This observation was also supported by decrease in the coating impedance.

The impedance of coatings with phosphate doped PPy/Al flake composite, and nitrate doped PPy/Al flake composite displayed ca. 4 orders of magnitude decrease in comparison with as received Al flake coating (Figure 3.3, and 3.4). This behavior was not due to the ion transport through the coating; instead it is suggested to be due to the presence of conductive pathways resulting from conductive nature of PPy. The semicircle was decreasing in case of phosphate doped PPy/Al flake composite coatings, and nitrate doped PPy/Al flake composite coatings as the time of exposure increased (Figure 3.3, and 3.4). The starting of the second semicircle loop with straight line also signified charge transfer and diffusion. The decrease in the impedance due to the conductive nature of PPy has been observed by many researchers [60, 61]. At higher frequencies of perturbation, the resulting current prefers conductive pathways through PPy instead of passing through dielectric component of the coating. If one uses the most accepted criteria for EIS, where the higher the impedance the greater the protection provided to the substrate, the impedance results are contradictory with the observations in salt spray exposure for a longer duration of time. Even after displaying a decrease in impedance, the phosphate doped PPy/Al flake composite coatings and nitrate doped PPy/Al flake composite coatings displayed better performance in salt spray testing as determined via visual assessment. The

electrochemical nature of PPy and the reactions occurring at PPy/Al flake interface as well as at PPy/Al substrate interface are inherently important in this coating system.

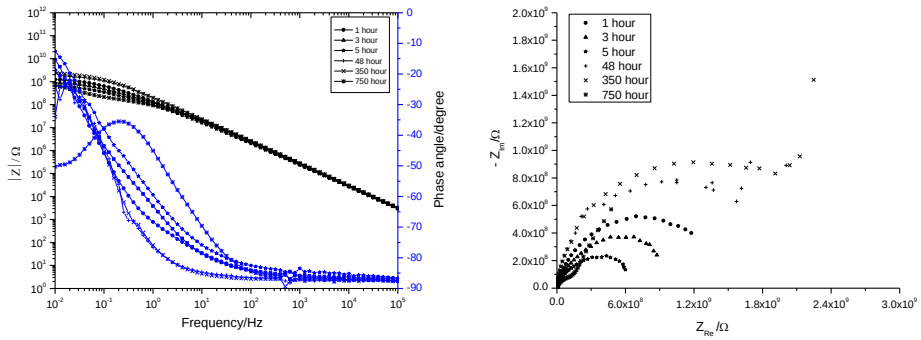

Figure 3.2: Bode plot (left), and Nyquist plot (right) of as received Al flake coating.

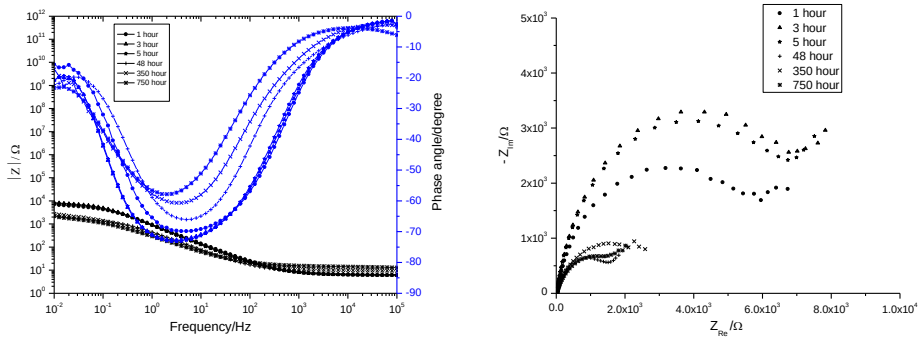

Figure 3.3: Bode plot (left), and Nyquist plot (right) phosphate doped PPy/Al flake coating.

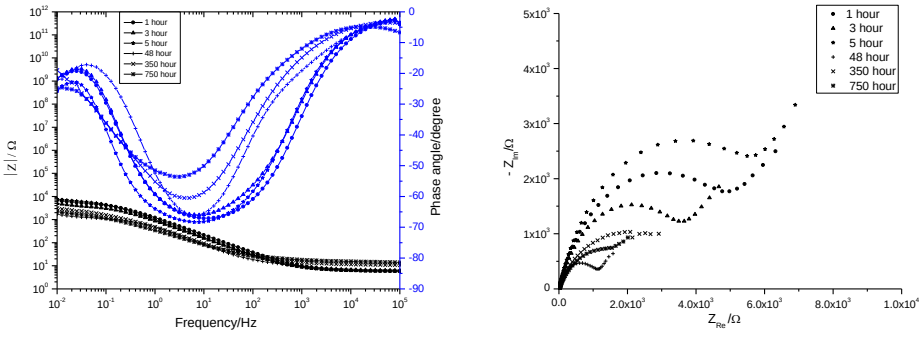

Figure 3.4: Bode plot (left), and Nyquist plot (right) nitrate doped PPy/Al flake coating.

The equivalent circuit provided in Figure 3.5 (a) was used to model the coatings based on phosphate doped PPy/Al flake composite, nitrate doped PPy/Al flake composite, and up to 350

hours of exposure of as received Al flake coating. The data was fitted to model circuits by using ZView 2 software (Scribner Associates Inc.). For 750 hours of exposure the as received Al flake coating was modeled using equivalent cell displayed in Figure 3.5 (b). This model included Warburg impedance element which confirms the physical phenomenon of ion diffusion through the coating [58]. In circuit modeling, Rs is the uncompensated solution resistance, Rc is the coating resistance, and CPE is the constant phase element which represents coating capacitance where CPE is obtained by equation 3.2.

$$Z_{(CPE)} = 1/(Y_0)(j\omega)^n \quad (3.2)$$

Where, Y_0 is CPE constant, j is an imaginary component, , ω is the angular frequency ($\omega = 2\pi f$, f is the frequency), n is the power ($0 \leq n \leq 1$), and $Z_{(CPE)}$ is the impedance of CPE. Circuit modeling results are shown in Table 3.1. An example of a fitted curve to obtained data for 750 hours of exposure of as received Al flake coating is shown in Figure 3.6. The green line is the fit while the red line is the obtained EIS data. It is apparent that the results obtained from equivalent circuit modeling closely matches with the actual data obtained from EIS experiments.

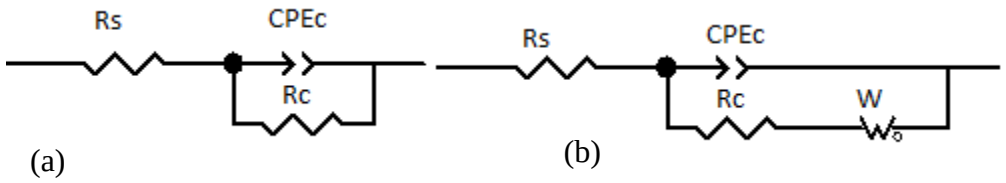

Figure 3.5: Equivalent circuit models used for (a) Phosphate doped PPy/Al flake coating, nitrate doped PPy/Al flake coating, and up to 350 hours of as received Al flake coating (b) 750 hours exposure of as received Al flake coating.

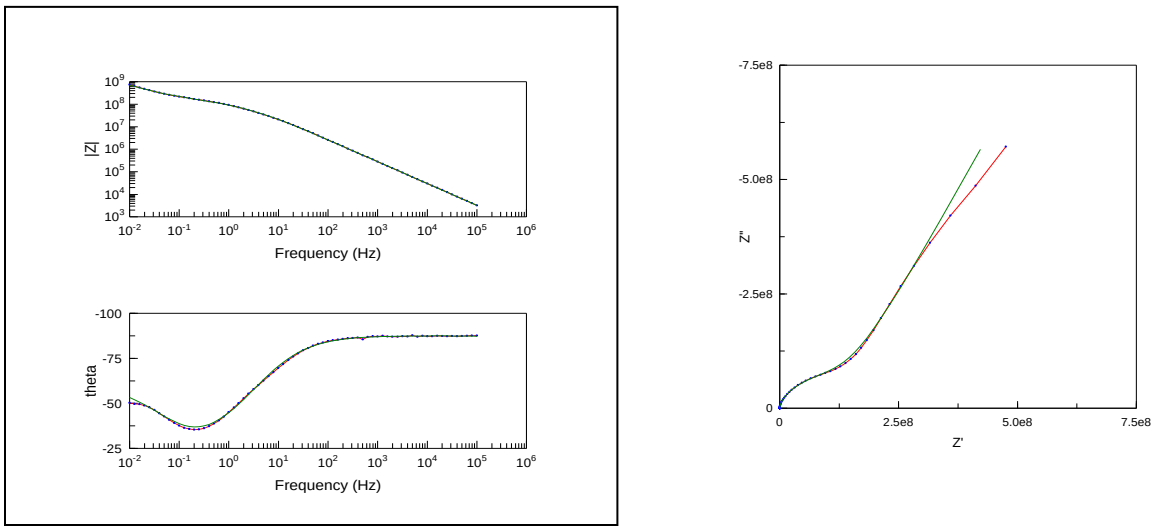

Figure 3.6: Fitted curve to obtained EIS data for 750 hours of exposure of as received Al flake coating (Red line is actual EIS data and green line is fit data).

Table 3.1
Fitted parameters for EIS spectra

Exposure duration/hours	Coating Resistance/Ω	Coating capacitance/F	Warburg resistance/Ω	Chi-sqr
As received Al flake coating				
1	1.09E+09	1.29E-09		0.070
3	7.90E+08	1.43E-09		0.085
5	5.28E+08	1.73E-09		0.080
48	1.72E+09	8.95E-10		0.048
350	2.08E+09	8.55E-10		0.049
750	2.48E+07	7.17E-10	3.49E+08	0.001
Wire PPy/Al flake composite coating				
1	6.74E+03	2.37 E-04		0.131
3	9.25 E+03	2.33 E-04		0.135
5	8.75 E+03	2.41 E-04		0.140
48	2.15 E+03	5.15 E-04		0.121
350	2.97 E+03	7.21 E-04		0.006
750	2.48 E+03	9.75 E-04		0.101
Spherical PPy/Al flake composite coating				
1	6.93 E+03	1.93 E-04		0.111
3	5.05 E+03	2.69 E-04		0.128
5	8.68 E+03	2.39 E-04		0.126
48	1.29 E+03	4.23 E-04		0.085
350	3.48 E+03	6.08 E-04		0.018
750	2.94 E+03	9.17 E-04		0.090

3.4.3. Scanning vibrating electrode technique (SVET)

SVET results for phosphate doped PPy/Al flake coating and nitrate doped PPy/Al flake coating are shown in Figure 3.7 and 3.8, respectively. A well defined scribe at the center of coating emulates a coating defect. Anodic dissolution in the scribe was signified by positive current in the defect. The corresponding cathodic reduction reaction was signified by negative current in the defect. As shown in Figure 3.7, for the phosphate doped PPy/Al flake coating, no cathodic or anodic current was observed in the scribe suggesting very little to no activity or corrosion in the defect for initial 48 hours of immersion in DHS solution. Interestingly, the oxidation and reduction currents were observed elsewhere on the coating rather than on the scribe. This activity can be attributed to the redox nature of PPy. As PPy is already in the oxidized form it tends to be reduced during the galvanic coupling with aluminum flakes and underlying aluminum substrate. This reduced PPy can scavenge oxygen responsible for corrosion reaction which will result in a decrease in the corrosion activity and a re-oxidation of the PPy [34]. The intensity of the currents observed on the surface of the coating was decreasing with the time of the immersion signifying reduced activity of the phosphate doped PPy/Al flake coating.

In the case of the nitrate doped PPy/Al flake coating, initially no activity was observed on the scribe or above the coating as shown in Figure 3.8. In this case, anodic current due to metal dissolution in the defect was observed after 24 hours of immersion in DHS solution. The magnitude of this current was low (ca. 10$\mu A/cm^2$). Most of the cathodic current was distributed over the coating. Even though slight anodic current was observed on the scribe in case of nitrate doped PPy/Al flake coating, the defect was still shiny after 48 hours of immersion in DHS, exhibiting almost no visible corrosion in the defect area (Figure 3.9). Also, in case of the

phosphate doped PPy/Al flake coating, the coating defect was shiny after 48 hours of immersion in the DHS solution.

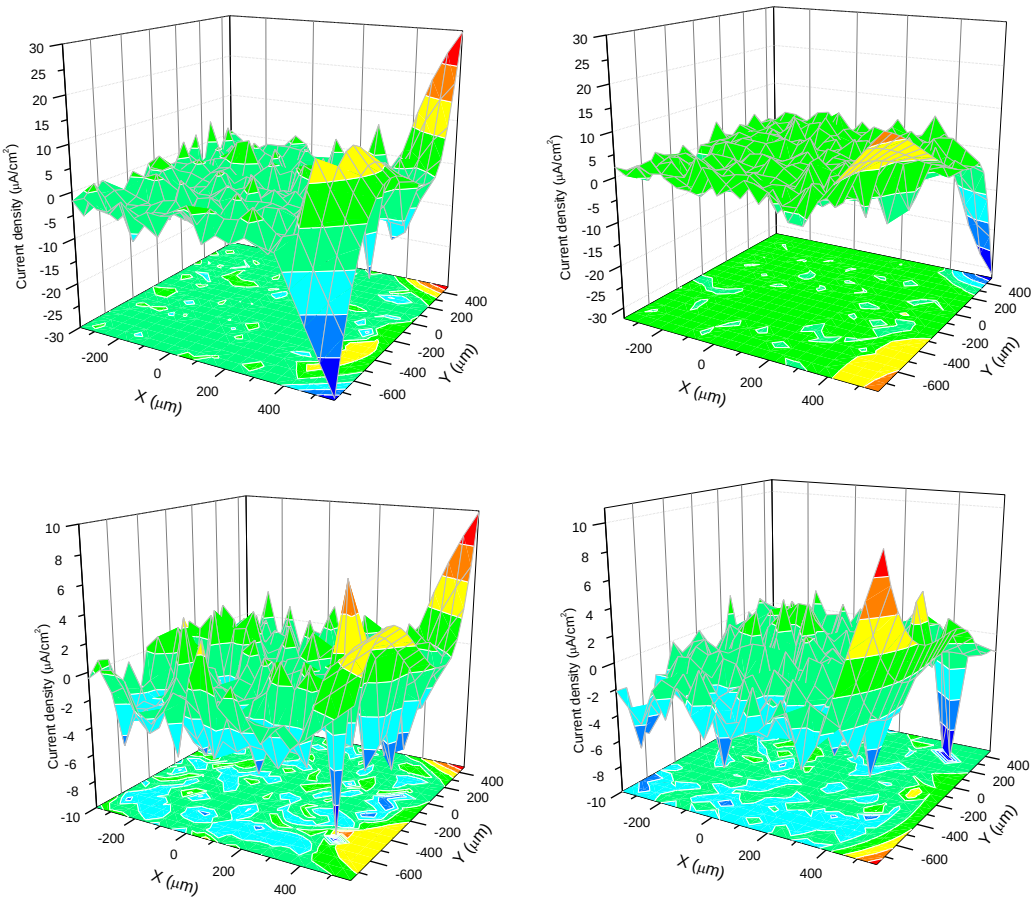

Figure 3.7: SVET current density maps for phosphate doped PPy/Al flake coatings: top-left (initial), top-right (12 hours), bottom-left (24 hours), and bottom-right (48 hours).

3.4.4. Anodic polarization

The results of the anodic polarization experiments are shown in Figure 3.10. A positive shift of almost 400 mV in the potentials for both phosphate doped PPy/Al flake coatings and nitrate doped PPy/Al flake coatings in nitrogen environment suggest the coupling between PPy and aluminum flakes. This coupling was not observed in case of as received aluminum flake coating as it showed more negative potential than phosphate doped PPy/Al flake coating and

nitrate doped PPy/Al flake coating. A more positive potential in case of both phosphate and nitrate doped PPy/Al flake coatings than as received Al flake coatings signify the protective and passivating nature of the doped PPy based coatings. Phosphate and nitrate are corrosion inhibiting anions which might have released in the reduction of PPy resulting in the passivation giving rise to the positive shift in the potential. It is interesting to note that while there was the aforementioned positive shift in potential for the PPy flake coatings, a corresponding decrease in corrosion current was not observed. It is suggested that this is due to the conductive nature of the coating effectively increasing the area under investigation during the experiment. This increase in area could correspond to an increase in measured current.

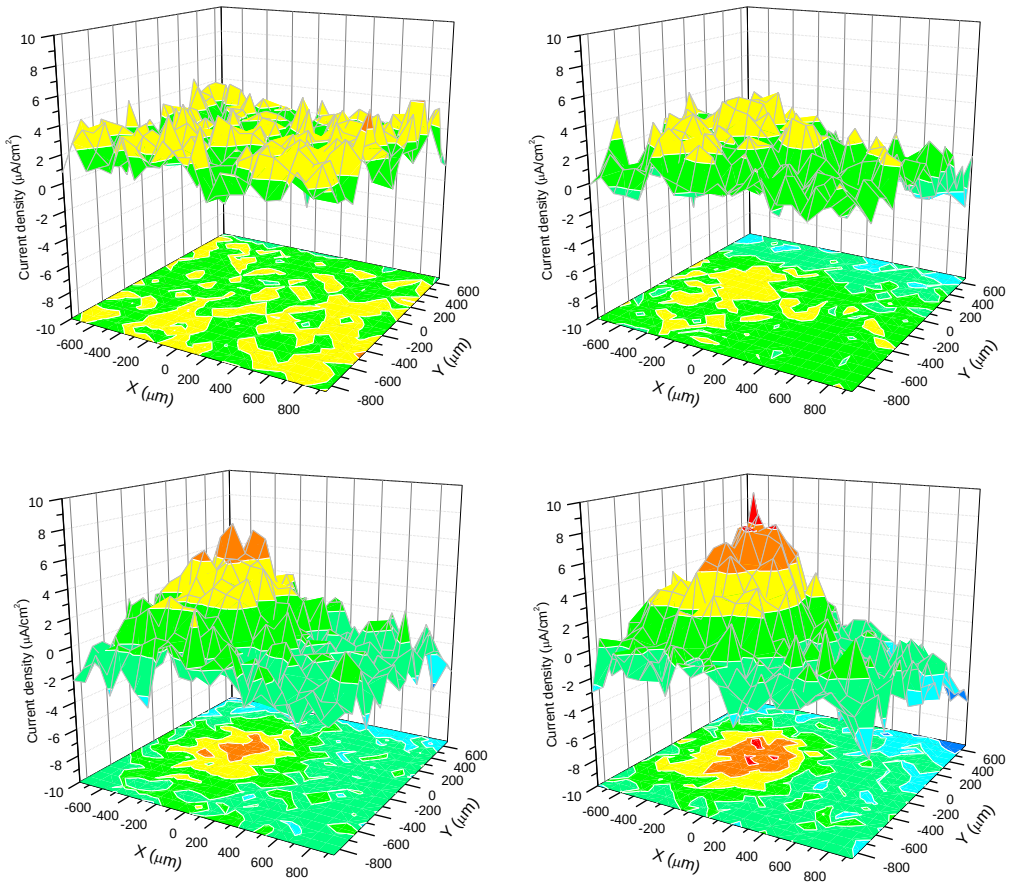

Figure 3.8: SVET current density maps for nitrate doped PPy/Al flake coatings: top-left (initial), top-right (12 hours), bottom-left (24 hours), and bottom-right (48 hours).

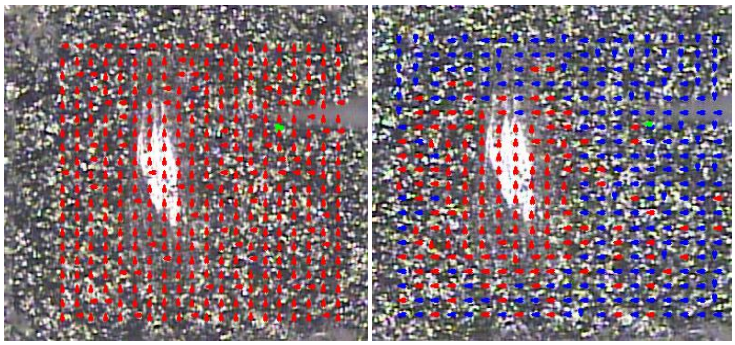

Figure 3.9: Optical image of nitrate doped PPy/Al Flake coating superimposed with current vectors, initial (left image), and 48 hours (right image) immersion in DHS solution.

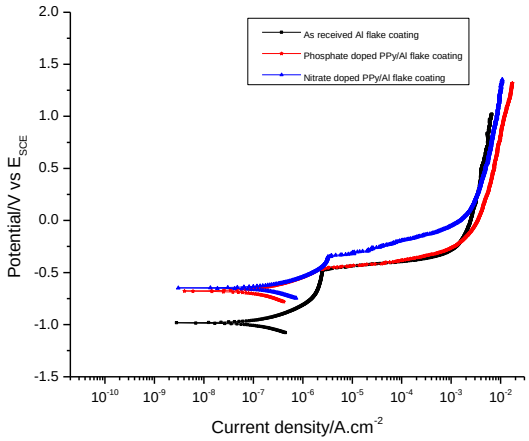

Figure 3.10: Anodic polarization curves in DHS solution in nitrogen environment.

3.4.5. Accelerated salt spray exposure test

After exposure to salt spray for 750 hours, the coated panels were assessed visually for the performance against corrosion. The optical images of exposed panels are shown in Figure 3.11. The as received Al flake coating exhibited blistering along the scribe signifying cathodic detachment underneath the coating, whereas it was not evident in case of phosphate doped PPy/Al flake coating and nitrate doped PPy/Al flake coating. As received Al flake coating is a barrier type coating, as indicated by the EIS results. It is suggested that this barrier allowed for the entrapment of the corrosion product (hydrogen gas) from escaping through the coating which resulted in the blistering. Phosphate doped PPy/Al flake coating and nitrate doped PPy/Al flake

coating are above the percolation threshold and porous in nature due to the porosity in PPy. Possibly, the oxygen scavenging effect of PPy when in its reduced form, coupled with activated aluminum flakes as observed in anodic polarization experiments was responsible for the protective nature exhibited by phosphate doped PPy/Al flake coating and nitrate doped PPy/Al flake coating.

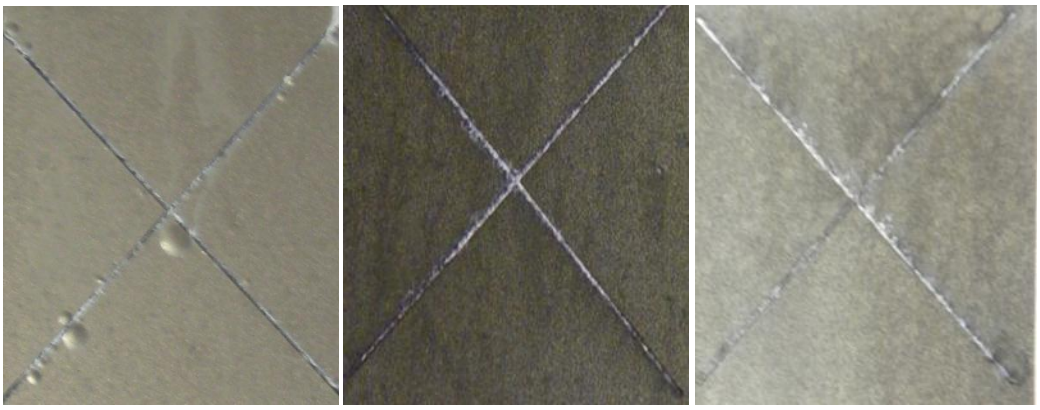

Figure 3.11: Salt spray exposure images (after 750 hours) of as received Al flake coating (left), phosphate doped PPy/Al flake coating (middle), and nitrate doped PPy/Al flake coating (right).

3.5. Conclusion

It was determined during this study that the phosphate and nitrate doped PPy/Al flake coating did not exhibit blistering with exposure to the salt spray for extended duration whereas blistering along the scribe was observed on as received Al flake coating. Additionally, during the anodic polarization experiments, a positive shift in the potential due to passivation was observed for both phosphate and nitrate doped PPy/Al flake coating. Furthermore, the SVET experiments did not find significant cathodic and anodic activity on the scribe suggesting the anticorrosive nature of phosphate and nitrate doped PPy/Al flake coating.

It is suggested that the reduced and neutral form of PPy in the given conditions was responsible for oxygen scavenging effect thereby protecting the substrate. The activation of the aluminum flakes and underlying aluminum substrate as observed in anodic polarization

experiments was responsible for the corrosion protection by phosphate and nitrate doped PPy/Al flake coating. Due to the reduction of PPy, release of corrosion inhibiting anions (phosphate and nitrates) lead to passivation as observed in anodic polarization experiments. Barrier properties of aluminum flakes combined with redox properties of doped PPy lead to superior corrosion protection on the surface of AA 2024-T3.

3.6. Acknowledgements

The authors gratefully acknowledge the support of this research by US Army Research Laboratory under grant no. W911NF-09-2-0014, W911NF-10-2-0082, and W911NF-11-2-0027.

3.7. References

[1] R. Rajagopalan and J.O. Iroh, *Applied Surface Science*, 218 (1-4), 5 (2003).

[2] H. Shirakawa, E.J. Louis, A.G. Macdiarmid, C.K. Chiang, and A.J. Heeger, *Journal of the Chemical Society-Chemical Communications* (16), 578 (1977).

[3] P. Zarras, N. Anderson, C. Webber, D.J. Irvin, J.A. Irvin, Guenthner, and J.D. Stenger-Smith, *Radiation Physics and Chemistry* 68 (3-4), 387 (2003).

[4] S. Zor, F. Kandemirli, E. Yakar, and T. Arslan, *Protection of Metals and Physical Chemistry of Surfaces* 46 (1), 110 (2010).

[5] A.L.P.S. Bailey, A.M. Pisanelli, and K.C. Persaud, *Sensors and Actuators B: Chemical*, 131 (1), 5 (2008).

[6] A. L.Kukla, A.S. Pavluchenko, Y.M. Shirshov, N.V. Konoshchuk, and O.Y. Posudievsky, Sensors *and Actuators B: Chemical* 135 (2), 541 (2009).

[7] U. Lange, N.V. Roznyatovskaya, and V.M. Mirsky, *Analytica Chimica Acta* 614 (1), 1 (2008).

[8] L. Torsi, M. Pezzuto, P. Siciliano, R. Rella, L. Sabbatini, L. Valli, and P. G. Zambonin, *Sensors and Actuators B: Chemical* 48 (1-3), 362 (1998).

[9] T.F. Otero and I. Cantero, Journal *of Power Sources* 81-82 (0), 838 (1999).

[10] S. Toshikatsu, *Journal of Membrane Science* 72 (1), 43 (1992).

[11] N. Kudo, Y. Shimazaki, H. Ohkita, and M. Ohoka, S. Ito, *Solar Energy Materials and Solar Cells* 91 (13), 1243 (2007).

[12] C. Gong, H.B. Yang, Q.L. Song, Z.S. Lu, and C.M. Li, *Solar Energy Materials and Solar Cells* 95 (3), 969 (2011).

[13] D. H.Huh, M. Chae, W.J. Bae, W.H. Jo, and T.W. Lee, Polymer 48 (25), 7236 (2007).

[14] Y. Kaminorz, E. Smela, T. Johansson, L. Brehmer, M.R. Andersson, and O. Inganäs, *Synthetic Metals* 113 (1-2), 103 (2000).

[15] A. Adhikari, P. Claesson, J. Pan, C. Leygraf, A. Dédinaité, and E. Blomberg, *Electrochimica Acta* 53 (12), 4239 (2008).

[16] A.J. Dominis, G.M. Spinks, and G.G. Wallace, Progress *in Organic Coatings* 48 (1), 43 (2003).

[17] P. Ocón, A. B.Cristobal, P. Herrasti, and E. Fatas, *Corrosion Science* 47 (3), 649 (2005).

[18] U. Rammelt, P.T. Nguyen, and W. Plieth, *Electrochimica Acta* 48 (9), 1257 (2003).

[19] K. Saravanan, S. Sathiyanarayanan, S. Muralidharan, and S.S. Azim, G. Venkatachari, *Progress in Organic Coatings* 59 (2), 160 (2007).

[20] Y. Shao, H. Huang, T. Zhang, G. Meng, and F. Wang, *Corrosion Science* 51 (12), 2906 (2009).

[21] C.K. Tan and D.J. Blackwood, *Corrosion Science* 45 (3), 545 (2003).

[22] Y. Wei, J. Wang, X. Jia, J.M. Yeh, and P. Spellane, *Polymer* 36 (23), 4535 (1995).

[23] J. Yano, K. Nakatani, Y. Harima, and A. Kitani, *Materials Letters* 61 (7), 1500 (2007).

[24] M.G. Hosseini, M. Sabouri, and T. Shahrabi, Progress *in Organic Coatings* 60 (3), 178 (2007).

[25] N.V. Krstajić, B.N. Grgur, S.M. Jovanović, and M.V. Vojnović, *Electrochimica Acta* 42 (11), 1685 (1997).

[26] B. Zeybek, N. Özçiçek Pekmez, and E. Kılıç, *Electrochimica Acta* 56 (25), 9277 (2011).

[27] Y.F. Jiang, X.W. Guo, Y.H. Wei, C.Q. Zhai, and W.J. Ding, *Synthetic Metals 139* (2), 335 (2003).

[28] G. Kousik, S. Pitchumani, and N.G. Renganathan, *Progress in Organic Coatings* 43 (4), 286 (2001).

[29] T. Tüken, B. Yazici, and M. Erbil, Progress *in Organic Coatings* 51 (3), 205 (2004).

[30] T. Tüken, B. Yazıcı, and M. Erbil, *Applied Surface Science* 239 (3-4), 398 (2005).

[31] M. Sharifirad, A. Omrani, A.A Rostami, and M. Khoshroo, *Journal of Electroanalytical Chemistry* 645 (2), 149 (2010).

[32] A. Tsirimpis, I. Kartsonakis, I. Danilidis, P. Liatsi, and G. Kordas, Progress *in Organic Coatings* 67 (4), 389 (2010).

[33] M. D. Cohen, B. Kargacin, C. B. Klein, and M. Costa, Critical *Reviews in Toxicology* 23 (3), 255 (1993).

[34] M. Yan, C. A. Vetter,and V. J. Gelling, *Electrochimica Acta* 55 (20), 5576 (2010).

[35] J. He, D. E. Tallman,and G. P. Bierwagen, *Journal of the Electrochemical Society* 151 (12), B644 (2004).

[36] M. Rohwerder, L. M. Duc, and A. Michalik, *Electrochimica Acta* 54 (25), 6075 (2009).

[37] M. Rohwerder and A. Michalik, *Electrochimica Acta* 53 (3), 1300 (2007).

[38] M. Sabouri, T. Shahrabi, H. R. Farid, and M. G. Hosseini, *Progress in Organic Coatings* 64 (4), 429 (2009).

[39] X. Qi, C. Vetter, A. C. Harper, and V. J. Gelling, *Progress in Organic Coatings* 63 (3), 345 (2008).

[40] S. Sathiyanarayanan, S. S. Azim, and G. Venkatachari, *Electrochimica Acta 52* (5), 2068 (2007).

[41] R. C. Patil and S. Radhakrishnan, *Progress in Organic Coatings* 57 (4), 332 (2006).

[42] S. Radhakrishnan, C. R. Siju, D. Mahanta, S. Patil, and G. Madras, *Electrochimica Acta* 54 (4), 1249 (2009).

[43] A. J. Dominis, G. M. Spinks, and G. G. Wallace, *Progress in Organic Coatings* 48 (1), 43 (2003).

[44] S. Sathiyanarayanan, V. Karpakam, K. Kamaraj, S. Muthukrishnan, and G. Venkatachari, *Surface and Coatings Technology* 204 (9-10), 1426 (2010).

[45] I. L. Lehr and S. B. Saidman, *Electrochimica Acta* 51 (16), 3249 (2006).

[46] M. G. Hosseini, M. Sabouri, and T. Shahrabi, *Progress in Organic Coatings* 60 (3), 178 (2007).

[47] J. Unsworth, P.C. Innis, B.A. Lunn, Z. Jin, and G.P. Norton, *Synthetic Metals* 53, 59 (1992).

[48] S.J. Sutton and A.S. Vaughan, *Synthetic Metals* 58, 391 (1993).

[49] G.A. Wood and J.O. Iroh, *Polymer Engineering and Science* 36, 2389 (1996).

[50] J. Ouyang and Y. Li, *Polymer* 38, 1971 (1997).

[51] D.S. Maddison and J. Unsworth, *Synthetic Metals* 30, 47 (1989).

[52] O.A. Semenikhin, L. Jiang, T. Iyoda, K. Hashimoto, and A. Fujishima, *Electrochimica Acta* 42, 3321 (1997).

[53] M.-L. Abel, J.-L. Camalet, M.M. Chehimi, J.F. Watts, and P.A. Zhdan, *Synthetic Metals* 81, 23 (1996).

[54] B. R. Hinderliter, S. G. Croll, D. E. Tallman, Q. Su, and G. P. Bierwagen, *Electrochimica Acta* 51 (21), 4505 (2006).

[55] C. G. Oliveira and M. G. S. Ferreira, *Corrosion Science* 45 (1), 139 (2003).

[56] Q. Le Thu, G. P. Bierwagen, and S. Touzain, Progress *in Organic Coatings* 42 (3-4), 179 (2001).

[57] V. Barranco, S. Feliu Jr, and S. Feliu, *Corrosion Science* 46 (9), 2203 (2004).

[58] S. Skale, V. Doleček, and M. Slemnik, *Corrosion Science* 49 (3), 1045 (2007).

[59] M. Nematollahi, M. Heidarian, M. Peikari, S. M. Kassiriha, N. Arianpouya, and M. Esmaeilpour, *Corrosion Science* 52 (5), 1809 (2010).

[60] A. C. Balaskas, I. A. Kartsonakis, G. Kordas, A. M. Cabral, and P. J. Morais, *Progress in Organic Coatings* 71 (2), 181 (2011).

[61] V. T. Truong, P. K. Lai, B. T. Moore, R. F. Muscat, and M. S. Russo, *Synthetic Metals* 110 (1), 7 (2000).

CHAPTER 4. TUNGSTATE AND VANADATE DOPED PPY/AL FLAKE COMPOSITES FOR THE CORROSION PROTECTION OF ALUMINUM 2024-T3

(Published in Proceedings of CoatingsTech Conference, American Coatings Association, Rosemont, Illinois, March 11-13, 2013)

4.1. Abstract

Conducting polymers (CPs), such as polypyrrole (PPy), can be used for the corrosion protection of the metals. Their redox activity, in conjunction with the corrosion inhibiting ion release ability, suggests CPs as a promising candidate for the replacement for hexavalent chromates. However their porous nature, inherent insolubility, stiff chains, and poor mechanical properties pose a significant hindrance towards their implementation in coatings. In order to overcome the problems associated with the CPs, and to extract maximum functionality, conducting polymer containing composites (CPCCs) were developed. CPCCs combines CPs with inorganic pigments in unique ways leading to excellent properties. In this work, PPy doped with Tungstate and Vanadate as counter anions were synthesized by chemical oxidative polymerization on the surface of aluminum flakes. This resulted in the deposition of PPy on the surface of the aluminum flakes. The composite pigments were characterized by Scanning Electron Microscopy (SEM), Energy Dispersive Spectroscopy (EDS), Conductive-Atomic Force Microscopy (C-AFM), Four point probe conductivity, and X-ray Photoelectron Spectroscopy (XPS). Furthermore these composites were incorporated in an epoxy-amide binder system in order to formulate a primer for an aluminum 2024-T3 substrate. The coatings were exposed to the Prohesion test conditions and corrosion resistance properties were monitored by Electrochemical Impedance Spectroscopy (EIS), DC Polarization, and galvanic coupling measurements. It was found that the doped PPy/Al flake coatings provided sacrificial protection

to the underlying aluminum 2024-T3 substrate. Additionally the release of dopants from PPy backbone resulted in the passivation in the defect areas improving the corrosion protection ability.

4.2. Introduction

Corrosion is a thermodynamically favored process which primarily involves conversion of metal to its original oxide form and is often described as extractive metallurgy in reverse [1-2]. Coatings are one of the oldest form of corrosion control for the metals and their alloys [3]. Barrier, inhibitors, and cathodic protection are some of the important mechanisms which are employed in coatings to combat against corrosion [4]. In modern times, the motivation behind the development of improved corrosion resistance coatings involves factors such as improved efficiency through multi-functionality, increased service times, ability to combat changing environmental conditions, and eco-friendly approaches. Well known corrosion inhibitors such as hexavalent chromates are being banned due to their toxicity [5-6], so environmental friendly and nontoxic alternatives are the focus of current research activities.

Conducting polymers (CPs) are a new class of materials which are the subject of great interest over the last four decades [7-10]. CPs posses several attractive properties including electrical conductivity [11], good thermal stability [12], oxidative and catalytic nature, non-toxicity, and easy synthesis by both chemical and electrochemical oxidative methods [13]. CPs are employed in variety of applications such as sensors and electrochemical devices [14-15], actuators[16], capacitors [17], batteries [18-19], light emitting diodes [20-21], control release devices [22-23], solar cells [24], radar and electromagnetic interference shielding [25-26], and corrosion protection of metals and their alloys[27-35].

Polyaniline (PAni), polypyrrole (PPy), polythiophene (PT), and their respective derivatives are important CPs which have exhibited promise towards mitigating corrosion [28-29, 36]. Among these, PPy is the most promising candidate for corrosion protection owing to its good conductivity, high environmental stability in its oxidized form, and low toxicity of pyrrole monomer [37]. However, PPy is insoluble in commonly used solvents in the coatings industry [38]. This insolubility coupled with its porosity, infusibility, poor mechanical properties, and insufficient adhesion leads to difficulty in processing and application in coatings [39]. In order to overcome these problems several strategies have been employed. First approach includes chemical structural modifications of the pyrrole monomer in order to alleviate solubility problems [40-41]. The second avenue investigated was the modification of PPy properties by incorporation of dopant counterion on its backbone [42-43]. The third strategy used was synthesizing a composite pigment of PPy and an inorganic flake, such as aluminum flake, for overcoming the shortcomings of PPy application in the coatings [38, 44]. In the current study, the combination of second and third strategy is employed, which involves not only an incorporation of corrosion inhibiting dopant anions on the backbone of PPy but also the deposition of this doped PPy on the surface of aluminum flake to form composite pigment. PPy doped with tungstate anion has been previously electropolymerized on carbon steel [45]. The results indicated that the tungstate anion participated in stable oxide layer formation resulting in improvement in corrosion resistance of carbon steel. The tungstate anion participated in a passivation process thereby forming primary passive layer [46]. Tungstate doped PPy has been also electropolymerized on the surface of aluminum 1100 with increased corrosion resistance. The improvement in corrosion protection was attributed to adsorption of tungstate anions at the defects and formation of passive film [12]. Vanadate has been shown corrosion

inhibition on aluminum 2024-T3 by forming adsorbed layer on its surface [47]. Vanadate adsorption, furthermore, reduced the oxygen reduction rate by blocking the sites for reduction. Composites of CPs with other materials (montmorillonite, carbon nanotubes, titanium dioxide, flakes, zinc, zinc oxide, etc.) have been synthesized and utilized for the corrosion protection of metals and metal alloys [48-52]. The functional properties and specific morphology of these materials exercise additional protection mechanism. For example, the platelet nature of flakes can result in the lengthening of the path for corrosive ions. The majority of the research found is literature for synthesizing doped CPs and composites have employed the electrochemical polymerization method. Whereas, in the current research, a chemical oxidative polymerization is used in which large scale synthesis of composite pigment is possible [44]. This composite pigment can be handled easily on industrial level for its application into the coatings.

Several mechanisms have been proposed for the corrosion protection by CPs for metals and their alloys. These include anodic passivation, surface ennobling, mediation of oxygen reduction, cathodic protection, barrier protection after initial galvanic coupling, and an intelligent dopant release mechanism [28-29, 53-55]. The efficacy of corrosion protection depends on application conditions including substrate preparation, type of substrate (aluminum or steel), methods of application, and different conductive forms of CPs [38, 56]. In the present work, a corrosion inhibiting dopant release mechanism, galvanic contact of PPy with aluminum flakes, and barrier protection resulting from the lamellar nature of aluminum flakes is suggested to provide the corrosion inhibition.

In this chapter, tungstate and vanadate doped PPy was synthesized on the surface of aluminum flakes by employing water a reaction medium. The composite pigments were investigated for morphology by SEM, for elemental composition by EDS and XPS, for

conductivity by CAFM and four point probe method, and for composition by FTIR. The corrosion protection properties of the formulated coatings with epoxy-amide binder system and applied on aluminum 2024-T3 substrate were evaluated by EIS, DC Polarization technique, and galvanic coupling measurements with the concomitant exposure to the Prohesion test conditions (ASTM G85-A5).

4.3. Experimental work

4.3.1. Materials

Aluminum (Al) flakes (Stapa Aloxal® PM 2010) were generously supplied by Eckart America. Sodium tungstate dihydrate and sodium metavanadate were procured from MP Biomedicals, LLC, and Strem chemicals respectively. Pyrrole was distilled prior to use and was obtained from Alfa Aesar Co. Ammonium persulfate (APS) was purchased from EMD chemicals Inc. Solvent used in the composite synthesis was 18.2 MΩ Millipore water. Epoxy resin, EPON 828 and polyamide curing agent, EPIKURE 3175 were obtained from Momentive Specialty Chemicals Inc. Coating solvent methyl ethyl ketone (MEK) was procured from Alfa Aesar Co. Aluminum 2024-T3 (0.063”x6”x3”) panels were obtained from Q-Panel Lab Products.

4.3.2. Synthesis of PPy/Al flake composite pigment

The quantities of chemicals used in the in the synthesis of PPy/Al flake composite pigment are outlined in Table 4.1. For the synthesis water was added to the Erlenmeyer flask followed by the addition of respective amounts of dopants as indicated in Table 4.1. After complete dissolution of the dopant salts, Al flakes were added. Dispersion of Al flakes in the reaction mixture followed the addition of APS. After complete dissolution of APS, pyrrole was added to the reaction mixture. The reaction was continued at ambient temperature under continuous mixing with magnetic stirrer. After 24 hours, the reaction mixture was filtered and

washed with copious amount of water. The product retained on filter paper was dried overnight in oven at 60°C. Finally, dried product was milled with the help of mortar and pestle and sieved through the sieve #400 (having 38 µm of opening diameter) and was stored in plastic vials at ambient conditions.

Acronyms were labeled for tungstate doped (0.1M) PPy/Al flake composite, Tungstate doped (0.01M) PPy/Al flake composite, vanadate doped (0.1M) PPy/Al flake composite, vanadate doped (0.01M) PPy/Al flake composite as CPCCW0.1, CPCCW0.01, CPCCV0.1, and CPCCV0.01 respectively.

Table 4.1
Synthesis reactions for PPy/Al flake composite pigment

	CPCCW0.1	CPCCW0.01	CPCCV0.1	CPCCV0.01
Water	500 ml	500 ml	500 ml	500 ml
Sodium tungstate dihydrate	9.15 grams	0.915 grams	-	-
sodium metavanadate	-	-	6.05 grams	0.605 grams
Al flakes	15 grams	15 grams	15 grams	15 grams
APS	11.4 grams	11.4 grams	11.4 grams	11.4 grams
Pyrrole	6.95 ml	6.95 ml	6.95 ml	6.95 ml

4.3.3. Coatings preparation

To prepare substrate for coating, sandblasting with 100 µm alumina grit was performed on the aluminum 2024-T3. The panels were then degreased with hexane. In order to achieve conducting primer, coatings were formulated at 20% pigment volume concentration (PVC) with epoxy resin, EPON 828 and polyamide curing agent, EPIKURE 3175. Stoichiometric ratio of 1:1 of epoxy resin to the hardener was used. Five different formulations were prepared: as received Al flakes, CPCCW0.1, CPCCW0.01, CPCCV0.1, and CPCCV0.01. The composite pigments were mixed with the epoxy resin followed by the hardener addition. MEK was added as a

solvent. A drawdown bar with 8 mils of wet film thickness was employed for coatings application. Coatings were cured at 80°C for 2 hours in oven followed by 8 days of ambient temperature curing for complete development of performance properties. The topcoat was also applied with similar application and curing conditions.

4.3.4. Composite characterization

Morphological studies of the synthesized composites and as received Al flakes were performed by JEOL JSM-6490LV SEM. For the sample preparation of SEM, powdered material under investigation was sprinkled over carbon tape attached to aluminum mount. Then it was covered with gold coating sputtered with Balzers SCD 030 sputter coater. For the ease of analysis, the magnification, accelerating voltage employed, and scale bars are listed on each micrograph later in this paper in the figures. NORAN System Six II system comprising a high-performance liquid-nitrogen-cooled energy-dispersive X-ray detector along with controlling software on a dedicated computer was employed for EDS analysis.

FTIR characterization was performed by employing NICOLET 8700 spectrophotometer from Thermo scientific. Prior to the analysis, all composite samples were ground fine with mortar and pestle and were mixed with KBr to make pallets for FTIR. To obtain the surface morphology and surface current density CAFM analysis was performed by employing a Veeco Dimension 3100 atomic force microscope in contact mode and with a current sensing probe. For CAFM measurements platinum-iridium (Pt/Ir) coated cantilevers were employed. For all the CAFM experiments, between sample and substrate 200mV DC bias voltage was applied. Conductivity measurements were performed with a four-point probe instrument consisting of a Keithley®2000 multimeter, a Keithley® 220 programmable current source, and Signatone® probes. The XPS measurements were performed on an SSX-100 system (Surface Science

Laboratories, Inc.) with a monochromated Al K_α X-ray source, a hemispherical sector analyzer (HSA) and a resistive anode detector. For the measurements, the base pressure was 3.0 x 10-10 Torr. For the data collection, the pressure was ca. 1.0 x 10-8 Torr. For analysis each sample was mounted separately on a sample holder using a piece of double-sized carbon tape. The X-ray spot size used for measurements was 1 x 1 mm^2, which in turn corresponded to an X-ray power of 200 W. The collection of the survey spectra was done using 12-14 scans at 150 eV pass energy and 1 eV/step. For the collection of the high resolution spectra, 50 eV pass energy and 0.1 eV/step was employed.

4.3.4. Coating characterization

Coatings prepared with CPCC were characterized by EIS measurements. For EIS, a Gamry Instruments R600 Potentiostat/Galvanostat/ZRA with Gamry Framework Version 5.58/EIS 300 software was employed with 10 mV of AC signal amplitude with 10 points/decade over 100,000 to 0.01Hz frequency range. Potentiodynamic experiments were performed on coated panels with defect of 1mm in width and 1.5 cm in length. EIS and potentiodynamic experiments were performed in three electrode cell with coated substrate as a working electrode, platinum mesh as a counter electrode, and saturated calomel as a reference electrode. The electrolyte used in EIS and potentiodynamic experiments was dilute Harrison's solution (DHS, 0.35% ammonium sulfate and 0.05% sodium chloride). Galvanic coupling experiments were performed in enclosed cell with two compartments connected with salt bridge. One compartment contained aluminum 2024-T3 panel whereas the other compartment was coated sample. The working areas of samples in both compartments was 1 cm^2 resulting in area ratio of 1. Experiments were performed in DHS solution and aluminum 2024-T3 panel compartment was bubbled with air whereas coated panel compartment was bubbled with nitrogen to stimulate

topcoated conditions. A Gamry Reference 600 Potentiostat was employed for galvanic coupling experiments in zero resistance ammeter (ZRA) mode and the coupling current and mixed potential values were measured between aluminum 2024-T3 paned and coated panel. Both primer and topcoated samples of coatings were exposed to Prohesion test conditions according to ASTM G85-A5. According to ASTM G85-A5, DHS mist is sprayed for an hour at 25˚C followed by an hour of a dry stage at 35°C in prohesion test chamber. EIS measurements were performed in triplicates whereas potentiodynamic and galvanic coupling experiments were performed in duplicates. The data reported is for the representative sample.

4.4. Results and discussion

4.4.1. Fourier transform infrared spectroscopy (FTIR)

The FTIR spectra of CPCCW0.1, CPCCW0.01, CPCCV0.1, and CPCCV0.01 are presented in Figure 4.1. Peak positions (cm^{-1}) and FTIR modes of vibrations are identified in Table 4.2. In the composites, N-H stretching was observed around 3400 cm^{-1} [57]. Due to the surrounding environment, in case of tungstate doped composite, this peak was broader due to the increased solubility of sodium tungstate dihydrate which lead to probable hydrogen bonding due to water molecules adsorption [58]. The band at 3100 cm^{-1} was observed due to the C-H bond aromatic stretching. The band around 1702 cm^{-1} was observed due to the formation of carbonyl group either due to the nucleophillic attack by water leading to chain terminations or due to the overoxidation [59]. The peak at 1702 cm^{-1} was not prominent in all of the four composite samples, suggesting minimal overoxidation and little loss in conjugation along the polypyrrole chain. The band at 1558 cm^{-1} represents ring stretching vibrations due to C-C and C=C bonds [58]. In case of the CPCCW0.1 and CPCCW0.01; this band was slightly red shifted at 1556 cm^{-1} and 1555 cm^{-1} respectively. Whereas in case of CPCCV0.1, and CPCCV0.01, this band was blue

shifted at 1569 cm^{-1} and 1566 cm^{-1} respectively. Delocalized π-electrons involving vibrations exhibit changes due to the doping and these observed shifts in this band might due to the varying degree of doping which might have been influenced by amount of dopant and nature of dopant [60-61].

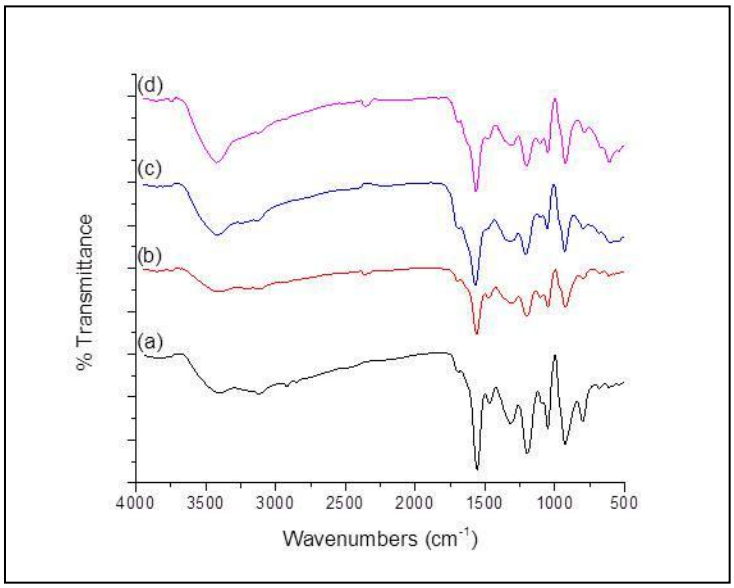

Figure 4.1: FTIR spectra of (a) CPCCW0.1, (b) CPCCW0.01, (c) CPCCV0.1, and (d) CPCCV0.01.

A combination of C-N and C=C bond stretching was observed at 1464 cm^{-1}. The band at 1464 cm^{-1} was not so prominent in the case of the CPCCV0.1 and CPCCV0.01 as compared to CPCCW0.1 and CPCCW0.01. An approximate conjugation length can be calculated by taking the ratio of intensities at 1465 and 1561 cm^{-1}[57-58, 62]. The band at 1295 cm^{-1} was observed due to the C-H and C-N in plane deformation [58, 63]. The shift in this band was observed for the doped composite samples. The band at 1198 cm^{-1} was attributed to ring breathing, as well as the band at 1090 cm^{-1} was from C-C in plane vibration, and the band at 1045 cm^{-1} was observed due to C-H deformation. These are characteristic band vibrations of PPy, including bands at 929 and 788 cm^{-1}.

Table 4.2
Peak positions (cm^{-1}) and FTIR modes of vibrations for CPCCW0.1, CPCCW0.01, CPCCV0.1, and CPCCV0.01

Wavenumbers (cm^{-1}) and modes of vibration	CPCCW0.1 (Wavenumber (cm^{-1}))	CPCCW0.01 (Wavenumber (cm^{-1}))	CPCCV0.1 (Wavenumber (cm^{-1}))	CPCCV0.01 (Wavenumber (cm^{-1}))
3400, N-H stretching	3398	3408	3421	3422
3100, C-H aromatic stretching	3118	3120	3100	3120
1702, carbonyl group	1700	1700	1698	1720
1558, C-C and C=C ring stretching	1556	1555	1569	1566
1464, C-N and C=C stretching	1470	1472	1463	1470
1295, C-H and C-N in plane deformation	1318	1311	1311	1311
1198, ring breathing	1197	1202	1209	1203
1090, C-C in plane deformation	1100	1102	1099	1099
1045, C-H deformation	1050	1049	1055	1050
929 and 788 PPy characteristic peak, 960-780 and 900-770 tungstate ion band, 1010-920 and 890-830 vanadate ion band, 750-490 Al-O stretching vibration	928, 801, 700, 680	926, 789, 675,613	429,789,681,600	926, 789, 672, 610
490 weak tungstate ion band	490	490,437	-	-
540-490 vanadate ion band	-	-	550	540

Regions of 960-780 cm^{-1} and 900-770 cm^{-1} for tungstate ion band in case of CPCCW0.1 and CPCCW0.01 were observed, whereas regions of 1010-920 cm^{-1} and 890-830 cm^{-1} for vanadate ion band were observed for CPCCV0.1 and CPCCV0.01. The region, 750-490 cm^{-1} was attributed for Al-O stretching vibration [64]. Also a weak tungstate ion band was observed at 490 cm^{-1} for CPCCW0.1 and for CPCCW0.01. Vanadate ion band was observed in 550 cm^{-1} and

at 540 cm^{-1} was for CPCCV0.1, and CPCCV0.01 respectively. The results obtained from FTIR indicate the presence of tungstate in tungstate doped PPy/Al flake composites and presence of vanadate in vanadate doped PPy/Al flake composites.

4.4.2. Scanning electron microscopy (SEM)

For the morphological investigations, SEM was performed on all CPCC samples. SEM micrographs of as received Al flakes, CPCCW0.1, CPCCW0.01, CPCCV0.1, and CPCCV0.01 are shown in Figure 4.2. For all of the micrographs, 5000X magnification, 15 kV accelerating voltage, and 1 μm scale bar were employed and are mentioned on respective micrographs (Figure 4.2). For the as received Al flakes (Figure 4.2(a)), a clear and smooth morphology was exhibited. For CPCCW0.1 (Figure 4.2(b)), spherical particles of PPy were found to be deposited on the surface of aluminum flakes. The distribution of PPy formation on the surface of aluminum flakes was dense. For CPCCW0.01 (Figure 4.2(c)), spherical PPy particles and circular wire formation of PPy was observed. For CPCCV0.1 (Figure 4.2(d)), spherical particles of PPy were formed on the surface of aluminum flakes whereas in case of CPCCV0.01 (Figure 4.2(e)), along with spherical particles of PPy wires of PPy were also formed.

It has been reported that the final surface morphology, mechanical and electrical properties are directly influenced by parameters employed in the synthesis of PPy [64-66]. The presence of dopants in the synthesis of PPy influences the morphology of resultant product [60]. The nature of dopants also influences the conductivity, mechanical properties and morphology of PPy [67-68]. Polyhydroxyl sulfonate has been used as a dopant for the synthesis of PPy. It was found that as the concentration of the dopant was increased in the synthesis, size of resultant PPy decreased [69]. Morphologies such as rings, frames, and platelets were obtained for PPy in presence of different flurosurfactants and β-naphthalenesulfonic acid [70].

Dodecylbenzenesulfonate doped PPy exhibited compact and globular morphology [60]. Also presence of dopant influences the rate of pyrrole oxidation resulting in different morphology [71]. Lowering the concentration of dopant from 0.1M to 0.01M in both tungstate and vanadate doped PPy/Al flake composite resulted into the formation of wires of PPy along with spherical particles on the surface of aluminum flakes. It is hypothesized that the effect of reduced concentration of dopant influences the rate of pyrrole polymerization and pyrrole nucleation for the polymerization resulting in different morphology.

4.4.3. Energy dispersive spectroscopy (EDS)

For elemental composition, EDS analysis was performed at two different points on same sample. According to product data sheet of as received aluminum flakes, it has a composition of 55-80% aluminum, 24-45% 1-methoxy-2-propanol, and up to 1% of proprietary phosphonic acid with undisclosed additive. There is presence of aluminum oxide layer on the surface of flakes. As observed in Figure 4.3, the as received aluminum flakes showed presence of carbon from 1-methoxy-2-propanol and oxygen from aluminum oxide and aluminum. Along with carbon, oxygen and aluminum; nitrogen, sulfur, and tungsten were also observed for CPCCW0.1 (Figure 4.4). These two areas were specifically selected with one having highly dense PPy and another area with less dense PPy.

As observed in Figure 4.4, area 2 (less dense PPy area) exhibited lower amount of nitrogen and tungsten where as it showed higher amount of aluminum. Even though PPy is not observed in this area (Figure 4.4) but it is present if the image is reformed at higher magnifications. Presence of nitrogen in area 2 also proves formation of PPy.

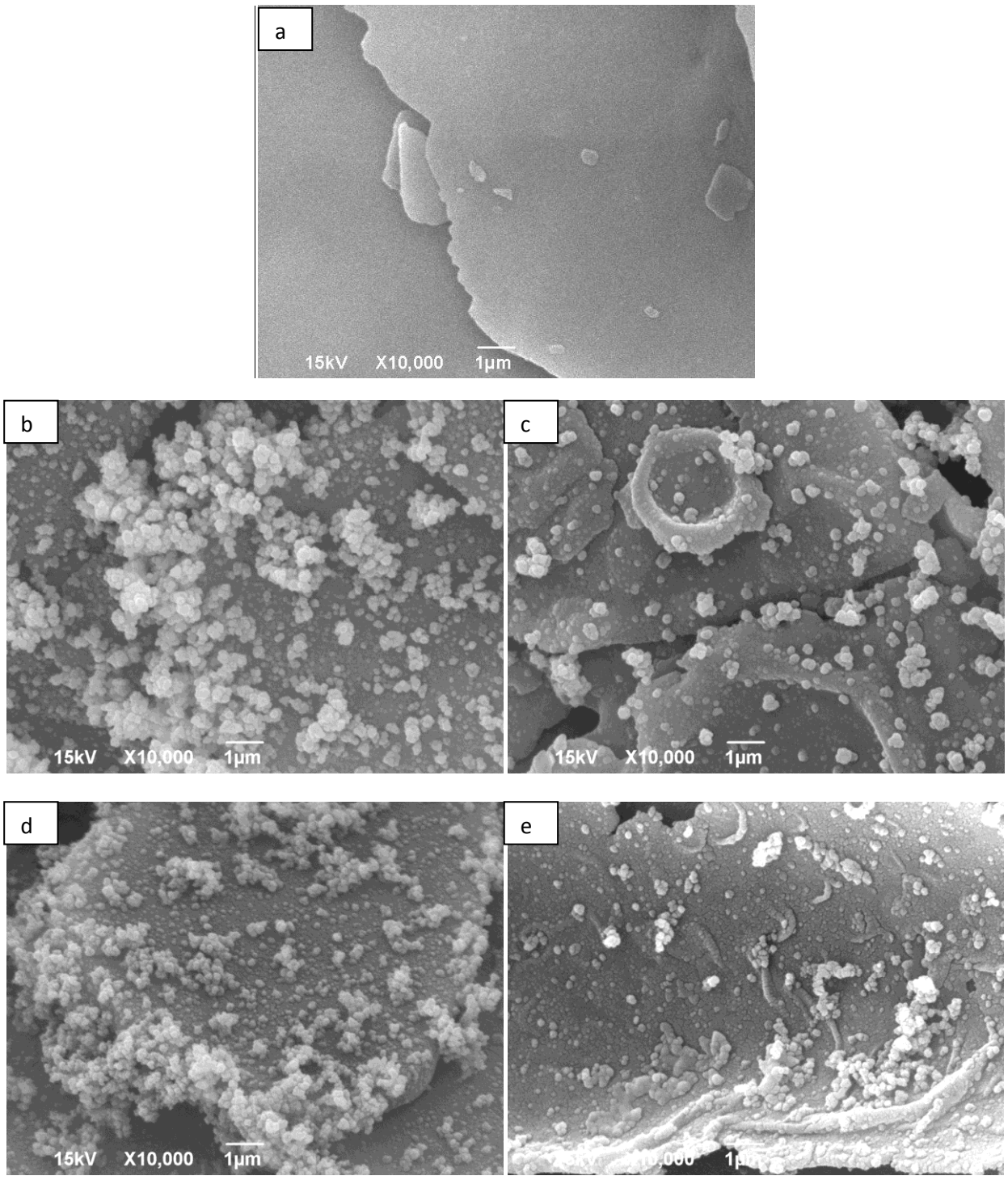

Figure 4.2: SEM micrographs of (a) as received Al flakes, (b) CPCCW0.1, (c) CPCCW0.01, (d) CPCCV0.1, and (e) CPCCV0.01.

For CPCCW0.01 (Figure 4.5), area 1 is on PPy wire and area 2 is on a flake. In this case lower amount of tungsten was observed as compared to CPCCW0.1. This may be due to the

lower concentration of tungsten dopant employed in the synthesis resulting in lower doping. In this case, on the wire PPy (area 1), significant amount of nitrogen was also observed confirming the wires made up of PPy.

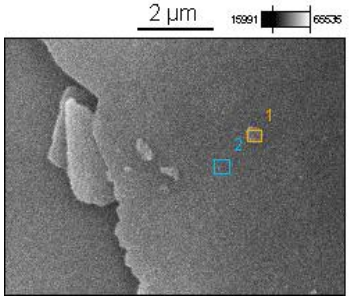

	C-K	O-K	Al-K
Area 1	33.36	19.68	46.96
Area 2	31.66	21.56	46.78

Figure 4.3: EDS of as received Al flakes.

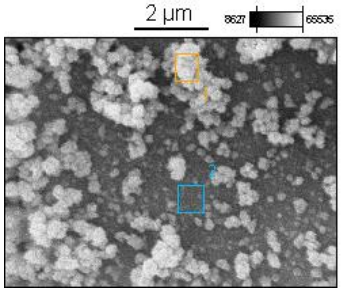

	C-K	N-K	O-K	Al-K	S-K	Cu-K	W-M
Area 1	61.33	10.68	11.19	15.42	0.20		1.18
Area 2	59.80	7.62	10.24	21.10		0.29	0.95

Figure 4.4: EDS of CPCCW0.1.

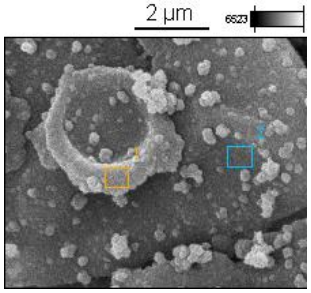

	C-K	N-K	O-K	Al-K	S-K	W-M
Area 1	58.53	11.20	16.40	13.37	0.37	0.15
Area2	56.02	8.72	14.56	20.62		0.09

Figure 4.5: EDS of CPCCW0.01.

For CPCCV0.1 (Figure 4.6), both areas 1 (less dense PPy) and 2 (more dense PPy) exhibited presence of vanadium confirming doping of PPy along with nitrogen, oxygen, carbon, and aluminum. For CPCCV0.01 (Figure 4.7), both areas 1 (less dense PPy) and 2 (more dense PPy) exhibited presence of vanadium but doping was lower than that in CPCCV0.1. In this case

of CPCCV0.01, sulfur doping was also observed along with vanadium. Lower concentration of vanadium dopant has to compete with sulfur from oxidant APS in the reaction.

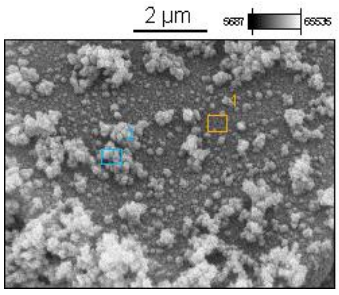

	C-K	N-K	O-K	Al-K	V-K
Area 1	55.79	9.15	10.30	24.42	0.34
Area 2	58.90	9.84	8.89	22.10	0.27

Figure 4.6: EDS of CPCCV0.1.

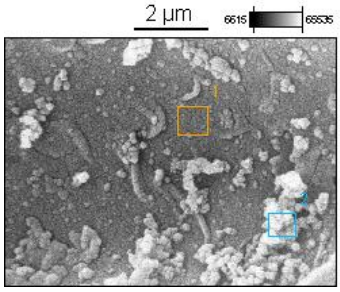

	C-K	N-K	O-K	Al-K	S-K	V-K
Area 1	51.54	8.02	23.99	15.47	0.75	0.23
Area 2	56.44	8.25	22.26	12.14	0.71	0.20

Figure 4.7: EDS of CPCCV0.01.

4.4.4. Conductivity

Topography, deflection and current images were obtained from CAFM experiments. Pellets of the composite sample and as received Al flakes were made in pellet presser from International Crystal Laboratories and were glued to an aluminum mount; the silver epoxy was used for CAFM studies. As received Al flakes did not show any current density on the current image as observed in Figure 4.8. Lack of conductivity in case of as received Al flakes could be attributed to the presence of aluminum oxide layer on the surface of aluminum flakes. Topography image for as received Al flake (Figure 4.8) also exhibited similar neat and pristine morphology as shown in SEM micrographs (Figure 4.2(a)). All of the CPCC samples namely

CPCCW0.1, CPCCW0.01, CPCCV0.1, and CPCCV0.01 displayed current density on current image as seen in Figure 4.9, 4.10, 4.11, and 4.12 respectively.

Four point probe conductivity method was employed for the quantitative measurement of the conductivity. Pellets prepared for CAFM experiments were used in four point probe conductivity measurements. The conductivity values were calculated by using equation 4.1.

$$\sigma = \left(\frac{\ln 2}{\pi t}\right).(I/V) \tag{4.1}$$

Here t, I, and V are thickness, current, and voltage respectively. Conductivity results obtained from four point probe method are displayed in Figure 13. Both tungstate doped composites (0.1M and 0.01M) have comparable conductivities whereas CPCCV0.01 showed an order of higher magnitude in conductivity than CPCCV0.1. A similar observation was found in the CAFM results as well. The current density observed in the case of the CPCCV0.01 (Figure 4.12) was higher than that of the CPCCV0.1 (Figure 4.11). The higher conductivity can be attributed to the doping due to both sulfur and vanadate, in case of CPCCV0.01 (EDS result in Figure 4.7) as against only of vanadate in case of CPCCV0.1 (EDS results in Figure 4.6). As observed in Figure 4.13, the conductivity of the vanadate doped composites was lower than that of tungstate doped composite. This could be due to the differences in the solubility of dopants in the reaction medium (water) at near ambient temperatures. Sodium metavanadate solubility in water at 25°C is 210 grams per liter of water whereas for sodium tungstate dihydrate it is 730 grams per liter of water at 20°C. Poor solubility in the reaction medium results in a smaller amount of incorporation of the vanadate dopant in the PPy backbone resulting in reduced conductivity. Polarons and bipolarons produced for the charge compensation of incorporated dopant anions results into the higher conductivities for the doped PPy [72-74]. There is possibility of formation of varied amounts of polarons and bipolarons in case of the different

CPCC. CPCC (tungstate and vanadate doped PPy composites) are the combination of inorganic aluminum flakes and PPy. Presence of inorganic flake could be also influencing the conductivity of the composite. It has been found that the presence of inorganic pigment titanium dioxide (TiO_2) resulted in decrease in conductivity after 20% by weight concentration in dodecylbezenesulfonate doped PPy- TiO_2 composite [75]. So presence of second component apart from CPs results in the changes in conductivity of CPCCs.

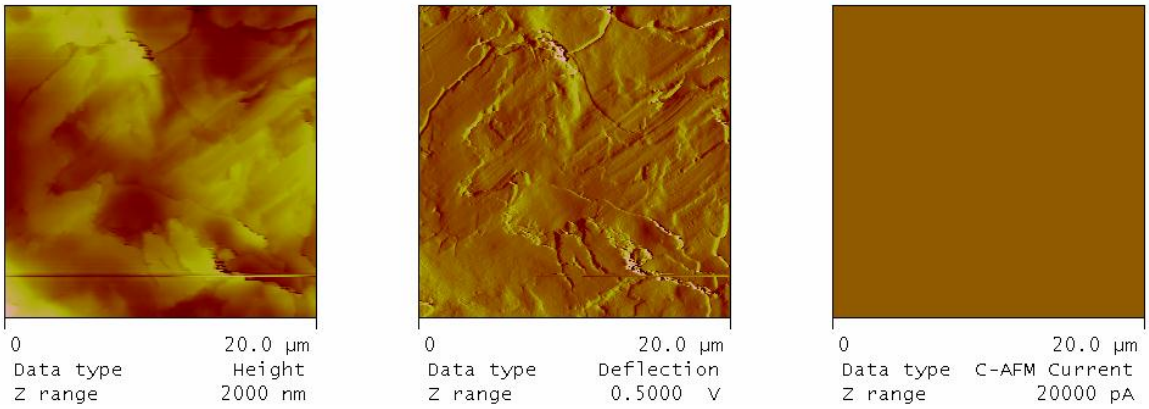

Figure 4.8: Height, deflection, and current images for as received Al flake.

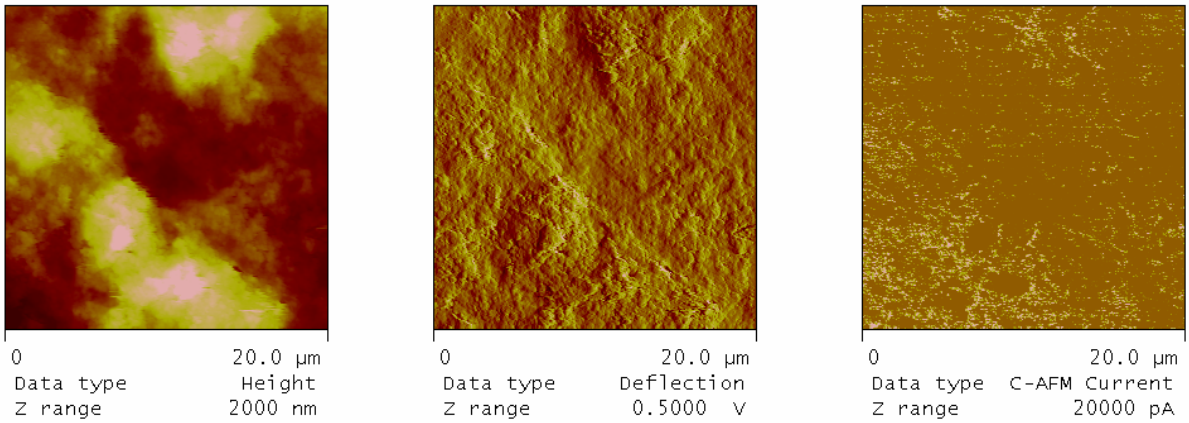

Figure 4.9: Height, deflection, and current images for CPCCW0.1.

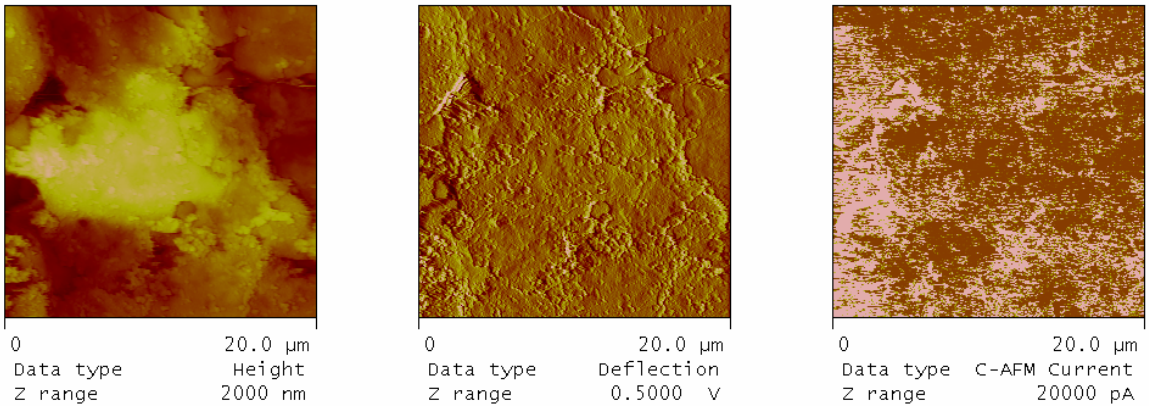

Figure 4.10: Height, deflection, and current images for CPCCW0.01.

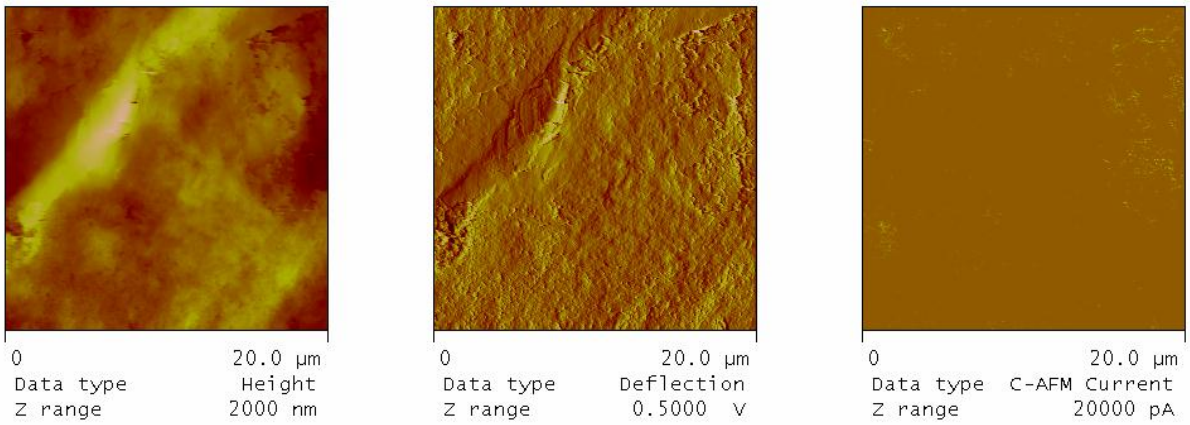

Figure 4.11: Height, deflection, and current images for CPCCV0.1.

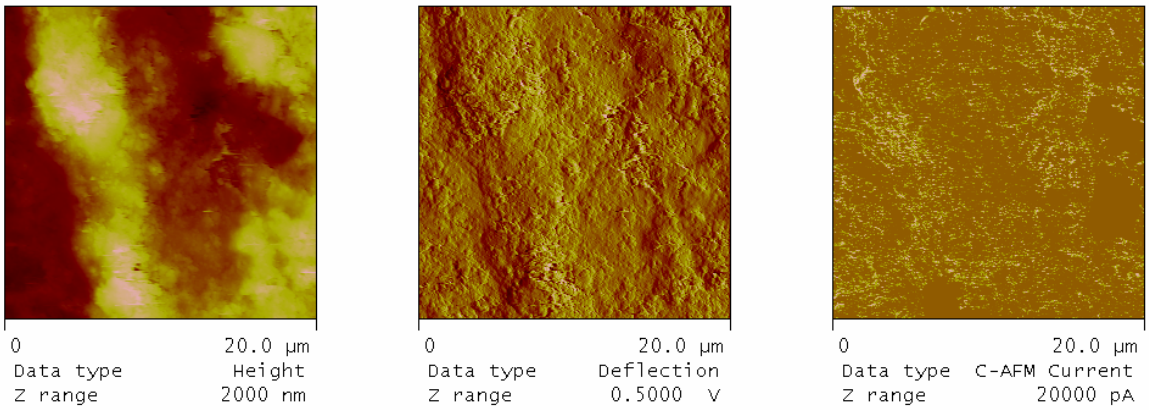

Figure 4.12: Height, deflection, and current images for CPCCV0.01.

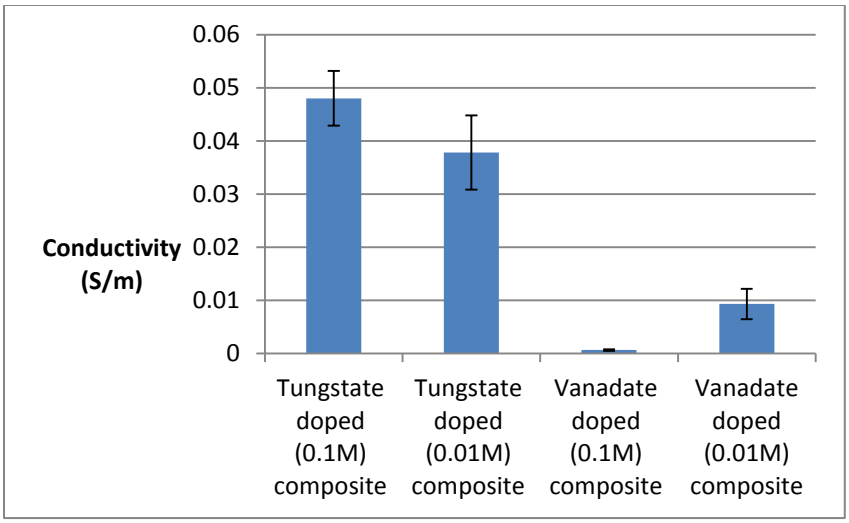

Figure 4.13: Conductivity values obtained by four point probe method.

4.4.5. X-ray photoelectron spectroscopy (XPS)

The doping level and elemental composition for the synthesized composites was obtained by XPS measurements. XPS measures composition at the surface with a depth of approximately 10 nm. As observed in Figure 4.14, both tungstate and vanadate doped composites were doped with tungstate and vanadate respectively. It was also found that dopant level was less in case of 0.01M concentration of dopant as compared to 0.1M concentration of dopant in the synthesis of both the composites as observed in Figure 4.14.

Table 4.3 demonstrates the different ratios of dopants with nitrogen. Dopant/nitrogen ratio signifies the level of doping in the composite of PPy and Aluminum flake. In case of CPCCW0.1, W/N ratio was higher than S/N whereas in case of CPCCW0.01, S/N ratio was higher than W/N. This signified greater amount of tungstate incorporation as compared to sulfur in the case of CPCCW0.1 and higher amount of sulfur incorporation in case of CPCCW0.01. With lower concentration of tungstate in the synthesis of CPCCW0.01, the tungstate anion pose possible competition with the sulfur anion to be incorporated into the PPy backbone. Similarity,

V/N ratio was greater than S/N for CPCCV0.1 and S/N ratio was greater than V/N ratio for CPCCV0.01 owing to the same reason as cited for the tungstate doped composite.

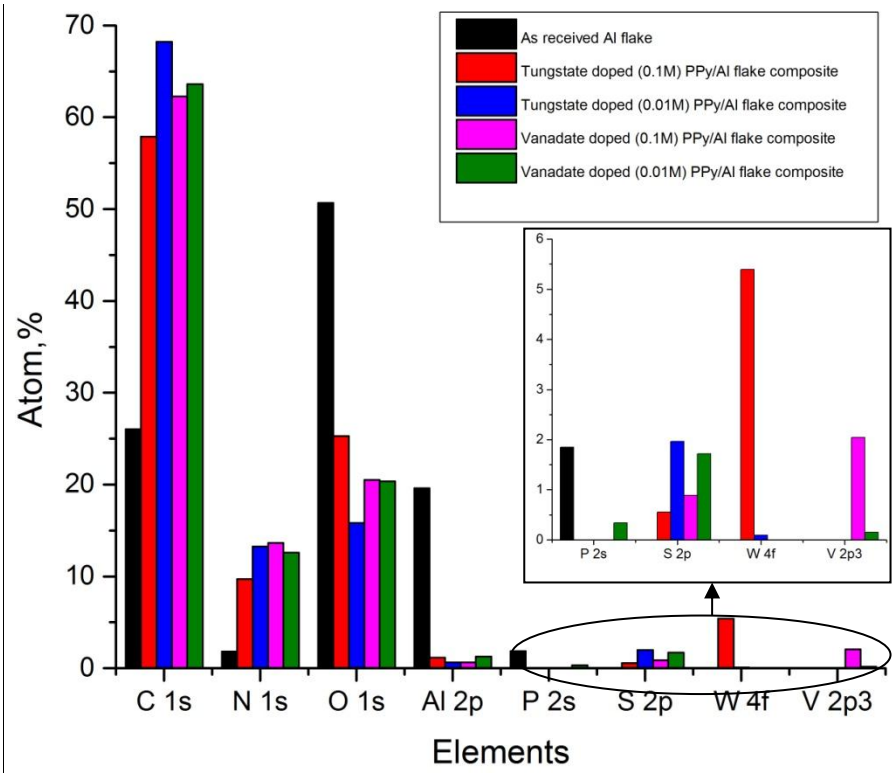

Figure 4.14: Elemental analysis by XPS.

Table 4.3
Dopant rations obtained by XPS

Dopant ratio	S/N	W/N	V/N
CPCCW0.1	0.056	0.556	-
CPCCW0.01	0.148	0.007	-
CPCCV0.1	0.065	-	0.150
CPCCV0.01	0.137	-	0.011

4.4.6. Electrochemical impedance spectroscopy (EIS)

EIS has been employed for the quantitative assessment of coatings against the corrosion [76-77]. EIS measurements were performed on CPCC containing primers of the composites for initial, 6 hours, 7 days, 15 days, and 35 days of exposure to the prohesion test conditions. Bode

plots for as received Al flake coating, CPCCW0.1 coating, CPCCW0.01 coating, CPCCV0.1 coating, and CPCCV0.01 coating are presented in Figure 4.15, 4.16, and 4.17 respectively. As observed in Figure 4.15, as received Al flake coating exhibited high impedance at low frequency and capacitive behavior with phase angle close to -90. This is typical EIS behavior observed for barrier type coating indicating no electrolyte has yet penetrated through the coatings [38]. There was a little drop in the low frequency impedance of the as received Al flake coating was observed as the exposure duration in Prohesion chamber was increased from initial time to the 35 days.

For the CPCCW0.1 coating and CPCCW0.01 coating as observed in Figure 4.16, lower impedance values were observed for the PPy containing Al flakes coatings. A similar observation was noted for CPCCV0.1 coating and CPCCV0.01 coating as shown in Figure 4.17. The low frequency impedance further decreased as the exposure to the Prohesion test conditions was increased from initial to 45 days. Impedance was almost constant at 45th day of prohesion exposure of all CPCCW0.1 coating, CPCCW0.01 coating CPCCV0.1 coating, and CPCCV0.01 coating.

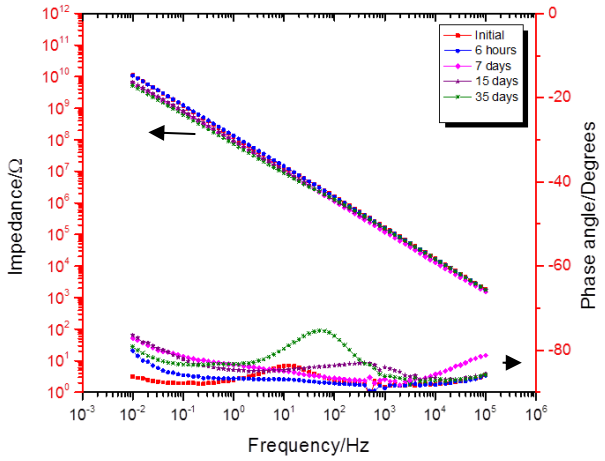

Figure 4.15: Bode plot of as received Al flake coating.

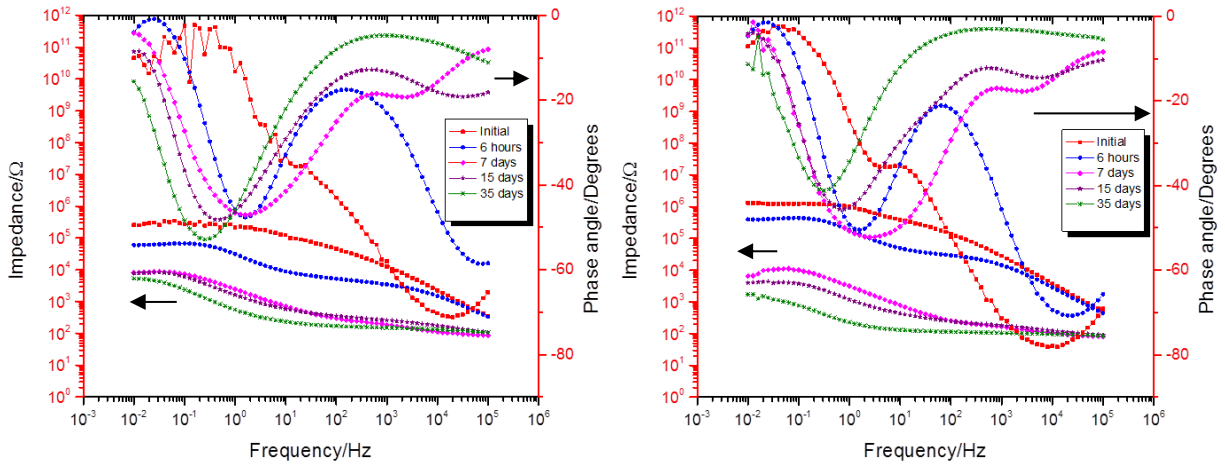

Figure 4.16: Bode plot of CPCCW0.1 coating (left) and CPCCW0.01 coating (right).

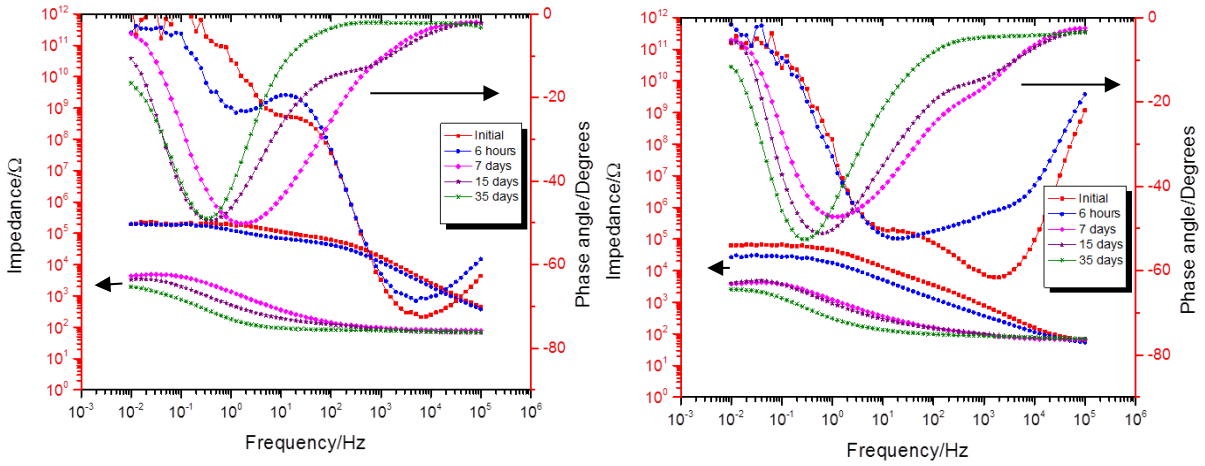

Figure 4.17: Bode plot of CPCCV0.1 coating (left) and CPCCV0.01 coating (right).

Lower impedance values in the PPy containing composite coatings can be attributed to the conducting nature of PPy. There is possibility of passing of alternating current (employed in EIS) current through the conducting pathways created by PPy instead of the dielectric pathways of epoxy binder [38, 44]. Lower impedance values in case of PPy doped composite coatings does not mean that these coatings are not protective in nature as will be evidenced by exposure tests mentioned in later in this paper. For PPy containing coatings, salt spray test results exhibited better corrosion protection even though lower impedance values were observed in EIS measurements for same coatings [78]. This behavior was attributed to the electroactive nature of

PPy. A similar behavior is observed here in this paper for CPCCW0.1 coating, CPCCW0.01 coating CPCCV0.1 coating, and CPCCV0.01 coating as observed in prohesion test results (Figure 19), the samples exhibited minimal corrosion. The active nature of PPy induces other forms of corrosion protection mechanism such as charge transfer mechanism for the corrosion protection instead of barrier type corrosion protection mechanism [79]. Another reason for lower impedance values observed for PPy containing composite can be the porosity of PPy resulting in extended percolation networks [80]. This is unlikely in this case as aluminum flake in the coating also serves as barrier for corrosion protection. The active nature of PPy along with its combination with aluminum flakes were further investigated for the corrosion protection mechanism in more controlled experiments of galvanic coupling in the following sections.

4.4.7. Equivalent electric circuit modeling and equivalent fitting

Equivalent electric circuit modeling and of the obtained EIS data was performed by using ZView2 software from Scribner® Associates Inc. The results of data fitting are presented in Table 4.4. The circuit models used for the fitting are shown in Figure 4.18. In Figure 4.18, R1 is solution resistance, R2 is coatings resistance, R3 is polarization resistance, Cc is coatings capacitance, Cdl is double layer capacitance, and CPE is constant phase element which represents pseudo capacitance. The impedance of CPE can be obtained by Equation 4.2,

$$Z_{(CPE)} = 1/[(T)(j\omega)^{P}] \quad (4.2)$$

Where, T is capacitance, j is an imaginary component, ω is the angular frequency ($\omega = 2\pi f$, f is the frequency), P is the power ($0 \leq n \leq 1$), and $Z_{(CPE)}$ is the impedance of CPE. P value close to 1 represents capacitor behavior. Only one time constant was evident for as received Al flake coating up to the 7^{th} day of exposure. This data was modeled by using circuit model as represented in Figure 4.18(a)**,** whereas after that two time constants were evident and that data

was modeled by using circuit model as represented in Figure 4.18(b). In the case of CPCCW0.1 coating, CPCCW0.01 coating, CPCCV0.1 coating, and CPCCV0.01 coating, two time constants were evident from the start of the exposure. A second time constant implied the reaction happening at interface of PPy and aluminum flake and not to the reaction at the interface of coating and surface as it was just starting of the exposure and no corrosion reaction was even started. This data was modeled by employing the circuit model represented in Figure 4.18(b). For the CPCCW0.1 coating, CPCCW0.01 coating, CPCCV0.1 coating, and CPCCV0.01 coating in the second time constant, initially were capacitive and CPE_{dl}-T started increasing as the exposure to the prohesion test conditions increased but still value of P remained close to one indicating capacitive behavior. Again for these coatings the value of R_{ct} did not decrease below 10^{-3} Ω after 35 days of exposure and it stayed at the constant value. These results of fit and modeling were in agreement with the results obtained from EIS.

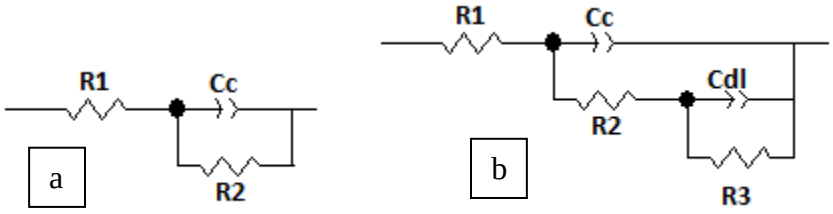

Figure 4.18: Equivalent electric circuit models (a, and b) for equivalent fitting based on EIS data.

4.4.8. Prohesion test exposure

Panels were exposed to Prohesion conditions according to ASTM G85-A5. Photographs of panels (without topcoat) exposed for 35 days and panels with topcoat exposed for 65 days are shown in Figure 4.19. As received Al flake coating without topcoat exhibited corrosion product in the scribe and delamination along the scribe. Lesser quantities of white corrosion product of

aluminum alloy most probably aluminum oxide was observed in the scribe for CPCCW0.1 coating, CPCCW0.01 coating CPCCV0.1 coating, and CPCCV0.01 coating but no delamination along the scribe was observed. For the topcoated as received Al flake coating severe delamination and corrosion was observed along the scribe where as for CPCCW0.1 coating, CPCCW0.01 coating CPCCV0.1 coating, and CPCCV0.01 coating, less delamination and less corrosion was observed. Minimum corrosion was observed for topcoated CPCCW0.1 coating possibility due to the high conductivity of the composite.

Table 4.4
Circuit elements obtained through EIS data

	Time	R_c (Ω)	CPE_c		R_{ct} (Ω)	CPE_{dl}		Chi-Sqr
			T (F)	P		T (F)	P	
As received Al flake coating	Initial	4.93×10^{11}	1.10×10^{-9}	0.97	-	-	-	0.003
	6 hours	7.48×10^{10}	1.11×10^{-9}	0.98	-	-	-	0.006
	7 days	3.11×10^{10}	1.94×10^{-9}	0.94	-	-	-	0.007
	15 days	3.17×10^{7}	1.21×10^{-9}	0.97	3.82×10^{10}	7.14×10^{-10}	0.79	0.001
	35 days	3.04×10^{6}	1.19×10^{-9}	0.97	5.55×10^{10}	1.03×10^{-9}	0.93	0.002
CPCCW 0.1 coating	Initial	4.77×10^{4}	6.15×10^{-8}	0.80	2.52×10^{5}	5.26×10^{-7}	0.63	0.017
	6 hours	5.16×10^{3}	2.99×10^{-7}	0.69	6.58×10^{4}	6.31×10^{-6}	0.79	0.009
	7 days	1.96×10^{2}	2.62×10^{-5}	0.42	1.18×10^{4}	8.42×10^{-5}	0.66	0.020
	15 days	3.88×10^{2}	4.91×10^{-5}	0.38	1.16×10^{4}	1.27×10^{-4}	0.74	0.009
	35 days	1.63×10^{2}	4.33×10^{-5}	0.35	7.41×10^{3}	4.82×10^{-4}	0.75	0.006
CPCCW 0.01 coating	Initial	2.89×10^{5}	1.98×10^{-8}	0.86	1.01×10^{6}	1.54×10^{-7}	0.77	0.005
	6 hours	3.33×10^{4}	4.60×10^{-8}	0.81	4.16×10^{5}	9.50×10^{-7}	0.87	0.006
	7 days	1.53×10^{2}	1.91×10^{-5}	0.47	1.28×10^{4}	6.17×10^{-5}	0.73	0.031
	15 days	2.37×10^{2}	7.43×10^{-5}	0.37	5.54×10^{3}	1.63×10^{-4}	0.72	0.018
	35 days	1.09×10^{2}	1.31×10^{-4}	0.27	1.67×10^{3}	1.40×10^{-4}	0.78	0.014
CPCCV 0.1 coating	Initial	8.91×10^{4}	4.37×10^{-8}	0.82	1.17×10^{5}	5.30×10^{-7}	0.84	0.010
	6 hours	6.72×10^{4}	9.13×10^{-8}	0.77	1.31×10^{5}	2.16×10^{-6}	0.80	0.005
	7 days	7.74×10^{1}	4.43×10^{-6}	0.46	5.80×10^{3}	1.85×10^{-4}	0.68	0.010
	15 days	8.94×10^{1}	8.11×10^{-5}	0.35	5.70×10^{3}	5.16×10^{-4}	0.66	0.030
	35 days	7.49×10^{1}	1.28×10^{-4}	0.25	2.23×10^{3}	1.53×10^{-3}	0.81	0.009
CPCCV 0.01 coating	Initial	8.27×10^{1}	5.69×10^{-6}	0.55	1.01×10^{5}	2.86×10^{-7}	0.88	0.004
	6 hours	4.30×10^{1}	9.94×10^{-7}	0.64	3.34×10^{4}	1.17×10^{-5}	0.62	0.008
	7 days	7.06×10^{1}	1.19×10^{-5}	0.45	5.70×10^{3}	2.19×10^{-4}	0.61	0.021
	15 days	9.42×10^{1}	3.72×10^{-5}	0.41	6.80×10^{3}	2.60×10^{-4}	0.66	0.035
	35 days	8.74×10^{1}	8.42×10^{4}	0.33	3.40×10^{3}	8.30×10^{-4}	0.76	0.015

4.4.9. Galvanic coupling measurements

Galvanic coupling measurements were performed on the samples without a topcoat in an oxygen free local environment. In order to simulate local environment with limited oxygen as under the topcoat, the coated sample compartment was purged with nitrogen. In these experiments, the cathode for bare aluminum 2024-T3 was signified by positive current. The results of coupling current and mixed potential are presented in Figure 4.20, and 4.21 respectively. All of the composite coatings exhibited positive coupling current suggesting that PPy/Al flake coatings were acting as anode and sacrificially protecting aluminum 2024-T3 (Figure 4.20). For CPCCW0.1 coating, coupling current increased rapidly. A similar behavior was also observed for CPCCV0.01 coating. The corrosion protection was also maximum for both of these coatings as observed in the prohesion test results (Figure 4.19). Again for both of these coatings, the mixed potential values were more negative and were decreasing with time suggesting cathodic polarization (Figure 4.21). For CPCCW0.01 coating and for CPCCV0.1 coating, the mixed potential values were more positive and stable but, still, the coupling current was positive suggesting the sacrificial protection by PPy/Al flake composite coatings.

It has been observed that, in contact with aluminum alloy, PPy tends to be reduced as it is coupled with aluminum alloy [53]. The reduction of PPy induces the anodic dissolution of aluminum; in this case activating aluminum flakes which further more protects sacrificially the underlying aluminum 2024-T3 substrate. The dissolution maintained high coupling current levels [38]. Reduced and neutral form of PPy has been also found to provide sacrificial protection to aluminum 2024-T3 [81]. The reduced PPy also serves as oxygen scavenger reducing corrosion rate and in the process itself gets oxidized. PPy which is oxidized again keeps aluminum flake dissolving and keeps galvanic current high till all aluminum flakes are

consumed. As soon as corrosion begins, the anodic reaction at metal surface results in the liberation of electrons which are utilized in CP reduction leading to the release of corrosion inhibiting dopant anion as shown in Scheme 4.1. Oxygen reduction at CPs surface causes replenishing of the depleted charge [82-84].

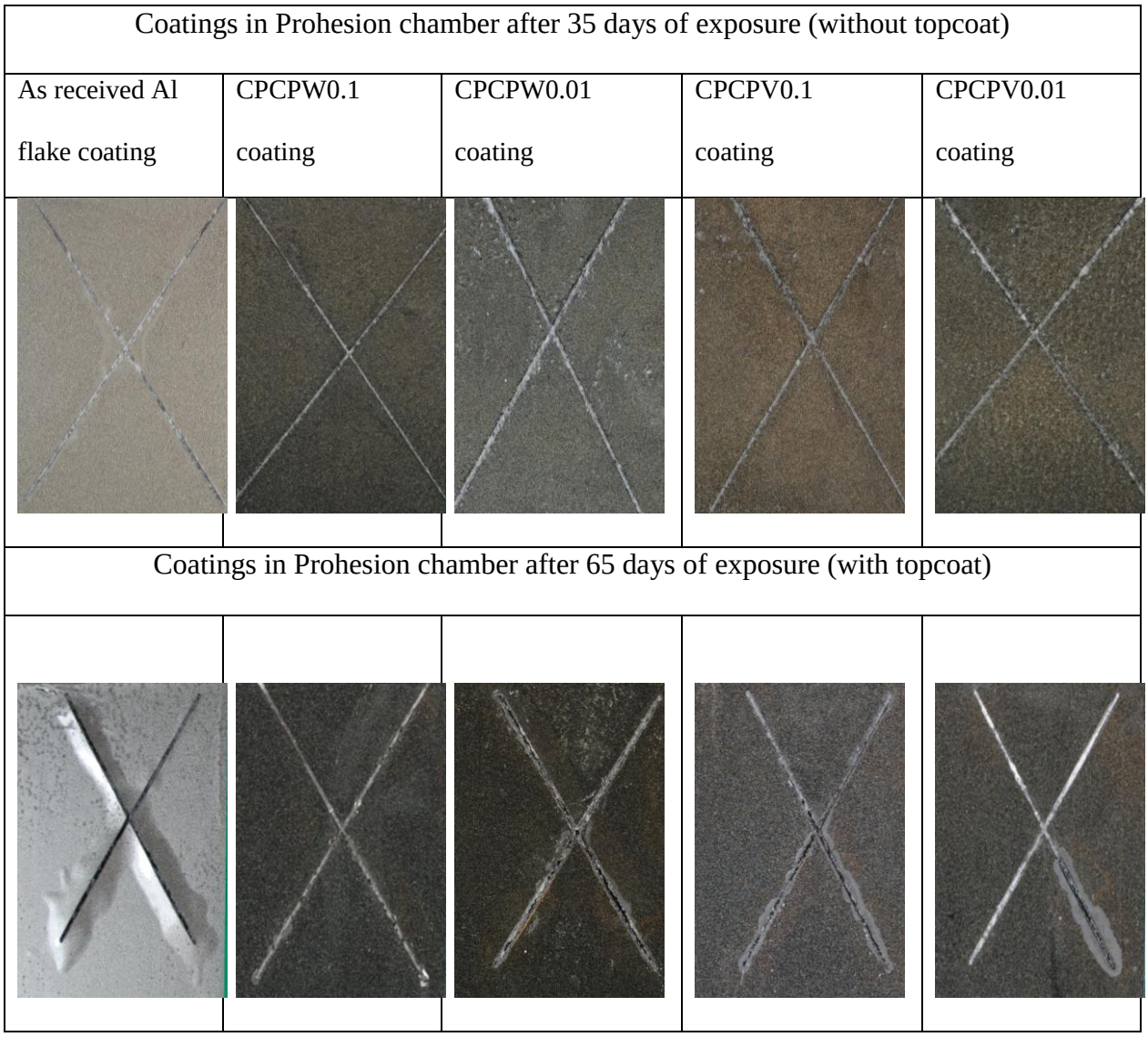

Figure 4.19: Panels in Prohesion chamber (top) after 35 days (without topcoat) and (bottom) after 65 days (with topcoat).

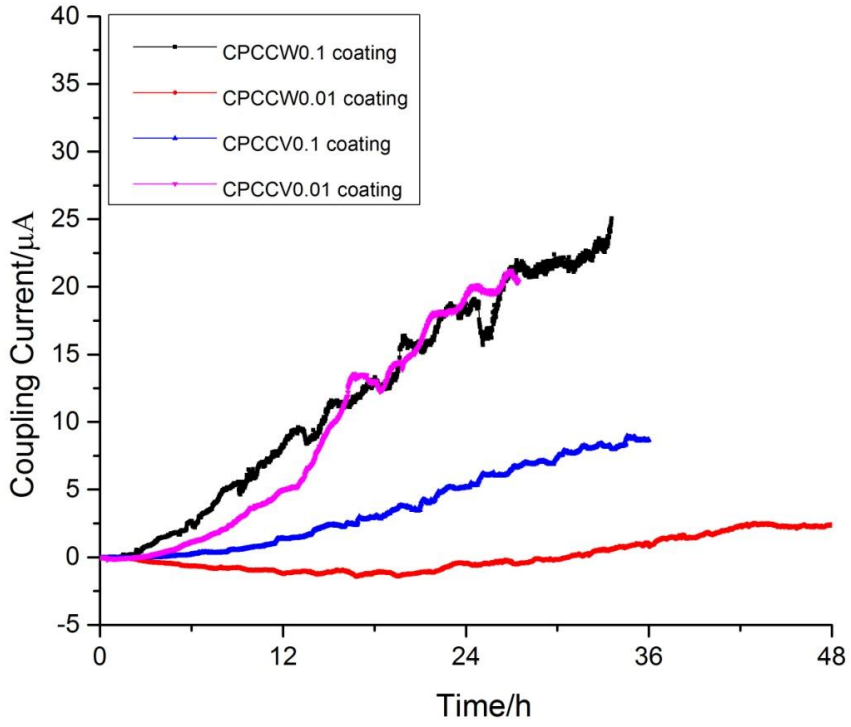

Figure 4.20: Coupling current measurements obtained by galvanic coupling experiment.

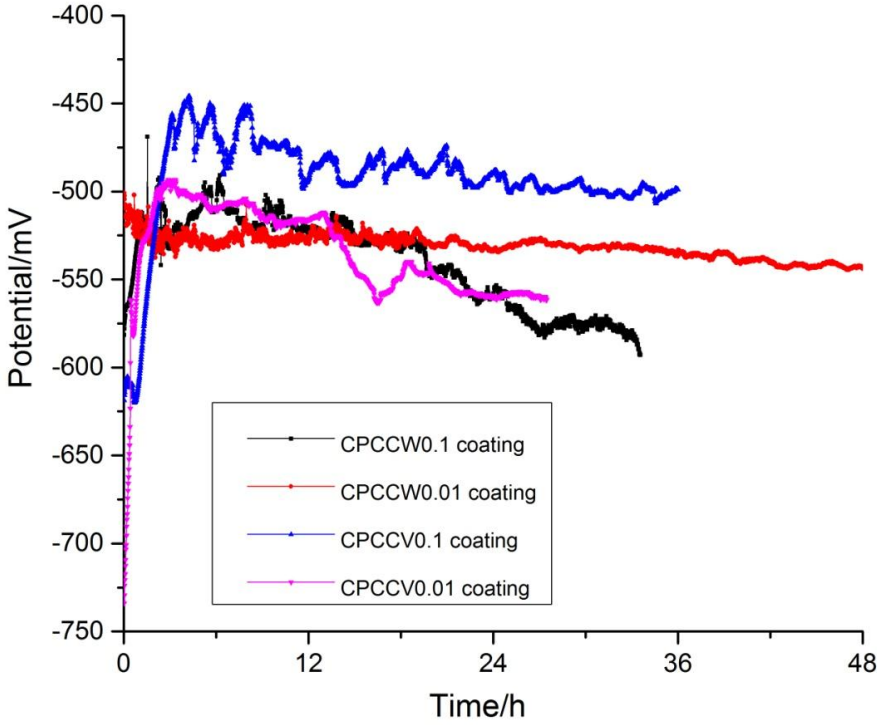

Figure 4.21: Mixed potential measurements obtained by galvanic coupling experiment.

As mentioned earlier, this reduction of oxygen leads to the oxygen scavenging by CPs resulting in reduced corrosion rates. The replenishment of the charge also results in the stabilization of the potential in the passive region on the metal surface [82]. In the case of the composite pigment of PPy and aluminum flakes, the galvanic contact of PPy with aluminum flakes results in the reduction of PPy and, thereby, the release of corrosion inhibiting dopant anions [38]. There is possibility of combination of released anions with cations of the substrate forming an impervious layer resulting in reduction of corrosion rate.

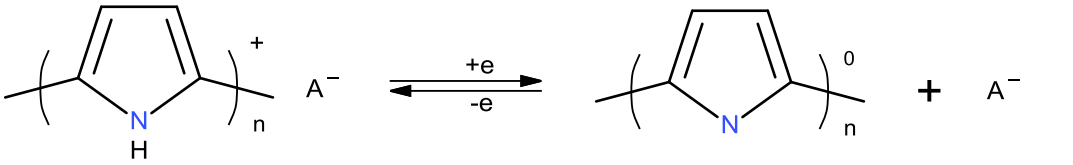

A^- is VO_3^- or WO_4^{2-}

Scheme 4.1: Anion release by PPy in redox reaction.

4.4.10. Potentiodynamic scans

As observed in the potentiodynamic scans (Figure 4.22), the corrosion potential values were shifted by approximately 300 mV in more noble for CPCCW0.1 coating, CPCCW0.01 coating CPCCV0.1 coating, and CPCCV0.01 coating as compared to the as received Al flake coating. This positive shift may be attributed to the release of the dopant (tungstate or vanadate) in to the defect area due to reduction of PPy in contact with aluminum flakes and underlying aluminum substrate. The dopant (tungstate or vanadate) may combine with aluminum cations forming impervious layer of oxide leading to passivation [45].

As observed in Figure 4.22, the corrosion current was also less in case of CPCCW0.1 coating, CPCCW0.01, and CPCCV0.01 than that of as received Al flake coating. Corrosion current did not decrease in case of CPCCV0.1 but passivation was still achieved as observed in

potentiodynamic scans. This might be due to the lower conductivity of CPCCV0.1 as compared to other composites resulting in slow release of dopant. The corrosion protection exhibited by PPy/Al flake composite pigment was due to the combined effect of active nature of PPy, galvanic coupling, and dopant release due to passivation.

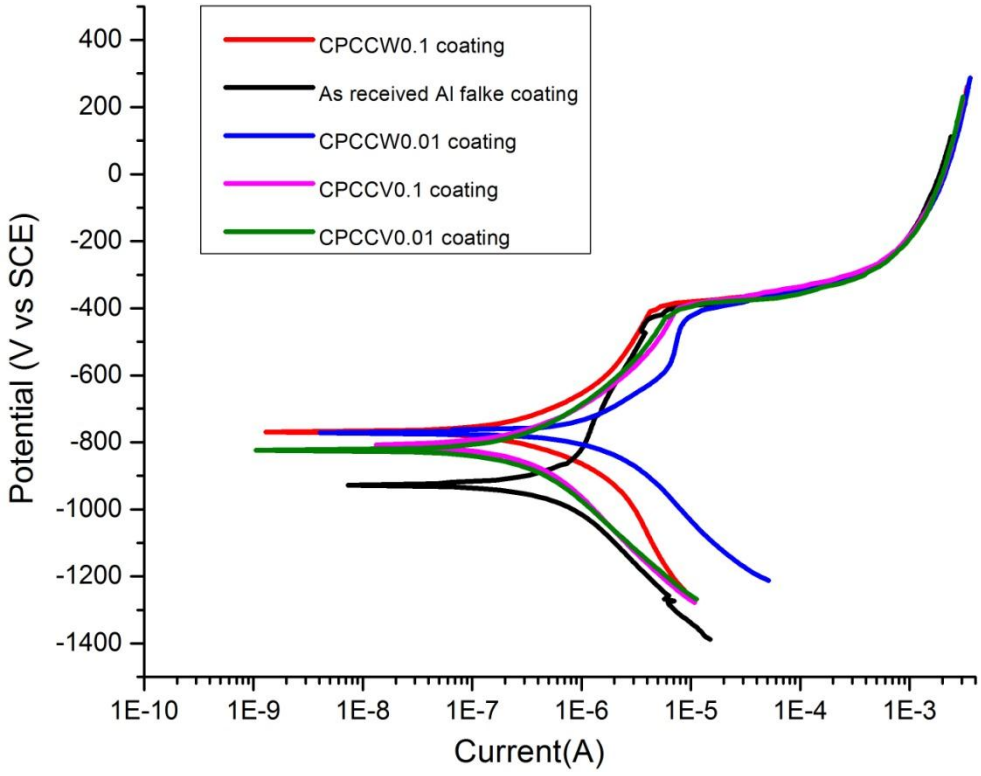

Figure 4.22: Potentiodynamic scans.

4.5. Conclusions

Tungstate and vanadate doped PPy/Al flake composites were synthesized by chemical oxidative polymerization. The synthesized composites were conductive in nature as observed in CAFM and four point probe measurements. Accelerated Prohesion test exposure showed improved corrosion protection for doped PPy/Al flake composite coatings. The galvanic coupling current measurements demonstrated sacrificial corrosion protection mechanism provided by doped PPy/Al flake composite coatings to the underlying aluminum 2024-T3 substrate. Potentiodynamic scans suggested dopant release from PPy, resulting in passivation in

the defect thereby enhancing the corrosion protection. In this way, sacrificial protection was combined with active dopant release mechanism in the formed doped PPy/Al flake composite coatings resulting in increased corrosion protection.

4.6. Acknowledgements

The authors gratefully acknowledge the support of this research by US Army Research Laboratory under grant no. W911NF-09-2-0014, W911NF-10-2-0082, and W911NF-11-2-0027.

4.7. References

[1] Z. Ahmad, Principles of Corrosion Engineering and Corrosion Control, Elsevier Science, 2006.

[2] D.A. Jones, Principles and prevention of corrosion, Prentice Hall, 1996.

[3] R.W. Revie, Uhlig's Corrosion Handbook, Wiley, 2011.

[4] T.A. Skotheim, J.R. Reynolds, Conjugated Polymers: Processing and Applications, CRC Press INC, 2007.

[5] S.M. Cohen, Corrosion, 51 (1995) 71-78.

[6] M.D. Cohen, B. Kargacin, C.B. Klein, M. Costa, Critical Reviews in Toxicology, 23 (1993) 255-281.

[7] A.G. Macdiarmid, J.C. Chiang, A.F. Richter, A.J. Epstein, Synthetic Metals, 18 (1987) 285-290.

[8] J. Heinze, Electronically conducting polymers Electrochemistry IV, in: E. Steckhan (Ed.), vol. 152, Springer Berlin / Heidelberg, 1990, pp. 1-47.

[9] J.D. Stenger-Smith, Progress in Polymer Science, 23 (1998) 57-79.

[10] G. Inzelt, Conducting Polymers: A New Era in Electrochemistry, Springer, 2012.

[11] M.G. Hosseini, M. Raghibi-Boroujeni, I. Ahadzadeh, R. Najjar, M.S. Seyed Dorraji, Progress in Organic Coatings, 66 (2009) 321-327.

[12] K. Castagno, D. Azambuja, V. Dalmoro, Journal of Applied Electrochemistry, 39 (2009) 93-100.

[13] M.G. Hosseini, M. Sabouri, T. Shahrabi, Journal of Applied Polymer Science, 110 (2008) 2733-2741.

[14] G. Bidan, Sensors and Actuators B: Chemical, 6 (1992) 45-56.

[15] G. Inzelt, M. Pineri, J.W. Schultze, M.A. Vorotyntsev, Electrochimica Acta, 45 (2000) 2403-2421.

[16] T.F. Otero, E. Angulo, J. Rodríguez, C. Santamaría, Journal of Electroanalytical Chemistry, 341 (1992) 369-375.

[17] A. Rudge, J. Davey, I. Raistrick, S. Gottesfeld, J.P. Ferraris, Journal of Power Sources, 47 (1994) 89-107.

[18] B. Scrosati, Polymer International, 47 (1998) 50-55.

[19] Z. Cai, M. Geng, Z. Tang, Journal of Materials Science, 39 (2004) 4001-4003.

[20] D. Braun, A.J. Heeger, Thin Solid Films, 216 (1992) 96-98.

[21] L. Dai, B. Winkler, L. Dong, L. Tong, A.W.H. Mau, Advanced Materials, 13 (2001) 915-925.

[22] L.M. Lira, S.I. Córdoba de Torresi, Electrochemistry Communications, 7 (2005) 717-723.

[23] L.L. Miller, Molecular Crystals and Liquid Crystals Incorporating Nonlinear Optics, 160 (1988) 297-301.

[24] Y. Saito, T. Azechi, T. Kitamura, Y. Hasegawa, Y. Wada, S. Yanagida, Coordination Chemistry Reviews, 248 (2004) 1469-1478.

[25] Y. Wang, X. Jing, Polymers for Advanced Technologies, 16 (2005) 344-351.

[26] K. Lakshmi, H. John, K.T. Mathew, R. Joseph, K.E. George, Acta Materialia, 57 (2009) 371-375.

[27] S. Sitaram, J. Stoffer, T. O'Keefe, Journal of Coatings Technology, 69 (1997) 65-69.

[28] D. Tallman, G. Spinks, A. Dominis, G. Wallace, J. Solid State Electrochem., 6 (2002) 73-84.

[29] G. Spinks, A. Dominis, G. Wallace, D. Tallman, J. Solid State Electrochem., 6 (2002) 85-100.

[30] N. Ahmad, A.G. MacDiarmid, Synthetic Metals, 78 (1996) 103-110.

[31] C.B. Breslin, A.M. Fenelon, K.G. Conroy, Materials & Design, 26 (2005) 233-237.

[32] U. Rammelt, P.T. Nguyen, W. Plieth, Electrochimica Acta, 48 (2003) 1257-1262.

[33] C.K. Tan, D.J. Blackwood, Corrosion Science, 45 (2003) 545-557.

[34] V. Annibaldi, A.D. Rooney, C.B. Breslin, Corrosion Science, 59 (2012) 179-185.

[35] G.S. Gonçalves, A.F. Baldissera, L.F. Rodrigues Jr, E.M.A. Martini, C.A. Ferreira, Synthetic Metals, 161 (2011) 313-323.

[36] S. Palraj, M. Selvaraj, M. Vidhya, G. Rajagopal, Progress in Organic Coatings, 75 (2012) 356-363.

[37] C.T. Lim, J.C.H. Goh, 13Th International Conference on Biomedical Engineering: ICBME 2008 3-6 December 2008, Singapore, Springer London, Limited, 2009.

[38] M. Yan, C.A. Vetter, V.J. Gelling, Electrochimica Acta, 55 (2010) 5576-5583.

[39] M. Trueba, S.P. Trasatti, Journal of Applied Electrochemistry, 39 (2009) 2061-2072.

[40] S.A. Ashraf, F. Chen, C.O. Too, G.G. Wallace, Polymer, 37 (1996) 2811-2819.

[41] V.J. Gelling, M.M. Wiest, D.E. Tallman, G.P. Bierwagen, G.G. Wallace, Progress in Organic Coatings, 43 (2001) 149-157.

[42] R.C.D. Peres, J.M. Pernaut, M.-A. De Paoli, Synthetic Metals, 28 (1989) 59-64.

[43] M.-K. Song, Y.-T. Kim, B.-S. Kim, J. Kim, K. Char, H.-W. Rhee, Synthetic Metals, 141 (2004) 315-319.

[44] X. Qi, C. Vetter, A.C. Harper, V.J. Gelling, Progress in Organic Coatings, 63 (2008) 345-351.

[45] M. Sabouri, T. Shahrabi, H.R. Farid, M.G. Hosseini, Progress in Organic Coatings, 64 (2009) 429-434.

[46] M. Sabouri, T. Shahrabi, M.G. Hosseini, Russ J Electrochem, 43 (2007) 1390-1397.

[47] M. Iannuzzi, G.S. Frankel, Corrosion Science, 49 (2007) 2371-2391.

[48] M.R. Mahmoudian, W.J. Basirun, Y. Alias, Applied Surface Science, 257 (2011) 3702-3708.

[49] E. Akbarinezhad, M. Ebrahimi, F. Sharif, M.M. Attar, H.R. Faridi, Progress in Organic Coatings, 70 (2011) 39-44.

[50] M.G. Hosseini, M. Jafari, R. Najjar, Surface and Coatings Technology, 206 (2011) 280-286.

[51] M.G. Hosseini, R. Bagheri, R. Najjar, Journal of Applied Polymer Science, 121 (2011) 3159-3166.

[52] M. Ioniţă, A. Prună, Progress in Organic Coatings, 72 (2011) 647-652.

[53] M. Yan, D.E. Tallman, G.P. Bierwagen, Electrochimica Acta, 54 (2008) 220-227.

[54] M. Rizzi, M. Trueba, S.P. Trasatti, Synthetic Metals, 161 (2011) 23-31.

[55] H. Nguyen Thi Le, B. Garcia, C. Deslouis, Q. Le Xuan, Electrochimica Acta, 46 (2001) 4259-4272.

[56] W.-K. Lu, R.L. Elsenbaumer, B. Wessling, Synthetic Metals, 71 (1995) 2163-2166.

[57] B. Tian, G. Zerbi, Journal of Chemical Physics, 92 (1990) 3886-3891.

[58] S.V. Kasisomayajula, X.N. Qi, C. Vetter, K. Croes, D. Pavlacky, V.J. Gelling, Journal of Coatings Technology and Research, 7 (2010) 145-158.

[59] W. Liang, J. Lei, C.R. Martin, Synthetic Metals, 52 (1992) 227-239.

[60] M. Omastová, M. Trchová, J. Kovářová, J. Stejskal, Synthetic Metals, 138 (2003) 447-455.

[61] B. Tian, G. Zerbi, The Journal of Chemical Physics, 92 (1990) 3892-3898.

[62] B. Tian, G. Zerbi, Journal of Chemical Physics, 92 (1990) 3892-3898.

[63] C. Saravanan, R.C. Shekhar, S. Palaniappan, Macromolecular Chemistry and Physics, 207 (2006) 342-348.

[64] A. Kaynak, Materials Research Bulletin, 32 (1997) 271-285.

[65] D.S. Maddison, J. Unsworth, Synthetic Metals, 30 (1989) 47-55.

[66] J. Unsworth, P.C. Innis, B.A. Lunn, Z. Jin, G.P. Norton, Synthetic Metals, 53 (1992) 59-69.

[67] S. Goel, N.A. Mazumdar, A. Gupta, Polymers for Advanced Technologies, 21 (2010) 205-210.

[68] L.F. Warren, J.A. Walker, D.P. Anderson, C.G. Rhodes, L.J. Buckley, Journal of the Electrochemical Society, 136 (1989) 2286-2295.

[69] C. Yang, P. Liu, Reactive and Functional Polymers, 70 (2010) 726-731.

[70] I. Díez, K. Tauer, B. Schulz, Colloid & Polymer Science, 284 (2006) 1431-1442.

[71] Y. Lu, A. Pich, H.-J.P. Adler, Macromolecular Symposia, 210 (2004) 411-417.

[72] J.L. Brédas, J.C. Scott, K. Yakushi, G.B. Street, Physical Review B, 30 (1984) 1023-1025.

[73] J.L. Bredas, G.B. Street, Accounts of Chemical Research, 18 (1985) 309-315.

[74] S. Kuwabata, J. Nakamura, H. Yoneyama, Journal of the Chemical Society, Chemical Communications, 0 (1988) 779-780.

[75] A. Shakoor, T.Z. Rizvi, Journal of Applied Polymer Science, 117 (2010) 970-973.

[76] L. Jianguo, G. Gaoping, Y. Chuanwei, Electrochimica Acta, 50 (2005) 3320-3332.

[77] F. Mansfeld, Journal of Applied Electrochemistry, 25 (1995) 187-202.

[78] V.T. Truong, P.K. Lai, B.T. Moore, R.F. Muscat, M.S. Russo, Synthetic Metals, 110 (2000) 7-15.

[79] J.O. Iroh, W. Su, Electrochimica Acta, 46 (2000) 15-24.

[80] M. Rohwerder, A. Michalik, Electrochimica Acta, 53 (2007) 1300-1313.

[81] M.C. Yan, D.E. Tallman, S.C. Rasmussen, G.P. Bierwagen, Journal of the Electrochemical Society, 156 (2009) C360-C366.

[82] P.J. Kinlen, V. Menon, Y. Ding, Journal of the Electrochemical Society, 146 (1999) 3690-3695.

[83] M. Kendig, M. Hon, L. Warren, Progress in Organic Coatings, 47 (2003) 183-189.

[84] D.E. Tallman, K.L. Levine, C. Siripirom, V.G. Gelling, G.P. Bierwagen, S.G. Croll, Applied Surface Science, 254 (2008) 5452-5459.

CHAPTER 5. TITANIUM DIOXIDE /CONDUCTING POLYMERS COMPOSITE PIGMENTS FOR CORROSION PROTECTION OF COLD ROLLED STEEL

(Published in Proceedings of CoatingsTech Conference, American Coatings Association, Rosemont, Illinois, March 11-13, 2013)

5.1. Abstract

Human civilization is heavily dependent on metals and their alloys. Corrosion is perennial problem faced by man-made structures which are made from metals and their alloys. Several technologies, including coatings, are employed for combating the problem of corrosion. Traditional coating systems such as barrier type coatings, metal rich coatings and inhibitor containing coatings have their own drawbacks. In order to overcome these drawbacks, TiO_2 /Conducting polymers composite pigments were synthesized by chemical oxidative polymerization technique in simple and eco-friendly manner. These composite pigments were characterized for morphology, conductivity, and elemental composition by various techniques. Coatings based on these pigments were formulated and applied on cold rolled steel substrate. Constant immersion in 5% sodium chloride was employed to accelerate corrosion. The corrosion resistance of the coatings with time was monitored by Electrochemical Impedance Spectroscopy (EIS) and DC Polarization technique. EIS results demonstrated increased corrosion protection for the core and shell TiO_2/Polypyrrole composite, TiO_2/Polypyrrole (Tungstate doped) composite, and TiO_2/Polyaniline composite. Additionally, potentiodynamic scan results demonstrated passivation achieved by synthesized composite based coatings improving corrosion protection.

5.2. Introduction

Worldwide yearly corrosion cost is at 2.2 trillion USD which amounts to almost 3% of worlds total GDP [1]. Out of total metal under utilization one-third is often destroyed by

corrosion [2]. Corrosion impacts several categories of human civilization such as infrastructure, transportation, manufacturing, utilities, and governments [3]. Taking into consideration of corrosion effects on human life and safety, corrosion associated costs, and need to conserve and prolong the usage of materials, it becomes imperative for researchers to study corrosion into details and find the necessary solutions for it [4]. Process of corrosion transforms metal to its native oxide form mostly by combining with oxygen and water. Metal oxide form is metals natural lowest energy state. Therefore it is very difficult to stop the corrosion. However it is possible to mitigate corrosion by applying various methods such as coatings, inhibitors, cathodic protection, judicial material selection, and proper design [5].

Application of protective coatings has been one of the most efficient methods for the corrosion protection. Of all the total paint produced one-third is applied on metal for its protection and decoration [6]. Protective coatings can be classified as barrier, conversion, anodic, and cathodic coatings. Barrier type coatings are further subdivided into four type's namely anodic oxides, inhibitive coatings, organic coatings, and inorganic coatings. Barrier type coatings prove ineffective once defect is formed. Chromates which are well known and highly effective corrosion agents are mutagenic and carcinogenic in nature [7]. Metal rich primers need high pigment volume concentration (PVC) for the corrosion protection. Furthermore these metals such as zinc have negative environmental impact. Taking into consideration limitations of existing coating systems along with changing environment, rapidly growing heavy industrialization, increasing pollutants, there is need to find environmentally benign solutions with superior properties.

Conducting Polymers (CPs) are the new class of materials with interesting properties such as conductivity, good environmental stability, easy supply, and facile synthesis procedures

[8-9]. Owing to these properties, CPs find numerous applications in the areas of science and technology including sensors [10], actuators [11], electrochemical devices [12], electrochromic cells [13], batteries [14], solar cells [15], light emitting devices [16], drug delivery [17], and corrosion protection [18]. CPs were first explored for corrosion inhibition by Mengoli et al.[19]. This was followed by several research articles in last three decades demonstrating usefulness of CPs for the corrosion inhibition [20-26]. CPs can be synthesized by chemical oxidative polymerization and electrochemical polymerization. Large scale synthesis is possible with chemical oxidative polymerization along with possibility of covalent modification of CPs backbone. Several new monomers and modified monomers can be easily polymerized by chemical oxidative polymerization [27].

Polyaniline (PAni), Polypyrrole (PPy), and Polythiophene are most widely studied CPs for the corrosion inhibition on metal and metal alloys substrates [28-29]. PPy is widely studied for the corrosion protection of metals and metal alloys owing to its properties such as good conductivity, better environmental stability, non-toxicity, thermal stability, and ease of synthesis [30-32]. However PPy has drawbacks such as insolubility, stiff chains, poor mechanical properties, difficult processibility, irreversible charge consumption in redox process, and porosity [33-35]. In order to overcome these problems associated with the application of PPy, various avenues have been employed by several researchers such as chemical modification of pyrrole monomer, dopant incorporation, copolymerization, composites and nanocomposites of CPs with inorganic materials, and multilayer's of CPs [36-38].

Composites of PPy and inorganic pigments are promising for overcoming drawbacks associated with PPy application to the coatings [39]. Inorganic pigments are widely used in coatings industry for hiding, color, mechanical strength, chemical resistance and thermal stability

[40]. Combination of these inorganic pigments with PPy could impart properties of both PPy and inorganic pigments for the synergistic effect. Composites of PPy and inorganic pigments have been synthesized for the corrosion protection of steel by electrochemical methods [41-43]. Titanium dioxide (TiO_2)/PPy composite was electrochemically prepared on AISI 1010 steel and it was found that the incorporation of TiO_2 in composite matrix about 6.5% by weight results in little improvement in corrosion resistance [43]. It was also found that TiO_2 did not interfere in the polymerization of pyrrole when electrochemical polymerization was performed on the surface of mild steel [44]. Sn-doped TiO_2 and PPy nanocomposite was prepared by chemical oxidative polymerization of pyrrole. It was incorporated into epoxy polyamide coating at 1% by weight and was applied on mild steel [45]. On the similar lines Ni-doped TiO_2 and PPy nanocomposite were also synthesized [46]. Both of these papers report improvement in corrosion resistance.

Corrosion inhibiting dopants can be incorporated on the backbone of PPy. Once PPy is reduced, these corrosion inhibiting dopants can combine with underlying metal to form an insoluble layer improving the corrosion resistance [47-48]. In contact with underlying metal, oxidation of metal can induce reduction of PPy resulting in release of dopant anion which could further passivate the defect demonstrating smart corrosion protection mechanism [49]. Tungstate doped PPy was electropolymerized on the surface of carbon steel which showed participation of tungstate anion in passivation resulting in improved corrosion protection [50]. Phosphate and tungstate anion doped PPy was electropolymerized on mild steel surface demonstrating better corrosion protection offered by tungstate anion doped PPy as compared to phosphate anion doped PPy [35]. Tungstate has demonstrated good corrosion inhibition for steel [51]. It has been reported that if effective passivation is not achieved in certain conditions such as in presence of

large defect, CPs can act as a corrosion mediator promoting corrosion [52]. In order to avoid this problem and the issues mentioned earlier about PPy incorporation in coatings and properties, conducting polymers containing pigments (CPCP) have been developed [42]. Aluminum flakes coated with PPy has been found to improve corrosion protection on the surface of Aluminum 2024-T3.

In current research paper, CPs redox activity and dopant release ability is combined and a composite with TiO_2 is synthesized by chemical oxidative polymerization. Three different types of CPCC were synthesized namely, TiO_2/PPy composite, TiO_2/PPy (Tungstate doped) composite, and TiO_2/PAni composite. These composites were characterized for morphology by SEM and TEM, composition by FTIR, elemental analysis with XPS, conductivity with CAFM and four point probe method. Coatings were formulated with epoxy-polyamide binder system with these pigments at 5 and 20% by weight composition on the surface of cold roll steel. Corrosion resistance ability of these coatings was evaluated by constant immersion studies in 5% sodium chloride (NaCl) and corrosion resistance was electrochemically analyzed by EIS and DC polarization techniques.

5.3. Experimental work

5.3.1. Materials

For the synthesis of composites, 18.2 MΩ Millipore water was used. TiO_2 (R-702) was obtained from DuPont with alumina as surface treatment. Dopant sodium tungstate dihydrate was purchased from MP Biomedicals, LLC. Oxidant ammonium persulfate (APS) was obtained from EMD chemicals Inc. Monomer pyrrole was purchased from Alfa Aesar Co. and was distilled prior to use. High purity grade monomer aniline was obtained from Sigma-Aldrich Corporation and was used as such without any purification. Hydrochloric acid was procured

from BDH. For coatings application, cold roll steel (0.032”x6”x3”) panels were procured from Q-Panel Lab Products. Epoxy resin (EPON 828) and polyamide curing agent (EPIKURE 3175) were supplied by Momentive Specialty Chemicals Inc. Methyl ethyl ketone (MEK) was used as a solvent for coating application and was procured from Alfa Aesar Co.

5.3.2. Synthesis of TiO_2/PPy composite and TiO_2/PPy (tungstate doped) composite

For the synthesis of TiO_2/PPy composite, TiO_2 pigment was soaked in pyrrole monomer for 5 days at ambient temperature. After 5 days of soaking, sample was centrifuged and separated TiO_2 was added to Erlenmeyer flask containing magnetic stir bar. This was followed by addition of 18.2 MΩ Millipore water to the flask. After proper dispersion of TiO_2 in the water, APS was added and reaction was continued for 24 hours. Product was filtered and washed with abundant amount of water. Washed product was dried in oven overnight at 60°C followed by grinding in mortar and pestle. In the end, the product was sieved with sieve #400 of 38 µm opening diameter and was stored at dry place.

For the preparation of TiO_2/PPy composite (tungstate doped), dopant sodium tungstate dihydrate was added to 18.2 MΩ Millipore water in above procedure just before the addition of centrifuged and separated TiO_2 to the Erlenmeyer flask. Rest of the procedure and materials are same as in the above mentioned synthesis of TiO_2/PPy composite. Quantities of all the ingredients used for the synthesis are mentioned in Table 5.1.

5.3.3. Synthesis of TiO_2/PAni composite

For this synthesis, TiO_2 pigment was soaked in aniline monomer for 5 days at ambient temperature. After 5 days of soaking, sample was centrifuged and separated TiO_2 was added to Erlenmeyer flask containing magnetic stir bar. This was followed by addition of 18.2 MΩ Millipore water to the flask. Prior to addition of water to the flask it was acidified with the

hydrochloric acid. After dispersion of TiO_2 in the water, oxidant APS was added and reaction was continued for 24 hours. Reaction product was filtered and washed with copious amount of water. This product was dried in oven overnight at 60°C followed by grinding in mortar and pestle. Finally, the product was sieved with sieve #400 of 38 µm opening diameter and was stored at dry place.

5.3.4. Coatings preparation

Prior to the coatings application, cold roll steel panels were sandblasted with 100 µm alumina grit. Hexane was used for the degreasing of the substrate. At stoichiometric ratio of 1:1 of EPON 828 and EPIKURE 3175, coatings were formulated with 5 and 20 % by weight of TiO_2, TiO_2/PPy composite, TiO_2/PPy composite (tungstate doped), and TiO_2/PAni composite. MEK was used as solvent to achieve application viscosity. Coatings were applied with drawdown bar with wet film thickness of 8 mils. Curing was performed in oven for 2 hours at 80°C. For complete curing samples were kept at room temperature for 8 days. Formulated coatings are denoted by acronyms as presented in Table 5.2.

5.3.5. Composite and coatings characterization

JSM-6490LV SEM (JEOL) and JEM-2100 TEM (JEOL) were employed for characterization of the morphology of the synthesized composites. NICOLET 8700 spectrophotometer (Thermo scientific) was employed for the FTIR characterization. SSX-100 system (Surface Science Laboratories, Inc.) was used for XPS analysis of the composites. Veeco Dimension 3100 atomic force microscope was employed for CAFM analysis of composite samples. Four point probe instrument consisting of Signatone® probes, a Keithley® 220 programmable current source, and Keithley®2000 multimeter was employed for the conductivity measurements of the composites. For performing EIS, Gamry Reference 600 Potentiostats with

Gamry Framework Version 5.58/EIS 300 software (Gamry Instruments) was employed with AC perturbation of 10 mV over frequency range 100,000-0.01 Hz at 10 points/decade. Potentiodynamic experiments were performed by using same setup of EIS.

Table 5.1
Synthesis reactions for composite pigments

Ingredients	TiO_2/PPy composite	TiO_2/PPy (Tungstate doped) composite	TiO_2/PAni composite
Pyrrole	30 ml	30 ml	-
Aniline	-	-	30 ml
TiO_2	3 g	3 g	3 g
Hydrochloric Acid	-	-	0.36 g
Water (18.2 MΩ Millipore®)	100 ml	100 ml	100 ml
Sodium Tungstate Dihydrate	-	1.83 g	-
Ammonium persulfate	2.28 g	2.28 g	2.28 g

Table 5.2
Formulated coatings with acronyms

Coating	**Designation**
Coating with 5 wt% of TiO_2	T5
Coating with 20 wt% of TiO_2	T20
Coating with 5 wt% of TiO_2/PPy composite	TiPPy5
Coating with 20 wt% of TiO_2/PPy composite	TiPPy20
Coating with 5 wt% of tungstate doped TiO_2/PPy composite	TiPPyW5
Coating with 20 wt% of tungstate doped TiO_2/PPy composite	TiPPyW20
Coating with 5 wt% of TiO_2/PAni composite	TiPAni5
Coating with 5 wt% of TiO_2/PAni composite	TiPAni20

5.4. Results and discussion

5.4.1. Morphology

All the mentioned composites (TiO_2/PPy composite, TiO_2/PPy (Tungstate doped) composite, and TiO_2/PAni composite) in this paper were synthesized in-situ with single step

chemical oxidative polymerization. SEM micrographs of TiO_2, TiO_2/PPy composite, TiO_2/PPy (Tungstate doped) composite, and TiO_2/PAni composite are shown in Figure 5.1. All the micrographs were obtained at same magnification and accelerating voltage which are mentioned on each micrograph respectively. As observed in Figure 5.1, TiO_2 as such is spherical and well separated without any agglomeration with particle size of individual particles in the range of 200-300 nanometers. In case of TiO_2/PPy composite, increase in the particle size of the particles is observed with varied particle size distribution and greater agglomeration. The observed morphology was also not spherical as in case of just TiO_2. For the TiO_2/PPy (Tungstate doped) composite, greater degree of agglomeration was observed possibly due to the presence of tungstate dopant. Nature and concentration of dopant in the synthesis of CPs result in order or disorder in the morphology of the CPs formation [53]. In case of TiO_2/PAni composite even larger amount of agglomeration was observed.

TEM images of TiO_2, TiO_2/PPy composite, TiO_2/PPy (Tungstate doped) composite, and TiO_2/PAni composite are shown in Figure 5.2. For as received TiO_2 as observed in Figure 5.2, spherical and needle like morphology was observed. For TiO_2/PPy composite, uniform thickness layer of PPy was observed around TiO_2 particles exhibiting core and shell morphology. This is the unique core and shell morphology of TiO_2/PPy synthesized in very facile manner. The average thickness of PPy shell was 50-60 nanometers around TiO_2 particles. Incorporation of PPy also resulted in agglomeration. In case of TiO_2/PPy (Tungstate doped) composite, much more dense layer of PPy was formed around TiO_2 particles. The average thickness of PPy shell was 80-100 nanometers around TiO_2 particles as well was growth of PPy particles was also more dense than that of in case of TiO_2/PPy composite. The compactness of PPy in the formation was found to be affected by the incorporation of the dopant anion [54]. For TiO_2/PAni composite,

PAni was randomly distributed around TiO_2 particles without any definite final morphology of TiO_2/PAni composite. Agglomerated morphology was also evident for TiO_2/PAni composite as observed in Figure 5.2. Even though resultant composite observed as agglomerated solids, size of agglomerates was small resulting into free flowing particles which could be easily incorporated into the coatings.

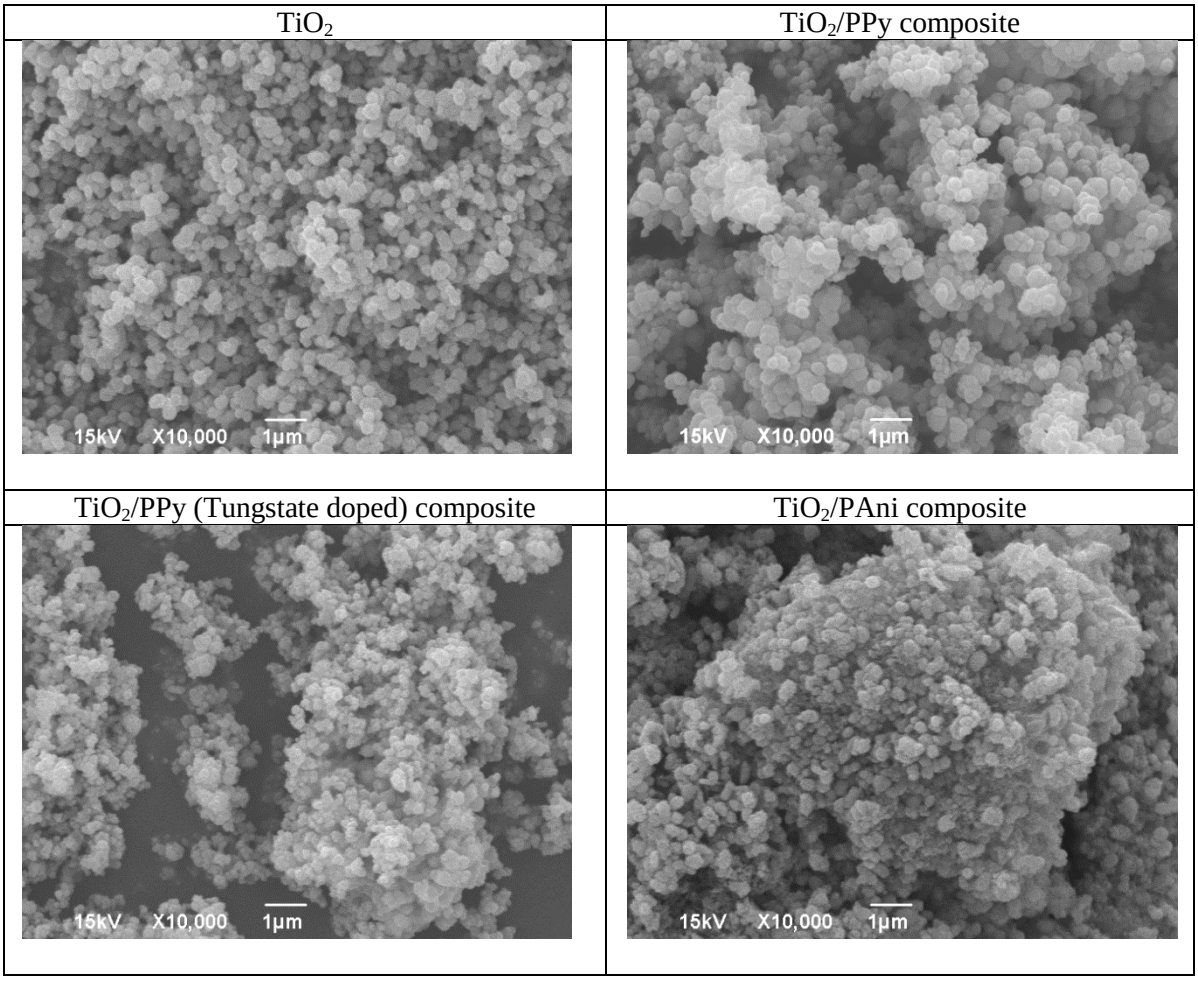

Figure 5.1: SEM micrographs of TiO_2 (Top left), TiO_2/PPy composite (Top right), TiO_2/PPy (Tungstate doped) composite (Bottom left), and TiO_2/PAni composite (Bottom right).

5.4.2. Chemical composition

Elemental composition was obtained by XPS analysis and the results are shown in Figure 5.3. As observed in Figure 5.3, in case of as received TiO_2 pigment particles, titanium, oxygen,

and aluminum content was high as compared to TiO_2/PPy composite, TiO_2/PPy (Tungstate doped) composite, and TiO_2/PAni composite. Presence of aluminum in case of TiO_2 pigment particles was attributed to the alumina surface treatment.

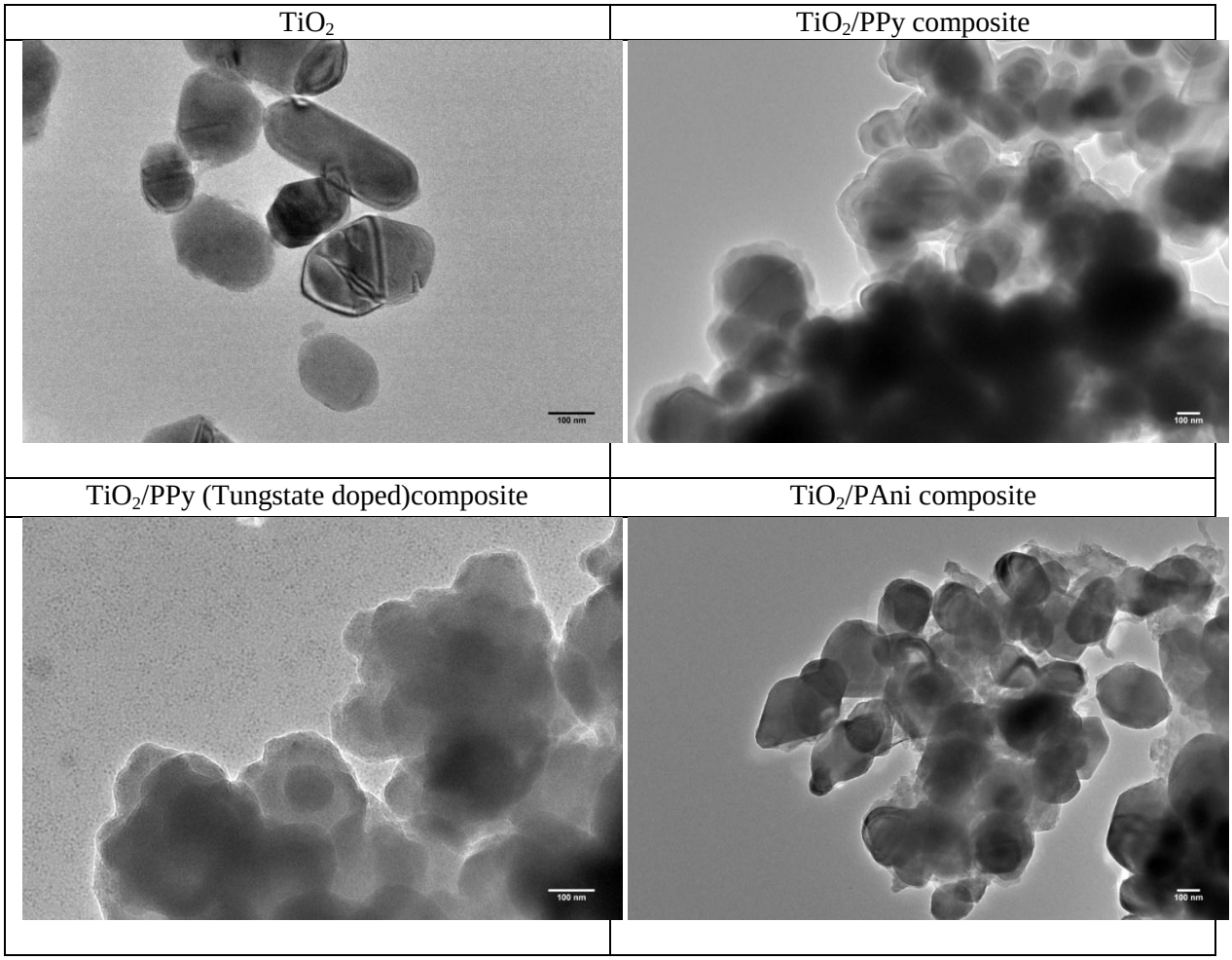

Figure 5.2: TEM images of TiO_2 (Top left), TiO_2/PPy composite (Top right), TiO_2/PPy (Tungstate doped) composite (Bottom left), and TiO_2/PAni composite (Bottom right).

Presence of nitrogen in case of TiO_2/PPy composite, TiO_2/PPy (Tungstate doped) composite indicated formation of PPy and in case of TiO_2/PAni composite indicated formation of PAni. Presence of sulfur in case of TiO_2/PPy composite and TiO_2/PAni composite indicated sulfur doping whereas presence of tungsten in case of TiO_2/PPy (Tungstate doped) composite indicated doping by tungsten anion. No sulfur was detected in case of TiO_2/PPy (Tungstate

doped) composite probably due to the possible competition by tungstate dopant. More titanium was observed in case of TiO_2/PAni composite, indicating bare particles of TiO_2 adjacent to the matrix of PAni. This morphology can be confirmed with TEM image as seen in Figure 5.2 (bottom right). No titanium was observed in case of TiO_2/PPy (Tungstate doped) composite indicating TiO_2 particles completely encapsulated in the PPy matrix as observed in TEM image (Figure 5.2 (bottom left)). The ratios of dopant to the nitrogen were obtained from the elemental analysis. For TiO_2/PPy composite, S/N ratio was 0.21, for TiO_2/PPy (Tungstate doped) composite, W/N ratio was 0.14 and for TiO_2/PAni composite, S/N ratio was 0.23.

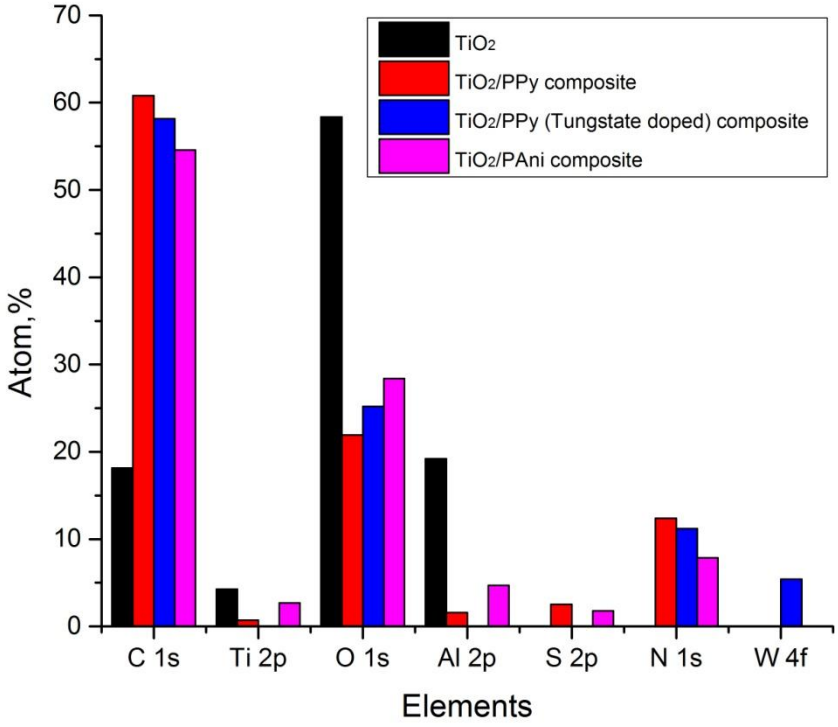

Figure 5.3: Elemental composition obtained by XPS.

High resolution core level spectrum of N 1s was obtained for TiO_2/PPy composite (Figure 5.4), TiO_2/PPy (Tungstate doped) composite (Figure 5.5), and TiO_2/PAni composite (Figure 5.7), whereas high resolution core level spectrum of W 4f was obtained for (Tungstate

doped) composite (Figure 5.6). The spectrum for N 1s and W 4f were deconvulated into the individual peaks and are tabulated in Table 5.3.

Table 5.3
Peak distribution for composites obtained by XPS

TiO_2/PPy composite			**TiO_2/PPy (Tungstate doped) composite**			**TiO_2/PAni composite**		
Peak eV	Species	Group %	Peak eV	Species	Group %	Peak eV	Species	Group %
398.02	-N= imine nitrogen	3.03	400.21	-NH- neutral amine nitrogen	68.67	398.50	-N= imine nitrogen	5.04
399.90	-NH- neutral amine nitrogen	71.44	401.25	$-N^+-$ positively charged nitrogen atom	31.33	400.25	$-N^+-$ localized positively charged nitrogen atom	79.27
401.19	$-N^+-$ positively charged nitrogen atom	25.53	35.68	W $4f_{7/2}$ W^{6+} oxidation state	51.16	401.56	$-N^+-$ positively charged nitrogen atom	15.69
			37.80	W $4f_{5/2}$ W^{6+} oxidation state	43.21			
			41.30	W loss peak	5.63			

Respective percentages of obtained species are also mentioned in Table 5.3. In case of TiO_2/PPy composite, the peak at 398.02 eV was ascribed to imine nitrogen (-N=) [55], the peak at 399.90 eV was attributed to neutral amine nitrogen (-NH-), and the peak at 401.19 eV was ascribed to positively charged nitrogen atom ($-N^+-$) [56]. In case of TiO_2/PPy (Tungstate doped) composite the neutral amine nitrogen (-NH-) and positively charged nitrogen atom ($-N^+-$) were found at 400.21 eV and 401.25 eV respectively. For TiO_2/PPy (Tungstate doped) composite deconvulated W 4f spectrum showed peaks at 35.68 eV, 37.80 eV, and at 41.3 eV. For this 35.68 eV and 37.80 eV correspond to W^{6+} oxidation state [51, 57] and 41.3 eV is a peak due to W loss.

In case of TiO_2/PAni composite, 398.50 eV peak was attributed to imine nitrogen (-N=), 400.25 eV peak due to the localized positively charged nitrogen (-N^+-), and at 401.56 eV due to the positively charged nitrogen atom (-N^+-) [58]. Protonation level can be obtained by [N^+]/[N] ratio [59]. Higher level of protonation signified higher doping for the composite pigments.

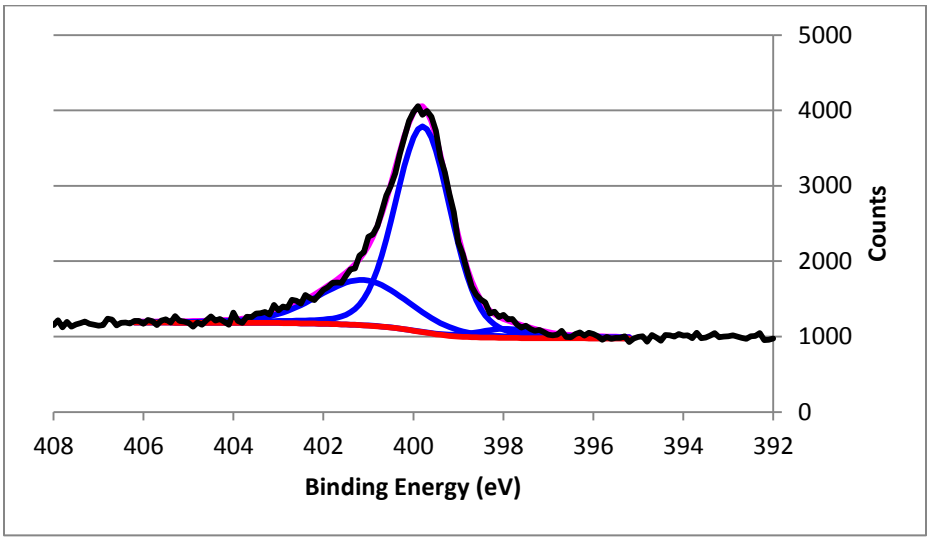

Figure 5.4: TiO_2/PPy composite N 1s high resolution.

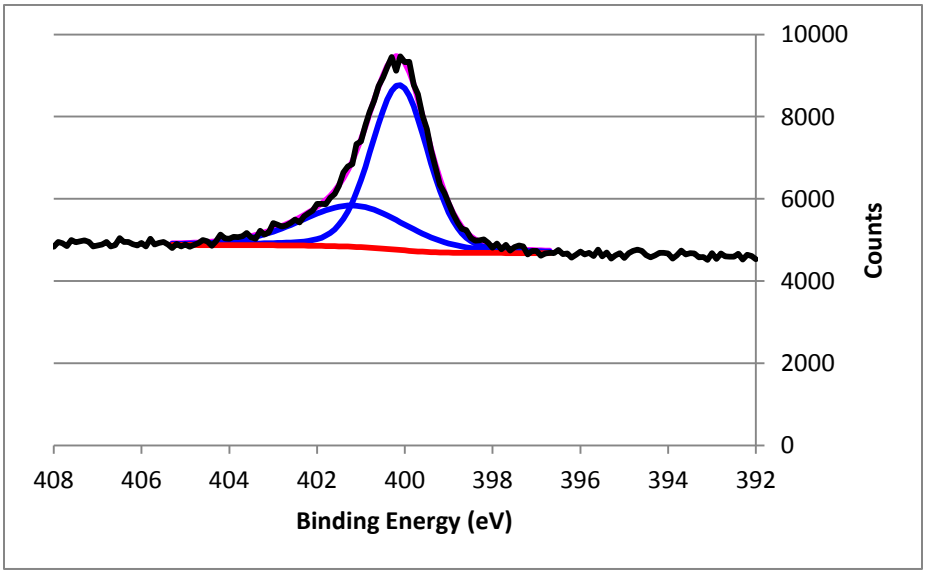

Figure 5.5: TiO_2/PPy (Tungstate doped) composite N 1s high resolution.

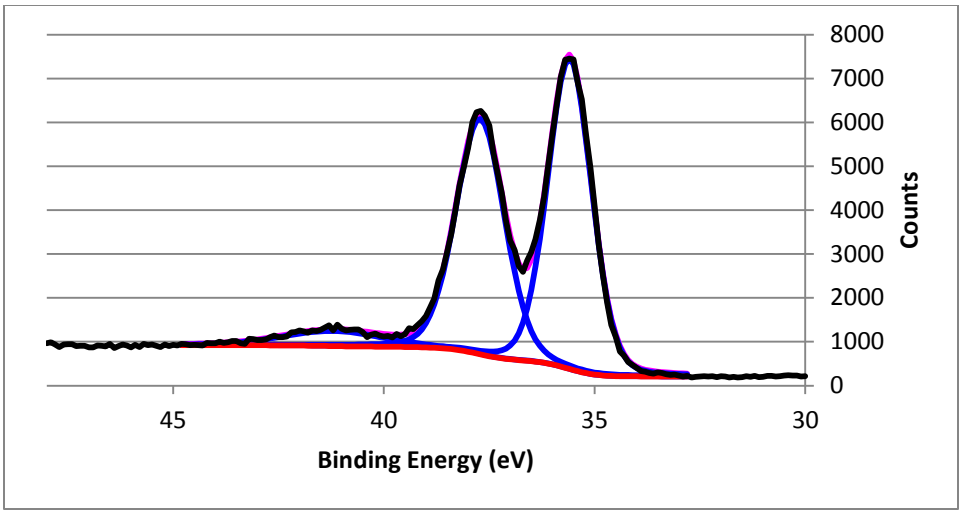

Figure 5.6: TiO_2/PPy (Tungstate doped) composite, W 4f high resolution.

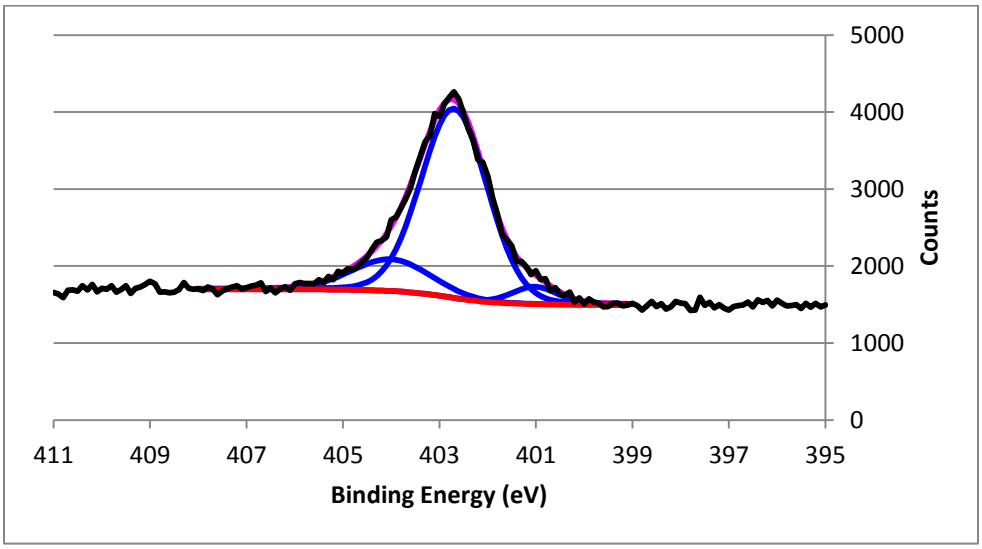

Figure 5.7: TiO_2/PAni composite N 1s high resolution.

FTIR spectra was collected for TiO_2, TiO_2/PPy composite, TiO_2/PPy (Tungstate doped) composite, and TiO_2/PAni composite and is shown in Figure 5.8 (a, b, c, and d). Respective wavenumbers (cm^{-1}) and modes of vibration are presented in Table 5.4. TiO_2 absorption band can be observed at 700-500 cm^{-1} [60] as observed in Figure 5.8(a). This peak for TiO_2 was overshadowed by other characteristic peaks for PPy in case of TiO_2/PPy composite (Figure 5.8(b)), PPy and tungstate ion band in case of TiO_2/PPy (Tungstate doped) composite (Figure 5.

8(c)), and by PAni characteristic bands in case of TiO_2/PAni composite (Figure 5.8(d)). This might be due to the possible interaction of the PPy or PAni or tungstate ion with the TiO_2 surface [61].

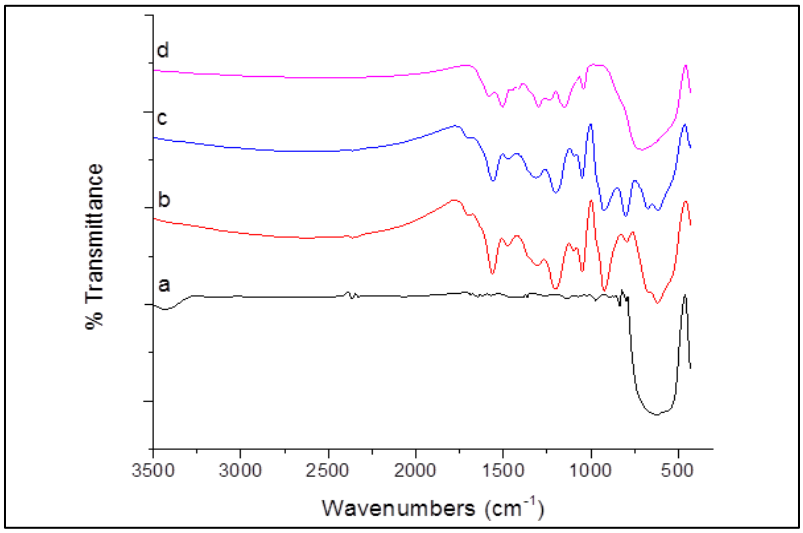

Figure 5.8: FTIR spectra of (a) TiO_2, (b) TiO_2/PPy composite, (c) TiO_2/PPy (Tungstate doped) composite**,** and (d) TiO_2/PAni composite.

Carbonyl group vibration band for TiO_2/PPy composite and TiO_2/PPy (Tungstate doped) composite was observed at 1701 cm^{-1} due to overoxidation of CPs but this band was not so prominent in both of the cases suggesting minimal loss in conductivity [62]. C-C and C=C ring stretching vibrations were observed at 1561 cm^{-1} and 1558 cm^{-1} in TiO_2/PPy composite and TiO_2/PPy (Tungstate doped) composite respectively. C-N and C=C stretching vibrations were observed at 1473 cm^{-1} and 1463 cm^{-1} for TiO_2/PPy composite and TiO_2/PPy (Tungstate doped) composite respectively [63]. C-H and C-N in plane deformations (1311 cm^{-1}) were observed for TiO_2/PPy composite and TiO_2/PPy (Tungstate doped) composite [64]. Pyrrole ring breathing vibration was observed at 1202 cm^{-1} and 1199 cm^{-1} for TiO_2/PPy composite and TiO_2/PPy (Tungstate doped) composite respectively [65]. Vibration around 1090 cm^{-1} C-C in plane deformation and 1045 cm^{-1} C-H deformation were observed in both TiO_2/PPy composite and

TiO_2/PPy (Tungstate doped) composite [66]. 929 cm^{-1} and 788 cm^{-1} PPy characteristic peak were also observed for TiO_2/PPy composite and TiO_2/PPy (Tungstate doped) composite. Tungstate ion band 960-780 cm^{-1} and 900-770 cm^{-1} was observed for TiO_2/PPy (Tungstate doped) composite as observed in Figure 5.8(c) [60].

Table 5.4
Peak positions (cm^{-1}) and FTIR modes of vibrations for TiO_2, TiO_2/PPy composite, TiO_2/PPy (Tungstate doped) composite, and TiO_2/PAni composite

Wavenumbers (cm^{-1}) and modes of vibration	TiO_2 (Wavenumber (cm^{-1}))	TiO_2/PPy composite (Wavenumber (cm^{-1}))	TiO_2/PPy (Tungstate doped)composite composite (Wavenumber (cm^{-1}))	TiO_2/PAni composite (Wavenumber (cm^{-1}))
1702, carbonyl group		1701	1701	
1580, quinoid stretching				1581
1558, C-C and C=C ring stretching		1561	1558	
1505, benzene ring stretching				1505
1464, C-N and C=C stretching		1473	1463	
1460, C=N stretching of quinoid ring				1448
1300, C-N stretching mode				1299
1295, C-H and C-N in plane deformation		1311	1311	
1229, C-C twisting				1229
1144, $-NH^+$ = vibration due to protonation				1148
1198, ring breathing		1202	1199	
1090, C-C in plane deformation		1090	1090	
1045, C-H deformation		1048	1049	
1045, C-H in plane bending				1042
929 and 788 PPy characteristic peak, 700-660 TiO_2 peaks, 960-780 and 900-770 tungstate ion band	700-500	923, 792, 678, 616	925, 801, 678, 617	707

For TiO_2/PAni composite, the band at 1581 cm^{-1} was observed due to quinoid stretching vibration mode and at 1505 cm^{-1} due to benzene ring stretching deformation as seen in Figure 5. 8(d) [67-68]. Band at 1460 cm^{-1} is due to the C=N stretching of quinoid ring [68] which was observed at 1448 cm^{-1} for TiO_2/PAni composite. Band at 1299 cm^{-1} was observed due to the C-N stretching mode [51]. The band at 1235 cm^{-1} is due to the C-C twisting and was observed at 1229 cm^{-1} as observed in Figure 5.8(d) [69]. The band at 1144 cm^{-1} is due to $-NH^+$ = vibration resulting from protonation and was observed at 1148 cm^{-1} for TiO_2/PAni composite [51]. Band at 1045 cm^{-1} is due to C-H in plane bending mode and was observed at 1042 cm^{-1} [68].

5.4.3. Conductivity

For surface current density, CAFM experiments were performed on the pressed pellets of composites glued to the aluminum mounts. For the CAFM measurements 100 mV DC bias was applied. Surface topography, deflection, and current images for TiO_2/PPy composite, TiO_2/PPy (Tungstate doped) composite**,** and TiO_2/PAni composite as presented in Figure 5.9, 5.10, and 5.11 respectively. As observed in Figure 5.9, current image illustrated dense current density for the TiO_2/PPy composite whereas for TiO_2/PPy (Tungstate doped) composite (Figure 5.10) current image exhibited less dense areas as compared to the TiO_2/PPy composite. For TiO_2/PAni composite (Figure 5.11), the current image did not exhibit significant current density. The conductive regions in CAFM measurements are on local scale so the current density image shows the local conductive representation whereas for global scale conductivity measurements were gathered by four point conductivity measurements. Same pellets as used for CAFM measurements were employed in four point probe conductivity measurements and the results are presented in Figure 5.12. In this case TiO_2/PPy (Tungstate doped) composite showed highest conductivity which might be possible due to the doping of tungstate ion in the backbone of PPy.

Again here conductivity of the composite material is measured which gets affected by the presence of TiO_2 in the total matrix. Even though XPS results suggest that TiO_2/PAni composite will be conductive but due to its presence in the blend with TiO_2 has resulted in the decrease in the conductivity. There is also possibility that in TiO_2/PAni composite, presence of TiO_2 in such a way that connectivity between PAni chains is not achieved and so lesser conductivity is observed or amount of PAni is not enough to provide high conductivity [70]. Conductivity value of TiO_2/PAni composite is 2.224×10^{-5} S/m. It has been observed that charge transport in PAni composites depends on the PAni percentage in the total composite [71].

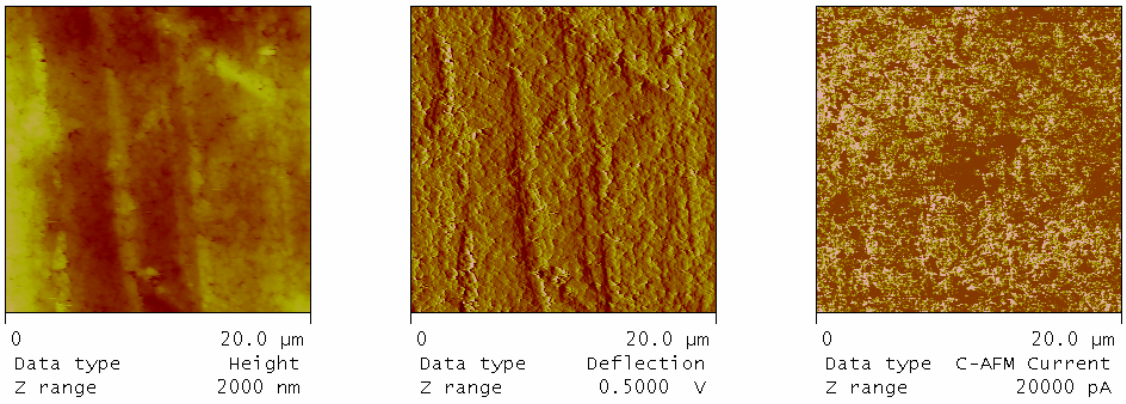

Figure 5.9: Height, deflection and current images for TiO_2/PPy composite.

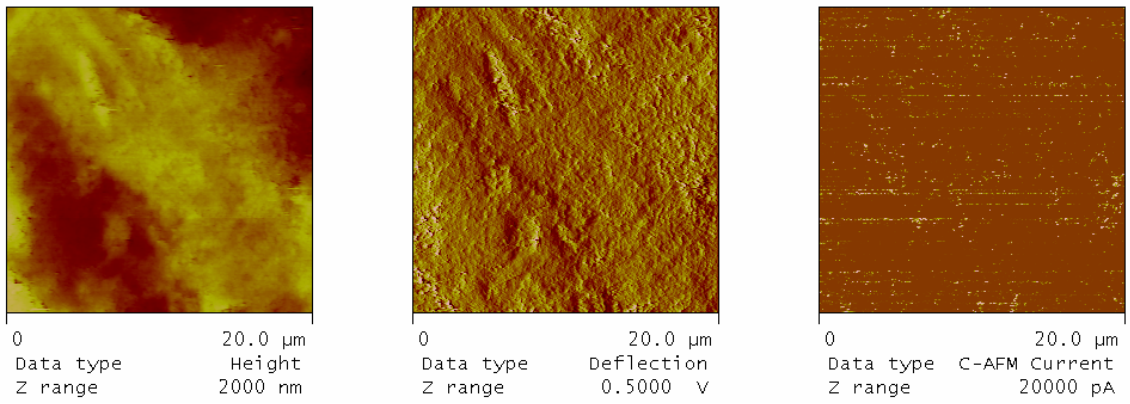

Figure 5.10: Height, deflection and current images for TiO_2/PPy (Tungstate doped) composite.

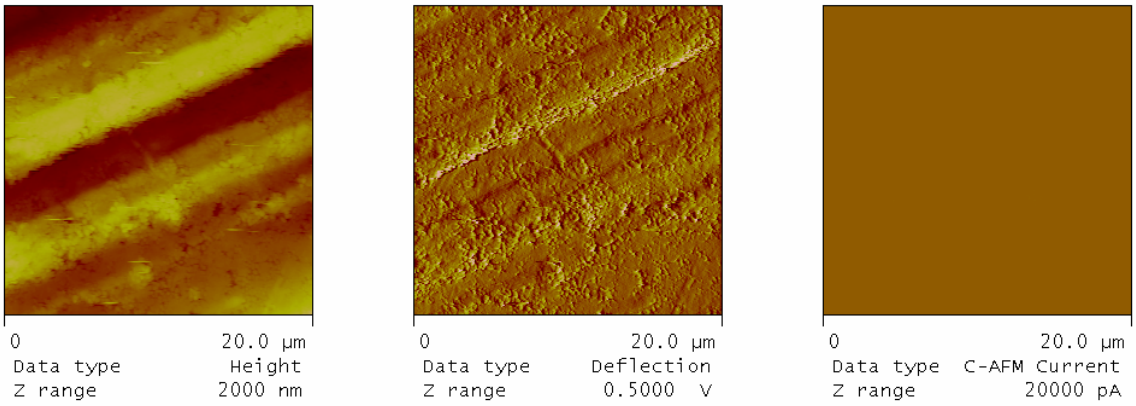

Figure 5.11: Height, deflection and current images for TiO_2/PAni composite.

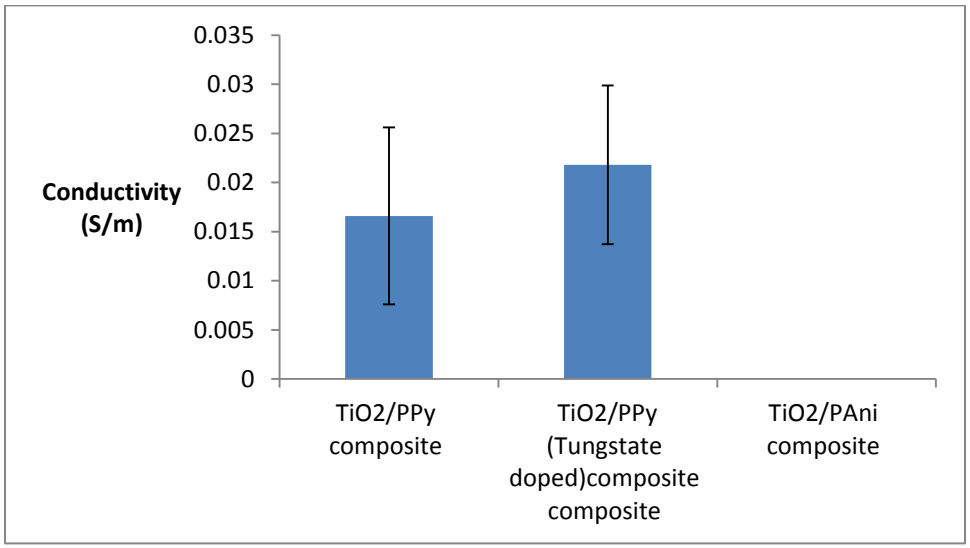

Figure 5.12: Conductivity values obtained by four point probe measurement.

5.4.4. Electrochemical impedance spectroscopy (EIS)

EIS is a powerful technique which has been employed for studying corrosion protection provided by coatings [72-75]. EIS was performed with three electrode cell with saturated calomel as a reference electrode, coated substrate as working electrode, and platinum mesh as a counter electrode. EIS was performed on the coated samples immersed in the 5% NaCl at initial, 24 hours, 7 days, 14 days, and 21 days. Bode plot of T5 and T20, TiPPy5 and TiPPy20, TiPPyW5 and TiPPyW20, TiPAni5 and TiPAni20 are presented in Figure 5.13, 5.14, 5.15, 5.16

respectively. For coating T5 (Figure 5.13 (left)), initial impedance (low frequency) was very high but as the duration of exposure to the electrolyte increased (21 days), the value of low frequency impedance decreased to lower than 10^5 indicating passage of electrolyte through the coating and reaching to interface leading to corrosion. In case of T20 coating (Figure 5.13(right)), low frequency impedance which was higher initially decreased to 10^8 as exposure duration to the electrolyte increased to 21 days. In case of TiPPy5 and TiPPy20 (Figure 5.14), initial value of low frequency impedance was 10^8, however after 21 days of exposure to the electrolyte, only an order of magnitude decrease to 10^7-10^6 was observed. For TiPPyW5 (Figure 5.15(left)), initial low frequency impedance decreased to 10^8 after electrolyte exposure for 21 days whereas for TiPPyW20 (Figure 5.15(right)), it reached to the value of 10^9. In case of TiPAni5 and TiPAni20 (Figure 16), after 21 days of exposure to the electrolyte, the value of low frequency impedance was decreased to 10^9. As observed in Figure 5.15 and 5.16, initial low frequency impedance values were very high (10^{10}-10^{11}) however as exposure duration to the electrolyte increased, the impedance was observed to be decreasing.

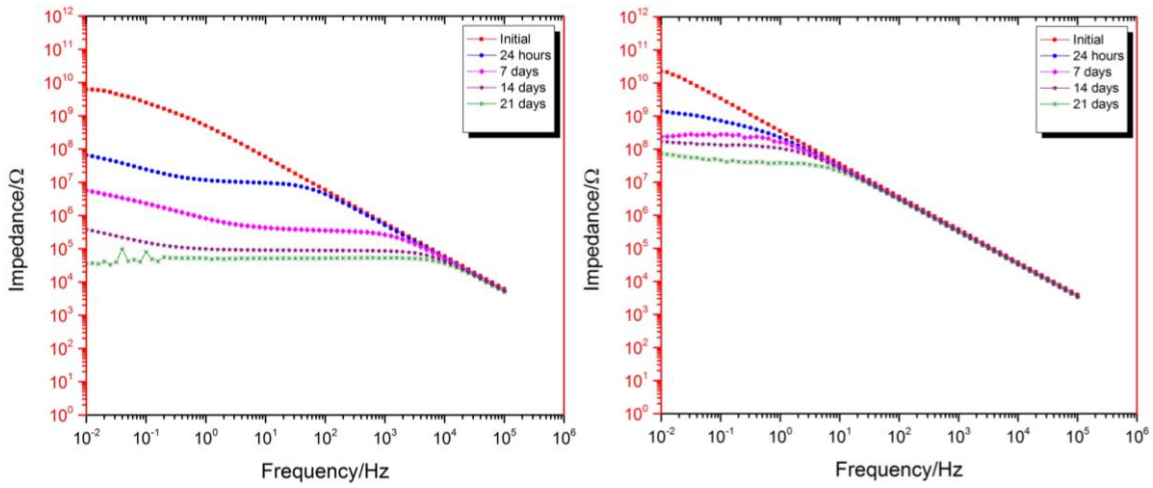

Figure 5.13: Bode plot of T5 (left) and T20 (right).

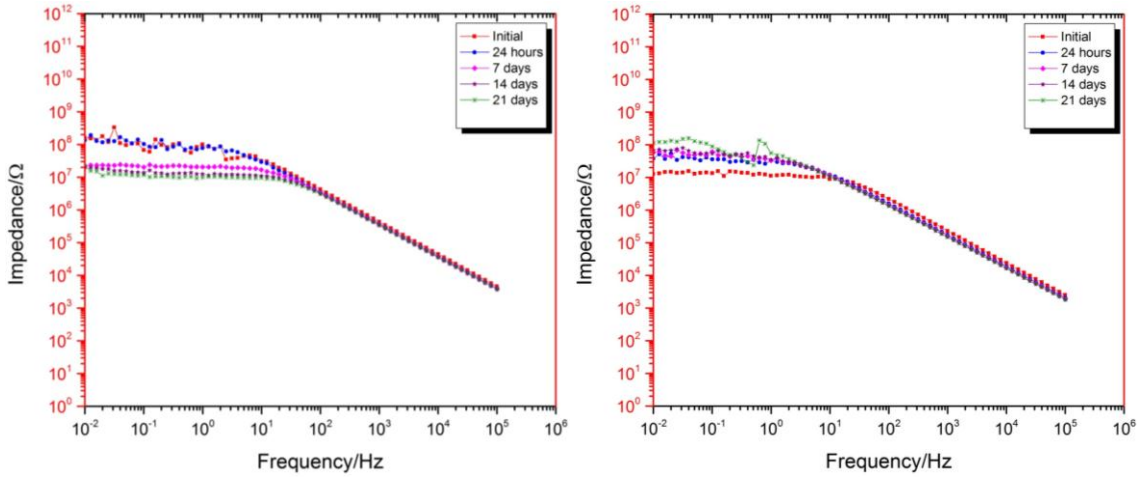

Figure 5.14: Bode plot of TiPPy5 (left) and TiPPy20 (right).

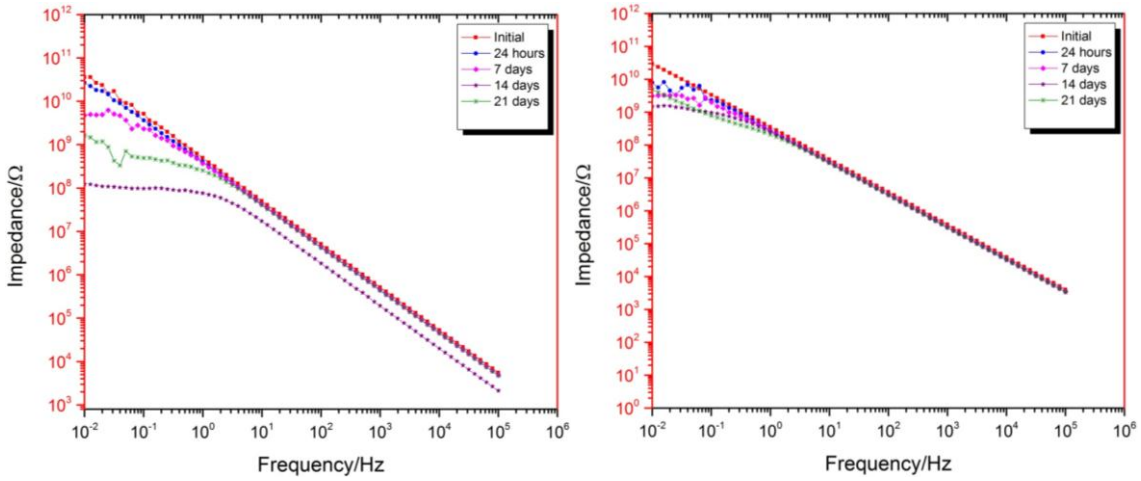

Figure 5.15: Bode plot of TiPPyW5 (left) and TiPPyW20 (right).

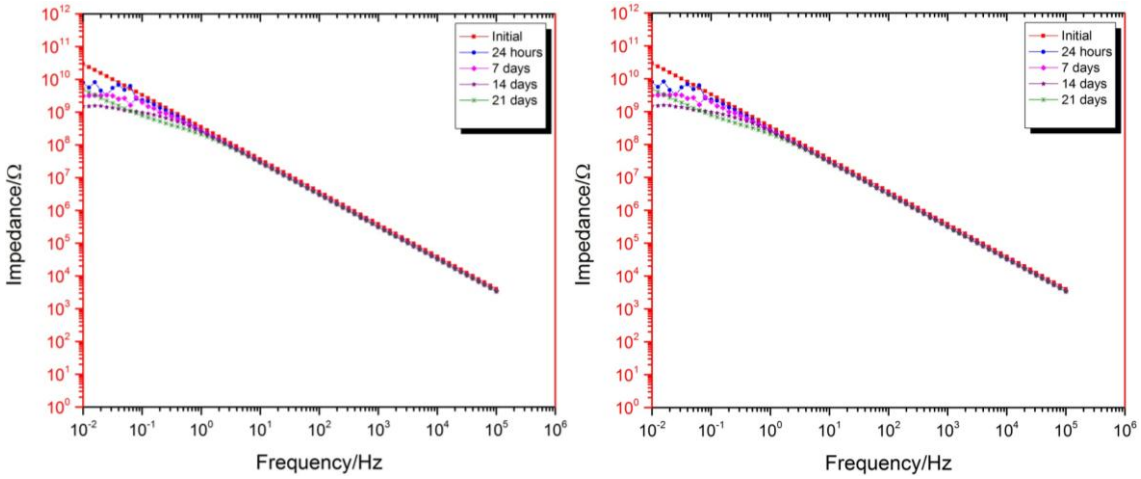

Figure 5.16: Bode plot of TiPAni5 (left) and TiPAni20 (right).

ZView2 software from Scribner® Associates Inc. was employed for the equivalent circuit modeling and fitting of the EIS data. The circuit models used for the data fitting are shown in Figure 5.17, and the circuit element fit results are presented in Table 5.5. In Figure 5.17, R1 is solution resistance, R2 is coatings resistance, R3 is polarization resistance, Cc is coatings capacitance, Cdl is double layer capacitance, and Ws is Warburg short element. Constant phase element (CPE) is a pseudo capacitor. Its impedance of CPE can be obtained by equation 5.1.

$$Z_{(CPE)} = 1/[(T)(j\omega)^{P}] \quad (5.1)$$

Where, T is capacitance, j is an imaginary component, ω is the angular frequency (ω = 2πf, f is the frequency), P is the power ($0 \leq n \leq 1$), and $Z_{(CPE)}$ is the impedance of CPE. P value close to 1 represents capacitor behavior. Diffusion phenomena observed in the coatings as time of immersion in electrolyte increased was modeled by employing equation 5.2.

$$Z_w = 1/\sigma(i\omega)^{(-1/2)} \quad (5.2)$$

Where, Z_w is Warburg impedance, i is imaginary component, σ is Warburg capacitance, and ω is the angular frequency.

For coating T5, after 24 hours of immersion in electrolyte, second time constant was observed in Bode plot (Figure 5.13(left)). Second time constant continued till 14 days and this data was modeled by circuit model presented in Figure 5.17(b). At 21st day, there was a possibility of second time constant in low frequency region but due to noise it was difficult to model. There is a possibility of complete damage of the coating due to the immersion [45]. This is also supported with the lower impedance observed at low frequency obtained from circuit modeling (10^4 Ω) (Table 5.5). Increase in the capacitance value (CPE_{dl}-T) suggested coatings degradation as exposure to the electrolyte increased. Increase in CPE_{dl}-T value with immersion

time was also observed in case of coating T20 (Table 5.5) however this increase was not significant as compared to the coating T5.

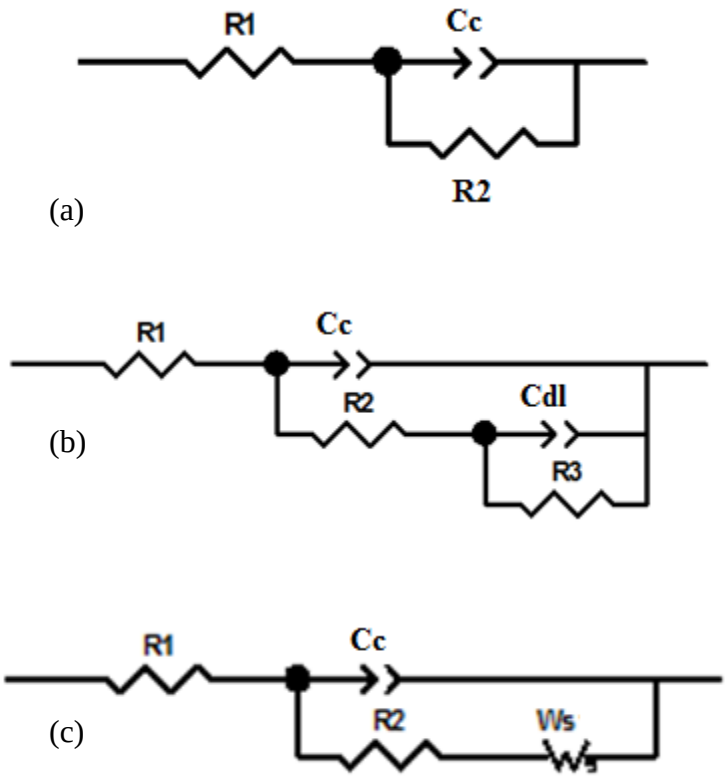

Figure 5.17: Equivalent circuit models for EIS data fitting.

For coating TiPPy5, coating resistance (Rc) steadily decreased as exposure time to the electrolyte increased however at the same time second time constant also appeared at 14th and 21st day of immersion indicating corrosion happening underneath the coating upon the substrate [76]. For coating TiPPy20, coatings resistance (Rc), increased at 21st day of immersion indicating formation of passive layer due to the corrosion production or the passivation achieved by PPy underneath the coating [28,77]. In case of coating TiPPyW5 and TiPPyW20, drop in the value of coating resistance (Rc) was followed by increase in the value of Rc at 21st day of immersion. A similar observation was made on mild steel substrate coated with tungstate doped PPy. Tungstate anion participated in the passivation process resulting in increase in coating

resistance value [35]. Increase in the values of polarization resistance (Rct) also suggested increase in charge transfer resistance in tungstate doped coatings. For TiPAni5 coating, Warburg element appeared at 24 hours and 7^{th} day indicating the diffusion of species through the coating however, at 14^{th} and 21^{st} day, second time constant appeared suggesting reaction happening at interface of the metal and the coating. However the coating resistance value was still at 10^7 Ω after 21 days of the immersion. For TiPAni20 coating, only one time constant was employed for modeling the data and coating resistance at 21^{st} day of immersion was still high. Protection mechanism suggested for the protection of mild steel substrate by PAni is mostly passivation resulting from the redox activity [78].

5.4.5. Potentiodynamic scans

Potentiodynamic scans were performed on the defect made up of size 1.5 cm in length and 1 mm in width. For T5, T20, TiPPy5, TiPPy20, TiPPyW5, TiPPyW20, TiPAni5, and TiPAni20 potentiodynamic scans are shown in Figure 5.18. Corrosion potential was shifted in positive direction by 100-200 mV for all of the coating systems as compared to T5, and T20. Almost 250 mV positive shift in potential was obtained for TiPPyW20. This might be due to the increase in storage charge in TiPPyW20 coating due to tungstate ion incorporation, resulting in improved corrosion protection [79]. There is also the possibility of participation in the passivation process by tungstate anion resulting in improved corrosion protection [50]. Due to the core and shell particles of PPy and TiO_2, effective area for redox activity and for metal surface interaction increased in case of TiO_2/PPy composite [46] . Another mechanism at work is the barrier posed by formed passivation layer to the corrosive species. Possibility of combining tungstate with ferrous ions resulting from the oxidation of the underlying steel also results in corrosion protection. Additionally PPy and PAni are p-type material whereas TiO_2 is n-type

semiconductor which acts as inhibitor to the transport of holes. Intimate contact of CPs with TiO_2 results into the formation of p-n junction which will decrease the charge transfer leading to decrease in the corrosion rate [45].

Table 5.5
Fit results obtained from equivalent circuit modeling of EIS data

	Time	Rc	CPEc		Rct	W-R	CPEdl	
			T	P			T	P
T5	Initial	5.28×10^{9}	3.55×10^{-10}	0.97				
	24 hours	9.44×10^{6}	3.48×10^{-10}	0.99	1.31×10^{8}		7.48×10^{-8}	0.68
	7 days	3.32×10^{5}	4.21×10^{-10}	0.97	9.46×10^{6}		5.60×10^{-7}	0.60
	14 days	8.81×10^{4}	4.55×10^{-10}	0.97	5.30×10^{6}		1.47×10^{-5}	0.69
	21 days	5.31×10^{4}	3.49×10^{-10}	0.99				
T20	Initial	8.21×10^{10}	4.79×10^{-10}	0.99				
	24 hours	2.91×10^{8}	5.57×10^{-10}	0.98	2.21×10^{9}		1.78×10^{-9}	0.49
	7 days	1.19×10^{8}	5.88×10^{-10}	0.98	1.58×10^{8}		1.06×10^{-9}	0.63
	14 days	1.26×10^{8}	6.78×10^{-10}	0.97				
	21 days	3.73×10^{7}	6.38×10^{-10}	0.98	3.88×10^{7}		9.06×10^{-8}	0.71
TiPPy5	Initial	1.20×10^{8}	5.07×10^{-10}	0.97				
	24 hours	1.14×10^{8}	6.05×10^{-10}	0.97				
	7 days	2.18×10^{7}	5.75×10^{-10}	0.97				
	14 days	1.20×10^{7}	5.61×10^{-10}	0.97	1.14×10^{7}		3.49×10^{-7}	0.56
	21 days	9.97×10^{6}	5.62×10^{-10}	0.97	6.78×10^{6}		6.44×10^{-7}	0.81
TiPPy20	Initial	1.28×10^{7}	8.51×10^{-10}	0.98				
	24 hours	3.52×10^{7}	1.37×10^{-9}	0.96				
	7 days	4.93×10^{7}	1.72×10^{-9}	0.94				
	14 days	5.80×10^{7}	1.95×10^{-9}	0.93				
	21 days	1.15×10^{8}	2.04×10^{-9}	0.94				
TiPPyW5	Initial	7.06×10^{10}	3.27×10^{-10}	0.99				
	24 hours	4.22×10^{10}	4.20×10^{-10}	0.98				
	7 days	5.25×10^{9}	4.63×10^{-10}	0.97				
	14 days	8.40×10^{7}	9.76×10^{-10}	0.98	7.89×10^{7}		5.88×10^{-8}	0.45
	21 days	4.36×10^{8}	4.36×10^{-10}	0.98	8.00×10^{8}		7.55×10^{-9}	1
TiPPyW 20	Initial	2.21×10^{11}	4.77×10^{-10}	0.98				
	24 hours	8.01×10^{9}	5.60×10^{-10}	0.99				
	7 days	4.01×10^{9}	6.76×10^{-10}	0.97				
	14 days	1.43×10^{9}	6.93×10^{-10}	0.97				
	21 days	4.88×10^{8}	6.03×10^{-10}	0.98	5.87×10^{9}		1.78×10^{-9}	0.86
TiPAni5	Initial	8.25×10^{10}	2.82×10^{-10}	0.99				
	24 hours	2.85×10^{7}	3.98×10^{-10}	0.98		2.54×10^{9}		
	7 days	5.70×10^{7}	4.16×10^{-10}	0.98		3.89×10^{8}		
	14 days	4.63×10^{7}	4.19×10^{-10}	0.98	2.27×10^{8}		2.11×10^{-8}	0.17
	21 days	5.03×10^{7}	4.39×10^{-10}	0.97	6.36×10^{7}		6.58×10^{-8}	0.65
TiPAni20	Initial	6.75×10^{10}	5.22×10^{-10}	0.97				
	24 hours	1.76×10^{8}	1.86×10^{-9}	0.90				
	7 days	1.04×10^{8}	2.63×10^{-9}	0.87				
	14 days	9.90×10^{7}	2.86×10^{-9}	0.87				
	21 days	1.87×10^{7}	2.70×10^{-9}	0.87				

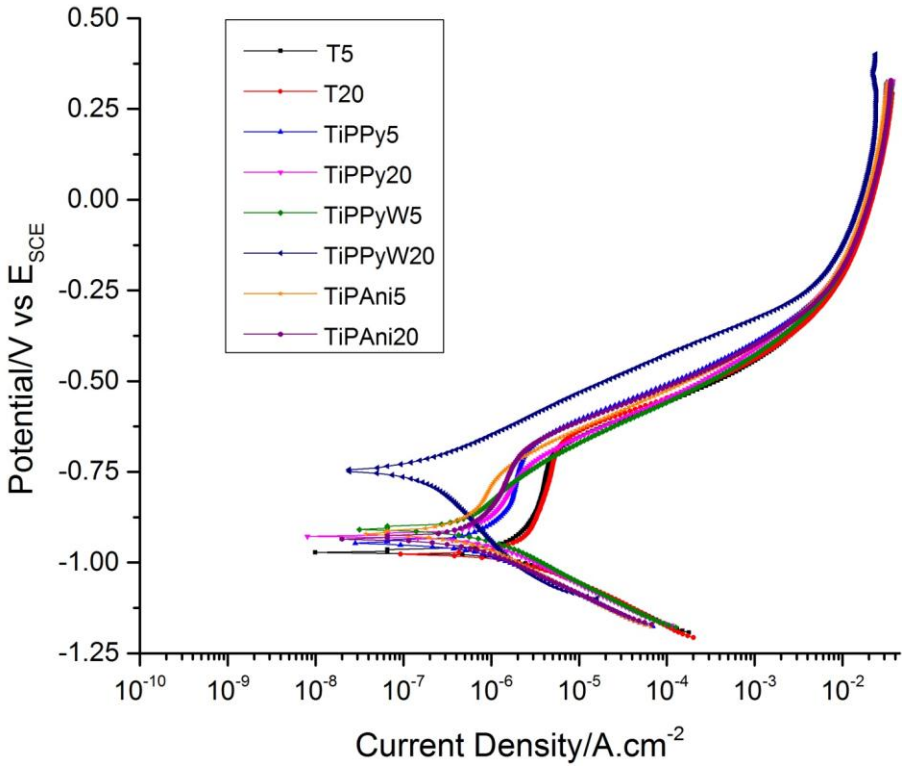

Figure 5.18: Potentiodynamic scans.

5.5. Conclusions

Core and shell composite of PPy and TiO_2 was successfully prepared by chemical oxidative polymerization with PPy shell thickness of 50-60 nanometers. Similar and denser morphology was also obtained for TiO_2/PPy composite doped with tungstate anion. TiO_2/PPy composite and TiO_2/PPy (Tungstate doped) composite were found to be conductive as observed in CAFM and four point probe conductivity measurements. TiO_2/PPy composite, TiO_2/PAni composite and TiO_2/PPy (Tungstate doped) composite based coatings exhibited improved corrosion protection on steel substrate as evidenced in EIS measurements and potentiodynamic scans. The suggested mechanisms for improved corrosion protection are effective area increase of CP, passivation and dopant release.

5.6. Acknowledgements

The authors gratefully acknowledge the support of this research by US Army Research Laboratory under grant no. W911NF-09-2-0014, W911NF-10-2-0082, and W911NF-11-2-0027.

5.7. References

[1] G.F. Hays, Corrodia (2010).

[2] N.S. Sangaj, V.C. Malshe, Progress in Organic Coatings, 50 (2004) 28-39.

[3] P. Roberge, Corrosion Engineering: Principles and Practice, McGraw-Hill Companies,Incorporated, 2008.

[4] E. McCafferty, Introduction to Corrosion Science, Springer, 2010.

[5] J.R. Davis, Corrosion: Understanding the Basics, Asm International, 2000.

[6] Z. Ahmad, Principles of Corrosion Engineering and Corrosion Control, Elsevier Science, 2006.

[7] M.D. Cohen, B. Kargacin, C.B. Klein, M. Costa, Critical Reviews in Toxicology, 23 (1993) 255-281.

[8] S.Y. Hong, D.S. Marynick, Macromolecules, 25 (1992) 4652-4657.

[9] S. Zor, F. Kandemirli, E. Yakar, T. Arslan, Protection of Metals and Physical Chemistry of Surfaces, 46 (2010) 110-116.

[10] H. Bai, G. Shi, Sensors, 7 (2007) 267-307.

[11] E. Smela, Advanced Materials, 15 (2003) 481-494.

[12] A. Rudge, J. Davey, I. Raistrick, S. Gottesfeld, J.P. Ferraris, Journal of Power Sources, 47 (1994) 89-107.

[13] P. Chandrasekhar, Conducting Polymers, Fundamentals and Applications: A Practical Approach, Kluwer, 1999.

[14] K. Gurunathan, D.P. Amalnerkar, D.C. Trivedi, Materials Letters, 57 (2003) 1642-1648.

[15] J. Hou, C. Yang, Y. Li, Synthetic Metals, 153 (2005) 93-96.

[16] J. Pei, W.-L. Yu, W. Huang, A.J. Heeger, Macromolecules, 33 (2000) 2462-2471.

[17] S. Geetha, C.R.K. Rao, M. Vijayan, D.C. Trivedi, Analytica Chimica Acta, 568 (2006) 119-125.

[18] D. Tallman, G. Spinks, A. Dominis, G. Wallace, J. Solid State Electrochem., 6 (2002) 73-84.

[19] G. Mengoli, M.T. Munari, P. Bianco, M.M. Musiani, Journal of Applied Polymer Science, 26 (1981) 4247-4257.

[20] D.W. DeBerry, Journal of the Electrochemical Society, 132 (1985) 1022-1026.

[21] Y. Wei, J. Wang, X. Jia, J.-M. Yeh, P. Spellane, Polymer, 36 (1995) 4535-4537.

[22] N. Ahmad, A.G. MacDiarmid, Synthetic Metals, 78 (1996) 103-110.

[23] D.E. Tallman, Y. Pae, G.P. Bierwagen, Corrosion, 55 (1999) 779-786.

[24] U. Rammelt, P.T. Nguyen, W. Plieth, Electrochimica Acta, 46 (2001) 4251-4257.

[25] E. Armelin, R. Pla, F. Liesa, X. Ramis, J.I. Iribarren, C. Alemán, Corrosion Science, 50 (2008) 721-728.

[26] A.F. Baldissera, C.A. Ferreira, Progress in Organic Coatings, 75 (2012) 241-247.

[27] N.K. Guimard, N. Gomez, C.E. Schmidt, Progress in Polymer Science, 32 (2007) 876-921.

[28] G. Spinks, A. Dominis, G. Wallace, D. Tallman, J. Solid State Electrochem., 6 (2002) 85-100.

[29] T. Tüken, B. Yazıcı, M. Erbil, Progress in Organic Coatings, 53 (2005) 38-45.

[30] K.R.L. Castagno, V. Dalmoro, D.S. Azambuja, Materials Chemistry and Physics, 130 (2011) 721-726.

[31] M. Sharifirad, A. Omrani, A.A. Rostami, M. Khoshroo, Journal of Electroanalytical Chemistry, 645 (2010) 149-158.

[32] Y. Li, M.Y. Leung, X.M. Tao, X.Y. Cheng, J. Tsang, M.C.W. Yuen, Journal of Materials Science, 40 (2005) 4093-4095.

[33] F. Jonas, L. Schrader, Synthetic Metals, 41 (1991) 831-836.

[34] J. Jang, B. Lim, J. Lee, T. Hyeon, Chemical Communications, 0 (2001) 83-84.

[35] M.G. Hosseini, M. Sabouri, T. Shahrabi, Journal of Applied Polymer Science, 110 (2008) 2733-2741.

[36] M.I. Khan, A.U. Chaudhry, S. Hashim, M.K. Zahoor, M.Z. Iqbal, Recent developments in intrinsically conductive polymer coatings for corrosion protection, 2010.

[37] A. Olad, B. Naseri, Progress in Organic Coatings, 67 (2010) 233-238.

[38] N. Bahrami Panah, I. Danaee, Progress in Organic Coatings, 68 (2010) 214-218.

[39] X. Qi, C. Vetter, A.C. Harper, V.J. Gelling, Progress in Organic Coatings, 63 (2008) 345-351.

[40] J. Zeno W. Wicks, F.N. Jones, S.P. Pappas, D.A. Wicks, Organic Coatings: Science and Technology, Wiley, 2007.

[41] M.G. Hosseini, R. Bagheri, R. Najjar, Journal of Applied Polymer Science, 121 (2011) 3159-3166.

[42] M. Yan, C.A. Vetter, V.J. Gelling, Electrochimica Acta, 55 (2010) 5576-5583.

[43] C.A. Ferreira, S.C. Domenech, P.C. Lacaze, Journal of Applied Electrochemistry, 31 (2001) 49-56.

[44] D.M. Lenz, M. Delamar, C.A. Ferreira, Journal of Electroanalytical Chemistry, 540 (2003) 35-44.

[45] M.R. Mahmoudian, W.J. Basirun, Y. Alias, M. Ebadi, Applied Surface Science, 257 (2011) 8317-8325.

[46] M.R. Mahmoudian, W.J. Basirun, Y. Alias, Progress in Organic Coatings, 71 (2011) 56-64.

[47] U. Rammelt, L.M. Duc, W. Plieth, Journal of Applied Electrochemistry, 35 (2005) 1225-1230.

[48] J. He, D.E. Tallman, G.P. Bierwagen, Journal of the Electrochemical Society, 151 (2004) B644-B651.

[49] G. Paliwoda-Porebska, M. Rohwerder, M. Stratmann, U. Rammelt, L. Duc, W. Plieth, J. Solid State Electrochem., 10 (2006) 730-736.

[50] M. Sabouri, T. Shahrabi, H.R. Farid, M.G. Hosseini, Progress in Organic Coatings, 64 (2009) 429-434.

[51] K. Kamaraj, V. Karpakam, S. Sathiyanarayanan, S.S. Azim, G. Venkatachari, Electrochimica Acta, 56 (2011) 9262-9268.

[52] M. Rohwerder, A. Michalik, Electrochimica Acta, 53 (2007) 1300-1313.

[53] L.F. Warren, J.A. Walker, D.P. Anderson, C.G. Rhodes, L.J. Buckley, Journal of the Electrochemical Society, 136 (1989) 2286-2295.

[54] M. Omastová, M. Trchová, J. Kovářová, J. Stejskal, Synthetic Metals, 138 (2003) 447-455.

[55] E. Pigois-Landureau, Y.F. Nicolau, M. Delamar, Synthetic Metals, 72 (1995) 111-119.

[56] K. Idla, A. Talo, H.E.M. Niemi, O. Forsén, S. Yläsaari, Surface and Interface Analysis, 25 (1997) 837-854.

[57] K. Senthil, K. Yong, Nanotechnology, 18 (2007) 395604.

[58] S. Golczak, A. Kanciurzewska, M. Fahlman, K. Langer, J.J. Langer, Solid State Ionics, 179 (2008) 2234-2239.

[59] D.Y. Kim, J.Y. Lee, C.Y. Kim, E.T. Kang, K.L. Tan, Synthetic Metals, 72 (1995) 243-248.

[60] G. Socrates, Infrared and Raman Characteristic Group Frequencies: Tables and Charts, Wiley, 2004.

[61] A. Shakoor, T.Z. Rizvi, Journal of Applied Polymer Science, 117 (2010) 970-973.

[62] W. Liang, J. Lei, C.R. Martin, Synthetic Metals, 52 (1992) 227-239.

[63] S.V. Kasisomayajula, X.N. Qi, C. Vetter, K. Croes, D. Pavlacky, V.J. Gelling, Journal of Coatings Technology and Research, 7 (2010) 145-158.

[64] C. Saravanan, R.C. Shekhar, S. Palaniappan, Macromolecular Chemistry and Physics, 207 (2006) 342-348.

[65] R. Turcu, A.L. Darabont, A. Nan, N. Aldea, D. Macovei, D. Bica, L. Vekas, O. Pana, M.L. Soran, A.A. Koos, L.P. Biro, Journal of Optoelectronics and Advanced Materials, 8 (2006) 643-647.

[66] T.M. Wu, H.L. Chang, Y.W. Lin, Composites Science and Technology, 69 (2009) 639-644.

[67] L. Li, G.P. Yan, J.Y. Wu, X.H. Yu, Q.Z. Guo, Journal of Colloid and Interface Science, 326 (2008) 72-75.

[68] K. Mallick, M.J. Witcomb, M.S. Scurrell, Journal of Physics-Condensed Matter, 19 (2007).

[69] N.P.S. Chauhan, R. Ameta, S.C. Ameta, Indian Journal of Chemical Technology, 18 (2011) 118-122.

[70] E.N. Zareh, P.N. Moghadam, E. Azariyan, I. Sharifian, Iranian Polymer Journal, 20 (2011) 319-328.

[71] M.N. Kalasad, M.A. Gadyal, R.K. Hiremath, I. Mohamed Ikram, B.G. Mulimani, I.M. Khazi, S.K. Anantha Krishnan, M.K. Rabinal, Composites Science and Technology, 68 (2008) 1787-1793.

[72] F. Mansfeld, Electrochimica Acta, 35 (1990) 1533-1544.

[73] F. Mansfeld, L.T. Han, C.C. Lee, G. Zhang, Electrochimica Acta, 43 (1998) 2933-2945.

[74] P.L. Bonora, F. Deflorian, L. Fedrizzi, Electrochimica Acta, 41 (1996) 1073-1082.

[75] A. Zomorodian, F. Brusciotti, A. Fernandes, M.J. Carmezim, T. Moura e Silva, J.C.S. Fernandes, M.F. Montemor, Surface and Coatings Technology, 206 (2012) 4368-4375.

[76] D. Loveday, P. Peterson, B. Rodgers, Jct Coatingstech, 1 (2004) 88-93.

[77] N.V. Krstajić, B.N. Grgur, S.M. Jovanović, M.V. Vojnović, Electrochimica Acta, 42 (1997) 1685-1691.

[78] S. Sathiyanarayanan, S.S. Azim, G. Venkatachari, Electrochimica Acta, 52 (2007) 2068-2074.

[79] M. Sabouri, T. Shahrabi, M.G. Hosseini, Russ J Electrochem, 43 (2007) 1390-1397.

CHAPTER 6. SYNTHESIS AND CHARACTERIZATION OF IRON OXIDE/POLYPYRROLE CORE AND SHELL COMPOSITE PIGMENTS AND THEIR APPLICATION IN COATINGS FOR CORROSION PROTECTION OF COLD ROLLED STEEL

(Published in Polymeric Materials: Science & Engineering (PMSE) 2012, 107, 536.)

6.1. Abstract

Core and shell composite pigments of iron oxide (Fe_2O_3) and polypyrrole (PPy) were synthesized by chemical oxidative polymerization using water as a reaction medium. Core and shell morphology of Fe_2O_3/PPy composite pigments was characterized by scanning electron microscopy (SEM) and transmission electron microscopy (TEM). The elemental composition was obtained by energy dispersive spectroscopy (EDS). Fourier transform infrared spectroscopy (FTIR) was performed for chemical composition analysis. Conductivity studies were performed with conductive atomic force microscopy (CAFM) and four point probe conductivity instrument. Density tests were performed for the analysis of adhesion between Fe_2O_3 and PPy. Coatings of Fe_2O_3 and Fe_2O_3/PPy were formulated at 10% pigment volume concentration (PVC) on cold rolled steel substrate and were exposed to salt spray test conditions according to ASTM B 117. Coatings were analyzed by electrochemical impedance spectroscopy (EIS) and equivalent circuit modeling was performed for corrosion assessment. As observed in EIS and circuit modeling of EIS data, better corrosion resistance was offered by Fe_2O_3/PPy composite pigments based coatings as compared to Fe_2O_3 pigment based coatings after 40 days of salt spray test exposure.

6.2. Introduction

Fabrication, characterization and application of core and shell particles have been the area of the interest of researchers for many decades. Multi-functionality can be exhibited by

hybrid core and shell particles. Tuning of properties of core and shell materials is possible by control over the synthesis conditions. Shell material tends to modify the surface reactivity, nature, charge, dispersibility and several other properties of the inside core materials giving rise to new set of functional properties [1]. Inorganic pigment core in micron size with nanometer size conducting polymer shell can give rise to hybrid and functional properties for various applications.

Conducting polymer PPy has good environmental stability and excellent conductivity but suffers from poor mechanical properties and porosity which can be overcome by combining it with inorganic compounds [2-3]. Silica, Fe_2O_3, and alumina have been employed as core to grow PPy on their surface as a shell [4-8]. These core and shell particles are finding their possible applications in gas and humidity sensors [9], electromagnetic shielding [10], material for microwave absorption [11], and electrochemical display devices [12-13].

Most of the methods used in conducting polymer and metal oxide composite synthesis are multistep, tedious, and sometimes requires low or high temperatures [14]. In order to improve adhesion between inorganic particles and conducting polymers for the formation of composites several approached have been attempted. This includes substituted pyrrole monomer, use of coupling agent, chemical modification of inorganic pigment, and use of surfactants [15-17]. However there are few reports in the literature about the synthesis of Fe_2O_3/PPy composites. Fe_2O_3/PPy composites have been synthesized before with chemical oxidative polymerization of pyrrole with the application of sonication or mechanical stirring and with the help of surfactants [18]. In the current work, we have synthesized core and shell particles containing Fe_2O_3 as core and PPy as shell in very simple manner without using any surfactants at ambient temperature with water as a medium for the reaction. By employing chemical oxidative

polymerization, a PPy shell on Fe_2O_3 core was synthesized. These Fe_2O_3/PPy core and shell particles were then characterized by SEM, EDS, TEM, FTIR, four point probe conductivity, and CAFM. Fe_2O_3/ PPy core and shell particles were further employed for the corrosion protection of cold rolled steel in the coating systems. Corrosion performance properties of Fe_2O_3 and Fe_2O_3/PPy composite pigment based coatings at 10% PVC on cold rolled steel were studied by exposing coatings to salt spray test conditions and EIS.

6.3. Experimental

6.3.1. Materials

Iron(III) oxide (Fe_2O_3) was procured from Sigma-Aldrich. Oxidant, Ammonium Persulfate (APS) was obtained from BDH. Pyrrole monomer was purchased from Alfa Aesar Co. and was distilled prior to the synthesis. In the synthesis, 18.2 MΩ Millipore® water was used as a reaction medium. The substrate was cold rolled steel with dimensions 0.032”x6”x3” and was purchased from Q-Panel Lab Products. Solvent, methyl ethyl ketone (MEK), was obtained from Alfa Aesar Co. Momentive Specialty Chemicals Inc. kindly provided epoxy resin (EPON 830) and polyamide hardener (Epikure 3015). Perchloroethylene used in density tests was procured from Alfa Aesar Co. All the chemicals, except pyrrole, were used as received without further purification.

6.3.2. Synthesis of Fe_2O_3/PPy core and shell composite pigments

The glassware and stir bar used for the synthesis were dried at 100-110°C for 24 h in oven. In 500 mL beaker, 15 grams of iron oxide was kept under immersion in pyrrole monomer for 5 days. After immersion of iron oxide in pyrrole for 5 days, it was centrifuged for 20 minutes at 7000 rpm to separate iron oxide particles for pyrrole. The pyrrole monomer adsorbed iron oxide was then transferred in 1000 mL Erlenmeyer flask to which 400 mL of 18.2 MΩ

Millipore® water was added. This mixture was subjected to gentle stirring. In separate beaker 11.4 grams of APS was dissolved in 100 mL of 18.2 MΩ Millipore® water. This APS solution was then slowly added to the mixture in previously described Erlenmeyer flask. The reaction was continued for 24 hours at ambient temperature. It was then filtered and washed with plentiful amount of water to remove any soluble ingredients. It was then subjected to 60°C overnight drying in oven followed by grinding with mortar and pestle. It was then sieved through the sieve of opening diameter 106 µm. The final product was stored in plastic vials for further characterization.

6.3.3. Fe_2O_3 pigment and Fe_2O_3/PPy composite pigment characterization

A JEOL JEM-2100 transmission electron microscope was employed for the identification of core and shell morphology. A JEOL JSM-6490LV scanning electron microscope was used to obtain the general morphology of samples. The sample preparation for SEM was performed by sprinkling the ground powder onto carbon tape, which was originally attached to aluminum mounts. EDS connected with SEM was used to obtain elemental composition. CAFM studies were performed using Veeco Dimension 3100 atomic force microscope in contact mode and current sensing probe to obtain surface morphology and current density. Four point probe instrument consisting of Signatone® probes, a Keithley® 220 programmable current source, and Keithley®2000 multimeter was employed for the conductivity measurements of the composites. FTIR measurements were performed in transmittance mode using NICOLET 8700 spectrophotometer from Thermo scientific.

6.3.4. Coatings preparation

Coatings were prepared on sandblasted and hexane degreased cold rolled steel substrate. Coatings were formulated at 10% PVC for Fe_2O_3 pigment and Fe_2O_3/PPy composite pigment

and 1:1 stoichiometric ratio of EPON 830 and Epicure 3015 used. MEK was used to reach application viscosity for proper drawdown application on the cold rolled steel surface. The coatings were applied with drawdown bar on cleaned cold rolled steel substrate. Coatings were cured at ambient temperature for 8 days for full development of the protective properties. Final dry film thickness of the coatings was 75-85 μm.

6.3.5. Corrosion assessment

The coatings were exposed to salt spray test conditions according to ASTM B 117. Corrosion performance was monitored by EIS with Gamry Reference 600 Potentiostats with Gamry Framework Version 5.58/EIS 300 software. For EIS, AC perturbation of 10 mV over frequency range 100,000-0.01 Hz at 10 points/decade was applied. For EIS experiments 5% NaCl was used as electrolyte. Experiments were performed in triplicates and data is collected from representative sample. The cell area for the EIS measurements was 7.1 cm^2. Open circuit potential (OCP) measurements were also performed with same set up used in EIS experiments.

6.4. Results and discussion

6.4.1. Scanning electron microscopy (SEM) and energy dispersive spectroscopy (EDS)

The SEM micrographs obtained for Fe_2O_3 pigment and Fe_2O_3/PPy core and shell composite pigment are shown in Figure 6.1 and 6.2 respectively. As observed in Figure 6.1, Fe_2O_3 pigment particles were spherical in shape. In Figure 6.2, PPy layer grown on the surface of Fe_2O_3 pigment was observed. A small increase in particle size was also evident in the SEM micrograph of core and shell particles of Fe_2O_3/PPy composite pigment. There is possibility of adsorption of pyrrole monomer on the Fe_2O_3 pigment surface [1, 9]. Further addition of monomer and oxidant resulted in the formation of PPy shell around the Fe_2O_3 pigment particles. Some of

the studies have suggested formation of monolayer of the PPy on the inorganic pigment surface [19-20]. There is another possibility of adsorption of formed oligomers on the shell of Fe_2O_3.

Results for elemental composition studied by EDS are shown in Table 5.1 and 5.2 respectively. As observed in Table 6.1, presence of carbon in Fe_2O_3 pigment was attributed to the carbon tape used in the sample preparation for the SEM/EDS. This carbon amount was increased in case of Fe_2O_3/PPy core and shell composite pigment (Table 6.2) due to the organic content of layer of PPy on the surface of Fe_2O_3 particles. Presence of nitrogen in Fe_2O_3/PPy composite pigment (Table 6.2) core and shell particles sample signified formation of PPy on the surface of Fe_2O_3 pigment particles. Sulfur was detected in Fe_2O_3/PPy core and shell composite pigment sample which was the dopant in the PPy backbone. The origin of sulfur was the APS which was the oxidant used in the synthesis of Fe_2O_3/PPy core and shell composite pigment. SEM and EDS results suggested the formation and growth of PPy on Fe_2O_3 pigment particles. Reduced amount of iron and oxygen in case of Fe_2O_3/PPy core and shell composite pigment and also signified PPy layer shell around the Fe_2O_3 pigment core.

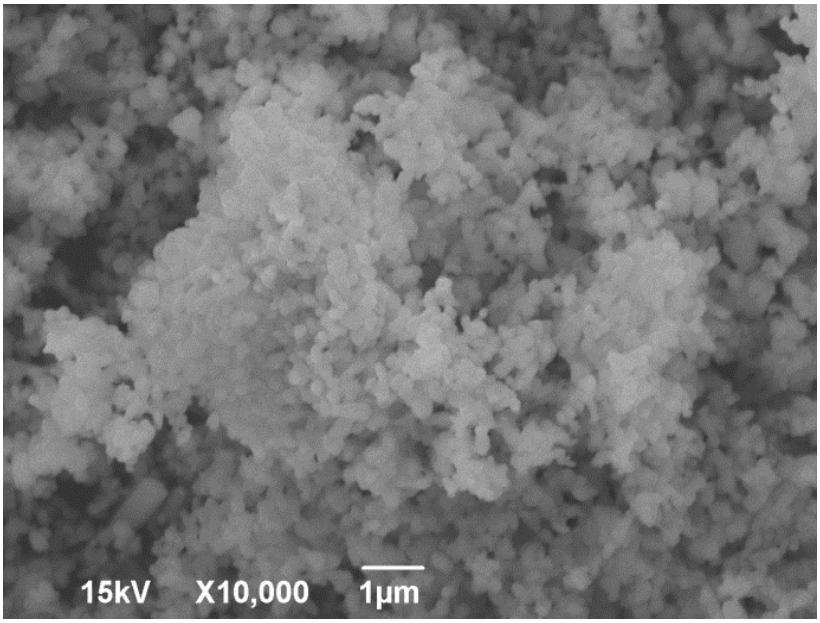

Figure 6.1: SEM micrograph of Fe_2O_3 pigment.

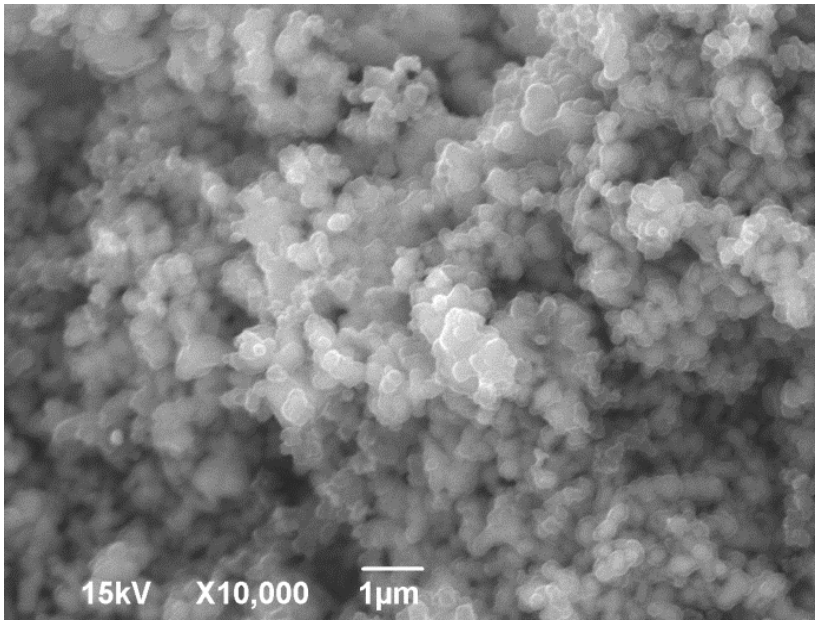

Figure 6.2: SEM micrograph of core and shell morphology of Fe_2O_3/PPy composite pigment.

Table 6.1
Elemental composition of Fe_2O_3 particles obtained by EDS

Element Line	Net Counts	Weight %	Weight % Error	Atom %	Atom % Error
C K	535	5.48	+/- 1.38	12.79	+/- 3.23
O K	23151	31.38	+/- 0.96	55.70	+/- 1.67
Fe K	27560	62.74	+/- 1.93	31.51	+/- 0.97
Total		100.00		100.00	

Table 6.2
Elemental composition of core and shell Fe_2O_3/PPy particles obtained by EDS

Element Line	Net Counts	Weight %	Weight % Error	Atom %	Atom % Error
C K	6867	41.40	+/- 0.51	57.12	+/- 2.12
N K	688	7.76	+/- 1.69	9.18	+/- 6.01
O K	8710	24.81	+/- 0.67	25.70	+/- 2.09
S K	2408	1.26	+/- 0.06	0.65	+/- 0.10
Fe K	11899	24.77	+/- 0.39	7.35	+/- 0.35
Total		100.00		100.00	

6.4.2. Fourier transform infrared spectroscopy (FTIR)

The FTIR spectra of Fe_2O_3/PPy core and shell composite pigment and Fe_2O_3 pigment are shown in Figure 6.3. As shown in Figure 6.3, the characteristic bands due to PPy were observed in Fe_2O_3/PPy core and shell composite pigment. C-C and C=C ring stretching vibrations were observed at 1561 cm^{-1} and C-N and C=C stretching modes in PPy were observed at 1481 cm^{-1}. At 910 cm^{-1} C-H deformation was observed in Fe_2O_3/PPy core and shell composite pigment [21]. C-H out of plane mode vibration was observed at 1040 cm^{-1} in Fe_2O_3/PPy core and shell composite pigment [22]. Breathing vibrations of PPy were confirmed at 1190 cm^{-1} in Fe_2O_3/PPy core and shell composite pigment [23]. Peak at 1321 cm^{-1} was observed in Fe_2O_3/PPy core and shell composite pigment due to C-N stretching vibrations [24].

Band in the regions 500 and 700 cm^{-1} are attributed to vibrations due to Fe-O and Fe_2O_3. Bands due to Fe_2O_3 pigment were also observed in the Fe_2O_3/PPy core and shell composite pigment signifying their combined nature [25-26]. The prominence of the bands due to Fe_2O_3 pigment was decreased in Fe_2O_3/PPy core and shell composite pigment suggesting the interaction between Fe_2O_3 and PPy.

6.4.3. Transmission electron microscopy (TEM)

In order to characterize core and shell morphology of Fe_2O_3/PPy particles in more details, TEM studies were performed. As shown in Figure 6.4, a layer of PPy was observed on the surface of Fe_2O_3 pigment particles. The thickness on the PPy layer was found to be approximately 20-40 nm. The interior core portion was iron oxide as observed in Figure 6.4. This confirmed the core and shell morphology of Fe_2O_3/PPy composite pigment particles.

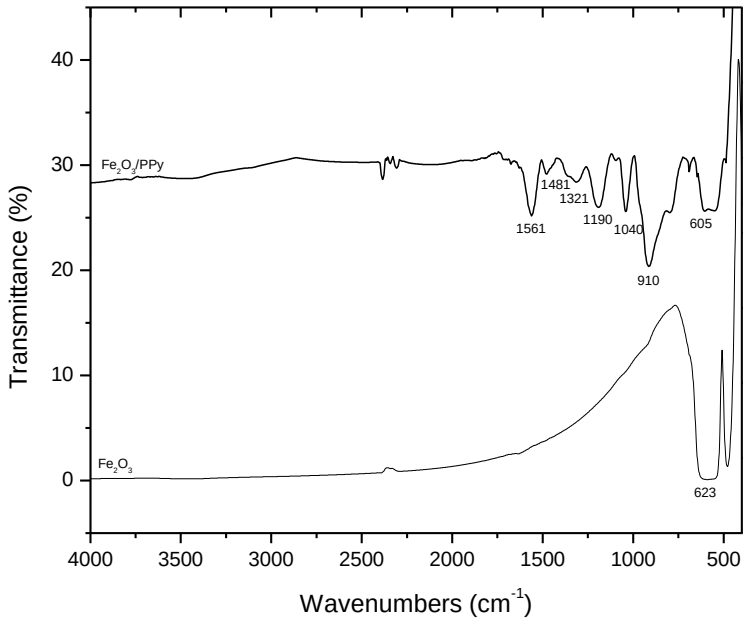

Figure 6.3: FTIR spectra of Fe_2O_3 pigment (Bottom) and Fe_2O_3/PPy core and shell composite pigment (Top).

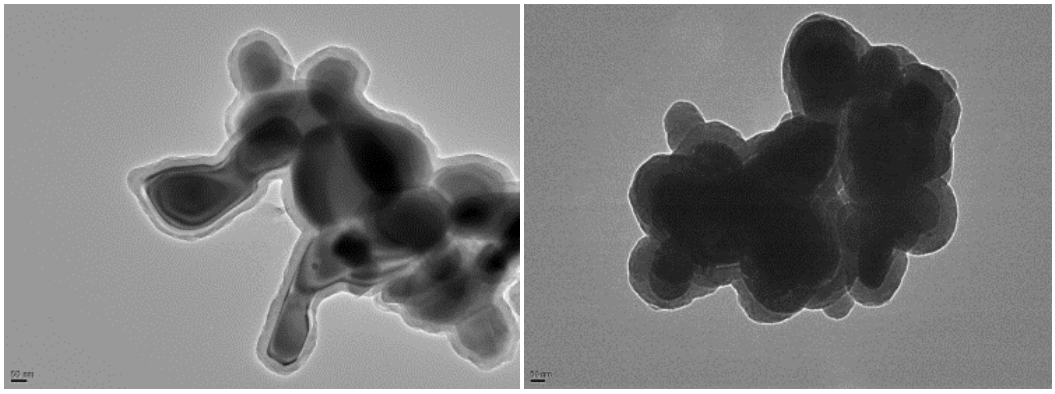

Figure 6.4: Core and shell morphology of Fe_2O_3/PPy core and shell composite pigment obtained by TEM.

6.4.4. Conductive atomic force microscopy (CAFM) and four point probe conductivity

CAFM experiments were performed for the conductivity studies. Height, deflection and current image of Fe_2O_3 pigment particles and Fe_2O_3/PPy core and shell composite pigments obtained by CAFM are shown in Figure 6.5, and 6.6 respectively. As shown in Figure 6.5, current was not observed on the current image in CAFM for Fe_2O_3 pigment particles whereas current was observed in current image obtained in CAFM for Fe_2O_3/PPy core and shell

composite pigment as shown in Figure 6.6. This conductive nature of Fe_2O_3/PPy core and shell composite pigment particles was attributed to the conductivity possessed by inherently conducting polymer (PPy) present on the Fe_2O_3 pigment particle surfaces. The conductivity value obtained by four point measurement for Fe_2O_3/PPy core and shell composite pigment was 0.034 S/m. The observed conductivity was a result of composite nature of Fe_2O_3/PPy core and shell composite pigment particles. The resultant conductivity is also dependant on the uniform distribution of inorganic pigment and reduced aggregation in the matrix [9, 27].

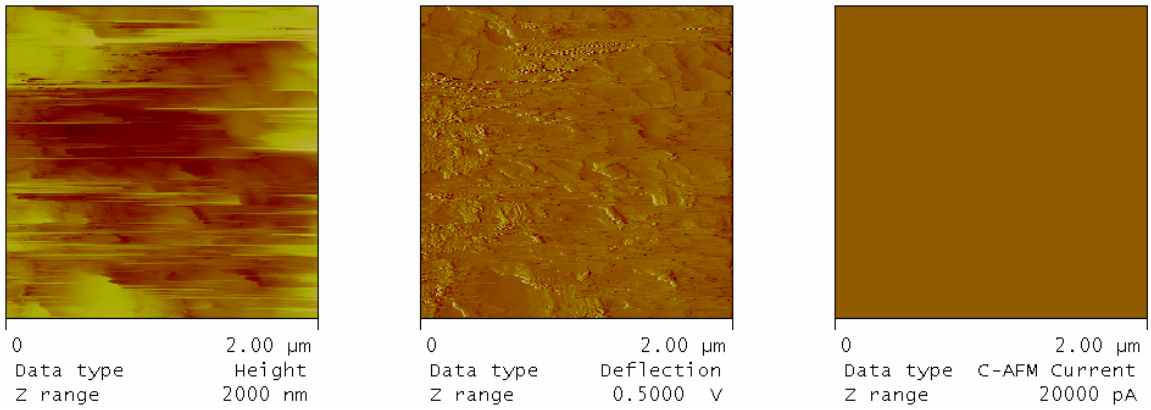

Figure 6.5: Height, deflection and current image of Fe_2O_3 particles obtained by CAFM.

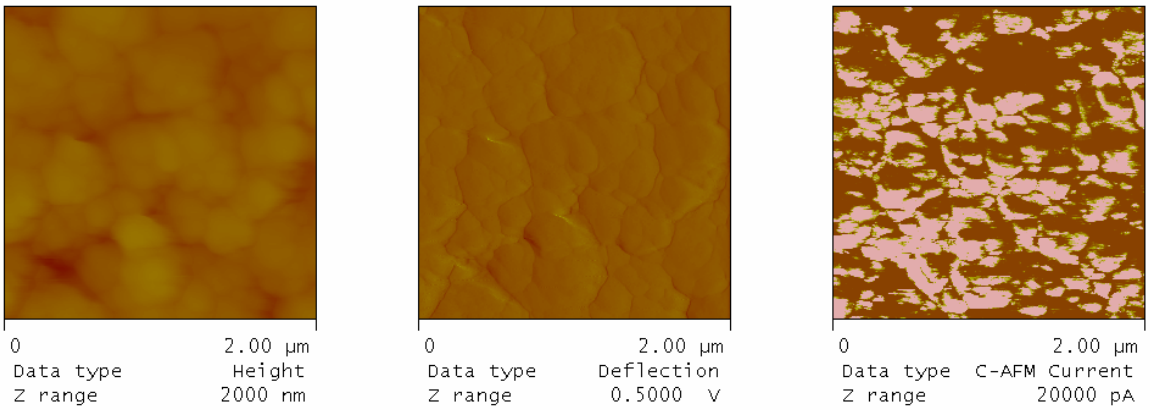

Figure 6.6: Height, deflection and current image of Fe_2O_3/PPy particles obtained by CAFM.

6.4.5. Density tests

In order to determine the adherent nature of PPy on Fe_2O_3 pigment particles, density tests were performed. Perchloroethylene was used as the medium for suspending Fe_2O_3 pigment particles and Fe_2O_3/PPy core and shell composite pigment particles. Perchloroethylene has density of 1.623 g/cm^3 and Fe_2O_3 has density of 5.24 g/cm^3 and PPy has density of 1.05 g/cm^3. Whatever is free PPy present in the Fe_2O_3/PPy core and shell composite pigment will float on perchloroethylene. As observed in Figure 6.7(b), no free PPy was floating in perchloroethylene suggesting intimate contact and core and shell morphology of Fe_2O_3/PPy composite.

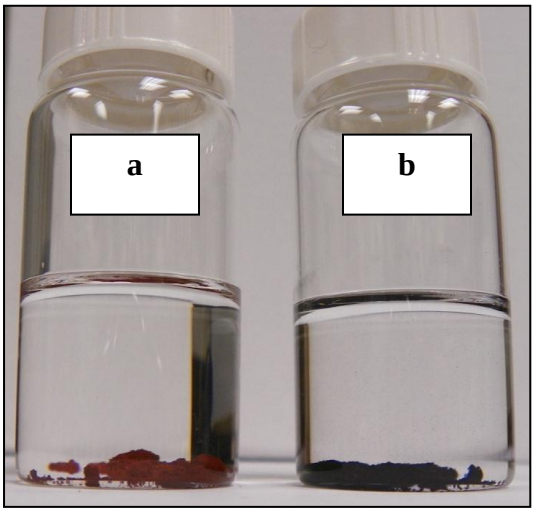

Figure 6.7: (a) Fe_2O_3 in perchloroethylene, (b) Fe_2O_3/PPy in perchloroethylene.

6.5. Corrosion performance of Fe_2O_3 pigment and Fe_2O_3/PPy composite coatings

6.5.1. Electrochemical impedance spectroscopy (EIS)

A three electrode cell consisting of substrate with coating as working electrode, saturated calomel as reference electrode and platinum mesh as a counter electrode was employed for performing EIS. As observed in Figure 6.8 and 6.9, low frequency (0.01Hz) impedance was very high initially for both Fe_2O_3 and Fe_2O_3/PPy coatings. As the duration of the salt spray exposure

increased, drop in low frequency impedance was observed for both Fe_2O_3 and Fe_2O_3/PPy coatings. The drop in impedance in this case represents decrease in protection offered by coating to the corrosion [28]. It represents the electrolyte ingress through the developed pores in the coating [29]. Appearance of second time constant in Fe_2O_3 coating is indicating the start of the corrosion reaction at coating and cold rolled steel interface [30].

The EIS data was modeled by using ZView 2 software from Scribner Associates Inc. EIS data was fitted to Randles circuit model equivalent circuit. Randles circuit model consists of solution resistance and constant phase element which is in parallel with coatings resistance (R_c). R_c for both Fe_2O_3 and Fe_2O_3/PPy coatings was plotted against the duration of the exposure in salt spray (Figure 6.10). Initially R_c was higher for Fe_2O_3/PPy coating as compared with both Fe_2O_3 coating. Even though the value of R_c decreased with duration of exposure to salt spray increased for Fe_2O_3/PPy coating it was still higher than that of Fe_2O_3 coating for the same duration of exposure. This suggested better corrosion performance offered by Fe_2O_3/PPy coating.

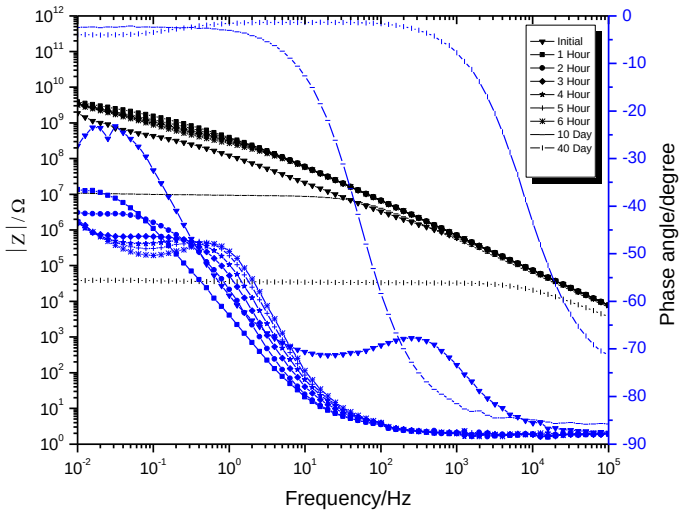

Figure. 6.8: Bode plot of 10 % PVC of Fe_2O_3 coating.

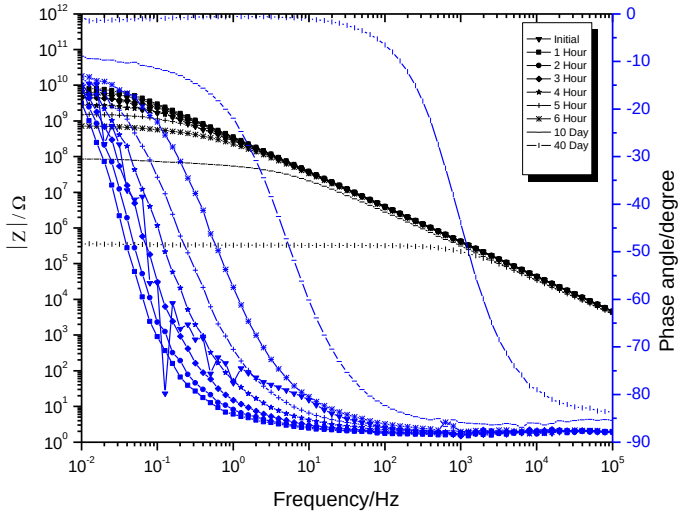

Figure. 6.9: Bode plot of 10 % PVC of Fe_2O_3 /PPy coating.

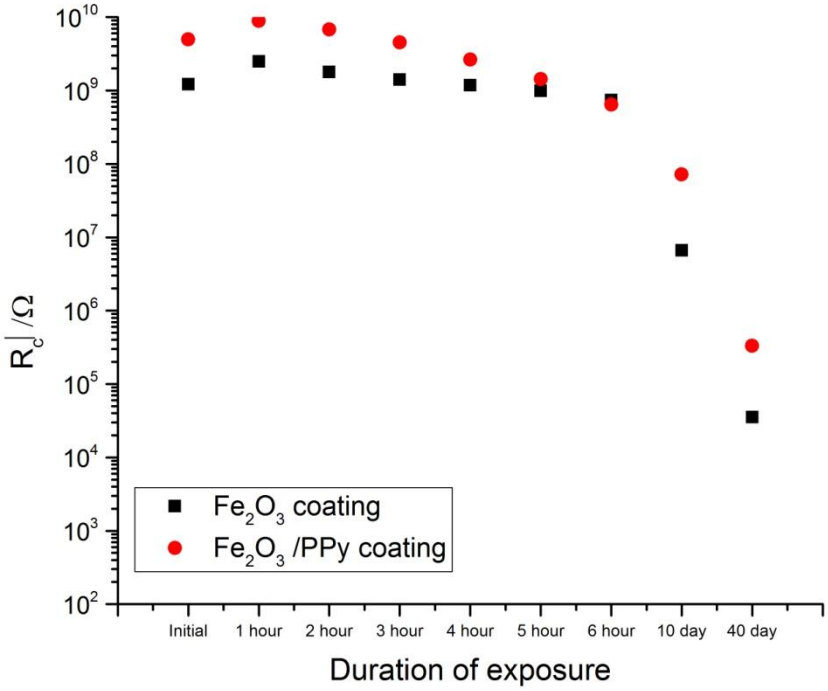

Figure 6.10. Change in coating resistance (Rc) with time of exposure.

6.5.2. Open circuit potential (OCP) measurements

Simultaneously with EIS experiments, OCP values were also collected. As shown in Figure 6.11, OCP of the Fe_2O_3 coating was more towards the OCP of the cold rolled steel. For

Fe_2O_3/PPy coating, OCP was more positive initially whereas it decreased over time as the duration to the salt spray exposure increased. Similar behavior was observed earlier in case of PPy doped with sulfate anions. The more positive values of the OCP were attributed to the doped nature of the PPy [31]. PPy tends to be reduced and also serve as an oxidant to passivate underlying iron substrate thereby further increasing corrosion protection [32]. The increased corrosion protection offered in case of Fe_2O_3/PPy coating can also be attributed to the increased surface area of PPy for redox reactions and interaction with metal substrate and corrosive ions [33]. The reduced PPy can also scavenge oxygen and get oxidized thereby decreasing rate of cathodic reaction and corrosion rate [34].

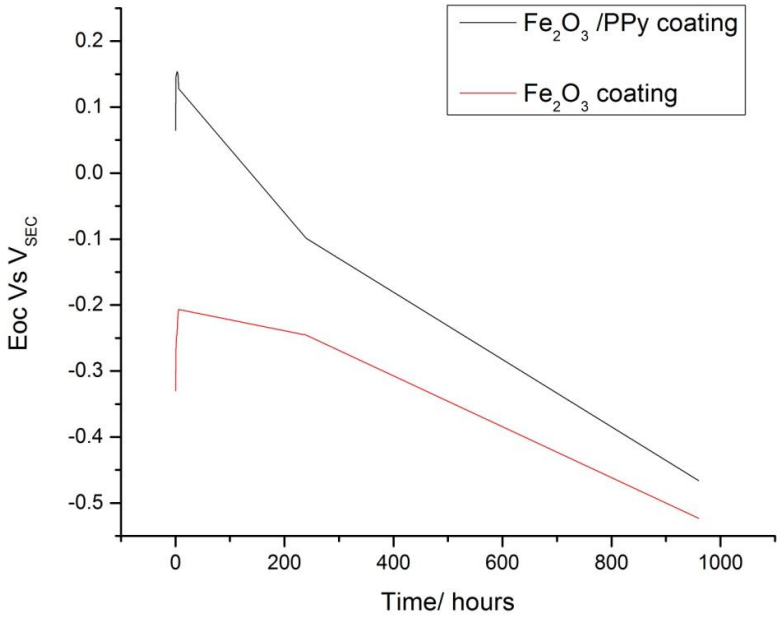

Figure 6.11: Open circuit potential (OCP) with time of exposure.

6.6. Conclusions

Core and shell Fe_2O_3/PPy particles were successfully prepared by simple chemical oxidative polymerization method. TEM results showed the layer of PPy in nanometer size (20-40 nm) on the surface of Fe_2O_3 pigment particles confirming the core and shell morphology. FTIR showed the presence of PPy in Fe_2O_3/PPy core and shell composite particles. These core and

shell Fe_2O_3/PPy composite particles exhibited conductivity as evidenced in current image of CAFM and four point conductivity measurements. Density tests revealed better adherence between PPy and Fe_2O3 particles in Fe_2O_3/PPy core and shell composite particles suggesting minimal free PPy. After exposure to salt spray test conditions, a lower drop in coating resistance in case of Fe_2O_3/PPy coating as compared to Fe_2O_3 coating suggested better corrosion protection offered by Fe_2O_3/PPy coating. Increased surface area for the interaction of ions with PPy and passivating ability of PPy was responsible for the improved corrosion protection offered by Core and shell Fe_2O_3/PPy particles based coatings.

6.7. References

[1] C.-L. Huang, E. Matijevic, Journal of Materials Research, 10 (1995) 1327-1336.

[2] K. Qi, Y. Qiu, Z. Chen, X. Guo, Corrosion Science, 60 (2012) 50-58.

[3] J. Jang, B. Lim, J. Lee, T. Hyeon, Chemical Communications, 0 (2001) 83-84.

[4] F. Yang, Y. Chu, S. Ma, Y. Zhang, J. Liu, Journal of Colloid and Interface Science, 301 (2006) 470-478.

[5] P. Montoya, F. Jaramillo, J. Calderón, S.I. Córdoba de Torresi, R.M. Torresi, Electrochimica Acta, 55 (2010) 6116-6122.

[6] H. Yang, W. Jiang, Y. Lu, Materials Letters, 61 (2007) 2789-2793.

[7] C.R. Lin, R.K. Chiang, J.S. Wang, T.W. Sung, J. Appl. Phys., 99 (2006).

[8] X. Liu, H. Wu, F. Ren, G. Qiu, M. Tang, Materials Chemistry and Physics, 109 (2008) 5-9.

[9] R.P. Tandon, M.R. Tripathy, A.K. Arora, S. Hotchandani, Sensors and Actuators B: Chemical, 114 (2006) 768-773.

[10] P. Saini, V. Choudhary, B.P. Singh, R.B. Mathur, S.K. Dhawan, Materials Chemistry and Physics, 113 (2009) 919-926.

[11] J. Hongxia, L. Qiaoling, Y. Yun, G. Zhiwu, Y. Xiaofeng, Journal of Magnetism and Magnetic Materials, 332 (2013) 10-14.

[12] J. Jang, J.H. Oh, Advanced Materials, 15 (2003) 977-980.

[13] F.-Y. Chuang, S.-M. Yang, Journal of Colloid and Interface Science, 320 (2008) 194-201.

[14] A. Malinauskas, Polymer, 42 (2001) 3957-3972.

[15] R. Gangopadhyay, A. De, Chemistry of Materials, 12 (2000) 608-622.

[16] F. Faverolle, A.J. Attias, B. Bloch, P. Audebert, C.P. Andrieux, Chemistry of Materials, 10 (1998) 740-752.

[17] H.P. de Oliveira, C.A.S. Andrade, C.P. de Melo, Journal of Colloid and Interface Science, 319 (2008) 441-449.

[18] Z. Guo, K. Shin, A. Karki, D. Young, R. Kaner, H.T. Hahn, J Nanopart Res, 11 (2009) 1441-1452.

[19] S. Maeda, S.P. Armes, Journal of Colloid and Interface Science, 159 (1993) 257-259.

[20] S. Maeda, S.P. Armes, Journal of Materials Chemistry, 4 (1994) 935-942.

[21] L. Liu, C. Zhao, Y. Zhao, N. Jia, Q. Zhou, M. Yan, Z. Jiang, European Polymer Journal, 41 (2005) 2117-2121.

[22] H. Kato, O. Nishikawa, T. Matsui, S. Honma, H. Kokado, The Journal of Physical Chemistry, 95 (1991) 6014-6016.

[23] M. Mazur, The Journal of Physical Chemistry B, 113 (2008) 728-733.

[24] S.P. Palaniappan, P. Manisankar, Materials Chemistry and Physics, 122 (2010) 15-17.

[25] S. Kasisomayajula, X. Qi, C. Vetter, K. Croes, D. Pavlacky, V. Gelling, J Coat Technol Res, 7 (2010) 145-158.

[26] H.-M. Xiao, W.-D. Zhang, M.-X. Wan, S.-Y. Fu, Journal of Polymer Science Part A: Polymer Chemistry, 47 (2009) 4446-4453.

[27] R.K. Sharma, A. Karakoti, S. Seal, L. Zhai, Journal of Power Sources, 195 (2010) 1256-1262.

[28] Q. Le Thu, G.P. Bierwagen, S. Touzain, Progress in Organic Coatings, 42 (2001) 179-187.

[29] A. Amirudin, D. Thieny, Progress in Organic Coatings, 26 (1995) 1-28.

[30] D. Loveday, P. Peterson, B. Rodgers, Jct Coatingstech, 1 (2004) 88-93.

[31] P. Ocón, A.B. Cristobal, P. Herrasti, E. Fatas, Corrosion Science, 47 (2005) 649-662.

[32] G. Spinks, A. Dominis, G. Wallace, D. Tallman, Journal of Solid State Electrochemistry, 6 (2002) 85-100.

[33] M.R. Mahmoudian, W.J. Basirun, Y. Alias, M. Ebadi, Applied Surface Science, 257 (2011) 8317-8325.

[34] M. Yan, C.A. Vetter, V.J. Gelling, Electrochimica Acta, 55 (2010) 5576-5583.

CHAPTER 7. SYNTHESIS AND CHARACTERIZATION OF MICACEOUS IRON OXIDE (MIOX)/ POLYPYRROLE (PPY) COMPOSITE PIGMENTS AND THEIR APPLICATION FOR CORROSION PROTECTION OF COLD ROLLED STEEL

(Communicated to Corrosion journal)

7.1. Abstract

Novel hybrid composite pigments consisting of Micaceous Iron Oxide (MIOX) and Polypyrrole (PPy) were synthesized by employing chemical oxidative polymerization method and water as a reaction medium. Three different particle shapes (5, 10, and 30μm) of MIOX namely MIOX5, MIOX10, and MOIX30 were used for the synthesis of MIOX/PPy composite pigments. The synthesized hybrid composite pigment was characterized by Scanning Electron Microscopy (SEM) for morphology, Energy Dispersive Spectroscopy (EDS) for elemental analysis, four point probe conductivity, and Conductive-Atomic Force Microscopy (C-AFM) for conductivity studies. Density tests were also performed for the adhesion between MIOX and PPy. MIOX30/PPy composite pigment based formulated coatings at 15, 25, and 35 % pigment volume concentration (PVC) on cold rolled steel were exposed to salt spray test conditions according to ASTM B 117. Corrosion performance was analyzed by electrochemical impedance spectroscopy (EIS) and Anodic polarization. Equivalent circuit modeling of the EIS data was performed for the understanding of the corrosion processes on the coated substrate. Smaller drop in impedance was observed for MIOX30/PPy composite pigment based coating at 100 days of salt spray exposure than MIOX30 pigment coating for the same duration of exposure.

7.2. Introduction

Coatings are considered as oldest method for the corrosion protection of the metal alloys [1]. For the protection and decoration of the metal substrates, one-third of the total coatings

produced are consumed [2]. Coatings can act as barrier for corrosive species. Coatings can block ionic pathways at metal/coating interface between local anode and cathodes, and can also act as carrier for corrosive inhibiting pigments which can act once corrosion is started [3]. However corrosion protection by barrier coatings is compromised in presence of pinholes and defects [4]. Active coatings (zinc rich and magnesium rich primers) suffer as the metal pigment gets transformed into the oxide form. Its effectiveness for the cathodic protection is compromised. Chromate conversion coatings which are very effective against corrosion are being phased out due to their environmental and health impacts [5]. For the corrosion protection in ecofriendly manner and in more smart approach, new coating systems and advanced materials are being studied [6-8]. Conducting polymers (CPs) such as polyaniline (PAni), polypyrrole (PPy), and polythiophene (PTh) have attracted considerable attention in the world of advanced materials. CPs posses conjugated π-electron system which renders them conductivity [9-10]. CPs can be prepared in simple chemical and electrochemical polymerization methods [11]. CPs have been employed in various applications such as batteries [12], sensors [13], electrochromic devices [14], tissue engineering [15], solid-phase microextraction [16], supercapacitors [17], electromagnetic interference (EMI) shielding [18], and anticorrosion coatings [19]. PPy is one of the most promising members of the CP family exhibiting properties such as good environmental stability, high conductivity, non-toxicity, and facile synthesis procedures which can be used in anticorrosion applications [20].

PPy can be employed in the coatings in several ways including as a pigment, as an additives in small quantities, as multilayer's, as copolymers of different CPs, composites and nanocomposites of the PPy and inorganic pigments. These various approaches have been sorted for PPy application in the coatings in order to overcome inherent drawbacks of PPy such as

insolubility, porosity, and poor adhesion [21-22]. PPy/TiO_2 composite was synthesized electrochemically on mild steel substrate. Good adhesion and no blistering was observed on the composite deposited mild steel samples exposed to salt spray conditions [23]. PPy/Montmorillonite (MMT) composite was solution casted in epoxy matrix on aluminum 5000 alloy substrate [22]. EIS studies demonstrated better corrosion protection for PPy/MMT composite owing to the combination of properties from MMT (hydrophobicity) and PPy (redox nature). MIOX is a lamellar form of Fe_2O_3 and is a very well know anticorrosion pigment [24]. MIOX has lamellar nature which reduces the migration of oxygen, water and corrosive ions to the substrate. MIOX provides long term corrosion protection by lengthening the path of corrosive species to the substrate by its platelet nature. MIOX often orients parallel to the substrate giving maximum possible barrier protection with mechanical reinforcement of coating and ultraviolet radiation blocking [25]. MIOX coatings fail at sharp edges as proper orientation is not achieved at the edges. In this paper, MIOX is combined with PPy in unique manner by in-situ synthesis of PPy on the surface of MIOX. MIOX will serve as a carrier particle for the PPy as well as will provide barrier protection. MIOX/PPy composite pigment will also alleviate problems associated with PPy incorporation in coating mentioned earlier. PPy will exhibit redox behavior and will pave a way for smart corrosion inhibition.

In the current research, composites pigments of MIOX/PPy are synthesized by chemical oxidative polymerization with three particle sizes of MIOX (5, 10, and 30μm). These composite pigments were characterized by SEM, EDS, CAFM, and four point probe conductivity. Coatings were formulated for 30μm particle size MIOX and PPy composite pigment at 15, 25, and 35 % pigment volume concentration (PVC) on cold rolled steel substrate. Coatings exposed to salt spray conditions were analyzed by EIS and anodic polarization experiments.

7.3. Experimental

7.3.1. Materials

MIOX SUBMICRO5, MIOX MICRO10, and MIOX MICRO30 of three different particles sizes of 5, 10, and 30 µm respectively were kindly supplied by Kish Company, Inc. Ammonium Persulfate (APS) was purchased from BDH. Epoxy resin (EPON 828) and polyamide hardener (EPIKURE 3175) were kindly supplied by Momentive Specialty Chemicals Inc. Methyl isobutyl ketone (MIBK) was supplied by Aqua solutions. Cold rolled steel (0.032”x6”x3”) panels were purchased from Q-Panel Lab Products. Perchloroethylene was procured from Alfa Aesar Co. Prior to the synthesis, pyrrole monomer was distilled. Rests of the chemicals were used as received in the synthesis and coating formulations without purification.

7.3.2. Synthesis of MIOX/PPy composite pigments

Three different particle sizes (5, 10, and 30µm) of MIOX were used for the synthesis of MIOX/PPy composite pigments. For the synthesis, 18.2 MΩ Millipore water (1000 ml) was used in which MIOX (30 grams) was dispersed. After the dispersion of MIOX, to the reaction mixture APS (22.8 grams) was added. After complete dissolution of APS, pyrrole monomer (13.9 ml) was added to the reaction mixture. The reaction was continued for 24 hours followed by filtration and washing with copious amount of water. It was dried overnight in oven at 60°C followed by grinding with mortar and pestle. The composite pigment was sieved through sieve of opening diameter 106µm. Final product was stored in plastic vials for characterization and application.

7.3.3. Composite and coatings characterization

For viewing the morphology of the MIOX/PPy composite pigments, A JEOL JSM-6490LV SEM was utilized. MIOX pigments and MIOX/PPy composite pigments in ground powder form were sprinkled onto carbon tape attached to aluminum mounts for the sample

preparation for SEM. EDS connected with SEM which was utilized to obtain elemental composition of MIOX pigments and MIOX/PPy composite pigments. C-AFM studies of MIOX30 and MIOX30/PPy composite pigments were performed for the surface morphology and surface current density analysis. This was accomplished by using Veeco Dimension 3100 atomic force microscope in contact mode and with current sensing probe. Conductivity measurements were performed with four point probe with instrument consisting of Signatone® probes, a Keithley® 220 programmable current source, and Keithley®2000 multimeter. For EIS studies, Gamry Instruments R600 Potentiostat/Galvanostat/ZRA with Gamry Framework Version 5.58/EIS 300 software was used. For these measurements, 5% sodium chloride was used as electrolyte solution. A saturated calomel reference electrode, platinum mesh counter electrode, and coated substrate as a working electrode were employed in the three cell assembly for EIS measurements. The frequency range for the measurement was 0.01-100,000 Hz with 10 points/decade using RMS of AC signal amplitude of 10 mV. Anodic polarization scans were performed with the same setup employed for EIS in Dilute Harrison's solution (DHS, 0.35% ammonium sulfate and 0.05% sodium chloride). A scribe of 1.5 cm in length and 0.1 cm in width was made on the surface of coatings by using Gravograph IM4 engraving system (Gravograph, USA) assisted with Gravostyle Quick software with 0.15 cm^2 as an area under analysis.

7.3.4. Coating preparation

Coatings were formulated at 15, 25, and 35 PVC of MIOX30/PPy composite pigment and MIOX30 pigment respectively on cold rolled steel substrate. The substrate was sandblasted with alumina grit and degreased with the hexane prior to the coating application. Stoichiometric ratio of 1:1 for epoxy resin EPON 828 and polyamide hardener EPIKURE 3175 was used for the formulation of the coatings and MIBK was used as a solvent to reach application viscosity for

the coatings application. Coatings were applied with drawdown bar on cleaned cold rolled steel substrate. Curing of the coatings was carried out for 2 hours at 80°C in oven. Coating samples were left as such at room temperature for 8 days for the full development of the performance properties. Thickness of the primer coat was 60±5 µm. Topcoat consisting of EPON 828 and EPIKURE 3175 was applied under similar conditions as primer for the salt spray exposure and furthermore EIS characterization. Thickness of the topcoat was also 60±5 µm. Designations for coatings prepared for corrosion assessment are shown in Table 7.1.

Table 7.1
Designations for coatings prepared for corrosion assessment

PVC, %	MIOX30 pigment	MIOX30/PPy composite pigment
15	15PVC, MIOX30 coating	15PVC, MIOX30/PPy coating
25	25PVC, MIOX30 coating	25PVC, MIOX30/PPy coating
35	35PVC, MIOX30 coating	35PVC, MIOX30/PPy coating

7.4. Results and discussions

7.4.1. Morphology of MIOX pigments and MIOX/PPy composite pigments

The morphology of the synthesized MIOX5/PPy, MIOX10/PPy, and MIOX30/PPy composite pigments and as received MIOX5, MIOX10, and MIOX30 pigments are shown in Figure 7.1. As observed in Figure 7.1A, MIOX5 pigments particles were observed with the particle size below 5 µm. Some of the particles were observed to be in size less than 1 µm. When polymerization of pyrrole monomer performed on the MIOX5 particles, the formation of PPy particles was observed to be on the surface of MIOX5 pigment particles as observed in Figure 1B. The size of PPy particles deposited on the MIOX5 pigment surface was observed to be 200-500 nm (Figure 7.1B). An overall increase in the total size of the MIOX5/PPy composite pigment was observed due to the formation of PPy on MIOX5 pigment surface.

As observed in Figure 7.1C, in case of MIOX10 pigment, the size of MIOX10 pigment particles was around 10 μm with some random distribution of smaller particles as well. After in-situ polymerization of pyrrole on the surface of MIOX10 particles, deposition of the PPy was observed on the surface of MIOX particles (Figure 7.1D). The size of the PPy particles deposited on MIOX pigment surface was found to be 200-500 nm. In case of MIOX30 pigment where size of MIOX pigment particles was around 30 μm (Figure 7.1E and 7.2A), the depositions of PPy lead to the formation of spherical particles deposited uniformly on the surface of MIOX 30 pigment (Figure 7.1E, and 7.2B). The size of deposited PPy was observed to be ca. 200-500 nm.

Aggregates of the PPy were deposited on nickel flakes in presence of surfactant sodium dodecyl sulfate and oxidant sodium persulfate by admicellar polymerization [26]. However in the current research herein deposition was obtained without the use of surfactant in the synthesis. Strong vander Waal's forces of attraction between π-conjugated polymer PPy and inorganic oxide can result in self-assembly [27]. This can result in deposition of PPy structures on MIOX. Hydrophobicity of PPy oligomers can also result in the deposition of PPy oligomers on MIOX which can further lead to polymerization on the surface of MIOX pigment leading to formation of PPy polymer particles. Increased surface area for deposition and possible adsorption of monomer pyrrole on MIOX can also lead to formation of PPy and MIOX pigment surface. Aggregation of cation radicals of PPy is also possible towards the electronegative oxygen atom of inorganic oxide surface [28]. Hydroxides on inorganic flake or pigment surface can also form H-bond with the nitrogen atom of PPy. So it is possible to deposit the PPy on the surface of inorganic flake such as MIOX in absence of the surfactant as well. One of the composite pigments MIOX30/PPy was selected for further characterization and the corrosion resistant coatings formulations owing to its well defined and dense morphology on the surface of MIOX.

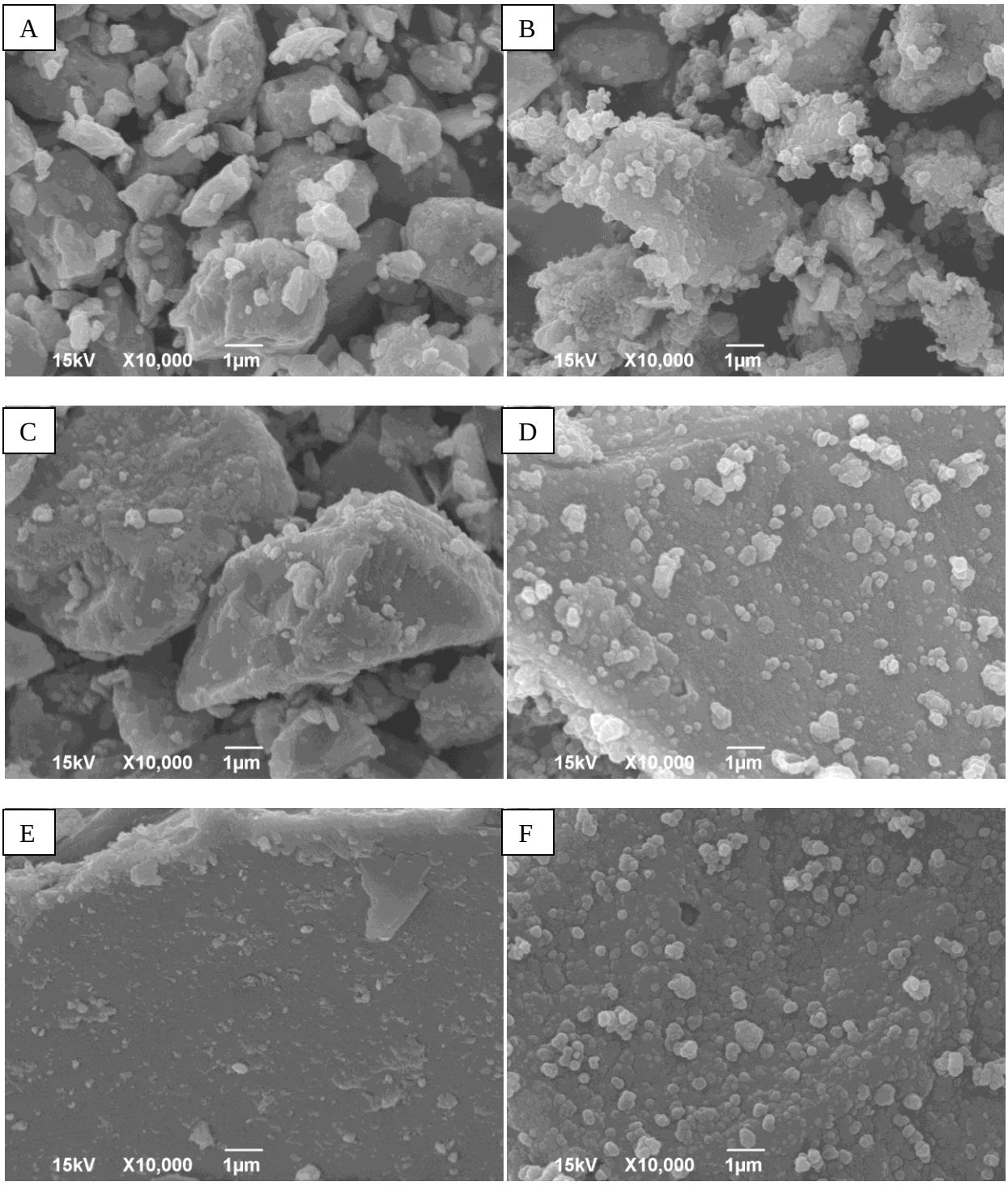

Figure 7.1: SEM micrographs of (A) MIOX5, (B) MIOX5/PPy, (C) MIOX10, (D) MIOX10/PPy, (E) MIOX30, and (F) MIOX30/PPy.

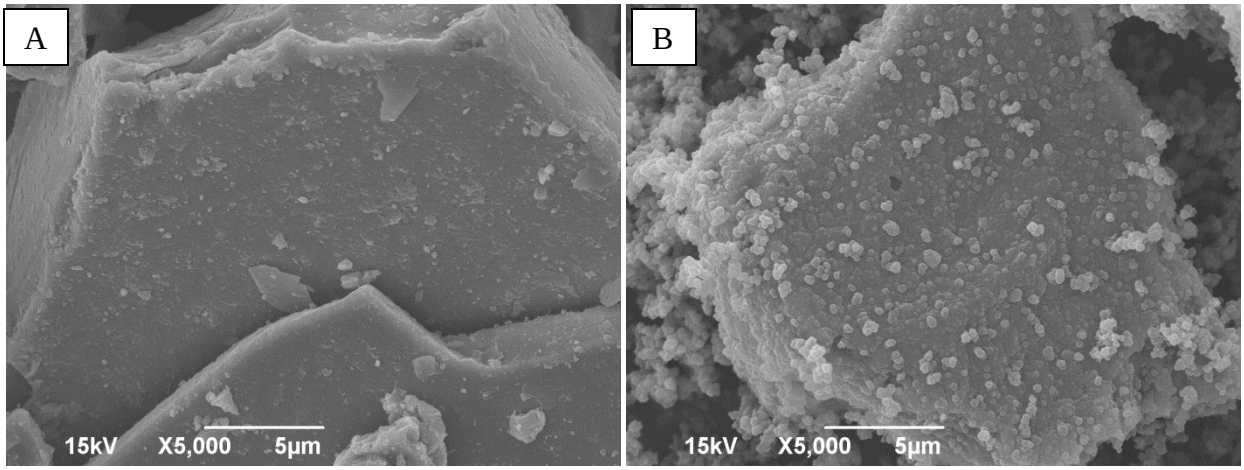

Figure 7.2: SEM micrographs of (A) MIOX30, (B) MIOX30/PPy.

7.4.2. Elemental composition

The elemental composition of the as received MIOX5, MIOX10, and MIOX30 pigments, and synthesized MIOX5/PPy, MIOX10/PPy, and MIOX30/PPy composite pigments was obtained by employing EDS attached to the SEM. The results obtained by EDS are shown in Figure 7.3A, 7.3B, and 7.3C, for MIOX5 and MIOX5/PPy, MIOX10 and MIOX10/PPy, and MIOX30 and MIOX30/PPy respectively. The carbon found in all of the samples (MIOX5, MIOX10 and, MIOX30) without any PPy was due to the carbon tape used in the sample preparation of SEM and EDS. Increased amount of carbon in all MIOX/PPy composite pigment samples indicated the organic carbon resulting from the formation of PPy on the surface of MIOX in composite pigments. The reduced amount of oxygen and iron in all of the MIOX/PPy composite pigment samples indicated that the MIOX particles were covered with PPy. Similar results were obtained supporting this claim by density tests as disused later. The presence of nitrogen in MIOX5/PPy, MIOX10/PPy, and MIOX30/PPy composite samples indicated the formation of PPy on the surface of the MIOX5, MIOX10, and MIOX30 pigments respectively. The presence of sulfur in minute amounts in MIOX/PPy composite pigment samples indicated also indicated doping of PPy from sulfur. The origin of the sulfur was oxidant APS used in the

synthesis. Due to presence of sulfur, the synthesized composite pigments exhibited conductivity as exhibited in CAFM and four point probe conductivity studies as discussed later.

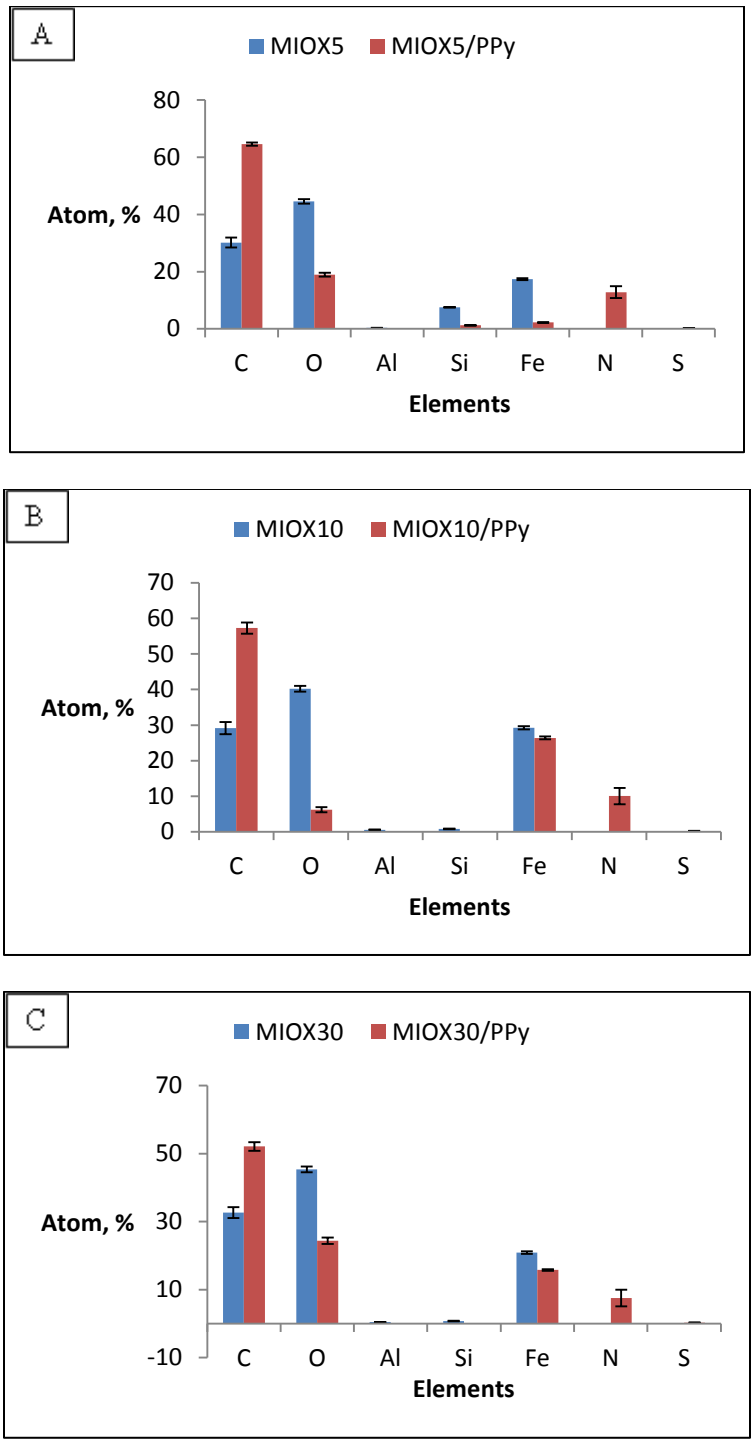

Figure 7.3: EDS of (A) MIOX5 and MIOX5/PPy, (B) MIOX10 and MIOX10/PPy, and (C) MIOX30 and MIOX30/PPy.

7.4.3. Conductivity

Height, deflection and current images were obtained for MIOX30 pigment and MIOX30/PPy composite and shown in Figure 7.4 and 7.5 respectively. The DC bias of 200 mV was applied for the CAFM experiments. As shown in Figure 7.4, no current was observed on the current image in case of MIOX30 pigment suggesting non-conducting nature of MIOX30 pigment. However in case of MIOX30/PPy composite pigment, current density domains were observed in current image (Figure 7.5). The conductivity is rendered due to the conductive nature of oxidized PPy doped with sulfur in this synthesis. However, the composite nature of MIOX30/PPy will change the conductivity of the prepared composite [29]. The conductivity value was obtained from four point conductivity measurement and was found to be 0.12 S/m.

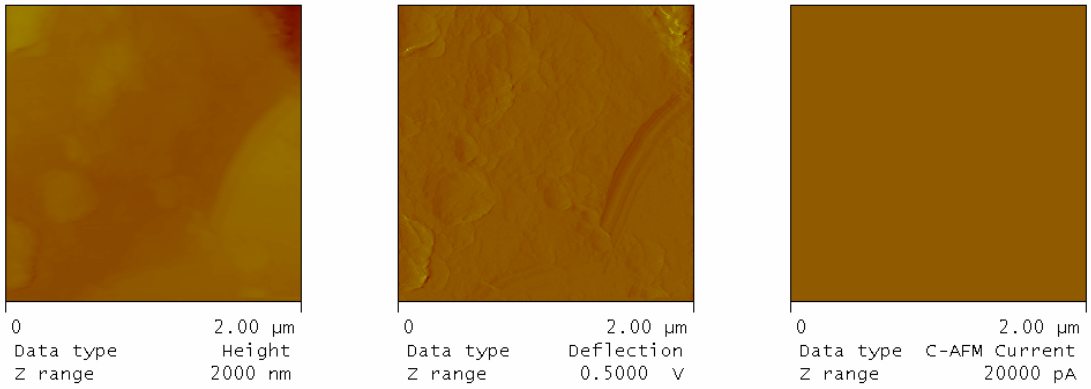

Figure 7.4: Height, deflection and current images for MIOX30 pigment.

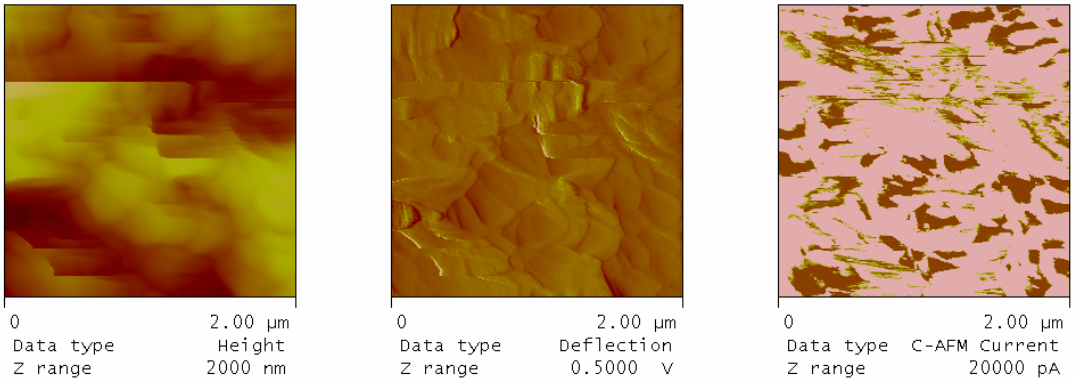

Figure 7.5: Height, deflection and current images for MIOX30/PPy composite pigment.

7.4.4. Density test

Density tests were performed for MIOX30 pigment and MIOX30/PPy composite pigment. Density tests were conducted for determining the adherence of PPy to the MIOX pigment surface and to provide a qualitative estimation of free PPy present in the MIOX30/PPy composite pigment. In the density tests, perchloroethylene with density of 1.623 g/cm^3 was added to MIOX30 pigment and MIOX30/PPy composite pigment respectively. The as received MIOX30 pigment has greater density (4.8 g/cm^3) than perchloroethylene, so it will settle to the bottom and PPy with density 1.05 g/cm^3 will float. The density test results are shown for MIOX30 pigment and MIOX30/PPy composite pigment in Figure 7.6. As shown in Figure 7.6, MIOX30/PPy composite pigment was well settled in the bottom in perchloroethylene. This suggested that, PPy was well adhered to the MIOX30 pigment surface. As observed in Figure 7.6, no free PPy was observed floating in the perchloroethylene.

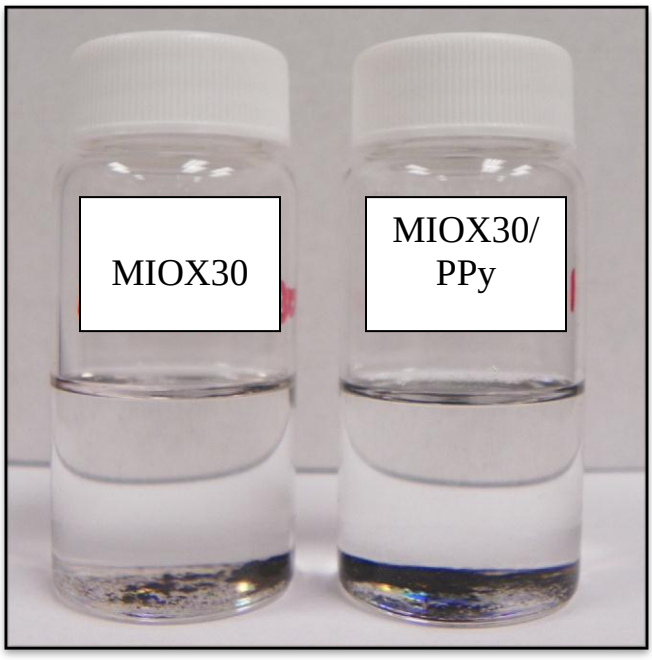

Figure 7.6: MIOX30 pigment and MIOX30/PPy pigment in perchloroethylene.

7.4.5. Electrochemical impedance spectroscopy (EIS)

Coatings were exposed to salt spray test conditions (ASTM B 117) and EIS was intermittently performed for the corrosion assessment. Bode plots of 15PVC, MIOX30 coating and 15PVC, MIOX30/PPy coating are shown in Figure 7.7. As observed in Figure 7.7, an initial low frequency (0.01Hz) impedance was ca. 10^{11} Ω for 15PVC, MIOX30 coating and 15PVC, MIOX30/PPy coating and coatings exhibited capacitive behavior. As exposure duration to salt spray conditions increased, the drop in low frequency (0.01Hz) impedance was observed for 15PVC, MIOX30 coating and coating showed resistive behavior. At 100 days of exposure, 10^{7} Ω was the low frequency impedance observed for 15PVC, MIOX30 coating. Drop in low frequency impedance for 15PVC, MIOX30/PPy coating was not as low as for 15PVC, MIOX30 coating. At 100th day of exposure, for 15PVC, MIOX30/PPy coating, 10^{9} Ω was value of low frequency impedance. This suggested the better resistance offered by 15PVC, MIOX30/PPy coating to the corrosive ions as well as to the corrosion.

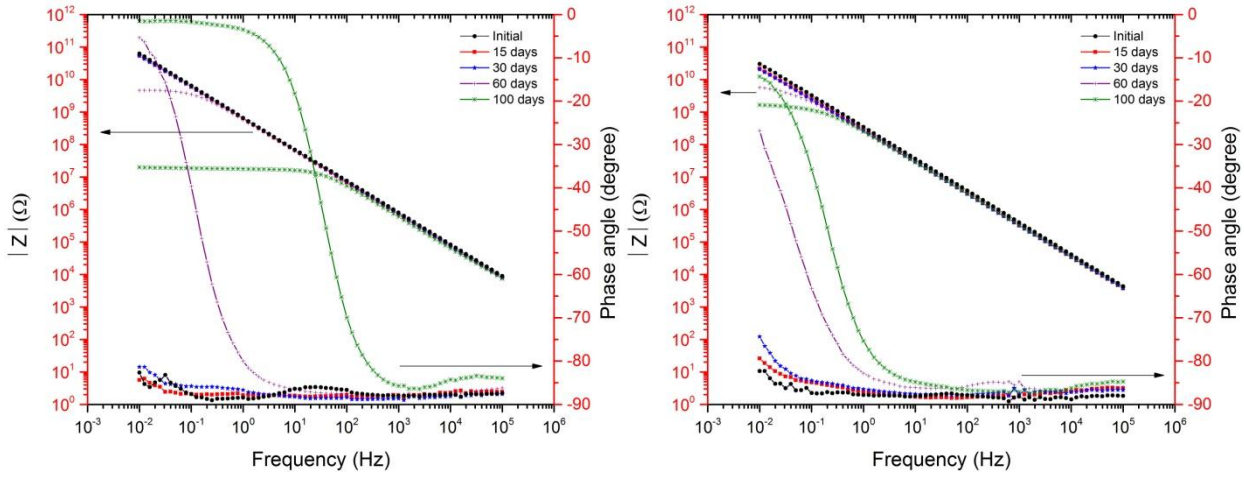

Figure 7.7: 15PVC, MIOX30 coating Bode plot (left), 15PVC, MIOX30/PPy coating Bode plot (right).

Bode plots of 25PVC, MIOX30 coating and 25PVC, MIOX30/PPy coating are shown in Figure 7.8. 25PVC, MIOX30 coating and 25PVC, MIOX30/PPy coatings showed very high

(10^{11} Ω) low frequency impedance. This impedance then gradually decreased as exposure duration to the salt spray increased in case of 25PVC, MIOX30 coating. At 100 days of exposure to the salt spray the low frequency impedance dropped to ca. 10^{7} Ω. The drop in impedance observed in case of 25PVC, MIOX30/PPy coatings was much lesser than that of in case of 25PVC, MIOX30 coatings. For 25PVC, MIOX30/PPy coatings, impedance at 100 days of the salt spray exposure was ca. 10^{9} Ω.

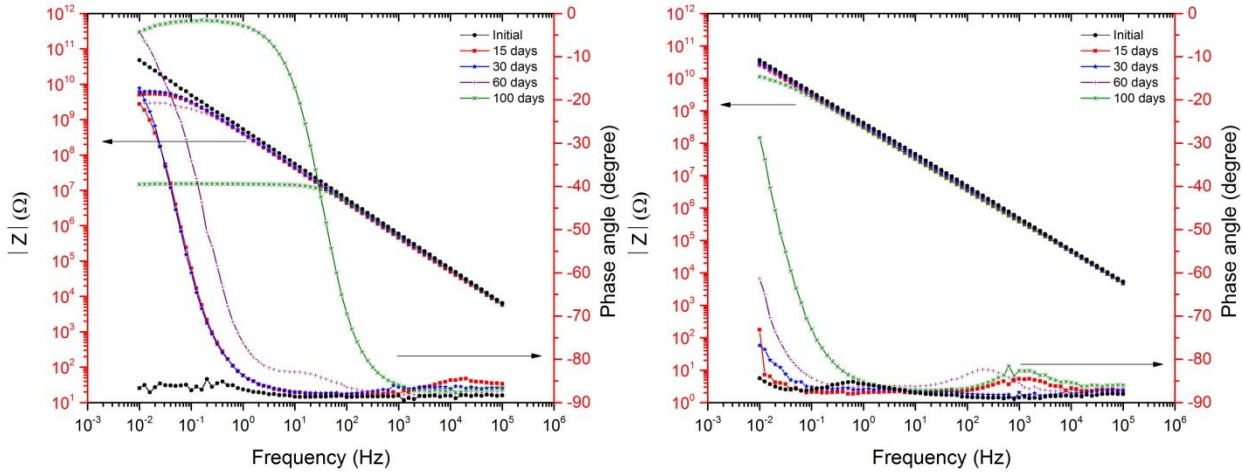

Figure 7.8: 25PVC, MIOX30 coating Bode plot (left), 25PVC, MIOX30/PPy coating Bode plot (right).

For 35PVC, MIOX30 coating and 35PVC, MIOX30/PPy coating, Bode plots are shown in Figure 7.9. As observed in Bode plot of 35PVC, MIOX30 coating and 35PVC, MIOX30/PPy coating, the very high (ca. 10^{11} Ω) low frequency (0.01Hz) exhibited by these coatings and the behavior of the coatings was capacitive. Exposure to the salt spray test conditions lead to decrease in the low frequency impedance in case of 35PVC, MIOX30 coating to less than 10^{7} Ω and to 10^{9} Ω in case of 35PVC, MIOX30/PPy coating and the coatings exhibited resistive behavior. The drop in impedance in case of 35PVC, MIOX30/PPy coating was much smaller than that of 35PVC, MIOX30 coating. In all the three cases of composite pigment based

coatings of MIOX/PPy, fewer drops in impedance was observed as compared to the just MIOX pigment based coatings.

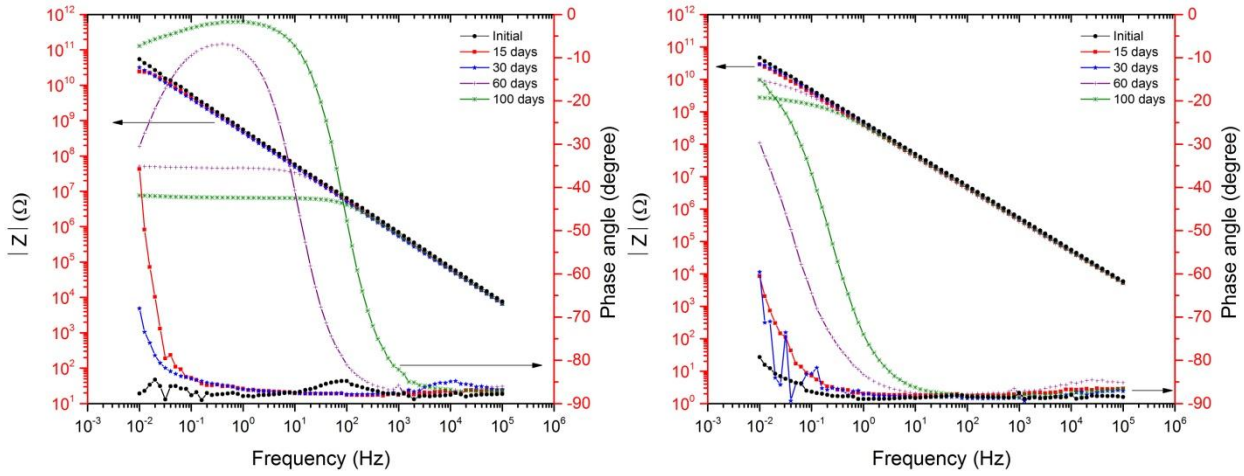

Figure 7.9: 35PVC, MIOX30 coating Bode plot (left), 35PVC, MIOX30/PPy coating Bode plot (right).

7.4.6. Equivalent circuit modeling and fitting of EIS data

Data obtained from EIS measurements was modeled and fitted to equivalent circuits using ZView 2 software from Scribner Associates Inc. EIS data of all the coated samples was modeled by employing Randles circuit model (Figure 7.10A) except for 35PVC, MIOX30 coating at 60 and 100 days of salt spray exposure (Figure 7.10B)

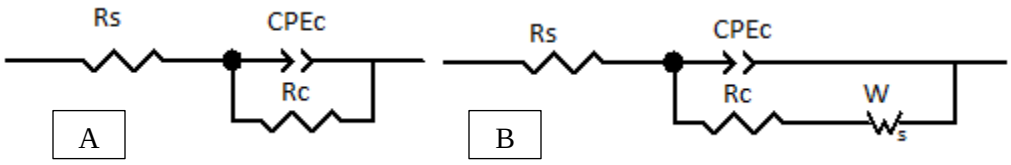

Figure 7.10: (A) Randles circuit model, (B) diffusion controlled model.

In Randles circuit model, Rs is the uncompensated solution resistance, Rc is the coating resistance, and pseudo capacitance is represented by constant phase element (CPEc). CPEc can be described by Equation 7.1.

$$Z(CPE) = 1/[(T)(j\omega)^{P}] \quad (7.1)$$

In Equation 1, Z(CPE) is the impedance of CPE, T is capacitance, j is an imaginary component, ω is the angular frequency (ω = 2πf, f is the frequency) and P is the power ($0 \leq n \leq 1$), Value of n=1 represents pure capacitor and value of n=0 represents pure resistor. Any value of n in between 0 and 1 represents mixed behavior. For 35PVC, MIOX30 coating at 60 and 100 days of salt spray exposure, Nyquist plot exhibited straight line at ca. 45 degree angle after first semicircle. This represented diffusion controlled region and was modeled by employing Warburg element (Figure 7.10 (B)). The impedance of the Warburg component is given by Equation 7.2.

$$Z_w = 1/\sigma(i\omega)^{(-1/2)} \quad (7.2)$$

Where, Z_w is Warburg impedance, i is imaginary component, σ is Warburg capacitance, and ω is the angular frequency (ω = 2πf, f is the frequency). Warburg element implies diffusion controlled process in the corrosion reactions [30-31]. Higher Warburg impedance in case of 35PVC, MIOX30 coating at 60 days of salt spray exposure as compared to its exposure at 100 days was observed from the circuit modeling. This implied longer diffusion pathways at 60 days of exposure and the diffusion pathway length decreased as exposure duration to the salt spray conditions increased resulting in lesser protection against corrosion [32-33].

The results obtained from equivalent circuit modeling are shown in Table 7.2. The results obtained closely match with the actual EIS data. One of the representative circuit model fitting (for 35PVC, MIOX30 coating at 100 days exposure to salt spray test conditions) was shown in Figure 7.11. As observed in Figure 7.11, actual obtained data is overlapping with the data of the model signifying closeness of fit.

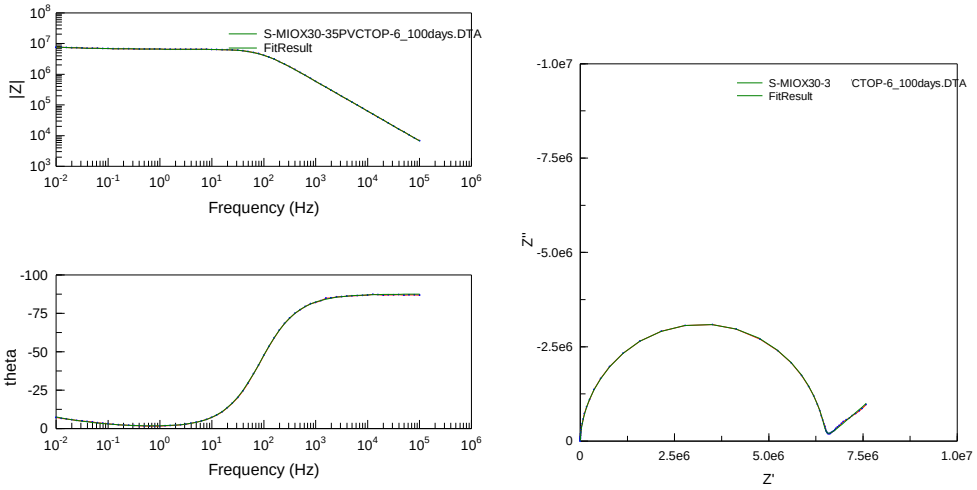

Figure 7.11: 35PVC, MIOX30 coating at 100 days exposure to salt spray test conditions (On left: Bode plot, on right: Nyquist plot, green curve is fitted data and red curve is actual data).

Coating resistance (Rc) values obtained by equivalent circuit modeling and fitting are plotted for all coatings with respect to the duration of exposure to salt spray (Figure 7.12). As observed in Figure 7.12, values of Rc were very high initially which steadily decreased as time to salt spray exposure increased. The drop in Rc was more in case of MIOX pigment coating system as compared to the MIOX/PPy composite pigment coating system. A minimal drop in Rc was observed for 25 PVC, MIOX30/PPy composite coating systems suggesting its better performance as compared to all other coating systems employed in this study [33].

An increased corrosion protection offered by MIOX30/PPy composite coating systems can be attributed to the PPy presence in the composite in intimate contact with the MIOX30 pigments. PPy, which contains conjugated double bonds and polar –NH group, acts as anodic inhibitor and tends to easily adsorbed onto the metal substrate due to the electron richness of the backbone [33]. Oxidized form of PPy is conductive in nature and it can easily take part in electrochemical reaction at the metal substrate thereby transferring electrons and stabilizing passive layer. PPy can also capture electrons at metal surface thereby reducing corrosion rate [34]. There is possibility of suppressing the active dissolution of steel in presence of PPy. This

can also result in the barrier protection offered by PPy coatings [35]. There is also possibility of limiting the flow of electrons to an oxidizing species from the metal in presence of conducting polymer thereby reducing the corrosion rate [36]. PPy couples with the iron metal in contact in presence of electrolyte which leads to auto-undoping with PPy reduction and overall increase in the impedance of the coating [37]. This might be the possible reason for the higher impedance of PPy based MIOX30 composites than that of just MIOX30 based composites. Along with these mechanisms there is mechanism of passivation at work which is described in anodic polarization section.

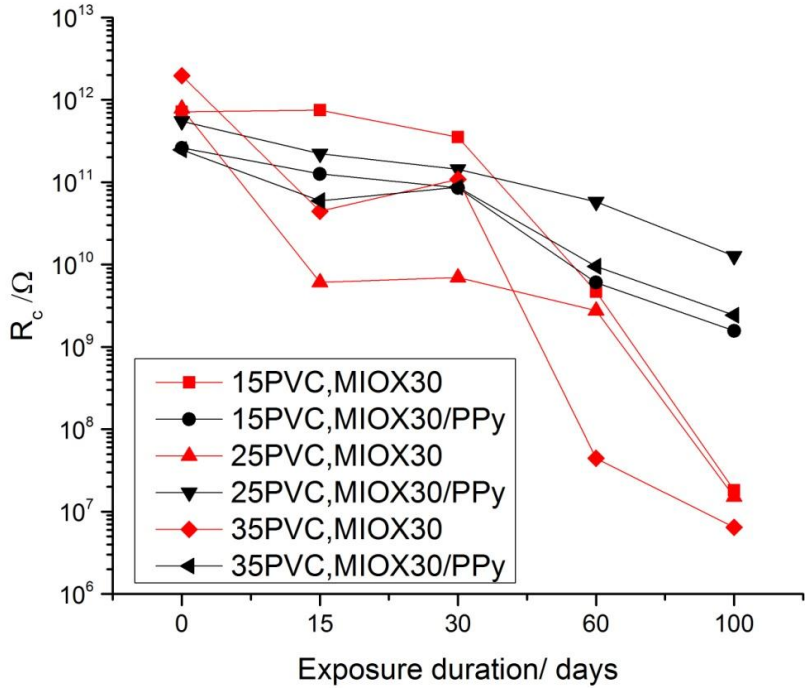

Figure 7.12: Changes in coating resistance (Rc) with exposure to salt spray test conditions**.**

Table 7.2
Equivalent circuit modeling results of EIS data

Exposure duration/Days	Rc/ Ω	CPE1		Ws-R/ Ω	Chi-Square
		Coating Capacitance/F	P1		
15PVC, MIOX30 coating					
0	7.19 x 10^11	2.47 x 10^-10	0.98		0.009
15	7.46 x 10^11	2.69 x 10^-10	0.98		0.002
30	3.51 x 10^11	2.63 x 10^-10	0.98		0.011
60	4.68 x 10^09	2.85 x 10^-10	0.98		0.001
100	1.82 x 10^07	3.79 x 10^-10	0.96		0.021
25PVC, MIOX30 coating					
0	7.85 x 10^11	3.14 x 10^-10	0.98		0.009
15	6.06 x 10^09	4.51 x 10^-10	0.97		0.020
30	6.99 x 10^09	4.13 x 10^-10	0.97		0.009
60	2.75 x 10^09	4.30 x 10^-10	0.96		0.016
100	1.51 x 10^07	3.69 x 10^-10	0.98		0.007
35PVC, MIOX30 coating					
0	1.97 x 10^12	2.93 x 10^-10	0.97		0.015
15	4.43 x 10^10	3.45 x 10^-10	0.97		0.018
30	1.08 x 10^11	3.91 x 10^-10	0.97		0.007
60	4.43 x 10^07	3.54 x 10^-10	0.97	8.87 x 10^07	0.007
100	6.44 x 10^06	3.36 x 10^-10	0.97	6.91 x 10^06	0.001
15PVC, MIOX30/PPy coating					
0	2.60 x 10^11	4.82 x 10^-10	0.98		0.002
15	1.26 x 10^11	6.23 x 10^-10	0.97		0.008
30	8.54 x 10^10	6.49 x 10^-10	0.97		0.003
60	6.03 x 10^09	6.94 x 10^-10	0.96		0.017
100	1.57 x 10^09	6.96 x 10^-10	0.96		0.018
25PVC, MIOX30/PPy coating					
0	5.48 x 10^11	3.98 x 10^-10	0.98		0.015
15	2.21 x 10^11	5.38 x 10^-10	0.97		0.014
30	1.44 x 10^11	4.68 x 10^-10	0.98		0.002
60	5.79 x 10^10	5.79 x 10^-10	0.95		0.010
100	1.27 x 10^10	6.07 x 10^-10	0.95		0.008
35PVC, MIOX30/PPy coating					
0	2.48 x 10^11	3.30 x 10^-10	0.99		0.003
15	5.96 x 10^10	4.27 x 10^-10	0.98		0.004
30	8.69 x 10^10	3.71 x 10^-10	0.98		0.040
60	9.52 x 10^09	5.01 x 10^-10	0.97		0.027
100	2.43 x 10^09	4.57 x 10^-10	0.97		0.051

7.4.7. Anodic polarization

Anodic polarization experiments were conducted for the coatings with scribe at scan rate of 5 mV/s. The results of anodic polarization are shown in Figure 7.13, 7.14, and 7.15 respectively. In case of 15 PVC, MIOX/PPy coatings and 25 PVC, MIOX/PPy coatings, 50-100 mV positive shift in the potential were observed with the reduction in corrosion current density (Figure 7.13 and 7.14).

The shift in potential towards positive direction is from the passivation in the scribe. Stored charge in the PPy which is already in oxidized form leads to the passivation in the defect [38]. PPy reduction gives rise to possibility of PPy re-oxidation by oxygen leading to decreased corrosion rate [39].The reason for the passivation is the strong oxidative power of conductive PPy which leads to the oxidation of metal and formation of the passive layer [19, 35]. In the case of steel substrate, stable passivating films of ferric oxide and ferrous oxide are formed at CP and metal interface [23]. The integrity of this layer which also comes from the addition of PPy is also responsible for the higher impedance values observed in EIS experiments.

In the case of 35PVC, MIOX/PPy coatings (Figure 7.15), a shift in potential in positive direction was observed. However, an increase in the corrosion current density was also observed. This would imply reduced corrosion protection [40]. These results might be due to the increased surface area of the 35PVC, MIOX/PPy coating. This increase might be from the approaching coatings PVC to critical pigment volume concentration (CPVC). Increased PVC of MIOX30/PPy also leads to more amount of PPy in the coating as compared to MIOX30 containing coating which also leads to the increase in the surface area due to the open porosity of the PPy. The area employed in these experiments is only the area of the scribe but the effective area might be larger. Similar behavior was observed in the 5% sodium chloride solution.

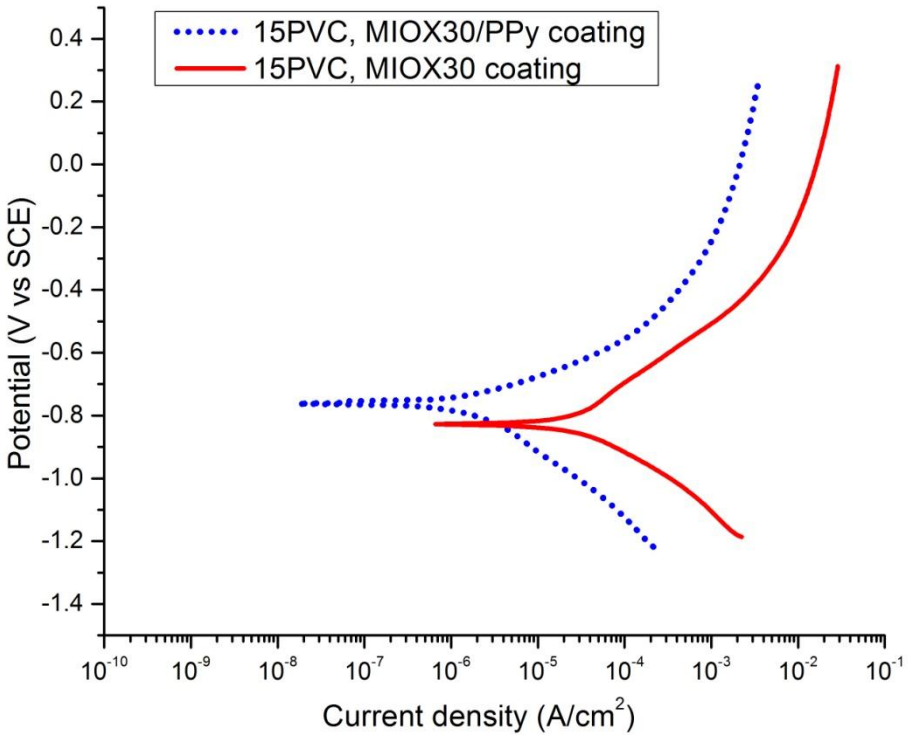

Figure 7.13: Anodic polarization scans for 15PVC coating.

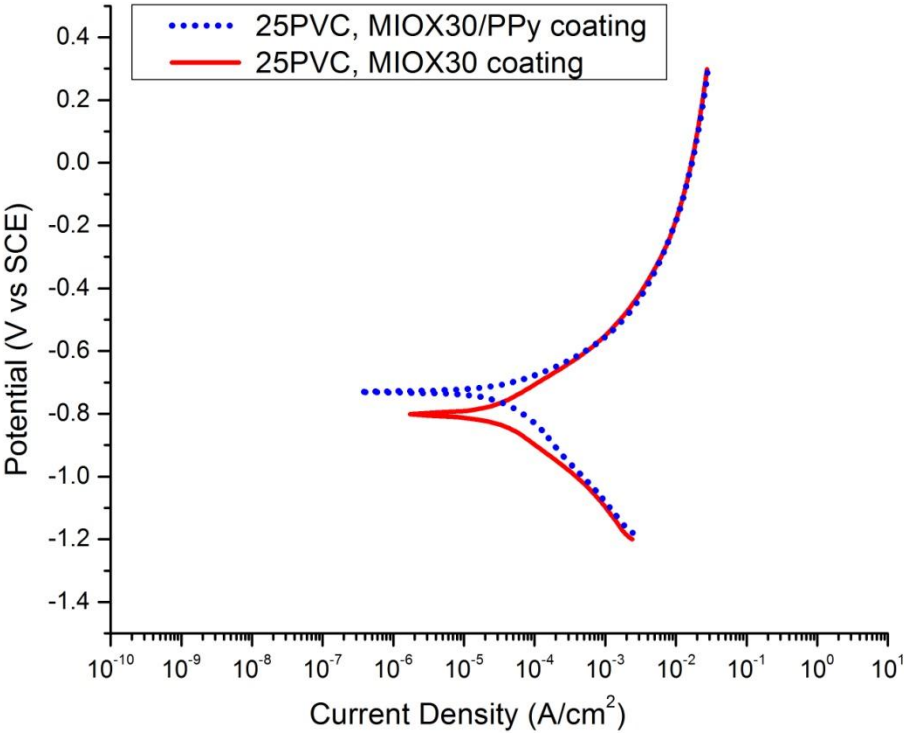

Figure 7.14: Anodic polarization scans for 25PVC coating.

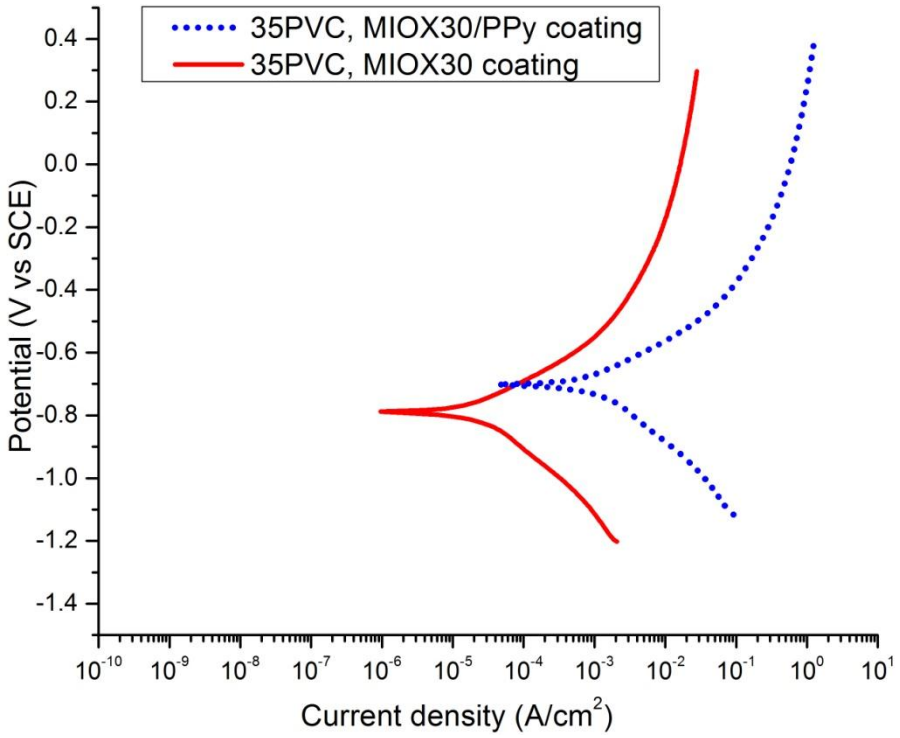

Figure 7.15: Anodic polarization scans for 35PVC coating.

7.5. Conclusions

Uniform growth of PPy particles was observed on the MIOX surface as evidenced in SEM micrographs. The presence of nitrogen and lesser amount of iron in EDS results indicated the formation of PPy on the surface of MIOX. The conductive regions found in C-AFM studies confirmed the conducting nature of synthesized MIOX30/PPy hybrid composite particles. During the last step of preparation of MIOX/PPy hybrid, it was ground using mortar and pestle. Despite of the mechanical force, PPy particles were found to be well adherent as observed in density tests. EIS studies showed higher coating resistance values for MIOX30/PPy composite coatings and anodic polarization studies confirmed that the passivation was achieved due to the presence of PPy in the MIOX30/PPy composites. Better corrosion protection in case of MIOX30/PPy composite coatings was attributed to the conductive and redox nature of the PPy.

7.6. References

[1] R.W. Revie, Uhlig's Corrosion Handbook, Wiley, 2011.

[2] Z. Ahmad, Principles of Corrosion Engineering and Corrosion Control, Elsevier Science, 2006.

[3] G. Grundmeier, W. Schmidt, M. Stratmann, Electrochimica Acta, 45 (2000) 2515-2533.

[4] M. Stratmann, Corrosion, 61 (2005) 1115-1126.

[5] D.E. Tallman, Y. Pae, G.P. Bierwagen, Corrosion, 56 (2000) 401-410.

[6] R.L. Twite, G.P. Bierwagen, Progress in Organic Coatings, 33 (1998) 91-100.

[7] S.A.S. Dias, S.V. Lamaka, C.A. Nogueira, T.C. Diamantino, M.G.S. Ferreira, Corrosion Science, 62 (2012) 153-162.

[8] A.K. S, H. Bhandari, C. Sharma, F. Khatoon, S.K. Dhawan, Polymer International, (2012) n/a-n/a.

[9] M. Gerard, A. Chaubey, B.D. Malhotra, Biosensors and Bioelectronics, 17 (2002) 345-359.

[10] M.R. Mahmoudian, W.J. Basirun, Y. Alias, M. Ebadi, Applied Surface Science, 257 (2011) 8317-8325.

[11] G. Inzelt, Applications of Conducting Polymers, in: Conducting Polymers, Springer Berlin Heidelberg, 2012, pp. 245-293.

[12] D. Kundu, F. Krumeich, R. Nesper, Journal of Power Sources, 236 (2013) 112-117.

[13] T. Patois, J.-B. Sanchez, F. Berger, J.-Y. Rauch, P. Fievet, B. Lakard, Sensors and Actuators B: Chemical, 171–172 (2012) 431-439.

[14] P.R. Somani, S. Radhakrishnan, Materials Chemistry and Physics, 77 (2003) 117-133.

[15] J.H. Collier, J.P. Camp, T.W. Hudson, C.E. Schmidt, Journal of Biomedical Materials Research, 50 (2000) 574-584.

[16] J. Wu, J. Pawliszyn, Journal of Chromatography A, 909 (2001) 37-52.

[17] M.D. Ingram, H. Staesche, K.S. Ryder, Solid State Ionics, 169 (2004) 51-57.

[18] Ö. Yavuz, M.K. Ram, M. Aldissi, P. Poddar, H. Srikanth, Synthetic Metals, 151 (2005) 211-217.

[19] J. Reut, A. Öpik, K. Idla, Synthetic Metals, 102 (1999) 1392-1393.

[20] Y. Han, X. Qing, S. Ye, Y. Lu, Synthetic Metals, 160 (2010) 1159-1166.

[21] M. Trueba, S. Trasatti, Journal of Applied Electrochemistry, 39 (2009) 2061-2072.

[22] M.G. Hosseini, M. Raghibi-Boroujeni, I. Ahadzadeh, R. Najjar, M.S. Seyed Dorraji, Progress in Organic Coatings, 66 (2009) 321-327.

[23] D.M. Lenz, M. Delamar, C.A. Ferreira, Journal of Electroanalytical Chemistry, 540 (2003) 35-44.

[24] C.A. Giudice, J.C. Benitez, Anti-Corrosion Methods and Materials, 47 (2000) 226-232.

[25] A. Forsgren, Corrosion Control Through Organic Coatings, Taylor & Francis, 2010.

[26] W.B. Genetti, W.L. Yuan, B.P. Grady, E.A. O'Rear, C.L. Lai, D.T. Glatzhofer, Journal of Materials Science, 33 (1998) 3085-3093.

[27] S. Biswas, L.T. Drzal, Chemistry of Materials, 22 (2010) 5667-5671.

[28] Y. Han, Y. Lu, Carbon, 45 (2007) 2394-2399.

[29] T.K. Vishnuvardhan, V.R. Kulkarni, C. Basavaraja, S.C. Raghavendra, Bull Mater Sci, 29 (2006) 77-83.

[30] S.U. Rahman, M.A. Abul-Hamayel, B.J.A. Aleem, Surface and Coatings Technology, 200 (2006) 2948-2954.

[31] S.H. Ahn, Y.S. Choi, J.G. Kim, J.G. Han, Surface and Coatings Technology, 150 (2002) 319-326.

[32] T. Hong, Y.H. Sun, W.P. Jepson, Corrosion Science, 44 (2002) 101-112.

[33] J.O. Iroh, W. Su, Electrochimica Acta, 46 (2000) 15-24.

[34] U. Riaz, S.M. Ashraf, S. Ahmad, Progress in Organic Coatings, 59 (2007) 138-145.

[35] T. Ohtsuka, International Journal of Corrosion, 2012 (2012) 7.

[36] P. Chandrasekhar, Conducting polymers, fundamentals and applications: a practical approach, Kluwer Academic Publishers, 1999.

[37] N.V. Krstajić, B.N. Grgur, S.M. Jovanović, M.V. Vojnović, Electrochimica Acta, 42 (1997) 1685-1691.

[38] T.A. Skotheim, J. Reynolds, Conjugated Polymers: Processing and Applications, Taylor & Francis, 2006.

[39] G. Spinks, A. Dominis, G. Wallace, D. Tallman, Journal of Solid State Electrochemistry, 6 (2002) 85-100.

[40] C.K. Tan, D.J. Blackwood, Corrosion Science, 45 (2003) 545-557.

CHAPTER 8. SUMMARY

Corrosion is a perennial problem faced by human civilization. Worldwide annual corrosion cost is at 2.2 trillion USD which is approximately 3% of worlds total GDP. As corrosion is thermodynamically favorable process it is difficult to completely stop it but it is possible to mitigate by applying various methods such as coatings, inhibitors, cathodic protection, judicial material selection, and proper design. Commonly used barrier type coatings prove ineffective once defect is formed on coated substrate. Chromates which are well known and highly effective anticorrosion agents are mutagenic and carcinogenic in nature. Metal rich primers need high pigment volume concentration (PVC) for the corrosion protection. Taking into consideration limitations of existing coating systems along with changing environment, rapidly growing heavy industrialization, increasing pollutants, there is need to find environmentally benign solutions with superior properties.

In the reported work, conducting polymer containing composites (CPPC) were synthesized in ecofriendly manner and coatings based on CPCC were formulated for aluminum 2024-T3 and cold rolled steel substrates and furthermore assessment of corrosion protection provided by these coatings by various electrochemical characterization methods was carried out. CPCC combines unique properties of conducting polymers (polypyrrole (PPy) and polyaniline (PAni)) such as conductivity, good environmental stability, ecofriendly nature, and facile synthesis procedures with inorganic pigments leading improved corrosion protection ability.

Two different morphologies of polypyrrole (PPy) aluminum flake composites, namely spherical PPy/Al flake composites and wire PPy/Al flake composites, were synthesized by chemical oxidative polymerization and the coatings based on them were applied to aerospace alloy aluminum 2024-T3. The wire PPy/Al flake composite coatings exhibited 3000 hours of salt

spray performance. The enhancement in anticorrosion performance was attributed to the unique morphology and electrochemical activity of the PPy on the surface of aluminum flakes as evidenced by electrochemical impedance spectroscopy (EIS) and galvanic coupling experiments. It was also revealed by scanning vibrating electrode technique (SVET) that the wire PPy/Al flake composite coating was sacrificially protecting the aluminum 2024-T3 substrate in larger defects.

Corrosion inhibiting dopants were incorporated on the backbone of PPy. Once the PPy was reduced, these corrosion inhibiting dopants could combine with underline metal to form an insoluble layer improving the corrosion resistance. Smart corrosion resistive coating systems based on the CPCC which included successful incorporation of corrosion inhibition dopants such as phosphate, nitrate, vanadate, molybdate, and tungstate on the backbone of PPy were applied to aluminum 2024-T3 substrate. In a defect these coatings exhibited better corrosion performance as evidenced by global and local electrochemical techniques. These doped CPCCs not only provided sacrificial protection to the underlying aluminum 2024-Ts substrate as observed in galvanic coupling experiments but also provided passivation in defect as suggested by potentiodynamic scans.

In vary facile manner, core and shell particles of TiO_2/PPy, iron oxide/PPy were also synthesized and coatings based on these composites were applied on cold rolled steel. Improvement in the corrosion protection was observed due to the presence of PPy in the composite coatings. Composite pigments of micaceous iron oxide (MIOX)/PPy were synthesized and were incorporated in the coating for the corrosion protection of cold rolled steel. Improvement in the corrosion protection performance was observed for MIOX/PPy composite based coatings for 100 day of Salt spray exposure.

In summary, in the reported research, new coating systems for the corrosion protection of aluminum and steel alloys were developed in ecofriendly manner with improved performance. These new coating systems were characterized with global and local electrochemical techniques which are nondestructive tests and have a potential of becoming industry standards.

CHAPTER 9. FUTURE STUDIES

The principle of synthesizing CPs in-situ on the inorganic flake surfaces can be extended to the other lamellar flakes such as talc and mica. Even though modification of inorganic surface is not necessary for the formation of PPy on lamellar pigments such as micaceous iron oxide (MIOX), surface treatments of these flakes will lead to the formation of different morphologies of PPy and changes in the corrosion protection performance. The MIOX/PPy composite pigment studies were performed at 30 μm particle size of MIOX pigment particles. In the future, it is possible to study corrosion performance at lower particle sizes of MIOX (5 and 10 μm) for MIOX/PPy composites. A mixture of different particle sizes of PPy can also lead to diverse corrosion performance of MIOX/PPy composite pigments.

Core and shell morphologies of inorganic pigments (titanium dioxide and iron oxide) and PPy can be characterized in more details for the corrosion protection of cold rolled steel for the optimization of quantities of PPy and inorganic pigments. Core and shell morphologies of metal particles such as iron and zinc with PPy can be obtained with proper control of reaction conditions. If the dissolution of the active metal can be controlled before the polymerization of monomer of CP then there is possibility of obtaining core and shell particles of active metals and PPy. This type of pigment can provide sacrificial protection to the underlying metal substrate. Flakes form of these active metals can also be obtained for the synthesis of CPCC in the similar manner as discussed for aluminum flakes in this dissertation.

In this study inorganic dopants were incorporated on the backbone of CPs in the formations of CPCCs. There is possibility of incorporation of organic dopants such as sodium p-toluene sulfonate, sodium dodecyl benzene sulfonate, and sodium 2-naphthalenesulfonate on the

backbone of PPy in CPCC. These bulky dopants will pose significant hindrance to the rapid ingress of chloride ions and will eventually provide long term corrosion protection.

Electroactive dopants such as sodium anthraquinone-2-sulfonate, 4 hydroxybenzenesulfonic acid sodium salt hydrate, 1 2-dihydroxybenzene-3 5-disulfonic acid disodium salt monohydrate, hydroquinonesulfonic acid potassium salt, and 4,5-Dihydroxynaphthalene-2,7-disulfonic acid disodium salt can be incorporated on be backbone of PPy in CPCC synthesis. Interactions of these electroactive dopants with metal substrate and with oxygen in the electrolyte can be studies with localized electrochemical techniques such as scanning electrochemical microscopy (SECM) and scanning vibrating electrode technique (SVET).